CRANFIELD INSTITUTE OF TECHNOLOGY

SILSOE COLLEGE

Ph.D THESIS

Academic Year 1981 - 85

TARA CHANDRA THAKUR

An Investigation into the Mechanics of Powered Rotary Tillage Tools

Supervisor: Dr. R.J. Godwin

January, 1985

This thesis is submitted in fulfilment of the requirement for the degree of Doctor of Philosophy

SYNOPSIS

A prediction model based upon Mohr-Coulomb soil mechanics theory has been developed to predict the interaction between the soil and a rotary tiller blade with horizontal axis of rotation by neglecting the 'leg-effect' of the cutter. The model has two major components, the quasi-static reaction and the dynamic soil reactions due to acceleration of the deformed soil slice and sinkage of the chamfered back face of the blade as a special case. The quasi-static force prediction model is dependent upon the passive general shear failure of the soil slice towards the curved free surface of a previous cut and the lateral local shear failure towards the undeformed soil due to the effect of the tip.

The effect of the tip of the blade was further investigated using a 20-gauge inextensible steel wire mounted on the leg of the cutter in geometrical similarity with that of the blade tip. The force prediction models of the wire are based on the type of failure mechanism observed at different fetch-ratios (bite length / depth of cut). The dynamic force due to acceleration of the deformed soil slice is based upon the principle of work-energy and that due to scrubbing/compression of the chamfered back face, upon the analogous static flat plate - sinkage test results. The predicted results for a wire and the blade are in close agreement with the results of the experimental studies.

The experimental studies were conducted in a sandy loam soil at the moisture content in the friable range under the controlled soil-bin conditions on a full-scale experimental apparatus developed primarily for this investigation. Bite lengths ranging from 50 mm to 250 mm and depths of cut ranging from 50 mm to 150 mm were used to cover a range of fetch-ratios from 0.33 : 1 to 5 : 1. The blade kinematics and soil reaction were measured using the monitors to record the angular position of the tip and a strain gauge transducer respectively. The signals from the transducer were converted to a graphical form onto both a graph plotter and a pre-programmed computer for further analysis.

The quasi-static force prediction model developed for the blade with the horizontal axis of rotation is extended to the blade with vertical axis of rotation by incorporating certain modifications. This model is based upon the observed soil failure mechanism from a limited number of preliminary investigations and predicts the forces with reasonable accuracy.

ACKNOWLEDGEMENTS

The author is sincerely grateful and indebted to Dr. R.J. Godwin for the encouragement and personal involvement during the course of this study. Gratitude is expressed to Professor G. Spoor and Mr. C.P. Crossley for their valuable suggestions and constructive criticism on many important aspects of the project.

Heartfelt thanks are expressed to Mr. Tony Reynolds who spent many hours assisting in the preparation of the soil and recording of the experimental data. To A.M.E. Mohammed and P.S.G. Magalhaes, colleagues at the Silsoe College Postgraduate Research Laboratory, for their general enthusiasm and encouragement.

Thanks also to the technical staff of Silsoe College for assistance in fabrication of the experimental apparatus developed for use in the project. To N. Marsh and B. Fletcher who in turn assisted in recording of the video film and preparation of the photographs. To Mrs. C. McAllister for typing the thesis.

The author acknowledges the financial support, in terms of Commonwealth Scholarship, offered by the Commonwealth Scholarship Commission in the U.K.; the Ministry of Education, Government of India; and the G.B. Pant University of Agriculture and Technology, Pantnagar (India), without which this study would not have been possible.

TABLE OF CONTENTS

LIST OF FIGURES

LIST OF TABLES

1. INTRODUCTION

1.1 Introduction

Equipment for rotary cultivation has found wide use in different agricultural operations with special application in strip or minimum tillage where controlled traffic methods may be used to minimise the extent of compaction. The negative draught of rotary tillage tools make them suitable for poor trafficability situations especially true in inundated regions of Asia or for high horsepower to low weight tractors. Although the agrotechnical effects of tilling soil by rotary tilling are widely known, their widespread use is restricted because of relatively high expenditure of energy. However, according to Söhne and Eggenmüller (1959) the high energy requirement may not necessarily be true on the basis of total power need for a given degree of soil pulverization.

A systematic research of the soil reactions on the tillage tools was initiated by Nichols (1930 and 1931) and Baver (1932) by the measurement of the dynamic properties of soil and relating them to the design and performance of tillage equipment. During almost the same period Clyde (1936 and 1937) resumed the work of defining the soil reaction forces on plough bodies, coulters and disc tools. Even so, most of the technological advances in soil manipulation equipment are evolved through 'Cut and Try' methods in the field over a period of years. The theoretical studies on the tillage tools mechanics gained greater impetus after the pioneering research of Payne (1956) who based the prediction of soil reaction forces on simple tines by adopting the retaining wall theory and Mohr-Coulomb soil failure mechanics. Since when some fundamental work has been developed for:

i. Two-dimensional soil failure situations such as wide tines or blades and theories developed by Osman (1964), Siemens et.al. (1965) and Hettiaratchi et.al. (1966).

ii. Three-dimensional soil failure cases with narrow tines by O'Callaghan and Farrelly (1964) and Hettiaratchi and Reece (1967) and

iii. Three-dimensional very narrow tines soil failure by Godwin and Spoor (1977).

These theories take into account the basic tool geometry and dynamic soil properties and predict the soil reaction forces with reasonable accuracy for most practical purposes.

Rotary tillage tools have not received the same fundamental research attention devoted to passive tillage tools. A comprehensive review on the design parameters of rotary tillers by Hendrick and Gill (1971, 1974 and 1978) and Elgin (1979), revealed that for the last three decades, researchers have tried to correlate the energy requirement of the tiller with special reference to the geometry of the tool. Throughout the reports, various figures have been quoted but the investigations from which they are derived are not entirely comparable since uniformity regarding the report on soil conditions, description of tool geometry or rotor diameter is lacking. Some workers present descriptions of initial soil conditions including moisture content and penetration resistance whilst others do not. Fundamental information on soil break-up in these experiments is often poorly reported and in some cases absent.

From the appraisal of the experimental evidence it is known that the designers of the rotary tillage tools have relied upon the empirical approach due to lack of suitable information on the relationship between the soil physical properties and performance of these tools. No apparent attempt has been made to investigate the performance of rotary tools using the principles of engineering soil mechanics. An increase in the power efficiency of rotary tools could result from the fundamental understanding of their mechanics.

A variety of rotary tools, now available, are driven from the tractor PTO in either of the two modes of operation:

i. A rotor with horizontal axis of rotation such as rotary tiller or rotavator, spading machine, spiked clod crushers and rotary ditch/canal diggers.

ii. A rotor with vertical axis of rotation such as rotary harrow and end blades of post hole diggers.

In these tools the major soil disturbance is performed by their blades. It was, therefore, thought logical to study the basic mechanics of a simple powered blade applicable to a variety of rotary tillage tools.

1.2 Objectives

i. To establish the effect of the blade parameters on the soil failure patterns in a frictional soil under controlled soil bin conditions.

ii. To relate the effect of blade geometry and physical conditions of the soil to the magnitude, direction and position of the resultant soil forces acting upon the blade.

iii. To develop a suitable model based on the soil mechanics parameters and blade geometry to predict the soil forces acting upon a rotary powered blade.

2. REVIEW OF LITERATURE

2.1 Introduction

This chapter deals with a brief review of literature reported on the rotary powered tillage tools and analogous cutting tools in the field of metal machining and coal cutting. A comprehensive review of research work on rotary tillers has been reported by Hendrick and Gill (1971, 1974 and 1978). The emphasis here is, therefore, given to the force/torque prediction models developed by various researchers for rotary tillers. The review on a specific area of interest has been presented in appropriate sections of the relevant chapters.

2.2 Rotary Powered Tillage Tools

2.2.1 Rotors with Horizontal Axis of Rotations

The total force of reactions in cutting-off a soil slice by a L-shaped cutter is the sum of reactions due to cutting with the leg and blade, the breaking of the soil slice from the monotilth and the friction of soil sliding over the surface of the working tool. The reaction to cutting by the leg of the rotary cutter has been studied in detail by many researchers. Dalin and Pavlov (1950) related the forces on the leg with its dimensional parameters i.e. thickness and tip angle, and depth of cut. It was shown that for a constant thickness of the leg, the forces increased with the decrease in tip angle and attributed due to the increase in the force of friction. The optimum value of tip angle was suggested by Dalin (1951) between 25^{o} and 30^{o} depending upon soil type and the amount of ground cover and was in agreement with Matsuo (1965) and Joshida (1965). However, a tip angle of more than 50^{o} was recommended for the cutter designed for soil loosening without surface covers.

The cutting resistance to the leg and blade of the cutter was found in the different order by Shamotaya and Surilov (1965). A considerable amount of cutting energy (30 to 40 %) was consumed by the leg whereas the blade consumed only 20 to 25 %. The breaking of

the slice along the lateral surface consumed approximately 40 to 48 % of the total energy. In the experiments with varying width of the blade from its leg Ahmad (1980) recorded a decrease in peak power for increasing the blade width to 50 mm. A further increase in width increased the power requirement linearly but decreased the specific power requirement. The higher power requirement of the leg was explained on the basis of the lateral soil failure phenomenon observed with narrow tines by Payne (1956), and Godwin and Spoor (1977).

The frontal reaction on the cutting edge of the blade has been described by Paltavtsev (1954) as a function of the cutting width, average length of the arc of a cut and the specific resistance to cutting along the arc. This concept was later used by Bernacki (1962) who postulated the cutting resistance of a rotary cutter as the product of specific soil resistance and cross-section of the soil slice which is proportional to the slice thickness. In a study on the characteristics of friction-loss due to compaction effect of the Japanes tiller blades, Sakai and Hai (1982) compared the single-edged blade with the double-edged. The single-edged blade was found to be more effective to decrease the tillage resistance and a saving of approximately 20 % in the power was reported from the results of field experiments. The greater resistance of the double-edged blade was attributed to the much greater value of friction between the blade and the untilled soil.

The power consumption in rotary tilling is dependent upon the diameter of the cutter drum, depth of cut, bite length, cutting angle, ratio of rotational and forward speeds, geometrical parameters of the blade and the soil physical conditions, and has been studied by Poltavtsev (1954), Popov (1963) and Surilov (1966). A change in any parameter during the working process entails a change in power consumption. The approximate methods of determining power consumption in rotary tilling adopted by Russian researchers are based on the formulas involving empirical coefficients. Developing the ideas of Goryechkin (1937) and Dalin (1950 and 1951); Lisunov (1968) suggested a general equation for the power consumption of a trailed-type rotary tiller given as overleaf:

$$N = N_c + N_t \pm N_p + N_T + N_r \quad \ldots\ldots\ldots (2.1)$$

where N_c = power consumed in cutting

N_t = power to throw the soil

N_p = power to pull the tiller, + for up-cut, - for down-cut

N_T = power loss in transmission

N_r = power to roll the machine

In analysing the equation 2.1, N_c and N_t appear to be the areas most suitable for a saving in power requirement and were considered by Bernacki (1962) who suggested an equation as a second order parabola by the relation between the specific work, and the forward and rotational speeds of the working tools.

Gosh (1967) using dimensional analysis technique identified the dimensionless parameters in rotary tilling and suggested a linear regression model for the torque requirement of the tiller on the basis that for a given soil condition, the torque is proportional to the depth of working and the forward speed of travel and inversely proportional to the speed of rotation. In a similar approach Purdok and Burema (1977) derived an empirical model based on the hypothesis that the torque of the tiller is proportional to the product of working width and bite length for a constant depth and rotational speed. After a comprehensive review on rotary tillage Elgin (1979) carried out dimensional analysis to reduce all the soil-tool variables into three non-dimensional numbers. A simple regression analysis of the data taken from Beeny (1970) and Chamen (1971 - 73) showed that about 87 % variability in torque was accounted for by the independent variable, cohesion alone and was used in the torque prediction model given overleaf:

$$T = 242 \frac{K\gamma}{\lambda} - \frac{51CK}{\lambda} + 5.66 \frac{C^2 K}{\gamma} \quad \ldots\ldots\ldots (2.2)$$

where K = machine variables number

$$= \frac{W L_b}{D/d}$$

w = width of cut

L_b = bite length

D = diameter of rotor

d = depth of cut

λ = speed ratio i.e. $\frac{V_c}{V_f}$

C = cohesion of soil

γ = density of soil

In deriving the equation 2.2, Elgin used the values of cohesion and bulk density considering the textural classification and previous crop history of the land and assuming the value of diameter of the rotor wherever necessary. The validity of the model was tested using experimental results from Beeny (1965) and Pascal (1967) which showed reasonable agreement between experimental and predicted values.

Tinker (1981) postulated a simple expression for the power requirement of a rotary cutter using basic soil properties and the blade geometry. The model was based on the assumption that the soil failed in a complete block along the arc of the blade motion. The force on the cutter was determined using cohesion and adhesion values of the soil and total area of the failure planes along the arc and sides. The model was verified using data from Ahmad (1981). This, however, was unsuccessful and both under or over estimated the predicted results with large variations. The model, however, can be considered as a first basic approach in introducing the soil physical properties in the force prediction model for a tiller blade.

2.2.2 Rotors with Vertical Axis of Rotation

Although a variety of tillers with vertical axis of rotations are now available, very little research has been reported on these machines. It is, therefore, possible to present only the physical significance of these machines to add to the historical developments.

One of the first vertical axis ploughs was English gyrotiller (1930) which had two drums (1,300 mm diameter) mounted with five ripper blades on each drum. The drums rotated towards each other at speeds of 15 to 18 r.p.m. and loosened the soil to a depth of upto 400 mm. Since the rotating ripper blades practically did not mix up different layers of soil, the gyrotiller was used for deep working of soil without bringing the lower layers of soil to the surface, Yatsuk et.al.(1981). Two types of working tools were mounted on later (1938) models with two drums rotating on vertical axis and ripper blades rigidly fixed to the chassis ahead of the drums to get loosening of the lower layers and thorough disintegration of the upper layer at the same time.

A machine similar to the gyrotiller was also produced in Germany (1930) for use with low-power tractors (16 to 18 h.p.). It consisted of two drums (total width of cut, 650 mm) with three vertical cutters on each and worked upto a depth of 250 mm. Panov and Melikhov (1963) after a series of tests concluded that the loosening of soil was more intensive than that with the common plough but the covering of plant residue with soil was inadequate.

The Chivello plough from Italy was incorporated with a single rotor of 400 mm width of cut and working upto a maximum depth of 350 mm with a rotor speed of 250 r.p.m. The plough worked in the speed range of 1 to 4 km/hr and needed a 20 - 35 h.p. tractor. The tests by Eggenmüller (1959) had shown that in terms of breaking of the soil it occupies a place in-between the plough and the rototiller.

Pascal (1967) reported a comparative study on various rotary soil working machines in terms of the power requirement and soil final conditions. In a comparison on a ploughed loam soil, the cultivators with vertical and horizontal axis of rotations required almost similar

amount of PTO power and the specific work was similar for both the rotors. However, the draught of the vertical rotor was approximately 3.5 times to that of the horizontal rotor. It was concluded that the cultivators with vertical axis of rotations are unlikely to match the cultivators with horizontal rotor because of their high initial cost and inability to deal adequately with surface trash. Nevertheless, certain specialised uses can be found for vertical rotor where a fine consolidated tilth is required in the preparation of discrete sites.

Harrison (1978) outlined a method to determine the optimum angle of the cutting face (rake) for a blade with vertical axis of rotation, to avoid compression of the uncut soil, to minimise the cutting force and allow adequate penetration. The rake angle was decided between 25^{o} and 45^{o} following Payne and Tanner (1959) for the total length of the curved blade such that the lower and upper portions of the blade had rake angles with respect to vertical and horizontal planes respectively.

2.3 Metal Cutting

It is not yet possible to predict with any great accuracy the forces involved in metal cutting, in spite of a large number of theories which have been developed. This is largely due to the extreme complexity and the lack of geometrical constraint which is characteristic of metal cutting. The first semi-empirical approach towards the prediction of tool forces in orthogonal machining is due to Merchant (1945) who was able to build up a picture of forces acting in the region of cutting which give rise to plastic deformation and sliding of the chip down to the tool rake face (Figure 2.1). The theory assumes that a continuous-type chip without a built-up edge is produced during the cutting and the shear angle adjusts itself to give minimum work. However, the theory does not give a completely satisfactory picture of metal cutting but is considered as a useful stepping-stone to much of the subsequent research which was based on the assumption that instead of a plane, shearing takes place in a narrow plastic zone, where it is necessary to allow for work hardening, Lee and Shaffer (1951); and Christopherson et.al. (1958).

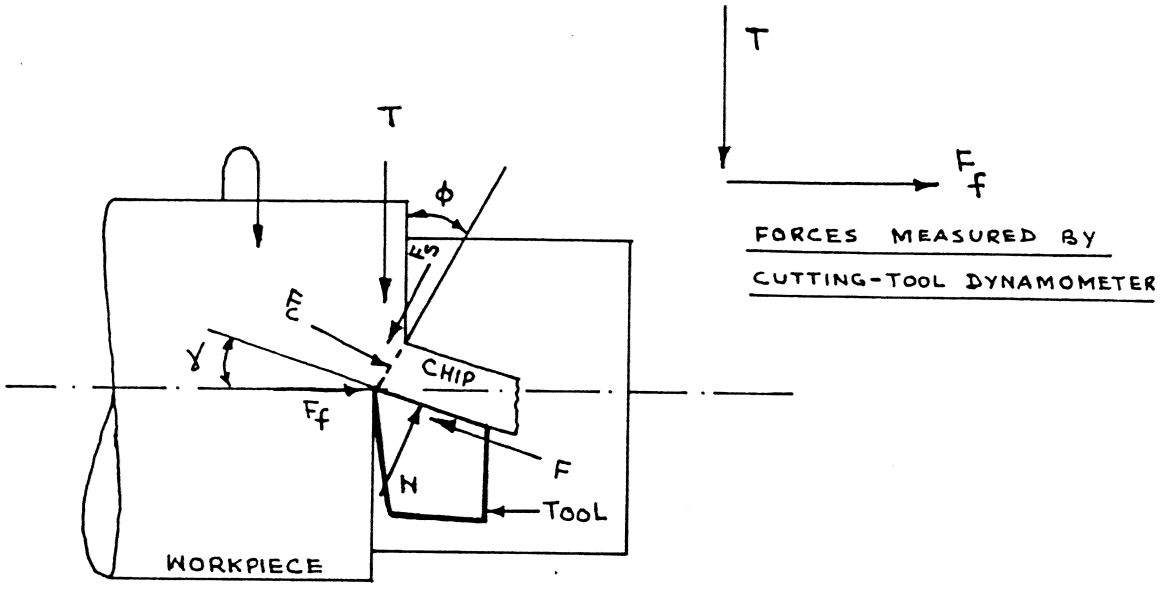

FIGURE 2·1 CHIP FORMATION AND FORCE SYSTEM AS POSTULATED BY MERCHANT (1945)

a. THE FORCES EXERTED BY THE WORKPIECE ON THE CHIP.

F_c = COMPRESSIVE FORCE ON THE SHEAR PLANE;

F_s = SHEAR FORCE ON THE SHEAR PLANE.

b. THE FORCES EXERTED BY THE TOOL ON THE CHIP

N = NORMAL FORCE ON THE RAKE FACE OF TOOL

F = FRICTIONAL FORCE ALONG THE RAKE FACE OF TOOL

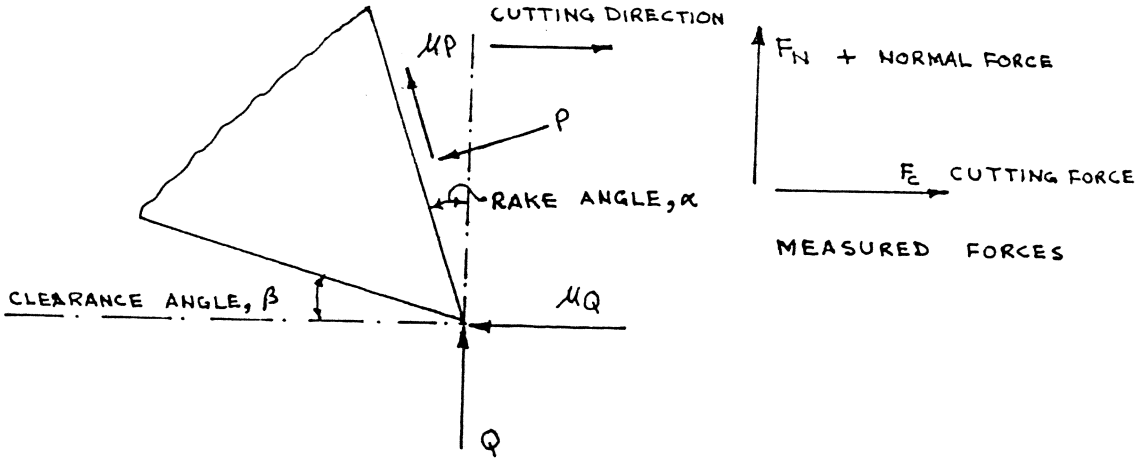

FIGURE 2·2 IDEALISED SYSTEM OF FORCES ACTING AT THE TIP OF A PICK IN COAL CUTTING
O' DOGHERTY (1964)

Milling cutters and grinding processes can be considered analogous to the rotary tilling process. The value of radial rake angle of a tooth (equivalent to the mounting angle of the tiller blade) see Figure 3.1, is dependent upon the speed of cutting and properties of metal according to Eaczmarek (1976). The radial rake angles applied in high-speed steel milling cutters are kept between 10^{o} (medium hard steel) and 20^{o} (soft steel) whereas in the case of rotary tillers the angle varies approximately from 50^{o} to 65^{o}. Although a substantial reduction in tangential force in metal machining has been recorded with the increase in rake angle, Kempster (1968), the smaller value of rake angle is recommended for high tool strength and minimum shank wear. The clearance angle of the teeth varies from 10^{o} to 20^{o} which is approximately in the same range as with the tiller blade.

The cutting resistance is influenced by the properties of the workpiece material and by the cutting angle of the milling cutter, the width and depth of cut, rate of feed (per tooth and per revolution of the cutter) and the cutter diameter, Baker (1969). Apparently, the application of shear theory on milling cutters has not been reported and the cutting resistance is still determined using empirical equations. Throughout the literature, the forces on the cutter teeth have been defined in terms of tangential and radial components and are, therefore, extremely useful. The peripheral cutting force acting on the tooth at any moment of cutting process has been determined as the product of specific cutting resistance and the instantaneous cross-sectional area of the undeformed chip in a manner similar to Bernacki (1962) for rotary tillers.

2.4 Coal Cutting

Evans and Murrell (1957) studying the phenomenon of cutting coal postulated that the cracks developed can be attributed to the tensile breakage radiating from the tip of the wedge. Despite the existence of the cracks, the mode of entry of the wedge was found primarily by crushing of coal against the surface of the wedge. At a later stage, Evans (1959) proposed a tensile breakage theory for the prediction of force required to cut-off a block of coal by a wedge-shaped tool.

The observed variation of tractive force (horizontal component acting on the face of the wedge) with wedge angle was found in agreement with theory for both a hard bituminous coal and a friable coal. There was, however, indication that shear strength might be important for other types of friable coal in which case Merchant's theory (1945) of metal cutting may be applicable.

O'Dogherty (1964) studied the effect of rake angle and back clearance angle on pick performance in coal cutting. The 24 cutter picks tested had rake angles from 0^{o} to 45^{o} and back clearance angles from 0^{o} to 30^{o}. The cuts were made in rectangular blocks of Garw coal over a range of depths of cut from 2.5 mm to 10 mm. It was shown that a positive clearance of 5^{o} could give optimum performance for all the rake angles. The cutting efficiency of a pick increased progressively with increase in rake angle and should be as large as possible consistent with strength and durability. O'Dogherty demonstrated a simple force system on the tip of a pick assuming its resultant to be acting at an angle of friction with the vertical (Figure 2.2). The tip force was found constant with the depths of cut and thought to be due to local stresses around the tip. Using Evan's tensile breakage theory (1959) for the forces on the front face of the pick semi-empirical equations were derived for the cutting and normal forces as the function of the rake angle and the depth of cut and are applicable for all the positive clearance angles.

2.5 Conclusions

From the review, it is evident that no fundamental soil or material mechanics exists for the prediction of forces in rotary cutting. However, some useful concepts can be utilised for rotary tilling of the soil from metal and coal cutting research as given below:

i. The forces on the tip of the rotary tiller blade may be represented as radial and tangential components similar to milling cutters in metal machining.

ii. The phenomenon of tip reaction should be investigated and as a first hand approximation use can be made of the concept derived in coal cutting.

3. MATERIALS AND METHODS OF INVESTIGATIONS

3.1 Introduction

The review of the literature reported in Chapter 2 reveals that most previous work has been primarily concerned with the development of the empirical relationships for the prediction of power consumption in rotary tilling of the soil and apparently no consideration has been given to the Mohr-Coulomb soil mechanics. In contrast, a considerable amount of work has been reported on passive tillage tools for the last two decades and the problems of blades and tines have been explained on the basis of soil and tool behaviour equations. It was, therefore, considered important to investigate the mechanics of a rotary tiller blade with a view to develop a suitable prediction model based on soil and blade parameters. The methods of approach to this problem and the way they have been carried out are reported in this chapter.

3.2 The Investigation

To enable the mechanics of a rotary tiller blade to be determined the following studies were planned to determine the soil reaction by measuring the tangential and radial force component and the resulting moment:

i. The L-cutter (knife) of a rotary tiller consists of a vertical section and a horizontal section termed as the leg and blade respectively. For the rotor with horizontal axis of rotation both the leg and blade comes into contact with the soil whereas with vertical axis of rotation only the blade is involved in the tilling operation. A simple blade was, therefore, selected according to the design criteria described in Section 3.3 to conduct soil cutting in two-dimension, to remove end effects, so that the mechanics could be applicable to a range of situations. Due to the high energy requirements, the rotary tillers are normally recommended to operate at the depths of cut and bite lengths of less than 150 mm. In this work, however, bite lengths

of upto 250 mm were selected to study the mechanics at the limit. The bite lengths and the depths of cut were varied in steps of 50 mm upto 250 mm and 150 mm respectively to cover a range of 'Fetch-Ratio' (the ratio between the bite length and depth of cut or L_b/d - Ratio) from 0.33 : 1 to 5 : 1.

ii. The consumption of energy by a rotary cutter is the sum of static and dynamic forces. According to Bernacki (1962), the static (quasi) force arises as the cutter passes through the soil at infinitesimal slow speeds. Therefore, a rotor speed of 5 r.p.m. was used to determine the quasi-static component of cutting a soil slice. The blade of a tiller traverses a complex path (cycloidal trajectory) in an actual working condition as shown in Appendix 2. However, as a simplification, the experiments were, initially, planned in a circular trajectory similar to Söhne (1957) which is a special case of a cycloidal trajectory. In the present investigations, the mechanism of soil failure, quasi-static and dynamic forces for a blade in a circular trajectory were determined alongside the respective components in a cycloidal trajectory.

iii. The tip effects of the blade can be determined by assuming the tip as a high strength and inextensible steel wire. Steffanelli (1968) measured the resistance to soil cutting with a wire in an attempt to estimate the equivalent of the width independent component but did not measure the Mohr-Coulomb soil properties or postulate a model by which the force could be estimated. Godwin (1974), however, postulated an empirical model for the prediction of forces on a wire applicable to the edge effects of a tine. Experiments were, therefore, planned with a 20-gauge wire working in the similar conditions to that of a blade so that the mechanics of a wire developed on the Mohr-Coulomb soil mechanics could be applied to the tip effects of a rotating blade.

3.3 Design of the Blade

The complex three dimensional shape of a rotary tiller blade has been defined by Beeny and Khoo (1970) and its kinematics has been

discussed by Bernacki (1962), and Hendrick and Gill (1974). Various kinematic parameters of a tiller blade are shown in Figure 3.1. The important parameters in the design of the blade are the size i.e. the width, length, thickness and the shape defined by the sharpening angle and the clearance angles with respect to circular and cycloidal trajectories. The minimum value that the apparent approach angle (mounting angle, γ) can take is limited by the blade sharpening angle (β) and the apparent clearance angle (δ_1). The effective clearance angle (δ') is a function of a number of design variables and varies throughout the cycle of rotation of the blade. Therefore, simply establishing one constant clearance angle that will be effective under all conditions is not possible.

Bernacki (1962) suggested a minimum tip angle (β) of 10^{o} and minimum cutting angle of 15^{o}. Spoor (1969), however, suggested a tip angle of approximately 16^{o} for minimum draught and better performance of the soil loosening and weed cutting equipment. According to Russian researchers a tip angle of 20^{o} to 25^{o} sharpened from outside and a clearance angle of 6^{o} to 8^{o} instead of 20^{o} for commercial blades is desirable to reduce the harmful effect of wear on the cutting angle.

The cutting width of the tiller blade normally varies between 80 - 120 mm. The specific power requirement for smaller cutting width is found comparatively high, Ahmad (1980), and the width greater than 150 mm is not recommended due to higher torsional stresses in the leg of the cutter. Therefore, the following parameters were selected for the blade on the basis of practical kinamatic relationship:

Dimensions of the blade: 140 mm (length) x 75 mm (width) x 8 mm (thickness)

Material: Ground - flat stock steel

Width of cut: 140 mm length of the blade for an effective cutting width of 100 mm

Tip angle (β): 18^{o} and 10^{o}

Apparent cutting angle (γ_o): 25^{o}

Apparent clearance angle (δ_1): 7^{o} for 18^{o} tip
15^{o} for 10^{o} tip

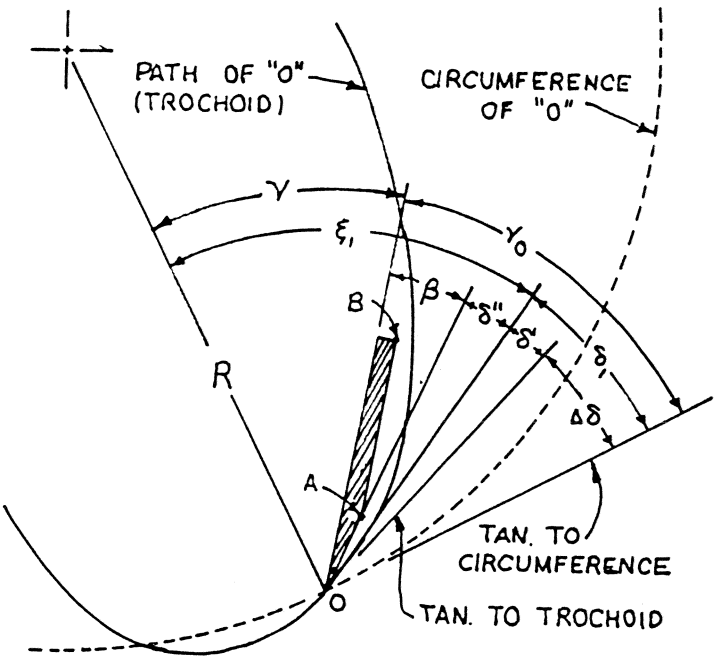

$\overline{OA}$ EFFECTIVE LENGTH OF THE SHARPENED EDGE, mm.

$\overline{OB}$ EFFECTIVE LENGTH OF THE BLADE, mm.

R RADIUS OF THE CUTTING EDGE AT "O" mm.

β SHARPENING ANGLE OF THE BLADE, deg

γ BLADE MOUNTING ANGLE, deg

γ_0 APPARENT CUTTING ANGLE.

$\gamma_0 - \Delta\delta$ EFFECTIVE CUTTING ANGLE, deg

δ_1 APPARENT CLEARANCE ANGLE (deg) BETWEEN $\overline{OA}$ AND THE TANGENT TO THE ROTOR CIRCUMFERENCE WHEN $\delta'' = 0$.

δ' EFFECTIVE CLEARANCE ANGLE (deg) BETWEEN $\overline{OA}$ AND A TANGENT TO THE TROCHOIDAL PATH AT "O" WHEN $\delta'' = 0$.

δ'' ACTUAL CLEARANCE ANGLE (deg) BETWEEN $\overline{OA}$ AND A POINT OPPOSITE A ON THE TROCHOIDAL PATH.

$\Delta\delta$ ANGLE (deg) BETWEEN CIRCUMFERENCE AND TROCHOIDAL PATH AT "O".

FIGURE 3·1 KINAMATICS OF A ROTARY TILLER BLADE (AFTER HENDRICK AND GILL, 1974)

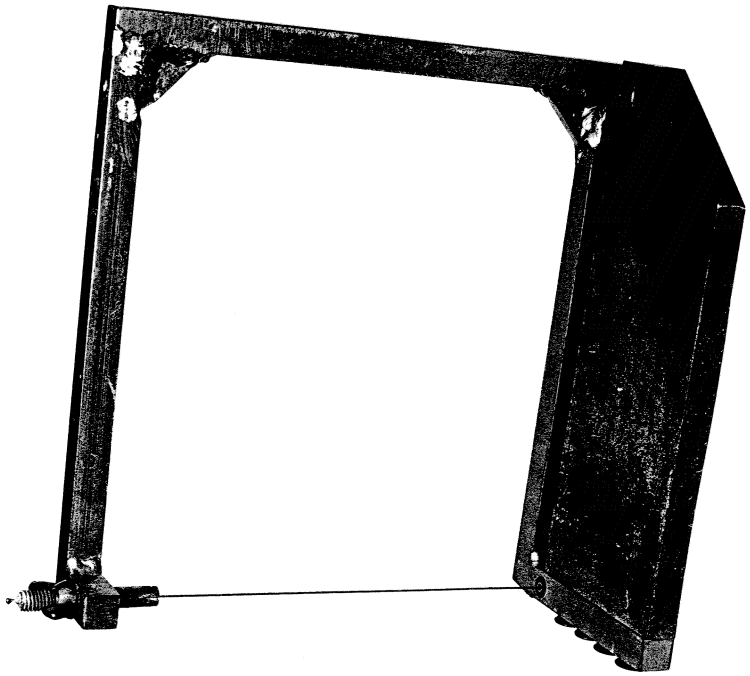

Figure 3.2 The Wire Mounting Frame

Blade mounting angle (γ) = ($90 - \gamma_o$) = 65^o

3.4 Design of the Leg

According to the main objectives of the investigation the leg of the cutter was designed only for mounting the blades and the wire mounting frame. The leg was fabricated from a mild steel plate and had the dimensions of 200 x 75 x 12 mm thickness. Four holes were drilled for mounting the blades at one end of the leg whereas at the other end two holes were drilled so as to provide a mounting angle of 65^o for the blade.

3.5 Design of the Wire Mounting Frame

An 'U' shaped mild steel frame of dimensions 204 mm wide and 210 mm deep was designed and fabricated for mounting a 20 - gauge wire such that the wire is kinematically similar to the tip of the blade. The size of the wire and the dimensions of the 'U' frame were selected on the basis of the strength requirements as well as to cover a range of depths of cut upto 150 mm and width of cut of 100 mm. The 'U' frame can be mounted on the leg described in section 3.4 by replacing the blade as shown in Figure 3.2.

3.6 The Apparatus to Study the Mechanism of Soil Failure and Quasi-Static Forces on the Blade and Wire

3.6.1 Introduction

The use of a 'single-shot' technique for the performance studies of a rotary tiller blade was first reported by Söhne (1957). He measured the rotor torque for a single cut and moved the apparatus to one bite length to perform the second cut. Umeda (1958) used a similar soil bin technique to measure the vertical and longitudinal force components in the steady state condition. Roming (1971), however, tested the validity of the 'single-shot' concept using the statistical analysis of the peak

value data and a complete spectral analysis. He recommended the steady state testing for the performance tests of the rotary tiller blades as this technique has the definite advantage over other methods in terms of:

i. lower total testing time,
ii. simpler test apparatus,
iii. balanced cutter heads,
iv. correct geometry of the blade on the rotor and
v. correct relation among the forces.

It was, therefore, decided to design and use an apparatus using the 'single-shot' technique for the study of quasi-static forces on the blade and wire at different 'fetch-ratios'.

3.6.2 Design Criteria

A container in which the soil can be prepared to a required condition and a system for cranking the instrumented rotor disc was the pre-requisite for the laboratory investigations. A wooden soil bin of 1440 x 240 x 280 mm height was available and was modified for mounting the rotor cranking apparatus. The apparatus consists of two mild steel plates shown in Figure 3.3 which can be mounted freely on two parallel rails by undoing the supporting bolts. A mild steel shaft of 15 mm diameter and 630 mm length is mounted on two bush bearings welded at the opposite ends of the upper plate. The interior of the shaft between the bearings is provided with grub screwed locking washers, one at each end, which can move freely on the shaft. A suitable cranking handle is welded at one end of the shaft whereas the other end is fastened to a flange with adjustable pin for mounting the instrumented rotor disc.

The apparatus can be moved linearly on the rails alongside which is a graduated scale to determine the required bite length. The apparatus can, also, be adjusted across the rails and locked to confine its lateral movement for a required width of cut adjustment. Two separate systems were adopted to monitor the position of the blade tip during cutting. The first, a visual system consisted of a dial graduated at every 5^{o}

LIST OF PARTS

NO	DESCRIPTION
1	SOIL BIN
2	SOIL BLOCK
3	ROTOR FLANGE
4	OCTAGONAL RING TRANSDUCER
5	BLADE
6	SUPPORTING RAIL
7	BOTTOM SLIDING PLATE
8	POINTER
9	ROTOR SHAFT
10	CLAMP
11	ROTARY POTENTIOMETER
12	LARGE PENION
13	SMALL PENION
14	VARIABLE DIAMETER SMALLER PULLEY
15	CRANKING HANDLE
16	VARIABLE DIAMETER LARGER PULLEY
17	UPPER SLIDING PLATE
18	LOCKING WASHER

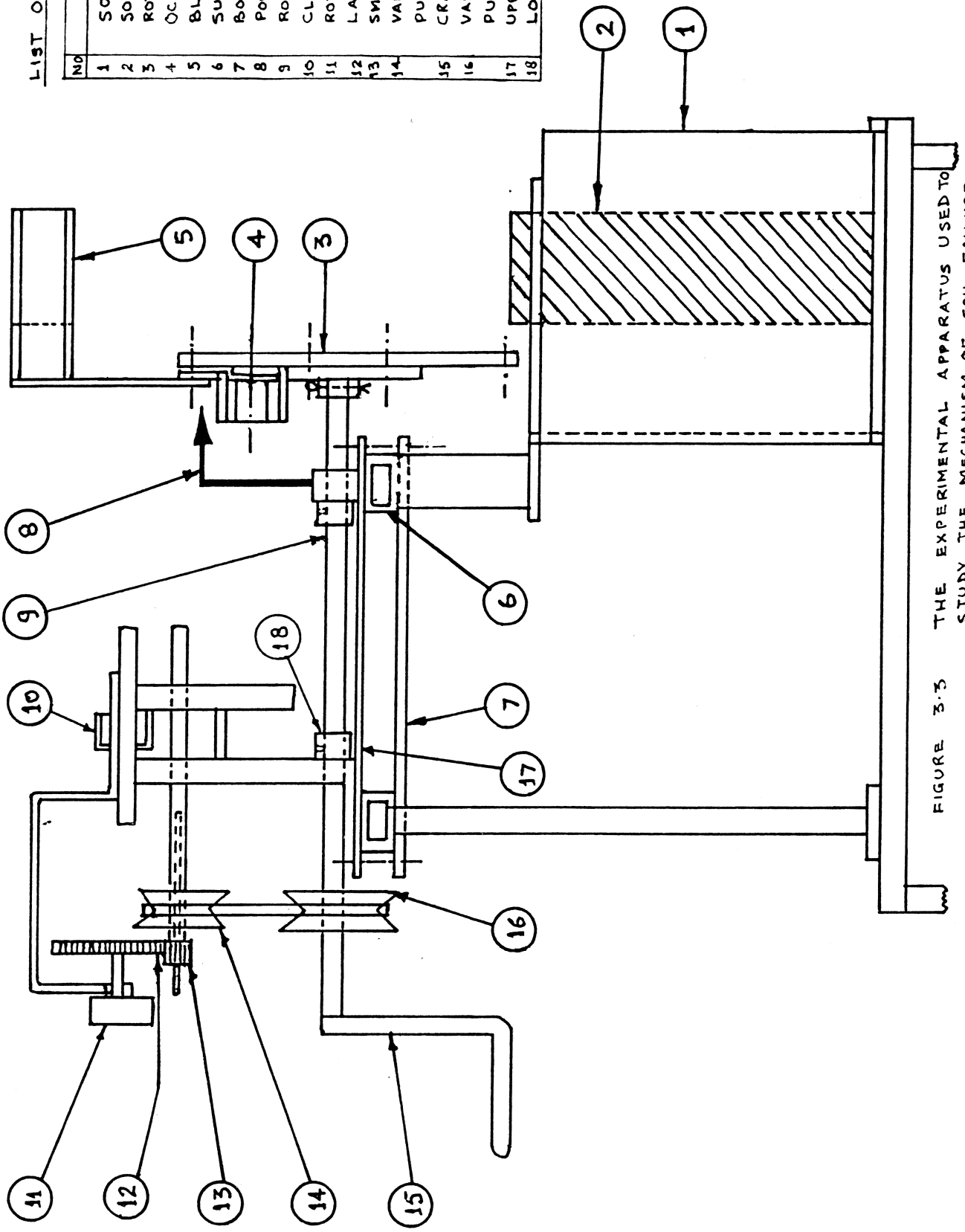

FIGURE 3.3 THE EXPERIMENTAL APPARATUS USED TO STUDY THE MECHANISM OF SOIL FAILURE

intervals on the rotor disc and a fixed pointer as a reference point of the tip. The second system comprised of a half turn rotary potentiometer driven from the shaft by a V-belt pulley and gear arrangements as shown in the figure. This drive system can turn the tip through approximately 240^{o} in about a quarter turn of the potentiometer.

3.7 The Apparatus to Study the Dynamic and Quasi-Static Forces on the Blade

Considerable thought was given to design a versatile apparatus so that it can be used in any desired mode of operation. A soil bin designed and developed by Godwin et.al. (1980) was incorporated with a semi-automatic soil processing trolley (1983) on which the apparatus can be mounted on its supporting elements.

3.7.1 General Description of the Soil Bin

The main characteristics of the soil bin and related equipment are described below:

i. Length and width of the bin can be varied from 5 m to 13 m and 0.8 m to 2 m respectively. Depth of the bin is 0.5 m which can accomodate a maximum of 0.4 m depth of soil.

ii. The power unit is a standard 30 kW tractor supported on three anti-vibration mountings and a winch drum replacing one of the drive wheels. Clutch, brake and differential lock control is achieved using solenoid activated pneumatic cylinders. The solenoid valves are activated from a single switch in the control room and de-activated by micro-switches mounted on the processing trolley.

iii. The soil processing trolley is comprised of a 7.5 kW electric motor to operate various hydraulic controls. A hydraulically operated soil bucket is mounted for spreading the soil in layers along and across the soil bin and gather it again to one end of

the bin after the experiment. The scraper-cum-leveller unit prepares a uniform layer of the soil which can be compacted to a desired density using an independent electric operated heavy roller.

An additional hydraulic unit with appropriate controls is mounted on the trolley to operate a hydraulic motor used as a power source for experimental apparatus. A square tool bar mounted at the rear of the extended frame of the trolley is used for mounting the supporting brackets of the implements or the experimental apparatus.

iv. The soil processing trolley can be operated at forward speeds of 0.1 m/sec to 2.5 m/sec from the tractor winch drum unit. A minimum possible speed of 11 mm/sec can be obtained in first gear by the starter motor using two pulleys and three rounds of cable arrangements. The trolley can also be moved independently using the hydraulic motor and rope arrangements provided to the sides of the trolley along the outside walls of the soil bin.

3.7.2 The Experimental Apparatus

3.7.2.1 Main Characteristics of the Apparatus

The salient features of the experimental apparatus are given below:

i. The apparatus can be mounted horizontally on the soil processing trolley's tool bar and its frame with appropriate brackets as shown in Figure 3.4. The rotor can be rotated in the clockwise or the anticlockwise directions, as necessary, for the down-cut and up-cut methods of rotary soil tilling.

ii. The apparatus can be turned through 90^{o} into its upright position to serve as a vertical rotor using a few additional brackets as shown in Figure 3.5.

iii. The apparatus is movable across the soil bin and can be clamped rigidly on the trolley to conduct more than one set of experiments along the width of the bin.

iv. The depths of cut are varied by lifting the complete assembly vertically and clamping the mounting plates of the apparatus with the appropriate holes of the brackets drilled at 50 mm intervals to obtain the depths of cut upto 200 mm with the present design of the rotor.

v. The apparatus is most versatile in that, all the components are detachable and independent which could be stored safely for any future use.

3.7.2.2 General Description of the Apparatus

The apparatus consists of an instrumented rotor disc, described in Section 3.8.2.4, mounted at the end of a 40 mm diameter shaft drilled through its centre with appropriate slots at the surface to carry the cable from the transducer to the slip rings without external interference. The shaft is supported on two self-aligned Y-bearings between the slip rings and rotor disc to reduce axial load on the rings and the torque-meter mounted at the other end of the shaft as shown in Figures 3.4 and 3.5. The torque-meter unit with slip rings can measure the torque, speed and power consumed by a rotating tool. However, in the present experimental study the torque-meter was, only, used to measure rotor speed. The torque-meter is, finally, connected, through a flange coupling, to a driving unit which acts as a power source for the rotor. The apparatus power source consists of a high torque and slow speed hydraulic motor or a variable speed electric motor. The electric motor is used for slow speeds upto 20 r.p.m. because of the erratic performance of the hydraulic motor at this low range of speeds. A spur gear mounted between the slip rings unit and the torque-meter unit alongwith a magnetic impulse transducer on a separate frame are used to record the position of the tip in a full rotation.

Specifications

a. Overall length of the apparatus: 1380 mm

b. Apparatus driving source

i. Hydraulic motor

ADAN-ABM Size 200, B series

Displacement: 200 cc/rev

Maximum pressure drop: 70 kg/cm^2 (continuous)

Maximum speed: 300 r.p.m.

Shaft speed: 120 r.p.m. (for a flow valve of 5.5 Imp. GPM capacity) speeds below 20 r.p.m. not recommended

Torque capacity: 17.5 kgf-m (at a maximum pressure of 70 kg/cm^2)

ii. Electric motor

Shunt, D.C. 3.3 amp.

Variable speed: (0 - 25 r.p.m.)

Power capacity: 0.5 h.p.

c. Slip rings

Make: D.J. Mouldings Ltd, England

PS-20-20 series

Overall length: 142 mm, overall diameter: 150 mm

Bore diameter: 40 mm, H8

Maximum speed: 3000 r.p.m.

20-way channels for five full bridge circuit

d. Torque transducer

Make: Experimental and Electronic Laboratories
British Hovercraft Corporation Ltd.

Range: 0 - 1000 lb-ft

Maximum axial load: 100 lb

Sensitivity: 2.757 mv/v

Maximum misalignment: $\pm$ 0.004 inch

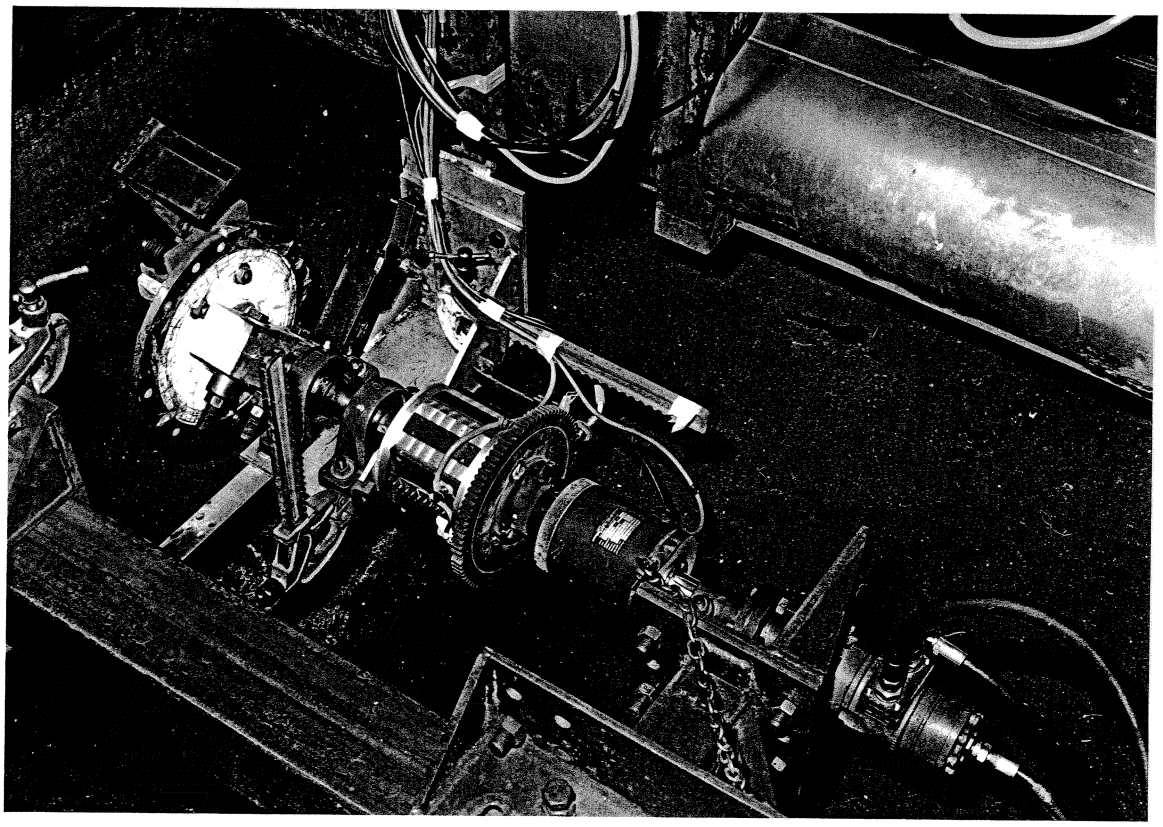

Figure 3.4 Experimental Apparatus in Horizontal Soil Cutting Mode, with Hydraulic Drive

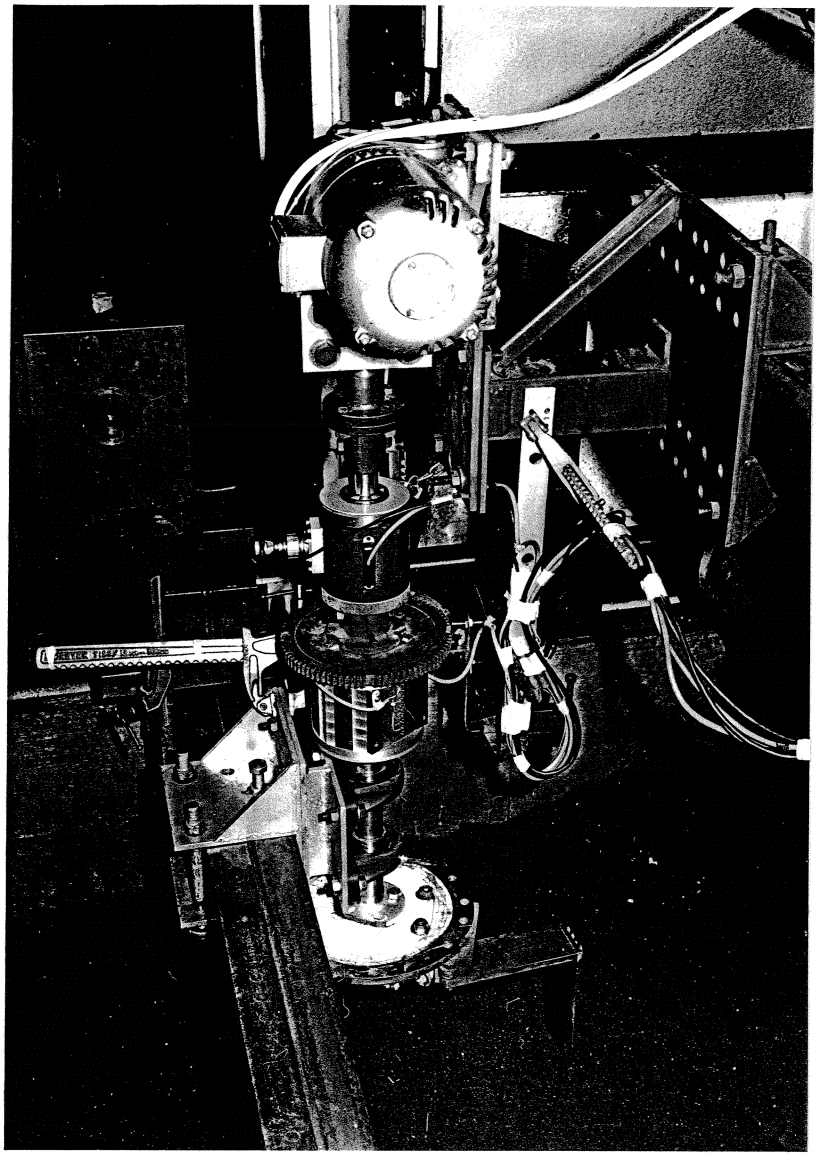

Figure 3.5 Experimental Apparatus in Vertical Soil Cutting Mode, with Electrical Drive

3.8 Instrumentation

3.8.1 Resolution of Forces in Rotary Tilling

In rotary tilling of the soil two reference systems can be adopted to represent the components of the cutting resistance:

i. The reference system connected with the rotor shaft comprised of the lateral force or the axial component (ΔL), the vertical component (R_Y) and the transverse component (R_X). This reference system does not depend upon the kinematics of cutting and is, therefore, stationary.

ii. Reference system connected with the blades on the rotor disc consisted of an axial component (Δl), the radial component (ΔS) and the peripheral or tangential component (ΔT). The resolution of forces in both the reference systems are shown in Figure 3.6.

Apparently, little information is available on the direct measurement of the component forces related to reference system (ii). The torque of the rotor has been considered as the main parameter, Bernacki (1962), to derive the circumferencial force by assuming the arm of the resultant force as constant and equal to the radius of the tiller drum. Povlov (1952), however, measured the tangential and horizontal components of cutting resistance and determined the resultant force by graphical methods. The theoretical presentation of the component forces on the leg and blade of the rotary cutter was, first, reported by Sakai (1979) but their nature and magnitude has not been investigated.

3.8.2 The Force Measuring Transducer

The tangential component of an L-shaped rotary cutter had been studied in detail by many researchers and triangular-like patterns have been reported. The resistance pattern of a cutter can be used to develop the total torque reaction of a rotary axle installed with multiple cutters Söhne (1957). It was, therefore, decided to measure

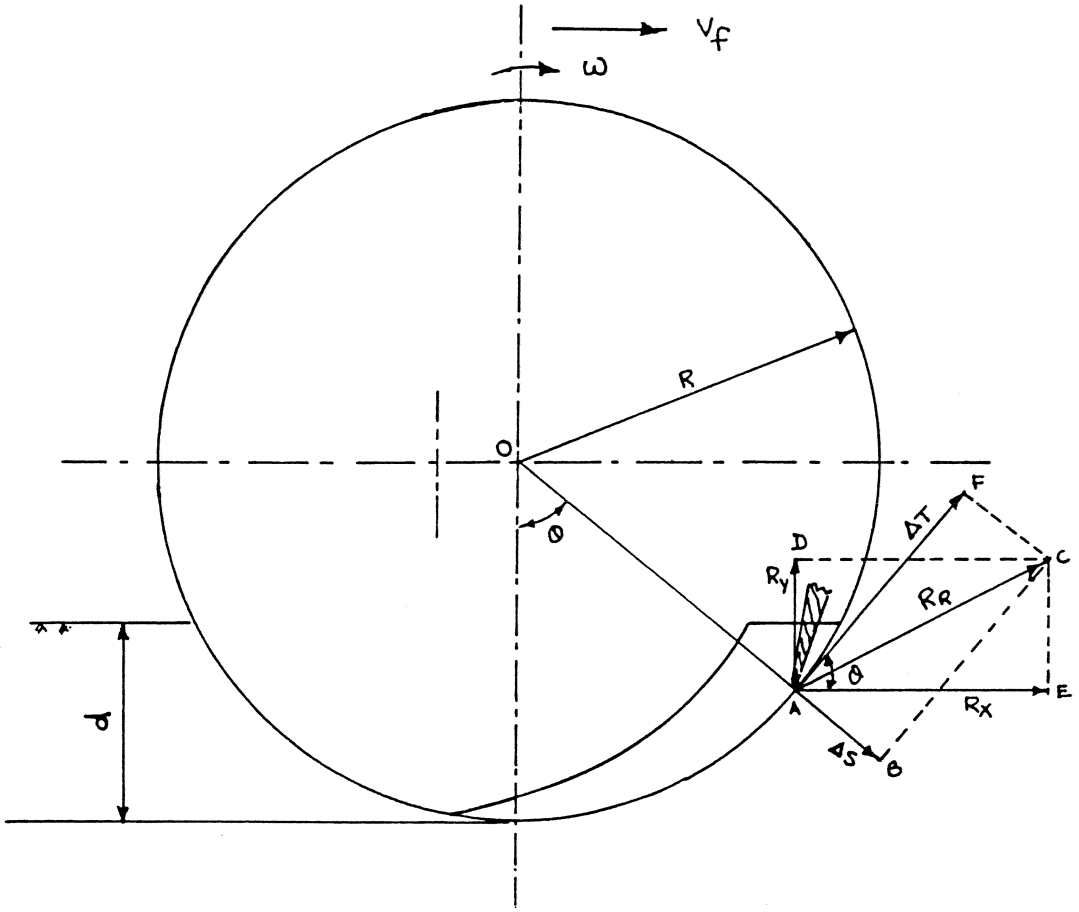

$$R_X = \Delta T \cos\theta + \Delta S \sin\theta$$

$$R_Y = \Delta T \sin\theta - \Delta S \cos\theta$$

$$\therefore R_R = \sqrt{R_X^2 + R_Y^2} = \sqrt{\Delta T^2 + \Delta S^2}$$

FIGURE 3.6 RESOLUTION OF FORCES IN ROTARY TILLING OF SOIL

the tangential and radial force components of a single blade by selecting a suitable transducer.

At the outset of the problem of selecting a transducer, an extended octagonal ring transducer machined integrally into the leg of the cutter, similar to the one used by Godwin et.al.(1981) to separate the foot forces of a mole plough from its leg, was considered. However, this was discarded because of the questionable rigidity of such a small device and a limited future use of the transducer. A separate extended octagonal ring transducer used by Siemens (1965), Godwin (1974) and O'Dogherty (1975) was found compatible and finally decided upon.

3.8.2.1 Design of the Transducer

The extended octagonal ring transducer was designed using the design criteria of Cook and Rabinowicz (1963) and Godwin (1975). The transducer was machined from a EN 24 A alloy steel stock to a length, width and side thickness of 112.26, 50 and 37.62 mm respectively. The details of the design are given in the Appendix 1. The strain gauges were bonded to the transducer at strain nodes, $\theta = 34^{o}$ and 90^{o}, after the recommendation of Godwin (1974) and connected into three four arm bridge networks, as shown in Figure 3.7. A fourth bridge was added after Seig (1982) for determination of side moment, although not required for this study.

3.8.2.2 Transducer Characteristics

The transducer was calibrated using a constant voltage data scanner unit and the following characteristics were observed:

i. The transducer signal was highly linear with coefficient of determination (r^2) being $\geqslant$ 0.9997.

ii. The variation of the output signal due to the position of the force was acceptable within the working range, the transducer is expected to be used and was less than 2.5 %.

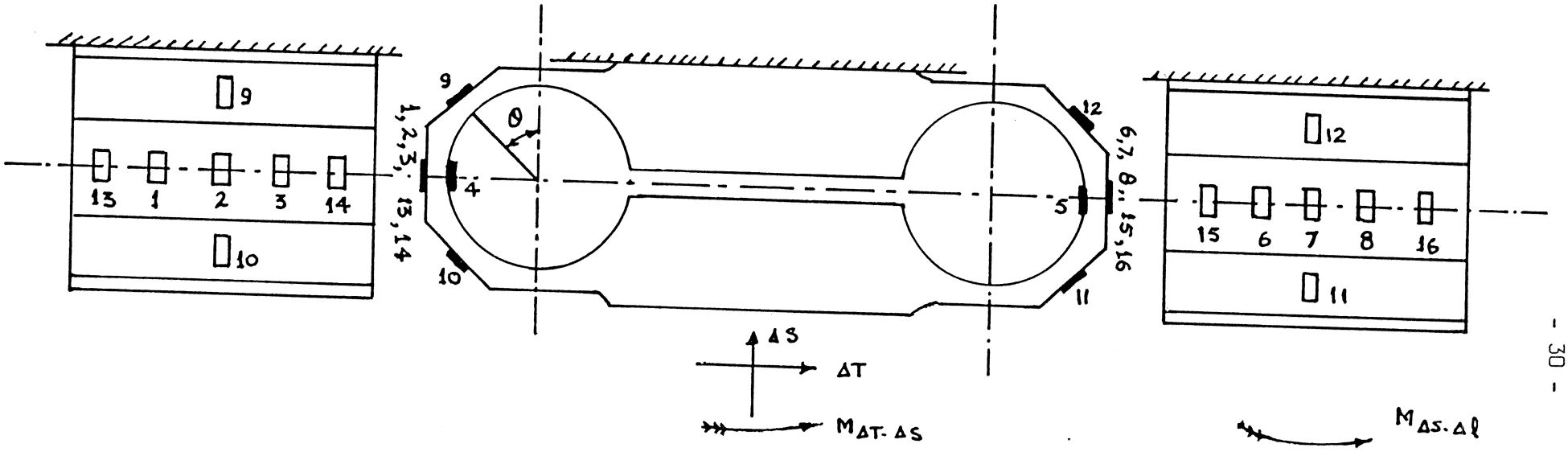

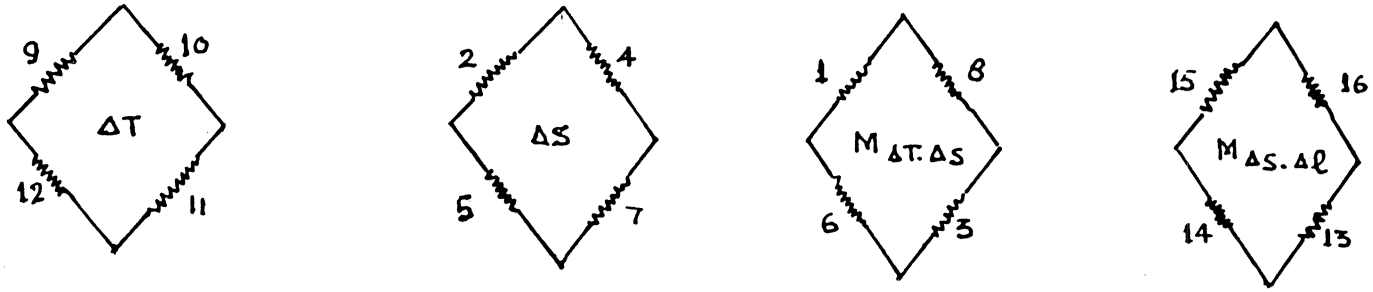

FIGURE 3·7 TRANSDUCER BRIDGE CIRCUIT

iii. The cross-sensitivity error was less than 3.5 % for the moment and side moment of 60 N-m when the transducer was loaded at 100 mm side and 100 mm across the centroid of the transducer. However, the cross-sensitivity error increased to approximately 5.5 % for a moment of 60 N-m and side moment of 120 N-m which can be reasonably acceptable considering the practical use of the transducer on the tiller blade.

iv. The output hysteresis effect was practically zero.

v. The sensitivities of the channels were found as below:

$$\Delta T = 0.38\ \mu v\ N^{-1} m^{-1} v^{-1}$$

$$\Delta S = 0.39\ \mu v\ N^{-1} m^{-1} v^{-1}$$

$$M_{\Delta T.\Delta S} = 6.16\ \mu v\ N^{-1} m^{-1} v^{-1}$$

$$M_{\Delta S.\Delta l} = 14.12\ \mu v\ N^{-1} m^{-1} v^{-1}$$

3.8.2.3 Knife Edge Balance of the Transducer Assembly

The weight of the transducer, its supporting elements and the experimental blade would act always outward due to the centrifugal force of the rotating mass at high peripheral speed of the rotor. It was, therefore, imperative that the complete assembly is balanced such that the centre of gravity of the assembly lies on the line passing through the centroid of the transducer and tip of the blade.

The L-shaped mild steel bracket designed for mounting the leg of the cutter was mounted rigidly onto one side of the transducer. The leg of the cutter with the experimental blade was placed onto the L-bracket with supporting washers to bring the longitudinal and traverse axes of the leg approximately in line with the respective axes of the transducer and afterwards secured rigidly on the bracket. A line was drawn through the centre of the transducer to the tip of the blade and the complete assembly was supported on a knife edge by inserting the edge through the central slot of the transducer close to its centroid. A thread with suitable weight was hung from the outer end

of the knife edge to represent one of the three axes (x - axis or radial) of the transducer. Theoretically, the centre of gravity of the complete assembly and the line marked through the centre of the transducer and tip of the blade should superimpose the x - axis to measure radial force on the tip of the blade. This was accomplished by adding necessary weights (280 grams) onto one side of the L-bracket so that the thread and the marked line superimpose each other. The complete assembly was, then, turned through 90^{o} and the leg was balanced on the knife edge to find the centre of gravity to approximately 83 mm from the centroid of the transducer on the marked line.

3.8.2.4 Mounting of the Transducer Assembly on the Rotor Disc

A rotor disc of 300 mm diameter and 120 mm thickness was fabricated from a mild steel plate and the leg mounting holes were drilled according to a standard 'Howard Rotavator Company' rotary tiller disc. The complete transducer assembly was mounted onto an L-shaped bracket and placed on the rotor disc such that the centre of the disc, centroid of the transducer and the tip of the blade are all in a line as shown in the Figure 3.8. In doing this, the leg of the cutter was brought over the two mounting holes of the disc representing a practical blade mounted on a rotavator. This instrumented rotor disc was used in all the experimental studies.

3.8.3 Monitoring the Position of the Blade Tip

The rotary potentiometer technique used to mark the position of the tip or wire on the apparatus described in section 3.6 was not compatible to the apparatus described in Section 3.7 because of the technical difficulties. A magnetic impulse transducer mounted to the side of a notched pulley was used successfully by Godwin (1974) to monitor the tine carriage speed. The use of this technique to mark the position of the tip was found compatible with the adopted data recording system and conformed with the design of the experimental apparatus.

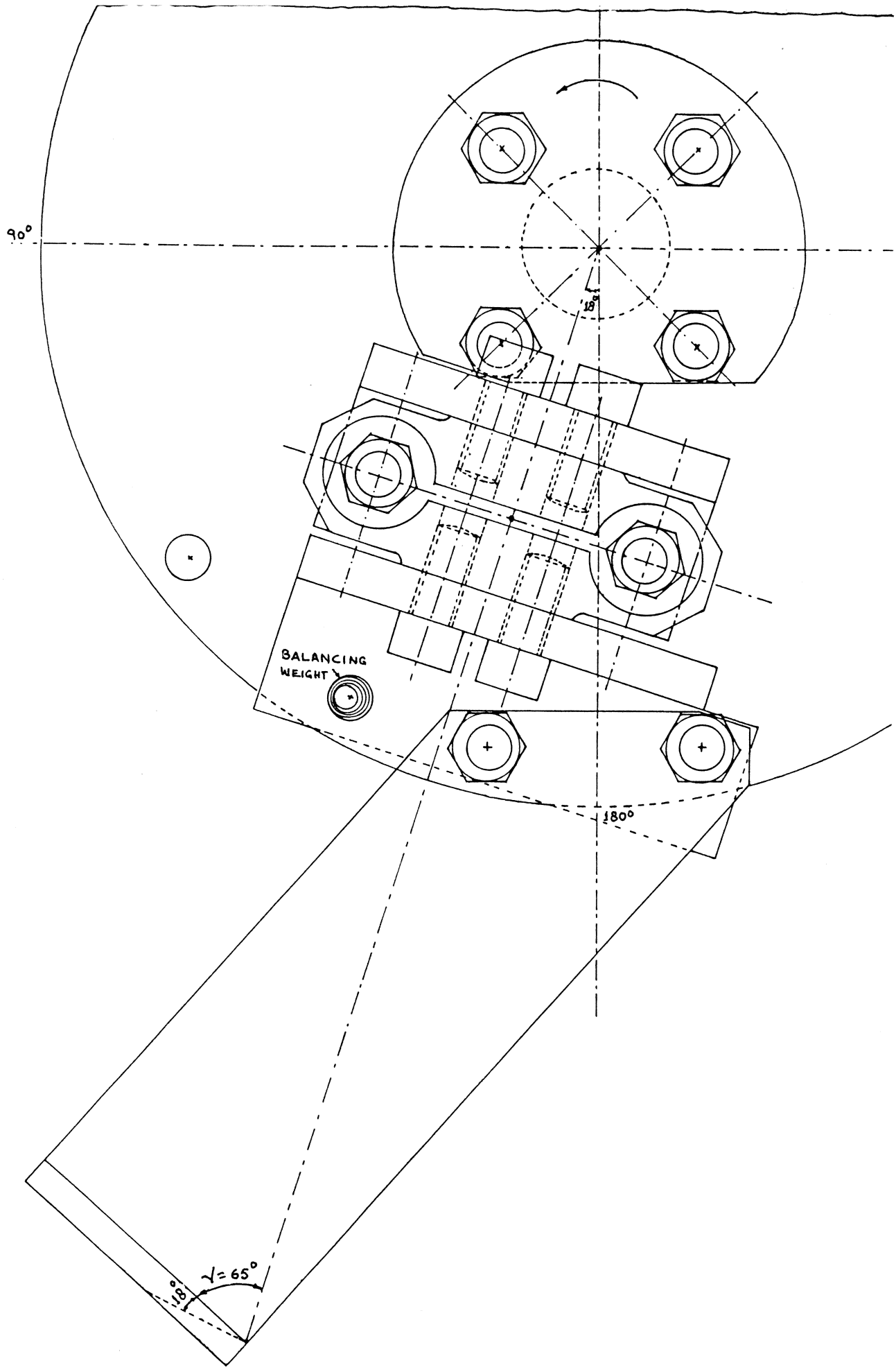

FIGURE 3·8 MOUNTING OF THE BLADE AND TRANSDUCER ASSEMBLY ON THE ROTOR DISC

A spur gear of 227 mm diameter with 88 teeth on its periphery was readily available and modified according to the design requirements. One tooth of the gear after every 21 teeth was removed to mark a reference point for the tip after every 90^{o} of the rotation. A suitable clamping device was welded at the centre of the gear and grub screwed between the slip rings unit and the torque meter as shown in Figure 3.9. The magnetic impulse transducer was positioned approximately 1 mm away from the periphery of the teeth and clamped rigidly with the supporting frame of the apparatus. The transducer was connected to the micro-computer through a screened co-axial cable. The pulsed output from the transducer was proportional to the rate of change of magnetic reluctance which recorded the position of each tooth (4.09^{o}) on the computer disc.

An on - off switch positioned at a suitable place can be actuated once every revolution of the rotor by a disc actuator mounted to the side of the gear. The position of the actuator was decided after positioning the centroid of the transducer at its top most position in a rotation and mounting the actuator to the side of the gear approximately 3^{o} beyond the 90^{o} reference mark of the gear. This arrangement switched on the micro-computer, automatically, after approximately 87^{o} travel of the tip from its top position.

3.8.4 Monitoring Rotational and Forward Speeds of the Rotor

The lower range of rotational speed was recorded manually by counting the number of revolutions in a particular time. For higher speeds i.e. greater than 40 r.p.m., the speed channel of the torque meter and its associated instrument was used. In most of the experiments, the rotor forward speed was small (less than 0.4 m/sec) and recorded manually by measuring the linear distance on a time base before the start and end of each experiment.

3.8.5 Signal Conditioning and Recording Equipment

Two separate systems were adopted for recording the data depending upon the types of experimental apparatus described in Sections 3.6 and 3.7.

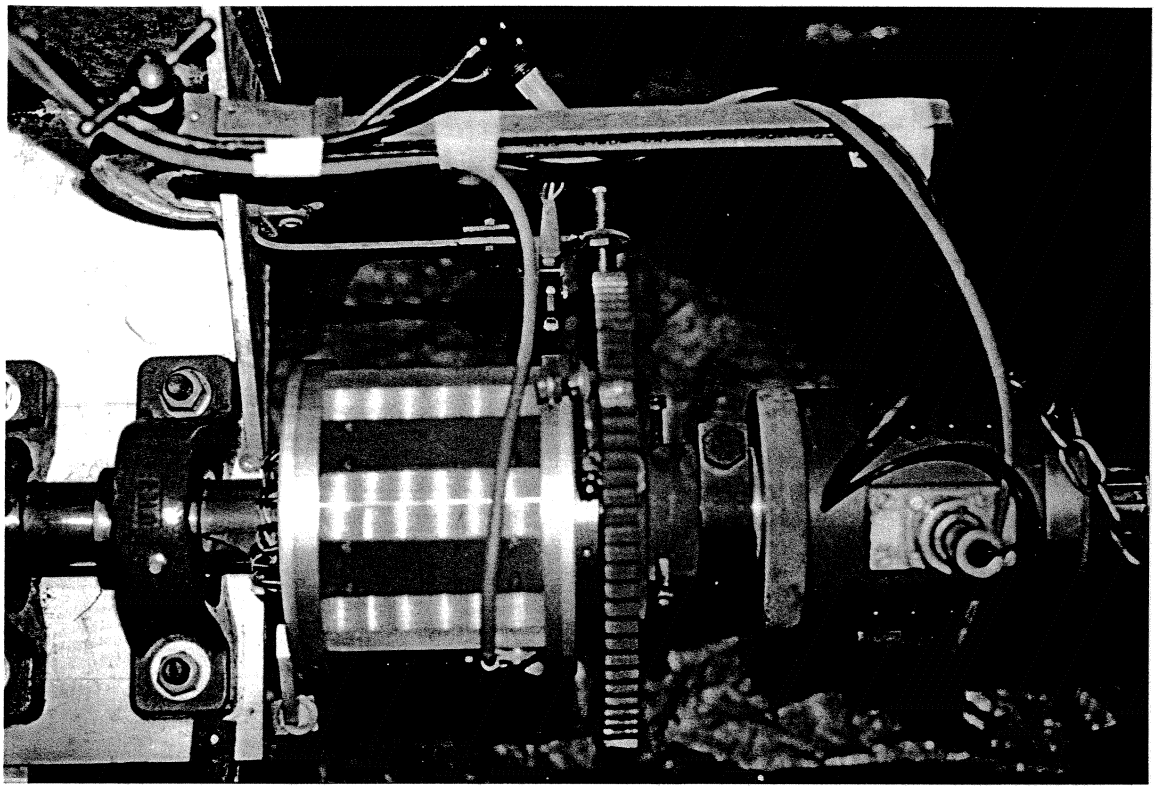

Figure 3.9 The Device for Monitoring the Position of the Blade Tip

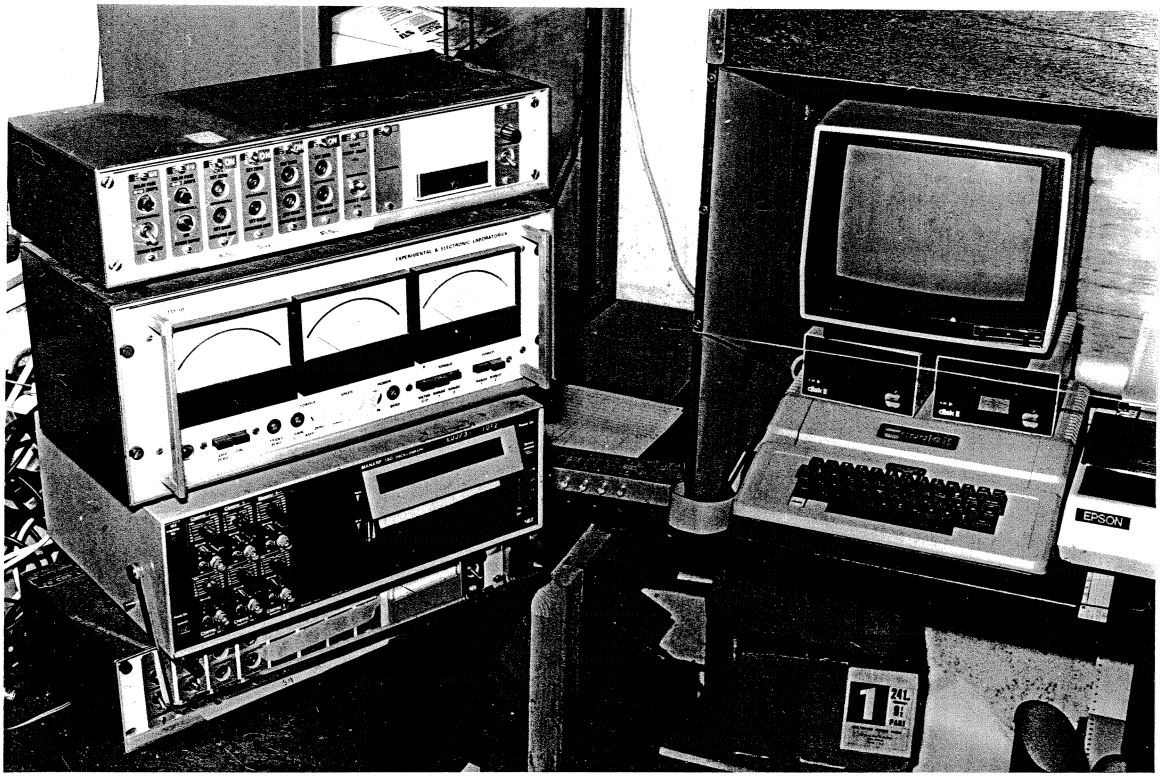

Figure 3.11 Data Conditioning and Recording Instruments

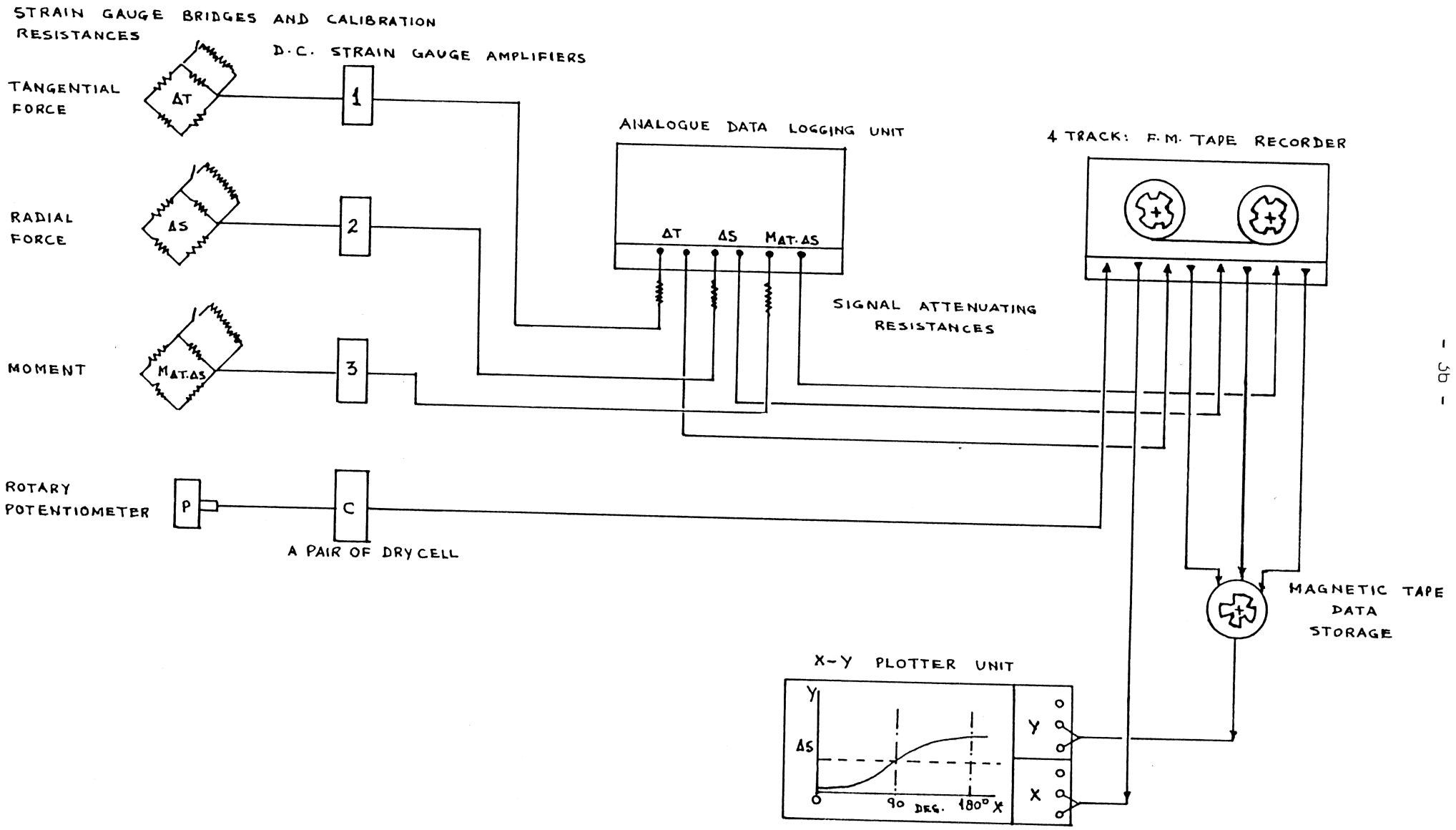

FIGURE 3.10 DIAGRAMATIC REPRESENTATION OF THE SIGNAL CONDITIONING AND RECORDING EQUIPMENT USED IN THE STUDY

3.8.5.1 Data Recording from the Apparatus in the Small Soil Bin

The complete system of data recording is illustrated diagrammatically in Figure 3.10. The output from each strain gauge bridge circuit was amplified using a d.c. differential amplifier which supplied the working potential for the strain gauge bridge circuit. High impedence signals from the strain gauge amplifier were connected to an analogue data logging unit incorporated with shunt resistance and switches for electrical calibration of strain gauge bridges.

The output signals from the data logging unit were connected to a four track F.M. Tape Recorder. The fourth tape recorder channel was used to connect the output signal from the rotary potentiometer powered by a pair of 1.5 volts (each) dry cells. The use of a tape recorder provided the most versatile record of the data for re-analysis at a later stage. The recorded data from the tape recorder was replayed on a pre-calibrated X - Y plotter which recorded the angular position of the tip of the blade or a wire on the X - ordinate and the forces with their resulting moment on the Y - ordinate.

3.8.5.2 Data Recording from the Apparatus in the Large Soil Bin

The output signals from the transducer, Section 3.7, were connected to a suitable plug mounted with the L-shaped bracket fixed on the rotor disc. A multi-channel cable connected with the plug was carried through the central hole of the shaft and inturn connected to a 20-way slip rings unit. This unit can accomodate upto five full bridge strain gauge circuits from the recording transducers. The output from the slip rings unit and the torque meter was connected to a junction box mounted on the soil processing trolley and thence via a trailing multi-way cable to the signal conditioning unit. The torque meter signals were connected to an independent amplifier and dial indicator unit shown as the top two units in Figure 3.11 whereas the slip rings unit signals were amplified and connected to a Multichannel Ultra Violet Oscillograph shown as the bottom two units in the figure. The signals from the U - V oscillograph were finally connected to a pre-programmed micro-computer which picked up the signals at a sampling frequency greater

than 200 Hz. The oscillograph was necessary only to check the calibration constants at the start and end of an experiment.

3.8.6 Insitu Transducer Calibration

The overall transducer characteristics are mentioned in Section 3.8.2.2. However, calibration constants were determined when the transducer was used in conjunction with the amplifier and recording equipment.

The rotary potentiometer used on the apparatus, Section 3.6, was calibrated for its linearity in the working range on the X - Y plotter. The octagonal ring transducer was brought upto the top most position in the vertical plane by cranking the rotor disc and its position was recorded as a zero setting. The rotor was turned slowly through every 10^{o} intervals by aligning the angular graduations on the rotor with the fixed pointer and marking the position on the X - ordinate of the plotter. The potentiometer showed a linear characteristic throughout its working range with coefficient of determination, $r^2 \geqslant 0.999$. The signal output levels from the transducer were obtained on the analogue data logger, tape recorder and X - Y plotter, simultaneously, by loading each channel. The calibration constants were found at the outset of the experiments and a record of zero-cut was obtained on the tape recorder by turning the transducer at approximately 5 r.p.m. from the top (zero position) to the bottom (180^{o}). The zero cut data was replayed from the tape recorder onto the X - Y plotter, Figure 3.13, which was considered as a standard record and checked periodically with a similar record obtained before the start and end of the experiments.

The calibration constants of the transducer when used on the large soil bin apparatus, Section 3.7, in conjunction with U - V oscillograph and micro-computer were dependent upon the gain and attenuation settings of the amplifier, sensitivity of the oscillograph galvanometers and sampling frequency of the computer. The calibration constants for each channel were determined from static calibration of the transducer by adding weights on the supporting frame shown in Figure 3.12. The dynamic calibration of the transducer was done by revolving the rotor at the

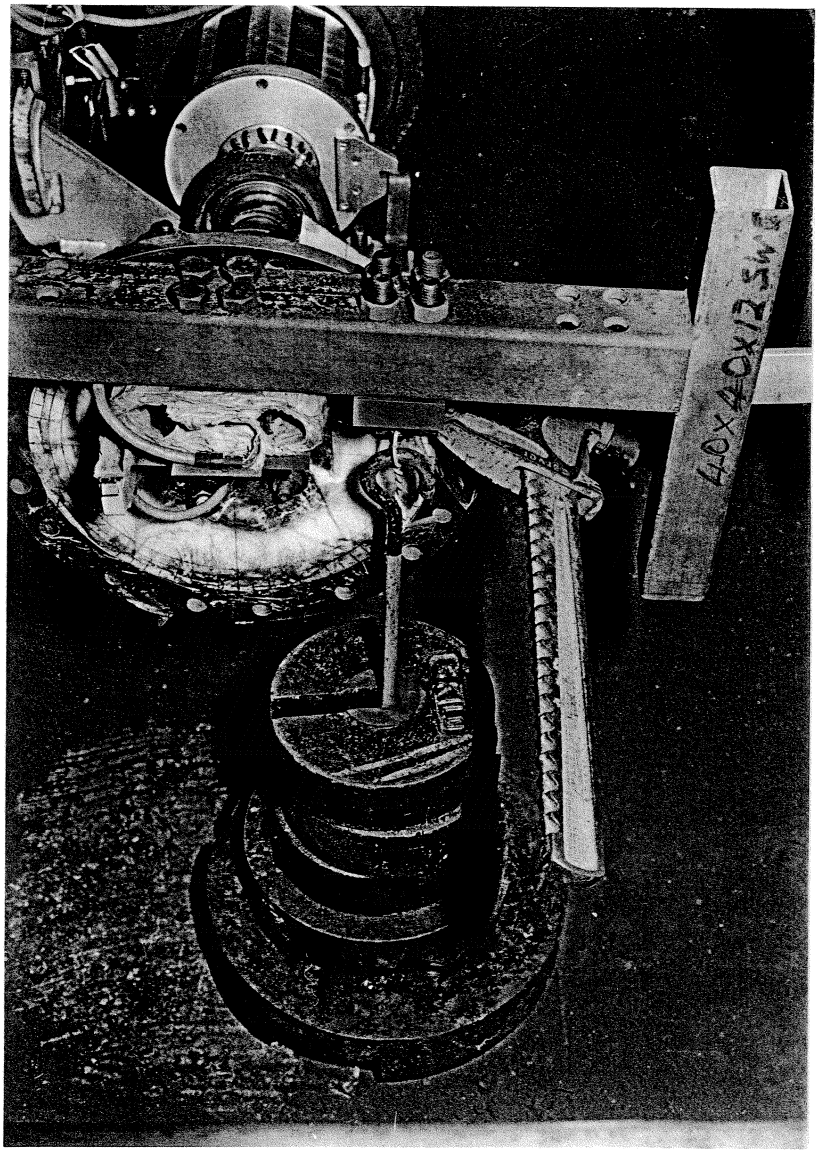

Figure 3.12 In-situ Calibration of Transducer for Radial Force (ΔS) and the Moment ($M_{\Delta T.\Delta S}$)

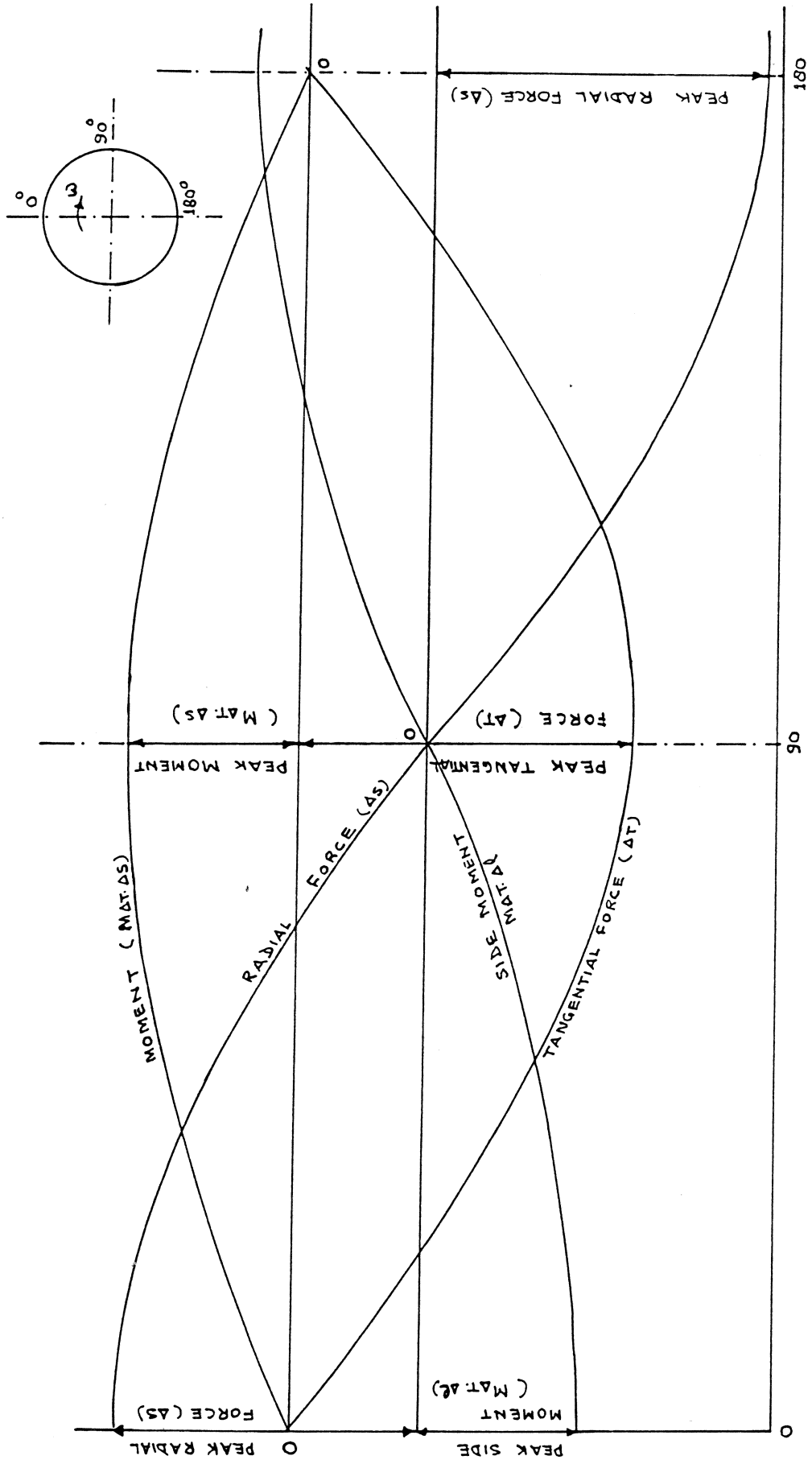

FIGURE 3.13 CALIBRATION OF THE TRANSDUCER ON THE EXPERIMENTAL APPARATUS (FIG. 3.3) AT A ROTOR SPEED OF 5 r.p.m.

desired experimental speeds and recording the signals for zero-cutting on the computer as shown in Figure 3.14.

3.8.7 Analysis of Data

A permanent record of the variations of component forces and moment at different speeds of cutting at zero cutting (rotor revolving freely) was obtained and transferred onto a transparent sheet. The variations of forces or moment at different angular position of the blade tip obtained either from the X - Y plotter or from the computer were superimposed on the respective zero cutting traces. The zero cutting traces were transferred on the traces obtained during cutting and ordinates were noted at different angular positions. The magnitude of the force was obtained using the calibration constants of the respective channel. The data could have been analysed by the computer which can print all the data at 1^{o} interval upto 180^{o} rotations of the blade for a single cut. Since, the primary objective was to measure only the peak forces due to shear failure of a slice, the use of the described technique was found more convenient.

3.9 Methodology

3.9.1 Choice of Soils

Two different types of soil exhibiting (i) cohesive and frictional properties, and (ii) purely cohesive property were used in the experimental investigations. For a frictional soil the choice was made to the sandy loam soil (sand 73 %, silt 10 %, clay 17 %) which was available in the bin and its other properties were known in detail, Godwin (1974). Purely cohesive soil was prepared by Omer (1977) using the 'English China clay' and Shell Carnea 21 oil and was available. The artificial clay soil was, however, used only in a limited number of experiments to check the validity of the model developed for a wire.

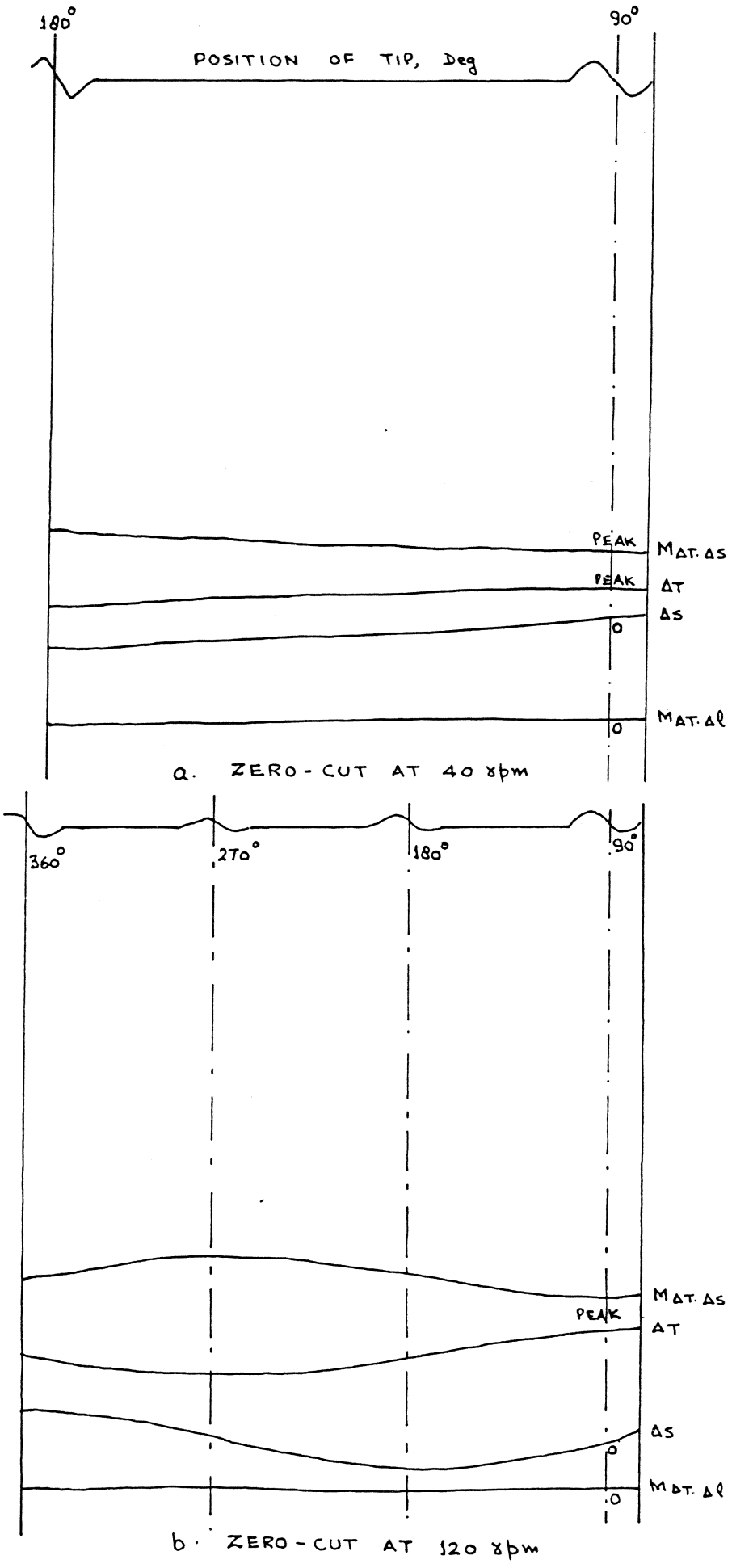

FIGURE 3·14 ZERO-CUT ON THE EXPERIMENTAL APPARATUS (Fig.3·4) AT DIFFERENT ROTOR SPEED

3.9.2 Soil Preparation, Bulk Density and Moisture Content

The sandy loam soil was prepared by seiving to remove foreign materials and stored in containers for its further use. A single bulk density of 1450 kg/m^3 was obtained using standard procedures. The choice of this density was because of the known mechanical properties of the soil, Godwin (1974). The moisture content was held within the friable range at 8 to 10 % on dry basis. The uniformity of the soil during the experiments was checked regularly by measuring the bulk density and moisture content. Since a limited number of experiments were planned with artificial clay soil, a single one pack of soil was enough, and the wet bulk density obtained was recorded as 1757 kg/m^3.

3.9.3 Preparation of the Soil Blocks

Considerable thought was given to the method of soil block preparation for a uniform density. Layered soil and roller technique used by Siemens (1963) and Godwin (1974) proved useful for preparing blocks of required depths. This technique, however, needed a large and heavy roller to prepare soil blocks of 100 mm width and 225 mm depth to a desired density of around 1450 kg/m^3 and therefore, disregarded on technical grounds. Drop hammer technique was found as an useful alternative and adopted for the preparation of the blocks with little modification depending upon the type of soil bin used for the experiments.

3.9.3.1 Block Preparation in the Small Bin

The soil bin used with the experimental apparatus in Section 3.6 was dismounted from the apparatus frame and turned horizontally on a level surface. A hollow trough of 100 mm (height) x 150 to 225 mm (width, depending upon the depth of cut) x 1440 mm (full length of the soil bin) was made using wooden boards and wedges. A measured volume of soil was poured in layers (50 mm) as suggested by Spoor (1982) for maximum compaction and compacted to the desired density by dropping a standard weight. The soil surface was hatch marked with a knife to

produce strong bonds between two layers. Each time 50 mm thick layers of loose soil were poured and compacted until the desired height (100 mm) was obtained. Finally, the soil bin was turned through 90^{o} to its upright position and all the boards and wedges were removed to obtain the experimental soil block. This technique of soil block preparation was essential to devoid the chances of soil failure by the blade along a weakest plane between two bonded layers. Three depths of cut (50, 100 and 150 mm) were obtained by varying the height of the soil block in the upright position of the bin using the wooden boards and wedges.

Preparation of a soil block from the artificial clay soil was similar to the sandy loam soil except that a layer of 50 mm was sliced each time and compacted by dropping a standard weight until the voids between the layers disappeared and the surface became smooth and level.

3.9.3.2 Block Preparation in the Large Bin

For the study of dynamic forces on the blade in the large soil bin, a longer length of soil blocks was required, therefore, the method described in Section 3.9.3.1 was found incompatible. A longer length (800 mm) and width (100 mm) of the soil block was obtained using the boards and wedges restrained along the wall of the soil bin as shown in Figure 3.15b. The layered soil (50 mm) was placed on the slopes of 35^{o} with the horizontal opposite to the direction of forward motion as shown in Figure 3.15a. The slope was decided to keep the bonded soil layers away from the natural shear planes as established from the small soil bin experiments. The layers were compacted using a sheep foot type rammer which eliminated the formation of any distinct bonded soil layers. Finally, all the supporting elements were removed to obtain the soil block.

Although the experimental apparatus used in the large soil bin is designed to move in the vertical plane for changing the depths of cut, it was found time consuming considering its immediate use. The depth of cut was, therefore, obtained by varying the height of the soil block using a hacksaw blade for scrapping the excess top soil.

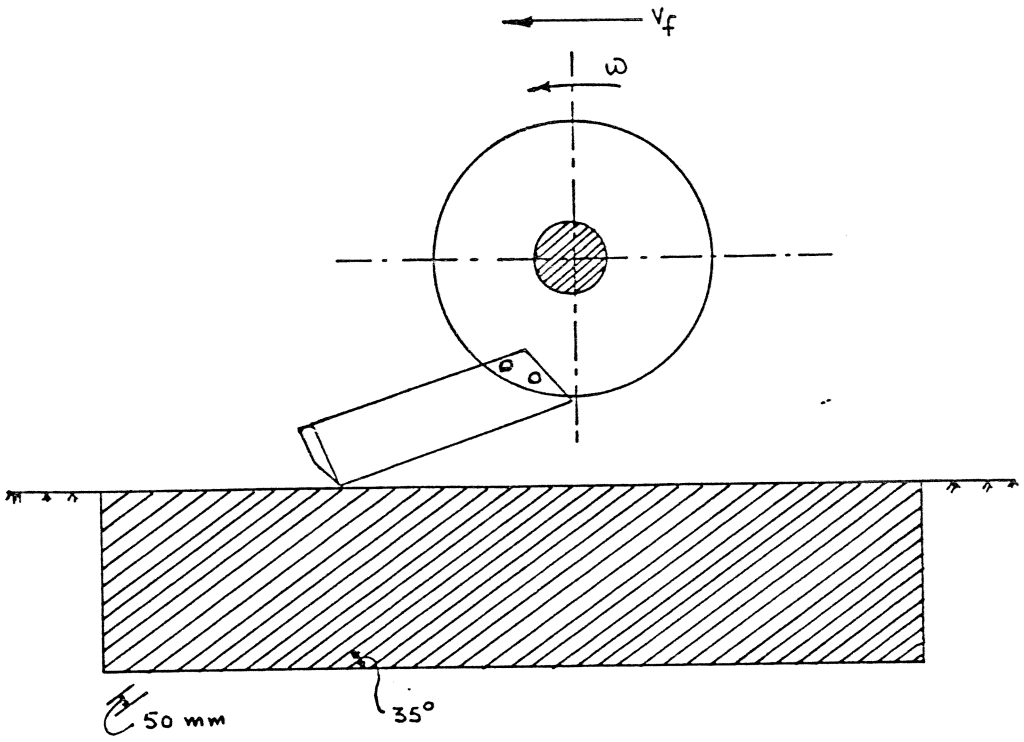

a. Orientation of Soil Layers with the Direction of Motion of the Blade

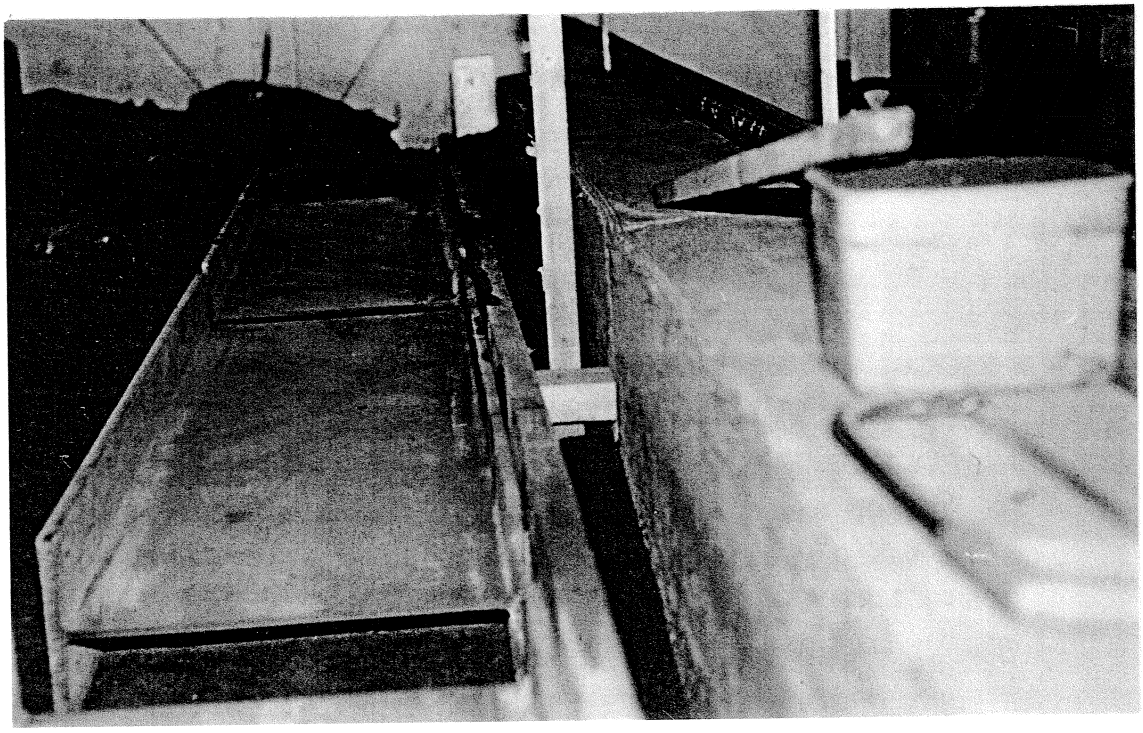

b. Equipment used in Block Preparation

Figure 3.15 Method of Soil Block Preparation in the Large Bin

The soil preparation for the rotor with vertical axis of rotation was made possible by spreading the soil layers (50 mm) in the centre of the bin upto a width of 1 m and compacting it to the required density, by treading, to avoid any distinct layering effects.

3.9.4 Measurement of Soil Properties

3.9.4.1 Introduction

The mechanical properties of a soil relevant to Mohr-Coulomb soil mechanics theory are:

i. Soil bulk density.

ii. Mohr-Coulomb parameters of angle of shearing resistance (ϕ) and cohesion (C).

iii. Soil-metal interface parameters of angle of soil-metal friction (δ) and adhesion (Ca).

The bulk density was determined using standard density rings and inserting into the packed, undisturbed experimental soil blocks in the soil-bin. The mean bulk density was found from the volume of the ring and weight of the soil. The other sets of parameters for each of the soil were determined as follows:

3.9.4.2 Mechanical Properties of Sandy Loam Soil

Godwin (1974) conducted a detailed analysis of various parameters of the experimental soil at three densities varying from very loose to a compact soil condition. It was, therefore, decided to make use of his results in the present investigation. The summary of the mechanical properties of the soil with their 95 % confidence limits are given overleaf:

Soil Treatment	1		2		3	
Density, γ, kg/m^3	1100		1500		1640	
Angle of shearing resistance, ϕ, deg	34.17	35.40 32.84	37.60	40.35 34.95	42.37	45.19 39.69
Cohesion, C, kN/m^2	00.00		4.616	6.407 2.825	7.560	11.24 3.88
Adhesion, Ca, kN/m^2	0.00		0.00		0.00	
Angle of soil-metal friction, δ, deg	----		22.00	23.76 20.17	----	

3.9.4.3 Mechanical Properties of Artificial Clay

Omer (1977) determined various parameters of artificial clay used in the present investigation and was subsequently analysed by Lawrance (1978) and Webb (1981). There was a significant change in the properties, probably, due to the loss of oil over a long period. It was, therefore, decided to determine the parameters at a density used in the experiments.

The soil shear strength parameters were determined using a standard triaxial test, Godwin (1974) and Omer (1977). Undrained compression tests, Hettiaratchi (1965), were conducted at four confining pressures (7.90, 34.76, 63.73 and 103.89 kN/m^2) strained at the fastest rate (2 % per minute) possible with the existing equipment. The Mohr-circles were drawn from the calculated principal stresses as shown in Figure 3.16. The shear strength parameters were determined using the procedure adopted by Godwin (1974) on the recommendation suggested by Lambe and Whitman (1969). The technique is to represent each of the Mohr circles by a single point, with co-ordinates p, q, and joining the points by a straight line denoting the stress path and referred as a K_f - line. The shear strength parameters are determined from the trigonometric relationship that exists between the K_f - line and the Mohr-Coulomb envelope. The 95 % confidence limits can be determined from the fitted regression model using the procedure outlined by Steel and Torrie (1960).

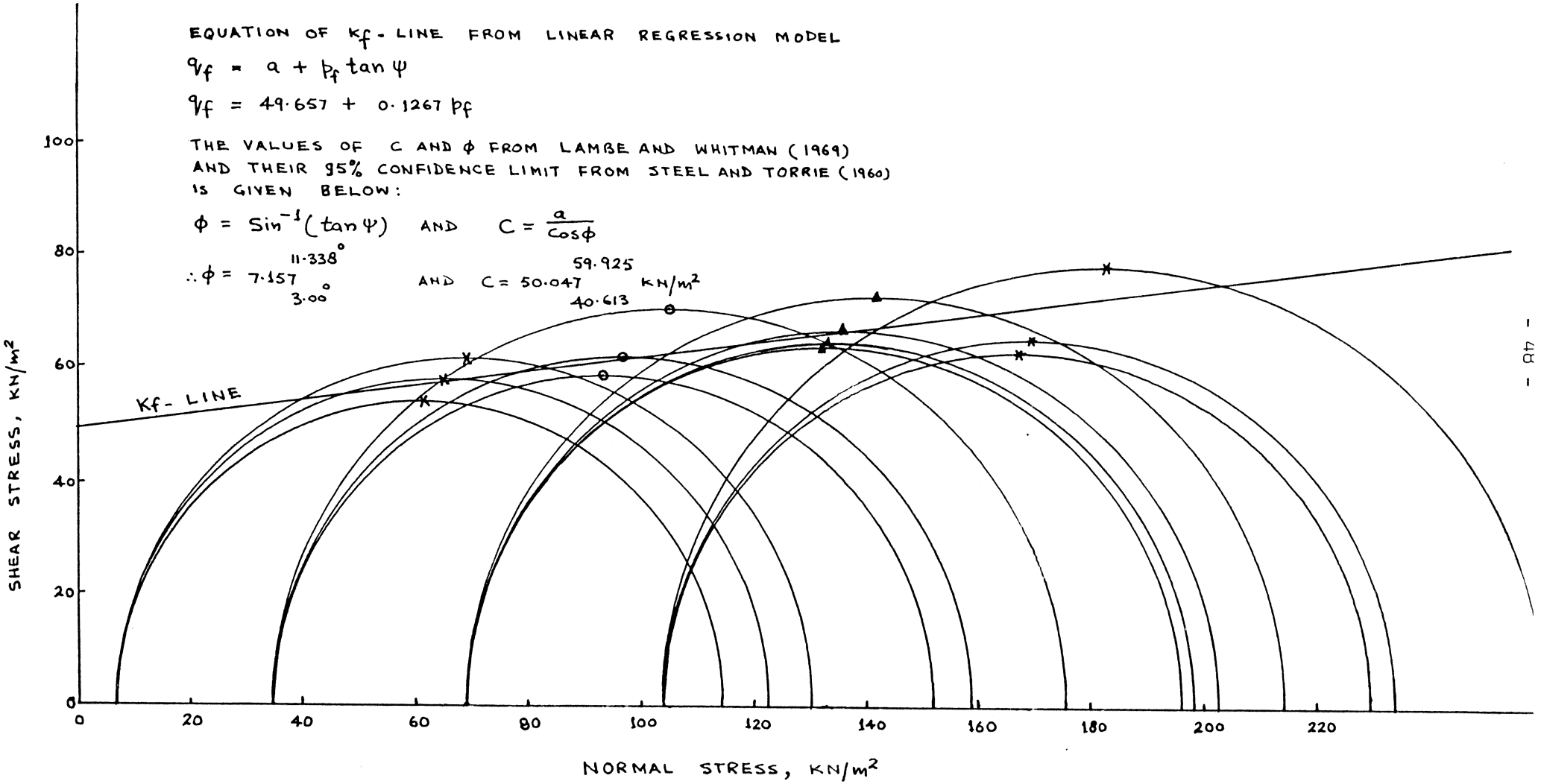

FIGURE 3.16 MOHR CIRCLES AND THE Kf - LINE FOR ARTIFICIAL CLAY SOIL AT 1757 kg/m³ DENSITY

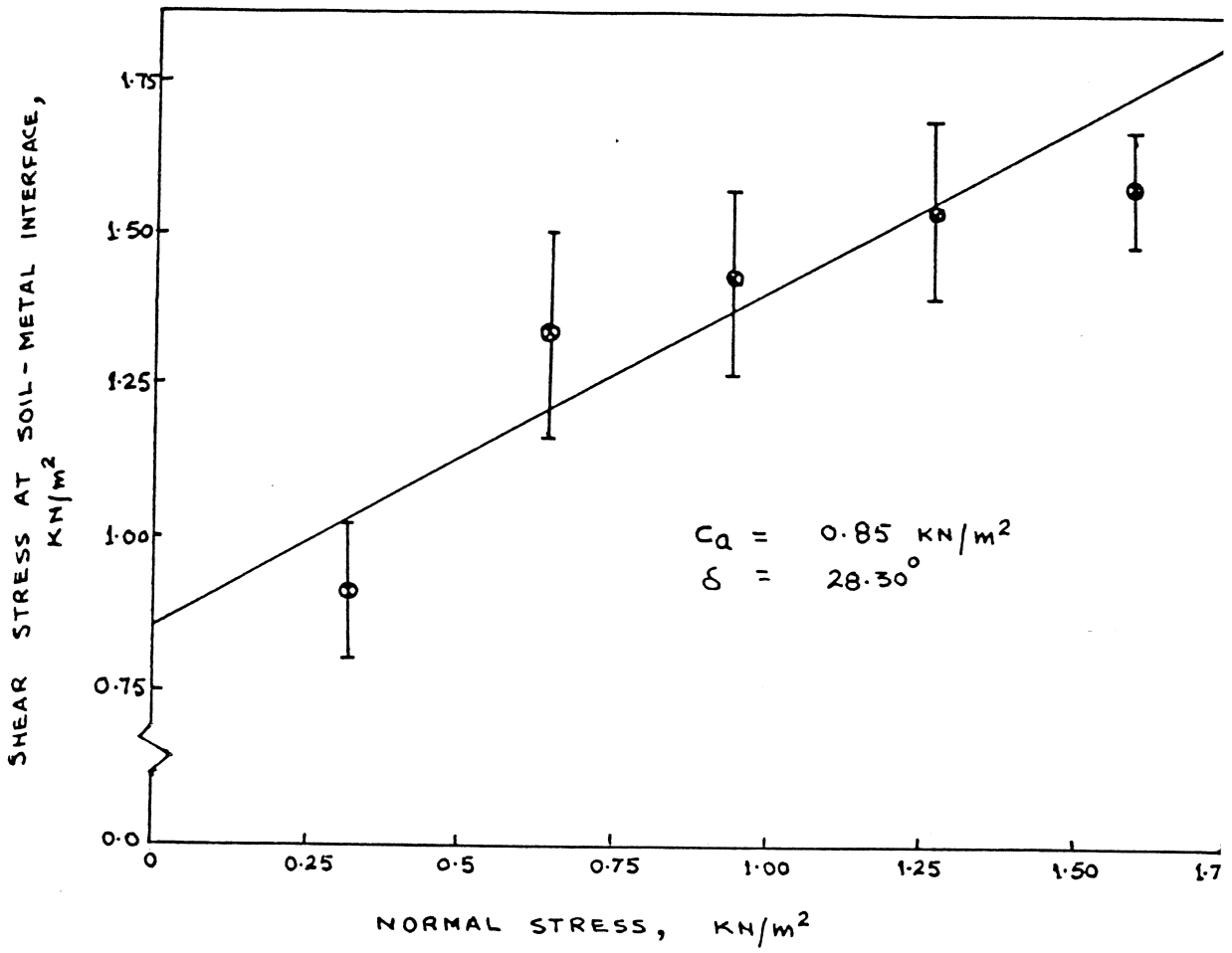

FIGURE 3·17 RELATIONSHIP BETWEEN SHEAR STRESS AT SOIL- METAL INTERFACE AND THE NORMAL STRESS FOR ARTIFICIAL CLAY SOIL

The soil-interface parameters were determined using a metal slider of known size (155 x 100 mm) and weight (166.1 grams) and recording the normal weight and the force required to pull the slider. The parameters were determined from the fitted regression model shown in Figure 3.17. The summary of the results is given below:

Soil Properties	Range	
Bulk density, γ, kg/m^3	1757	
Cohesion, C, kN/m^2	50.05	59.93 40.61
Angle of shearing resistance, ϕ, deg	7.15	11.34 3.01
Adhesion, Ca, kN/m^2	0.85	
Angle of soil-metal friction, δ, deg	28.30	

Radial Force		Resultant Force	
Observed	Predicted	Observed	Predicted
ΔS_V, Newton		R_{RV}, Newton	
+19.41	-1.23	69.68	94.21
+47.57	+25.21	106.76	127.15
+88.02	+70.88	154.76	190.82
+50.48	+4.83	109.32	101.29
+69.89	+50.29	129.94	161.50
+143.68	+97.04	224.69	228.85
46.60	+21.31	111.69	122.02
115.20	+60.28	210.07	175.64
214.88	+165.64	339.32	330.65

4. QUALITATIVE EXPERIMENTS TO DETERMINE THE MECHANISM OF SOIL FAILURE

4.1 Introduction

In any soil-tool interaction, there are three major areas of interest for a clear understanding of the processes involved in soil cutting. The areas shown in Figure 4.1 can be listed as below:

i. The first area extends along the shear plane, bc and is the boundary between the deformed and undeformed soil slice and the uncut soil mass. The main interest in this area may be in the failure patterns of the soil.

ii. The second area includes the interface between the deformed slice and the tool face with an emphasis on the frictional characteristics of the soil-tool combination.

iii. The third area includes the processes involved underneath the tip of the tool which requires an understanding of the deformation of the soil mainly compression due to thickness of the tip. This area is, in fact, independent of the other two areas and does not contribute in the removal of the soil slice.

All these areas are described in the foregoing chapters, however, this chapter concentrates mainly on the general shear failure (area, i) of the soil in front of a single rotating blade as it made a single cut through the soil block. The soil failure caused by a 20-gauge wire was investigated to understand the tip-effect of the blade and related to the failure mechanism of a rotating blade with horizontal and vertical axis of rotations. The selection of the size of the wire was mainly on the basis of its strength and suitability to the designed frame and was greater by 0.3 mm from the thickness of the blade.

4.2 Experimental Variables

i. Bite lengths (L_b) : 50 to 250 mm in steps of 50 mm

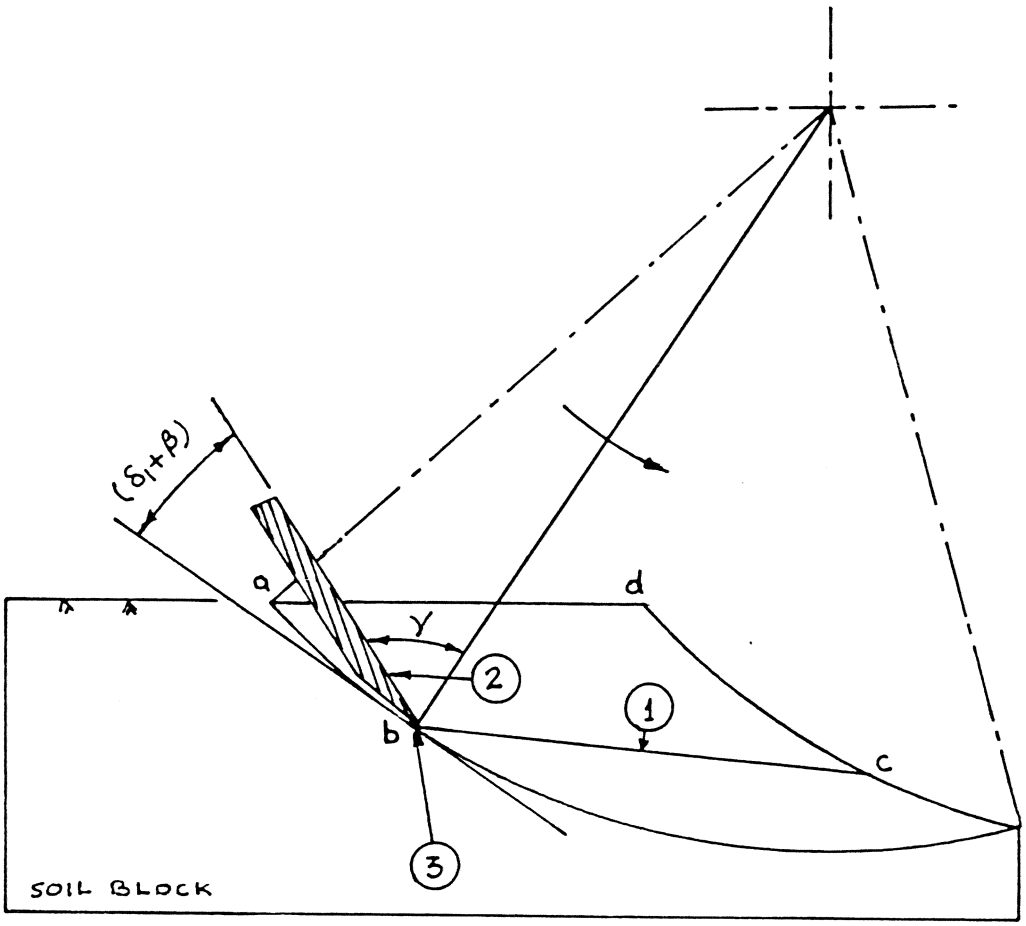

(1) SHEAR FAILURE PLANE, bc

(2) SOIL-METAL INTERFACE PHENOMENON

(3) LOCAL STRESSES DUE TO 'TIP-EFFECT'

FIGURE 4.1 MAIN AREAS OF INTEREST IN SOIL-TOOL INTERACTION

ii. Depths of cut (d) : 50 to 150 mm in steps of 50 mm

iii. Width of cut (w) : 100 mm
This covers a range of 'fetch-ratios' from 0.33 to 5:1

iv. Systems of cutting : (a) blade with 18^{o} tip angle
(b) 20-gauge wire

v. Modes of cutting : (a) blade with horizontal and vertical axis of rotations
(b) wire with horizontal axis of rotation

4.3 Experimental Technique

The experimental apparatus used in these experiments is described in Sections 3.6 and 3.7 and the method of soil block preparation is explained in Section 3.9.3. At the outset of an experiment, the rotor on the respective apparatus was held stationary at a predetermined position and the first false cut was made to remove the excess soil. The rotor was then positioned to give the desired bite length and cranked slowly (5 r.p.m.) to perform an experimental cut. A permanent record of the mechanism of soil failure was obtained using both a video recorder and a still camera. The orientation of the shear planes was measured with respect to the tangent to the circular path of the blade tip at the point of incipient failure.

4.4 Experimental Results

4.4.1 The Mechanism of Failure

The failure of a soil or any other homogeneous material under stress occurs when there is an appreciable departure from the linearity between stress and strain that is observed during elastic behaviour. Two main types of failure are distinguished as plastic flow and brittle fracture and have been observed with soil engaging tools by Hettiaratchi

and Reece (1967), Spoor (1969), Hendrick and Gill (1973), Godwin and Spoor (1977) and Stafford (1979) depending upon:

i. The soil type and physical conditions,

ii. The confining stress of the soil around the tool,

iii. The size and shape of the tool and

iv. The speed of cutting.

From the analysis of the video recording it was evident that there was, at first, compression and compaction of the soil in front of the blade tip (wire). This continued as long as the compressive force acting on the soil slice was insufficient to break the internal bonds and overcome the shear forces between the soil particles. Once the compression reached its limiting value, a slice of soil broke-off in a section from the main soil block by developing a shear plane and was then ejected. The formation of the shear planes, generally, started from the tip of the blade (or the wire) and the deformed slice section was pushed ahead by the front face of the blade. The successive shear planes were formed in a similar manner throughout the cutting of a full soil slice.

4.4.2 Orientation of Shear Planes in Soil Cutting by a Rotating Wire and a Blade

The resistance to cutting or pure tenacity acting on the cutting edge (tip) of a blade can be demonstrated by assuming the tip as an inextensible thin steel wire (Stefanalli, 1968). As a simplest case, the 'blade-effect' can be neglected so as to avoid interface friction of the blade and assuming wire as perfectly smooth. The results obtained with the wire can, then, be compared with the blade to observe the effect associated with the interface friction on the orientation of the shear planes.

The results of the experiments with a wire are shown in Figures 4.2a to 4.4a and that with the blade are shown in Figures 4.6a to 4.8a for two limiting 'fetch-ratios' (i.e. very small and very large) at

three depths of cut. The point of actual formation of the shear planes are marked with appropriate numbers. It can be seen that at small 'fetch-ratios', there is multiplicity of shear planes developed from the wire or tip of the blade. The average measured angle of shear planes with respect to the tangent for a wire and a blade was recorded (30 ± 3) degrees with a trend to the higher value at the larger 'fetch-ratios'. It can be deduced that the friction on the interface of the blade does not have a significant effect on the orientation of the shear planes. At large 'fetch-ratios' for a depth of cut of 150 mm, there are, however, two exceptions listed below:

i. After the entry of the wire or the blade, the first few shear planes develop by taking the path of least resistance towards the horizontal free surface.

ii. The largest shear plane develops by taking another least resistance path towards the base of the previous cut. However, even at the largest 'fetch-ratio', after the first largest shear plane, the successive shear planes develop within the recorded angle of (30 ± 3) degrees with the tangent.

At failure, the soil behaves like a plastic material and obeys the Mohr-Coulomb failure criteria. The failure plane makes an angle of $(45 - \frac{\phi}{2})$ degrees with the direction of the major principal stress. It can be noted that the observed orientation of the shear planes with the tangent is very close to a value $(45 - \frac{\phi}{2})$ degrees i.e. 26.5^{o}. This, in fact, shows that the direction of the tangent (or tangential stress) should be considered as the major principal stress. The direction of the principal planes should, therefore, be fixed according to the angular position of the blade tip (or wire) in cutting a full soil slice. The theoretical shear planes have been developed at an angle of $(45 - \frac{\phi}{2})$ degrees with the direction of major principal stress (tangent) and are shown in Figures 4.2b to 4.4b for the wire and Figures 4.6b to 4.8b for the blade. A comparison between the observed and theoretical shear planes reveals a close agreement.

The mechanics of a rotating blade can be explained on the basis of the failure mechanism by a simple blade operating at small rake angle (α)

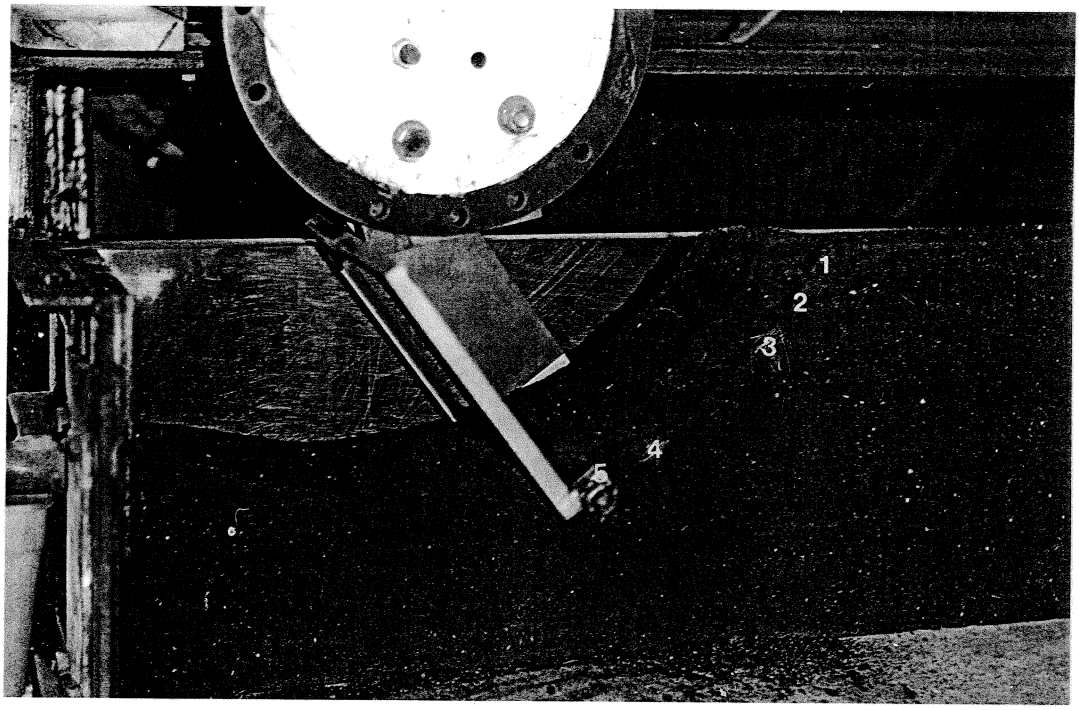

(i) 'Fetch-Ratio' or (L_b/d - Ratio) = 0.33 : 1

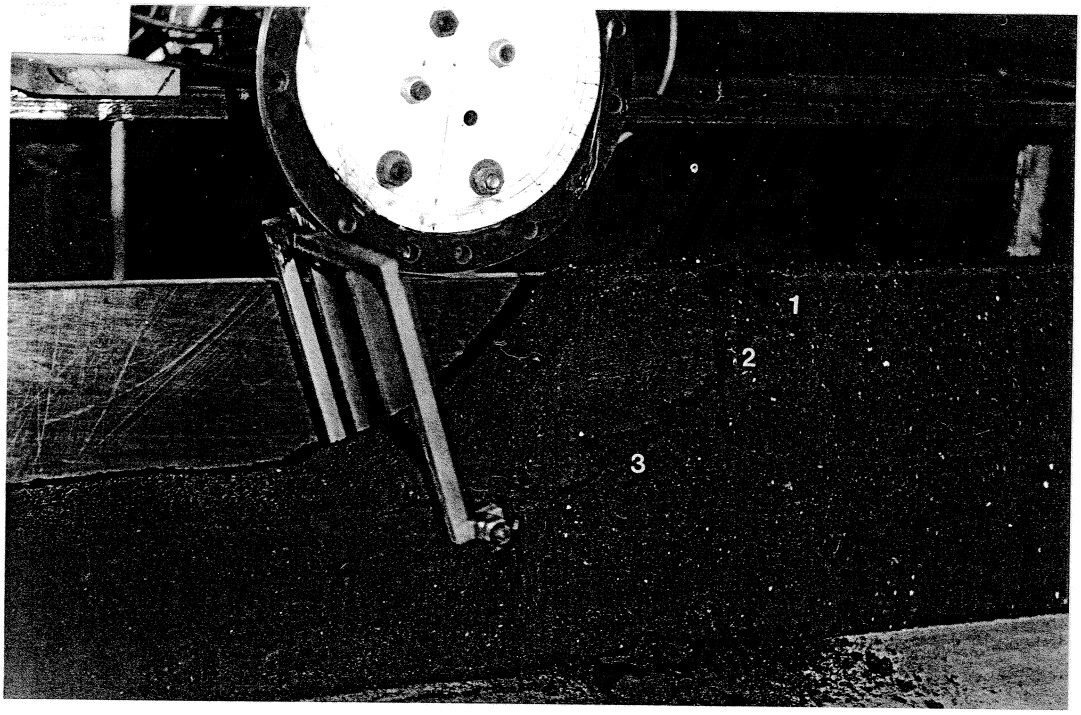

(ii) 'Fetch-Ratio' = 1 : 1

Figure 4.2a Observed Shear Planes Developed by a Wire, for 150 mm Depth of Cut

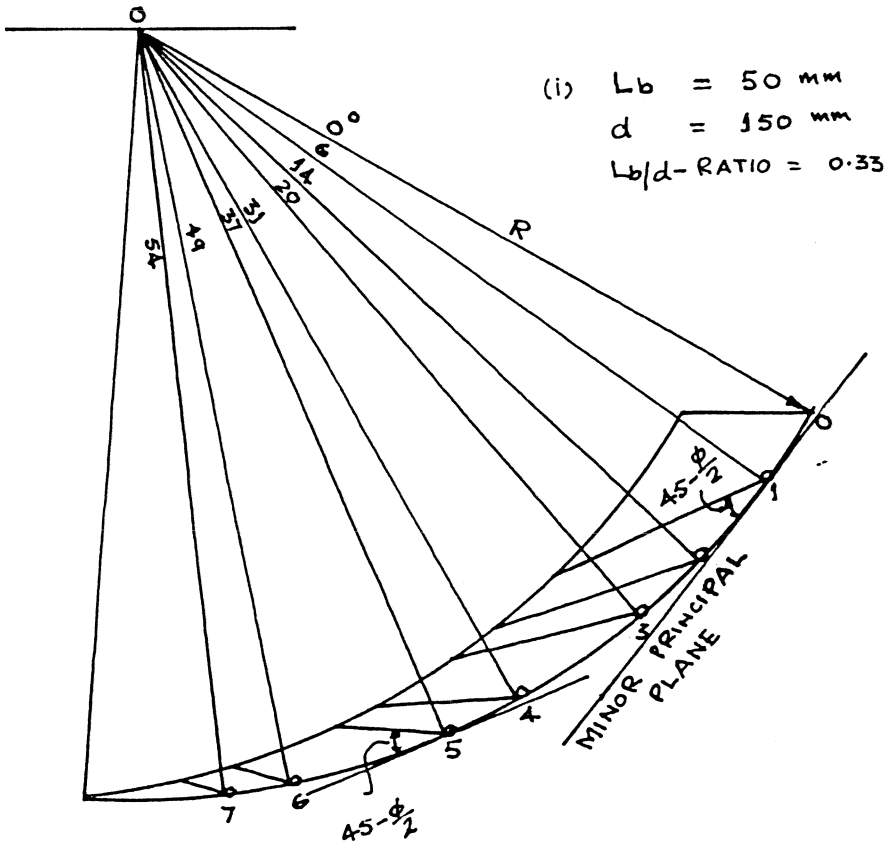

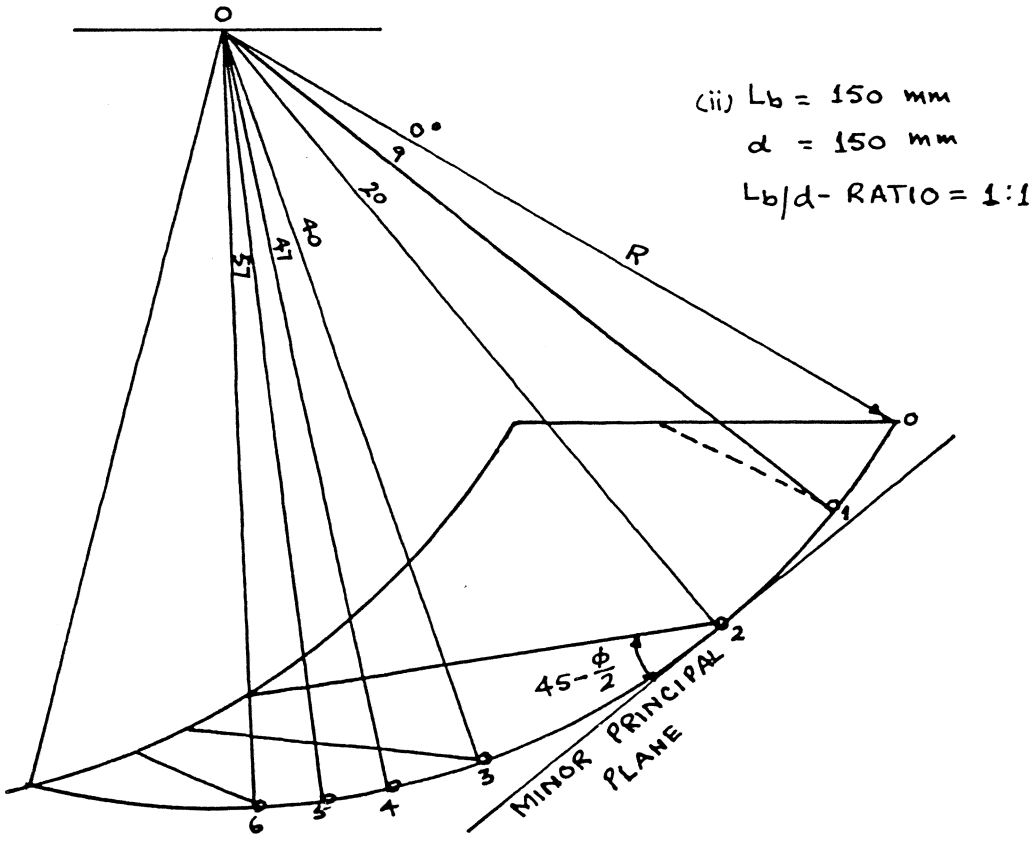

FIGURE 4·2b THEORETICAL SHEAR PLANES DEVELOPED BY A WIRE, FOR 150 MM DEPTH OF CUT

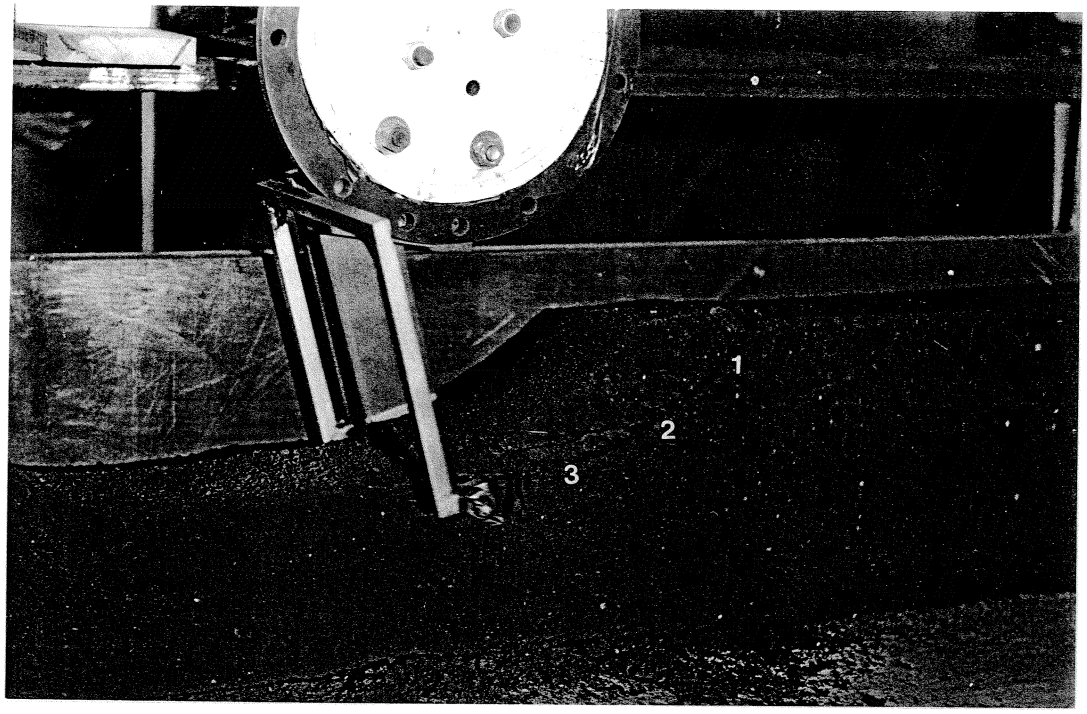

(i) 'Fetch-Ratio' = 1 : 1

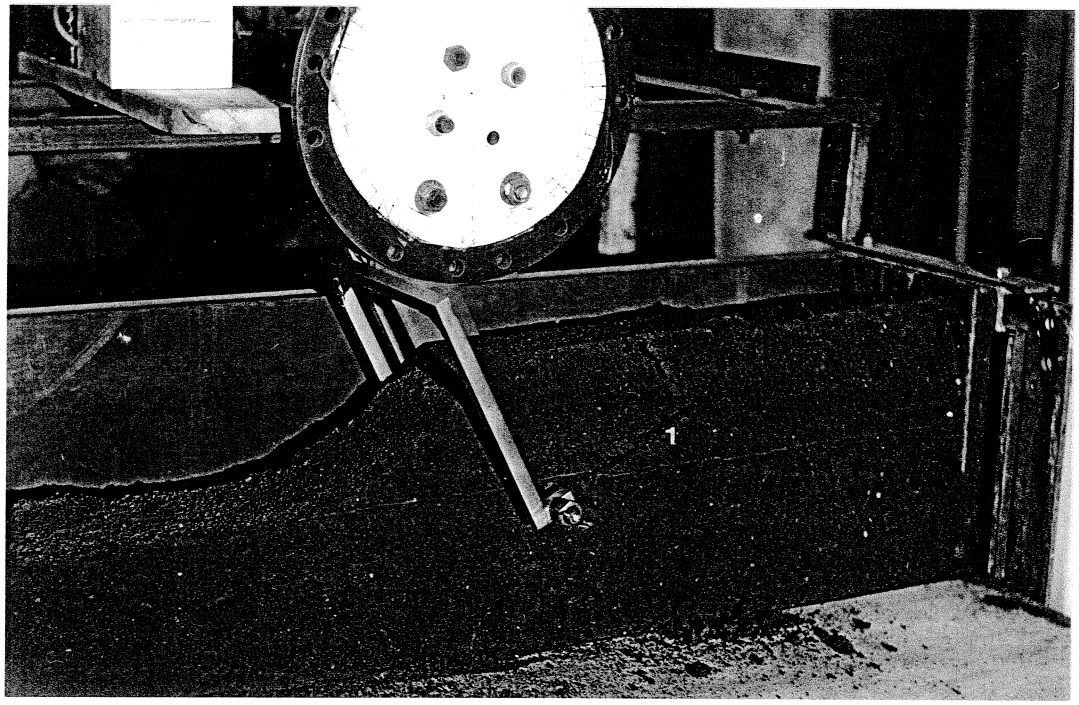

(ii) 'Fetch-Ratio' = 2.5 : 1

Figure 4.3a Observed Shear Planes Developed by a Wire, for 100 mm Depth of Cut

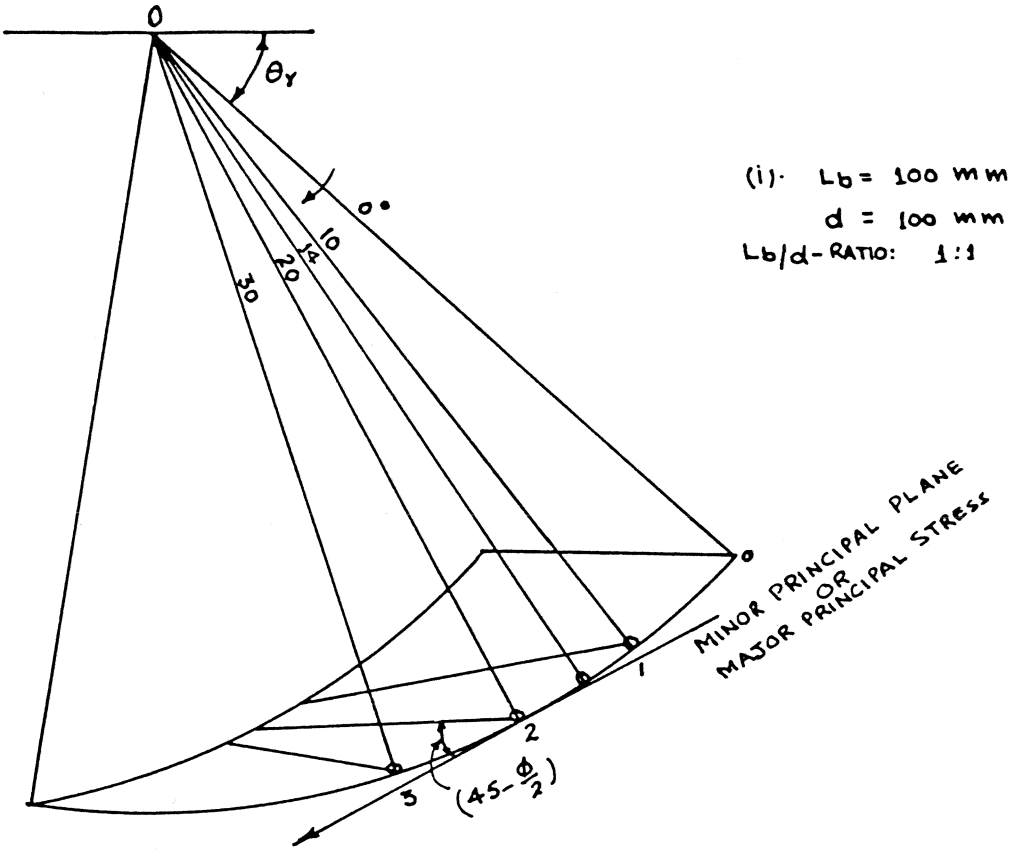

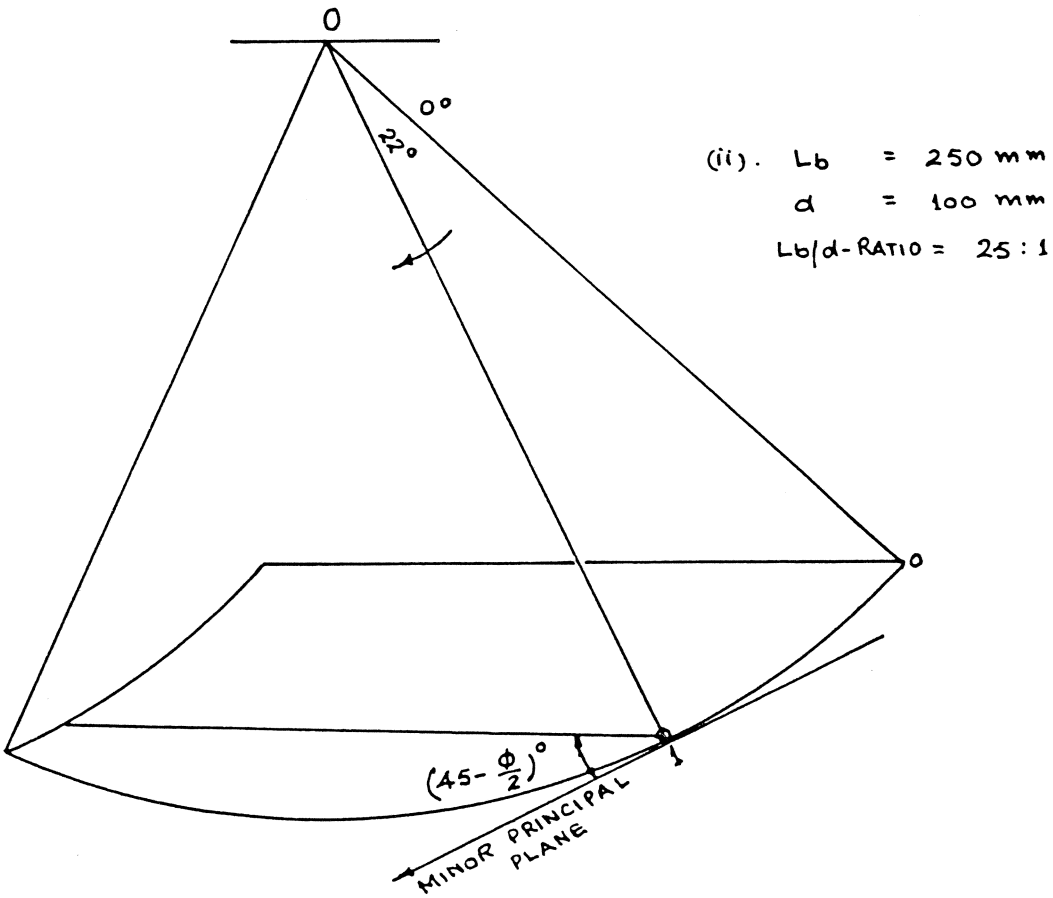

FIGURE 4·3b THEORETICAL SHEAR PLANES DEVELOPED BY A WIRE, FOR 100 mm DEPTH OF CUT

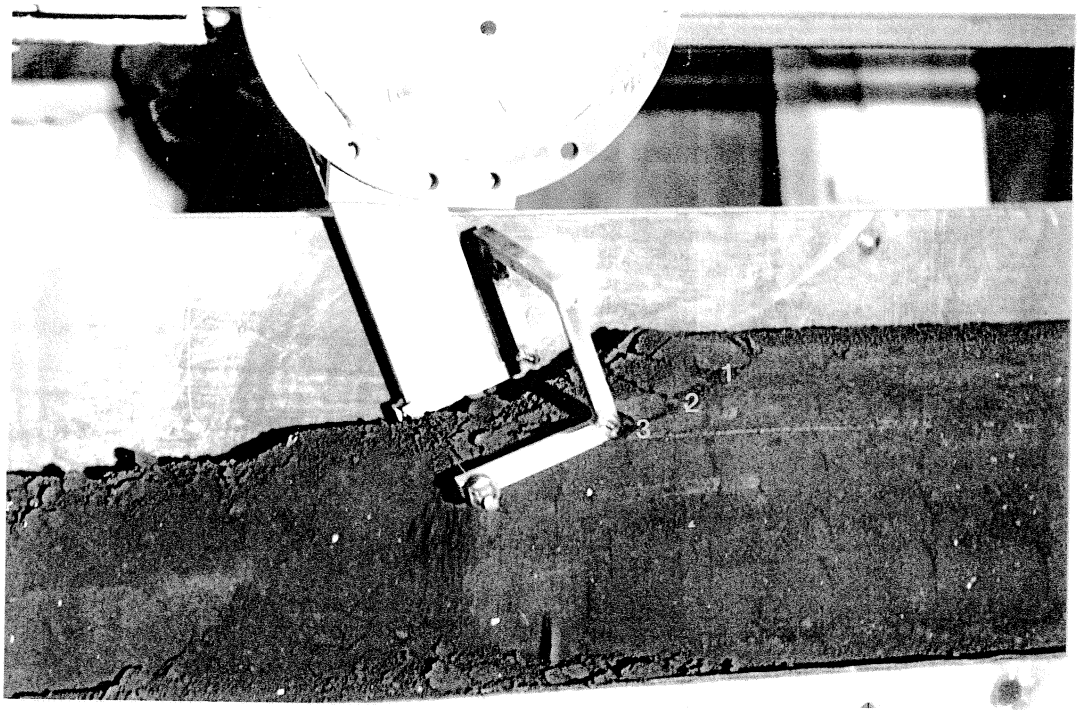

Figure 4.4a Observed Shear Planes Developed by a Wire, for 50 mm Depth of Cut

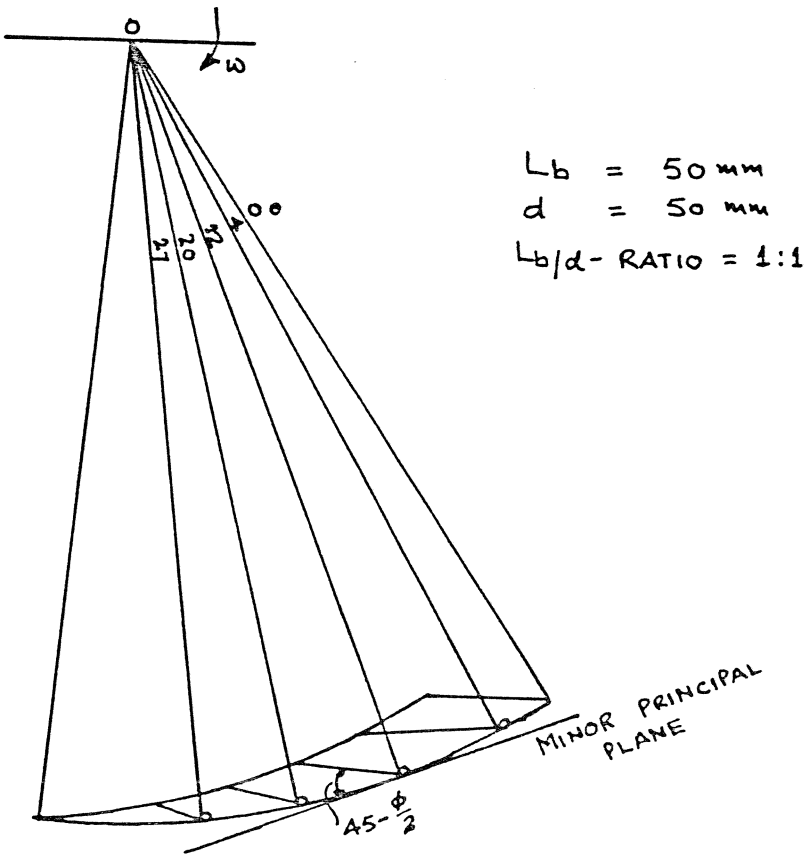

Figure 4.4b Theoretical Shear Planes Developed by a Wire for 50 mm Depth of Cut

shown in Figure 4.5. According to Hettiaratchi and Reece (1973) for a constrained adhesion case, the position of the radial shear plane with the interface of a simple blade can be determined using the following relationships to fix the position of the pole of the log-spiral for minimum passive resistance.

$$2\theta = 90^{o} + \phi + \delta + \sin^{-1}\frac{\sin\delta}{\sin\phi} \qquad \ldots\ldots\ldots (4.1)$$

$$2\beta_1 = 90^{o} + \phi - \delta - \sin^{-1}\frac{\sin\delta}{\sin\phi} \qquad \ldots\ldots\ldots (4.2)$$

The angles θ and β_1 are considered in a clockwise and anticlockwise directions from the interface respectively and are shown in Figure 4.5. However, at rake angles less than critical rake angle of $\alpha_c = (90 + 45 + \frac{\phi}{2} - \theta)$ degrees defined by Hettiaratchi and Reece (1974), the interface zone runs into the Rankine zone and the leading edge of the blade starts to cancel out the logarithmic spiral (radial zone) to such an extent that the position of the centre of the spiral becomes indeterminate. The rupture surface may be taken as a single straight line for two limiting conditions of rake angles as suggested by Hettiaratchi and Reece (1973) i.e.

i. $\alpha = 90^{o}$ for perfectly smooth blade (Rankine theory) or,

ii. $\alpha = 45 - \frac{\phi}{2}$ for perfectly rough interface.

The apparent cutting angle (γ_o) shown in Figure 3.1 of a rotating blade can be taken equivalent to the rake angle (α) of a simple blade with a centre of rotation at infinity. In practice, the geometry of the tiller blade is such that the interface will be always in or around the passive Rankine zone of a simple blade and in any case, the angle (γ_o) will be less than the critical rake angle, α_c. It can, therefore, be postulated that the shape of the failure plane developed by a rotating blade may remain as a straight line.

In a particular condition of a rotating blade (Figure 4.6b) the theoretical shear planes can be drawn either with respect to the interface or the tip. In Figure 4.6b (Upper) if the blade was moving in the direction shown by the dotted arrow, the shear plane will develop from the tip of the blade with respect to the interface similar to a simple blade depending upon the rake angles. This may, however, happen only if there was a semi-infinite mass of soil in front of the interface. When the blade was moving along the circular trajectory shown by the direction of the solid arrow, the shear planes develop from the tip of the blade at an angle of $(45 - \frac{\phi}{2})$ degrees with the major principal stress (tangent). The theoretical shear planes at large 'fetch-ratios' shown in Figure 4.6b to 4.8b (Lower) are drawn with respect to the face of the blade at an angle, $\theta \simeq 97^{o}$, after the entry of the tip. Under this situation, the rotating blade behaves similar to a simple blade because of the semi-infinite mass of soil in front of the interface. From the practical consideration, however, these first few planes are least important because the largest shear plane develops only when there is a sufficient strain applied by the blade to cut-off the slice along an angle of $(45 - \frac{\phi}{2})$ degrees with the tangent or an angle closest to the tangent.

The condition of the blade shown in Figures 4.6a and 4.6b with 'fetch-ratio' of 1.33 : 1 and higher (not shown) for 150 mm depth of cut, it is evident that the first largest shear plane can not be developed, theoretically, at an angle of $(45 - \frac{\phi}{2})$ degrees with the direction of major principal stress. According to the observed orientation of the shear planes, the first largest shear plane can be developed at an angle closest to $(45 - \frac{\phi}{2})$ degrees from the tip towards the base of the previous cut. The theoretical largest shear plane for a large 'fetch-ratio' shown in Figure 4.6b, would have only developed according to the concept when the base of the soil block was at large depth as shown by a dotted curved line. This, however, is a non-typical situation, hence, and in general for all practical regimes under which the rotary tiller may be operated, the direction of the failure planes can be fixed according to the theoretical concept. It can be noted that even at the largest 'fetch-ratio' after the first largest shear plane, the successive planes can be derived according to the theoretical concept.

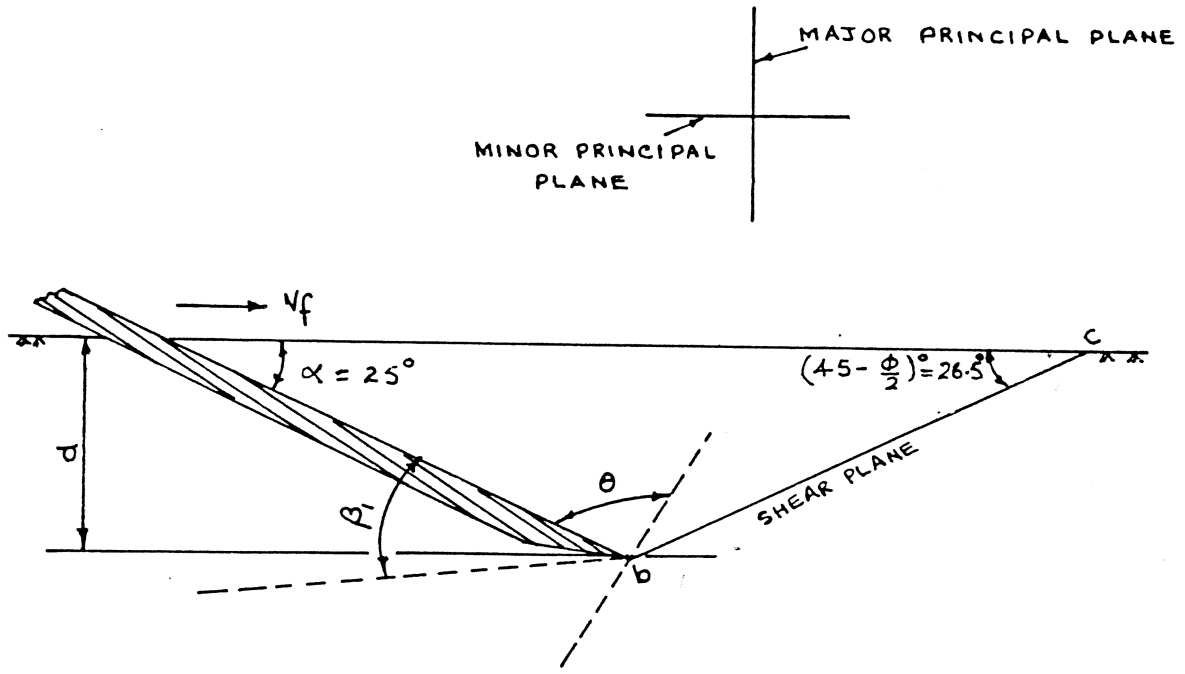

RAKE ANGLE, (α), OF A SIMPLE FORWARD MOVING BLADE $\equiv$ CUTTING ANGLE, ($\delta_1 + \beta$), OF A ROTATING BLADE

LET, $\delta = 24^\circ$ AND $\phi = 37^\circ$

$$\therefore 2\theta = 90^\circ + \phi + \delta + \sin^{-1}\left(\frac{\sin\delta}{\sin\phi}\right) \qquad \therefore \theta = 96.76^\circ$$

$$2\beta_1 = 90^\circ + \phi - \delta - \sin^{-1}\left(\frac{\sin\delta}{\sin\phi}\right) \qquad \beta_1 = 30.24^\circ$$

FIGURE 4.5 FAILURE SURFACE DEVELOPED BY A ROUGH SIMPLE BLADE OPERATING AT RAKE ANGLES (α) LESS THAN $(45 - \frac{\phi}{2})$ DEGREES

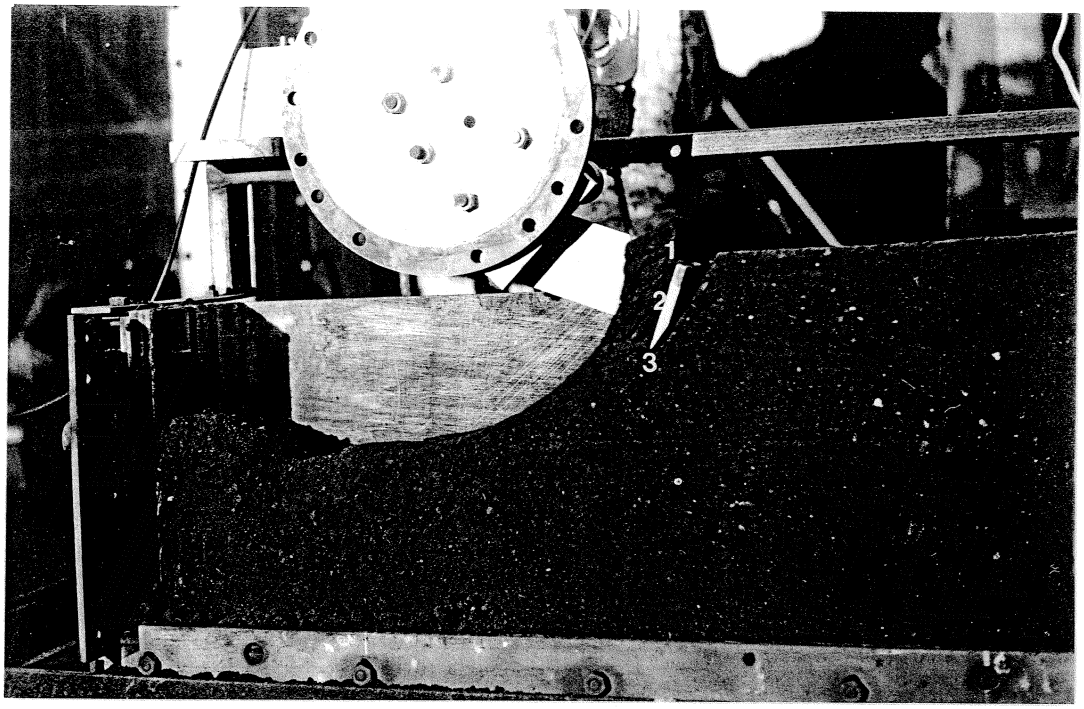

(i) 'Fetch-Ratio' = 0.33 : 1

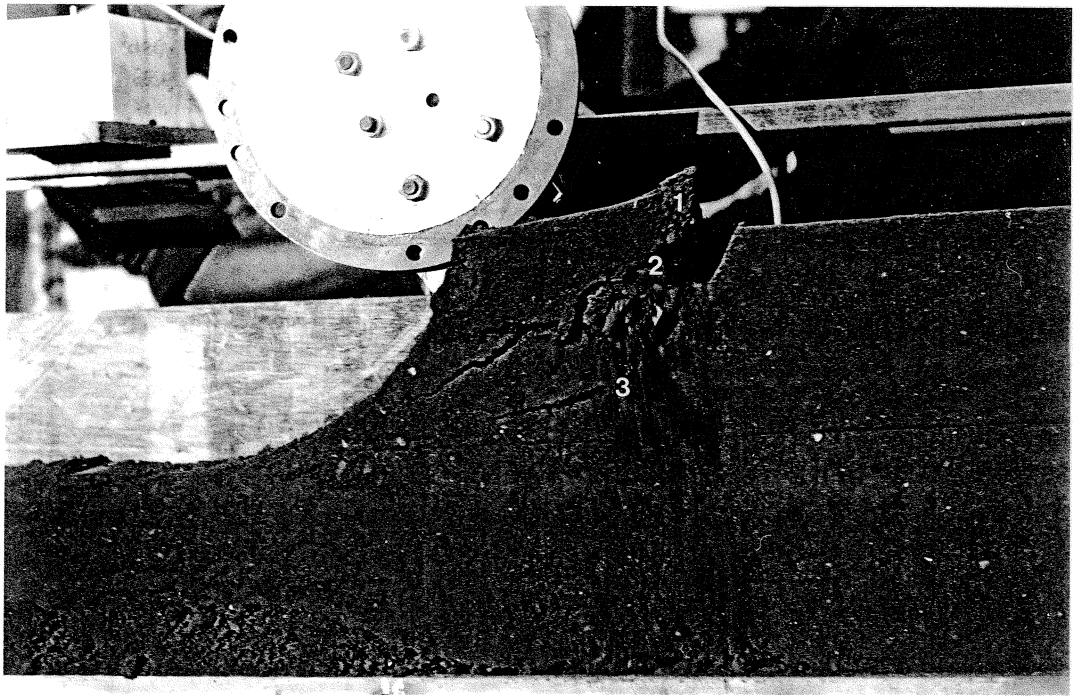

(ii) 'Fetch-Ratio' = 1.33 : 1

Figure 4.6a Observed Shear Planes Developed by a Blade, for 150 mm Depth of Cut

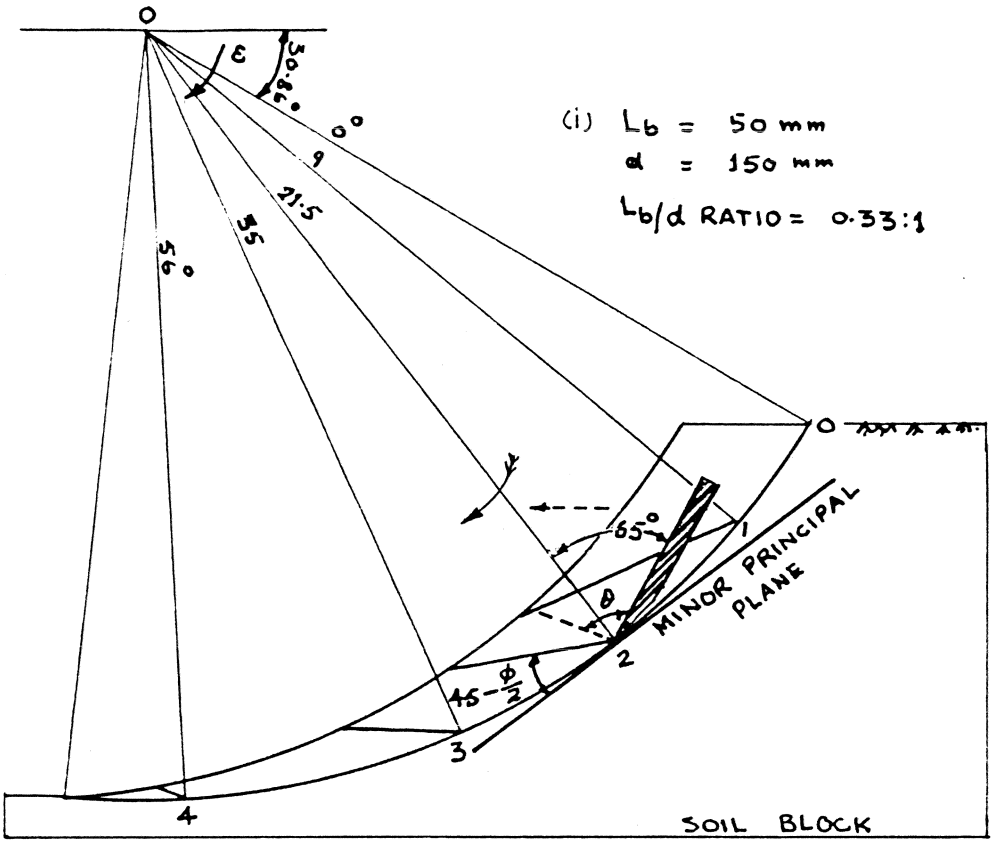

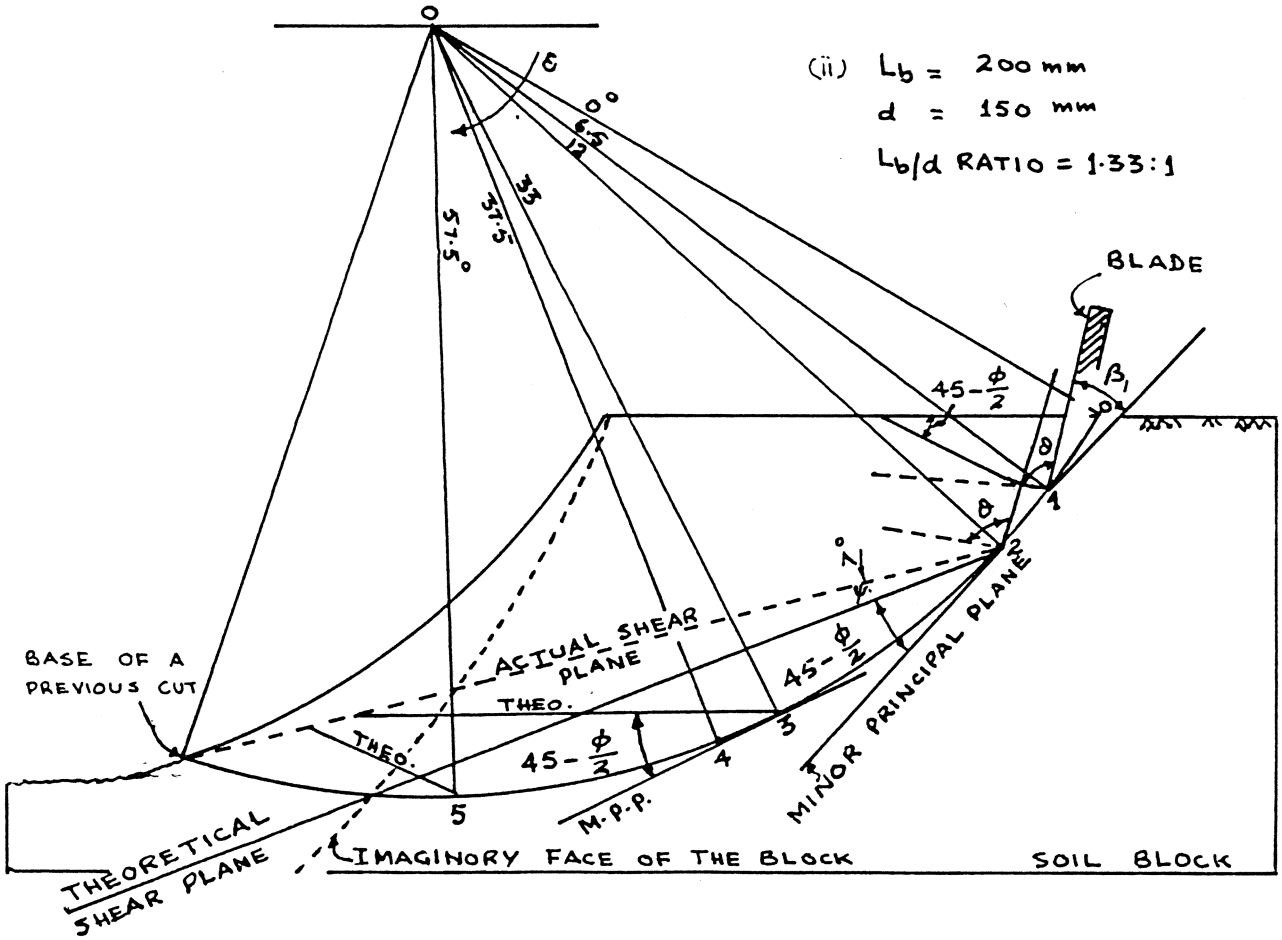

FIGURE 4.6b THEORETICAL SHEAR PLANES DEVELOPED BY A BLADE, FOR 150 mm DEPTH OF CUT

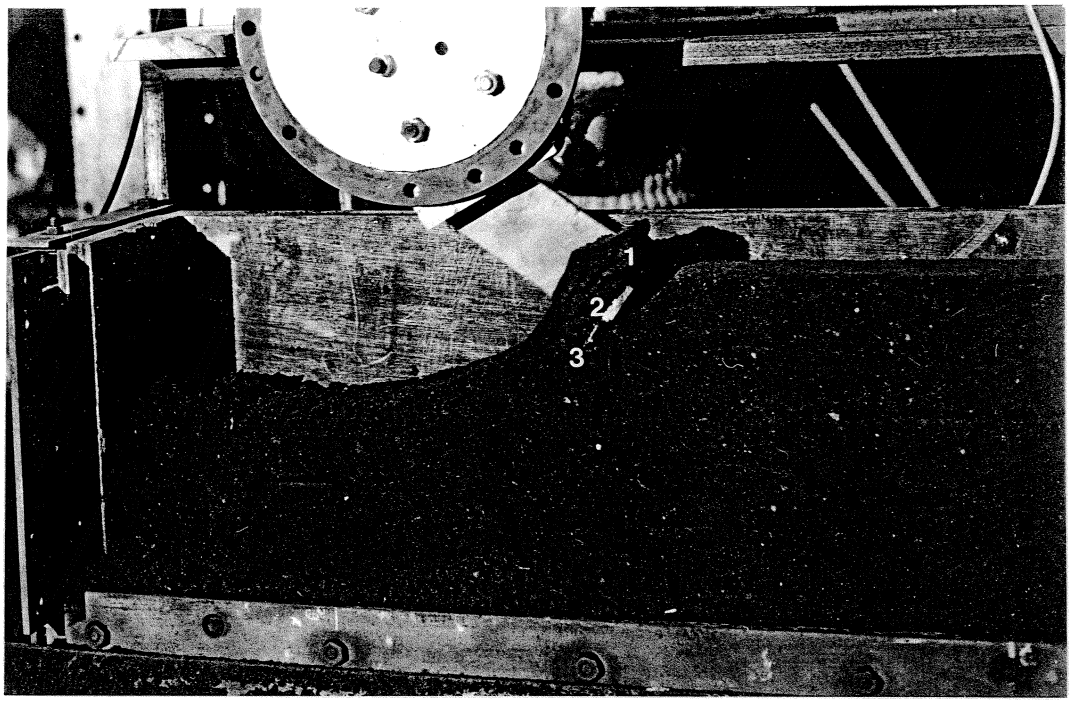

(i) 'Fetch-Ratio' = 0.5 : 1

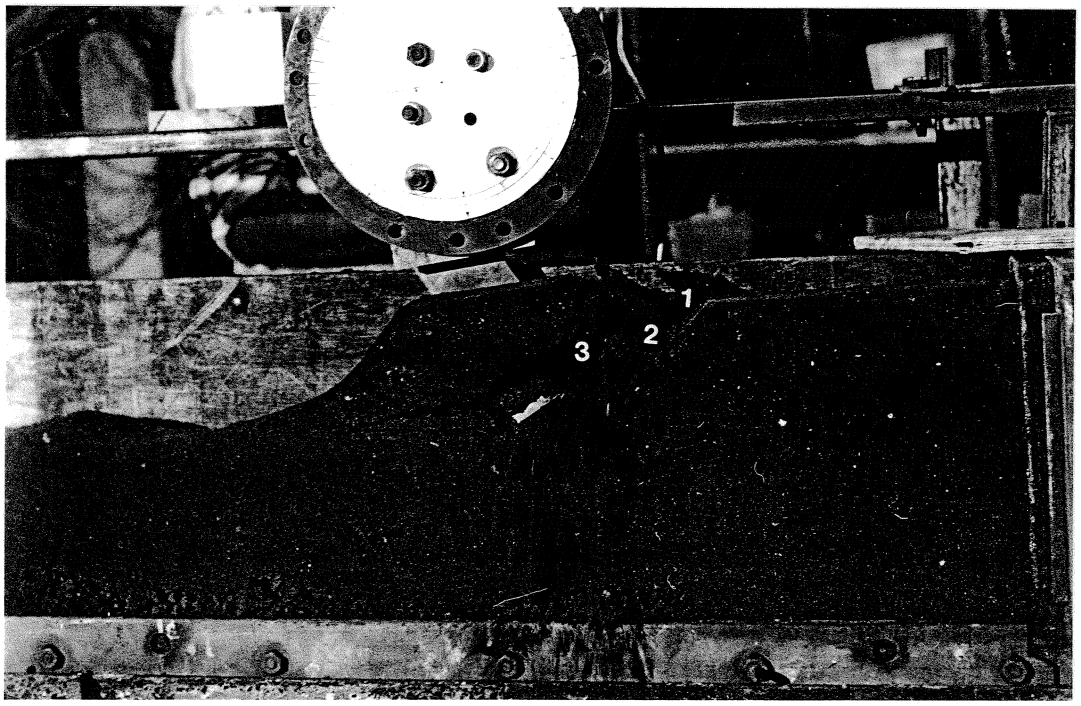

(ii) 'Fetch-Ratio' = 2.5 : 1

Figure 4.7a Observed Shear Planes Developed by a Blade, for 100 mm Depth of Cut

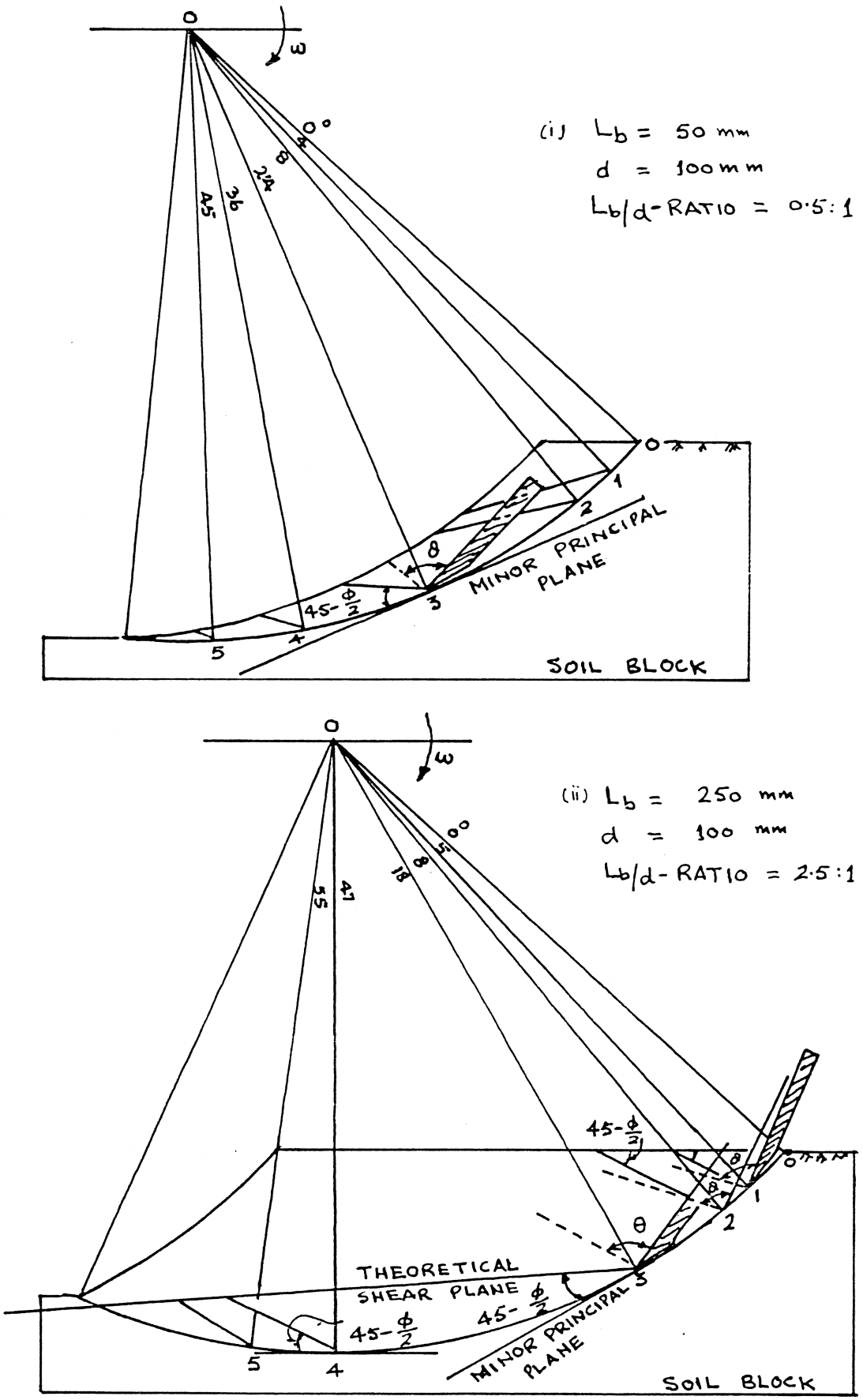

FIGURE 4·7b THEORETICAL SHEAR PLANES DEVELOPED BY A BLADE, FOR 100 mm DEPTH OF CUT

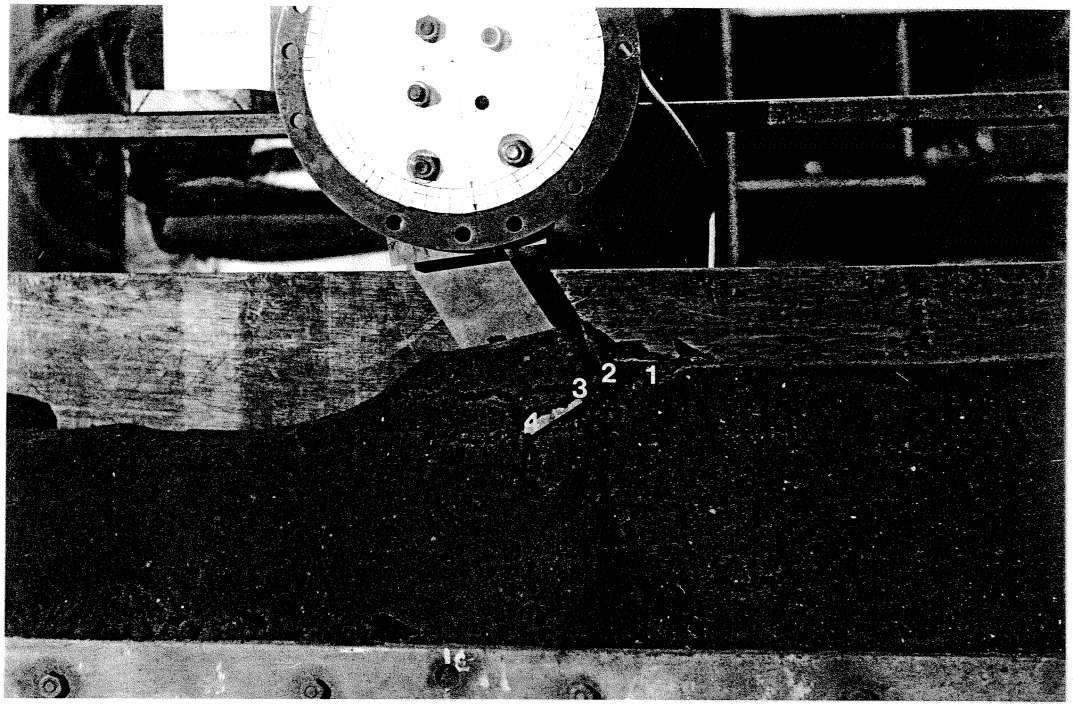

FIGURE 4.8a OBSERVED SHEAR PLANES DEVELOPED BY A BLADE, FOR 50 mm DEPTH OF CUT

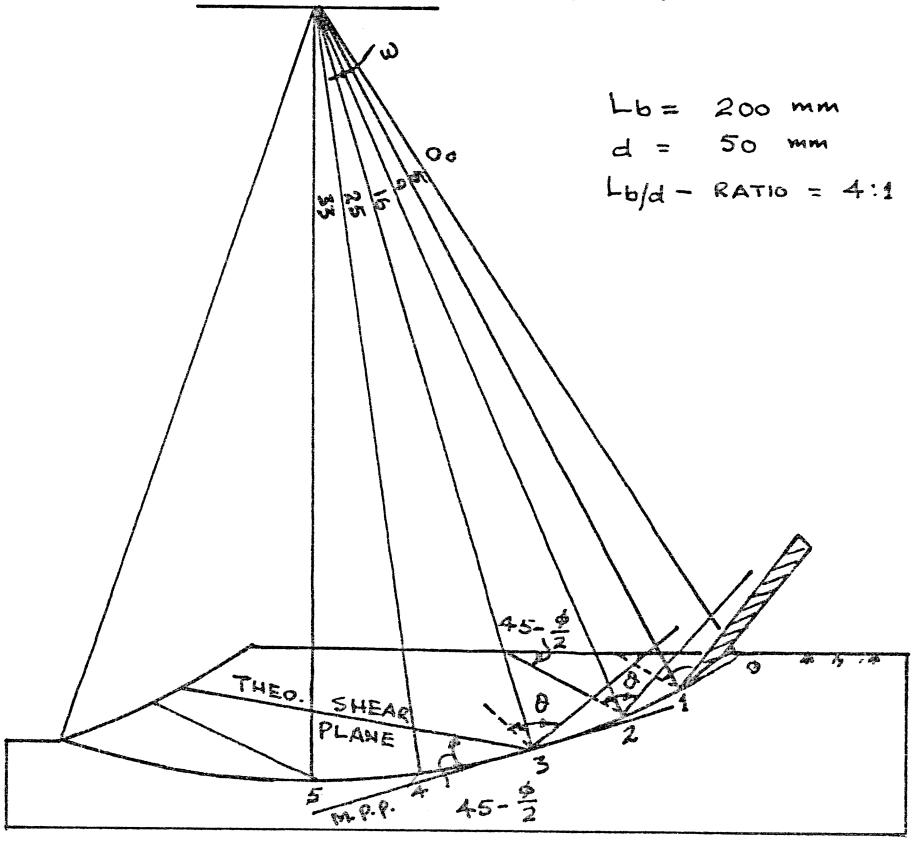

FIGURE 48b THEORETICAL SHEAR PLANES DEVELOPED BY A BLADE, FOR 50 mm DEPTH OF CUT

4.4.3 Orientation of the Shear Planes for a Blade with Vertical Axis of Rotation

4.4.3.1 Introduction

A limited number of experiments were conducted with the axis of rotation of the blade vertical with a view to observe the application and limitations of the theoretical concepts developed in Section 4.4.2 for a blade with horizontal axis of rotation. The full plan of the experiments is described in Figure 5.17. The mechanism of soil failure was observed under two situations:

i. The blade cutting a soil slice in less than a quarter of a circle at a working regime similar to the blade with horizontal axis of rotation and

ii. The blade operating in a full half-circle.

4.4.3.2 Results

Preliminary investigations reveal that the nature of the soil failure in less than a quarter of a circle cut is similar to the blade with horizontal axis of rotation as shown in Figure 4.9a. The shear planes were observed to develop from the tip of the blade at an angle of less than 30^{o} from the direction of the maximum principal stress (tangent) towards the curved free surface even though a bottom shear failure plane was present in these experiments. The theoretical shear failure planes shown in Figure 4.9b for a small (0.5 : 1) and a larger (1 : 1) 'fetch-ratios' are drawn at an angle of $(45 - \frac{\phi}{2})$ degrees with the major principal stress and are in correspondance with the observed soil failure.

The mechanism of soil failure in half circle cuts was similar to the experiments (i) for bite lengths less than 50 mm and the theoretical shear planes can be developed according to the concept of $(45 - \frac{\phi}{2})$ degrees to the major principal stress. For large bite lengths, however, the theoretical shear planes can only be developed according to this concept for the zone towards the end of a cut as shown at the lower right hand

side of Figure 4.10b. This case is, in fact, similar to a cut less than a quarter of a circle. On the basis of limited observations, the theoretical planes for the other position of the blade can be derived using the concept of least resistance observed with the blade in horizontal axis of rotation at a larger 'fetch-ratio' (Figure 4.6b, Lower). It can be seen in the figure that the largest shear plane develops at an angle greater than $(45 - \frac{\phi}{2})$ degrees towards the base of the previous cut. The concept of developing a theoretical shear plane for a blade working in a half circle cut is shown in Figure 4.10b. The figure shows the directions of the maximum principal stress (tangent), bc_1; shear planes drawn at an angle of $(45 - \frac{\phi}{2})$ degrees with the tangent, bc ; a plane drawn at an angle of $\theta = 97^{o}$ (value of θ shown in Figure 4.5) with the interface, bc_2; and the shear planes drawn as planes of least resistance at shallowest angles with the tangent (bc_1) which touch the curved free face, bc_3. The theoretical shear planes, bc_3, are drawn at -10^{o}, 0^{o}, $+10^{o}$, 80^{o}, 150^{o} and 170^{o} of rotation of the tip. The theoretical shear planes marked as 1, 2 and 3 after -10^{o}, 0^{o} and $+10^{o}$ rotation of the tip in Figure 4.10b are in close agreement with the observed shear planes shown in Figure 4.10a.

4.5 Conclusions

i. The mechanism of soil failure by a rotating wire, assumed analogous to the tip of a blade, can be explained by Mohr-Coulomb soil mechanics and the boundary of the shear planes can be determined at an angle of $(45 - \frac{\phi}{2})$ degrees with the direction of major principal stress considered as a tangent to the tip parallel to the direction of rotation.

ii. The presence of a face of the blade has no significant effect on the orientation and shape of the failure planes and can be determined according to (i) for most practical cases. However, for a blade with horizontal axis of rotation in a special situation (very large 'fetch-ratio'), the theoretical failure planes can be determined from the tip of the blade either;

   a. With respect to the interface towards the horizontal free surface immediately after the entry of the blade, or

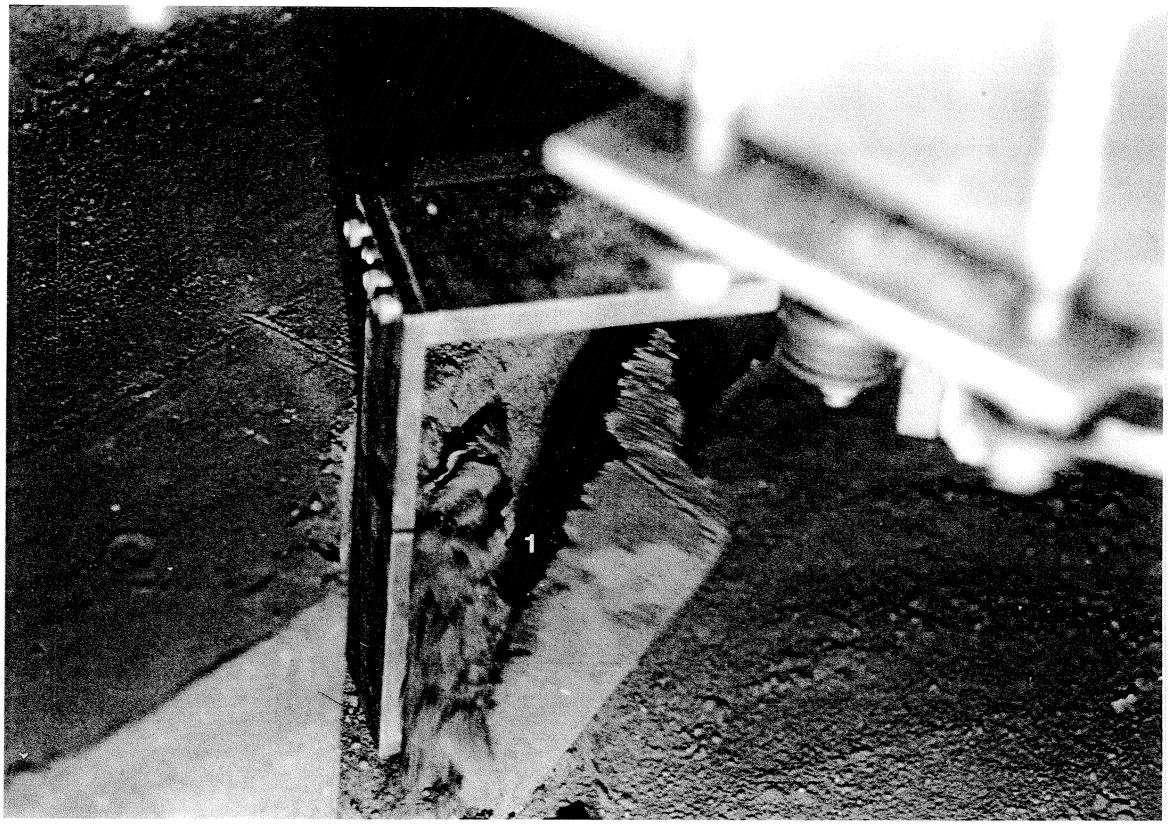

(i) Bite Length (L_b) = 50 mm

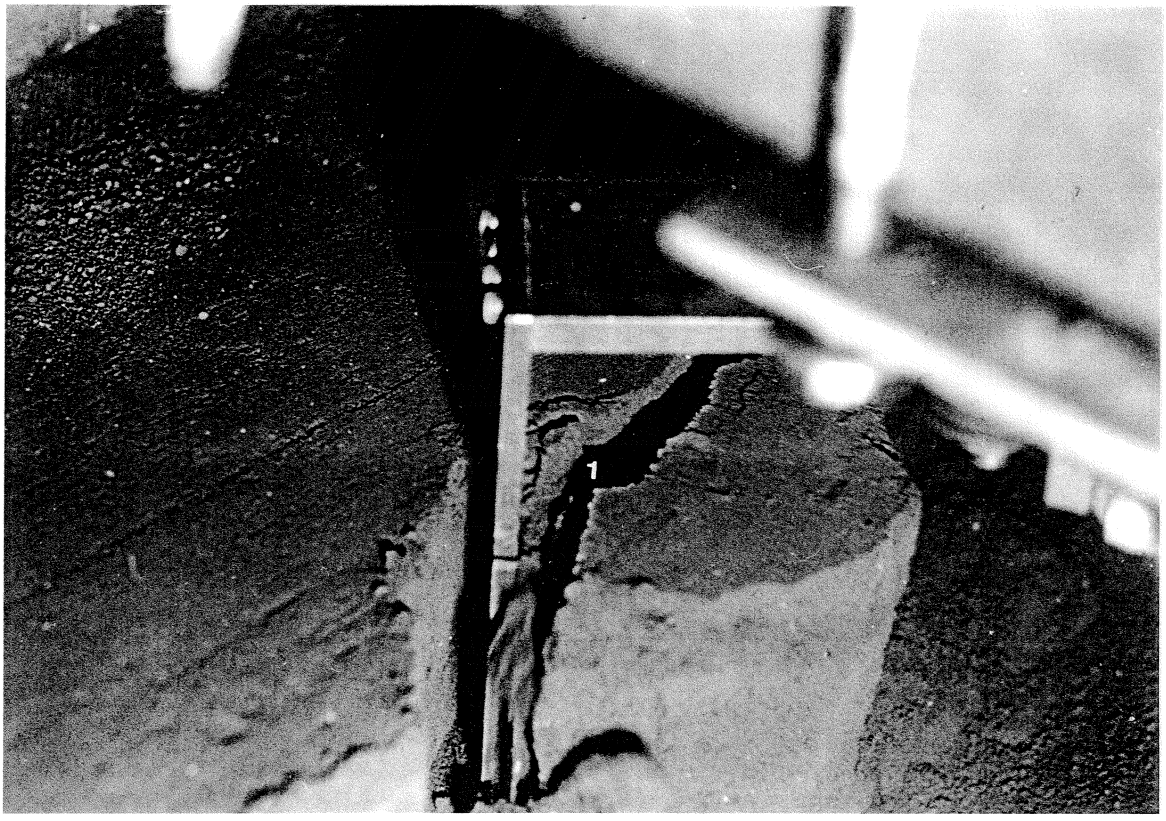

(ii) Bite Length (L_b) = 100 mm

Figure 4.9a Observed Shear Planes Developed by a Blade with Vertical Axis of Rotation, for Less than a Quarter of a Circle Cut

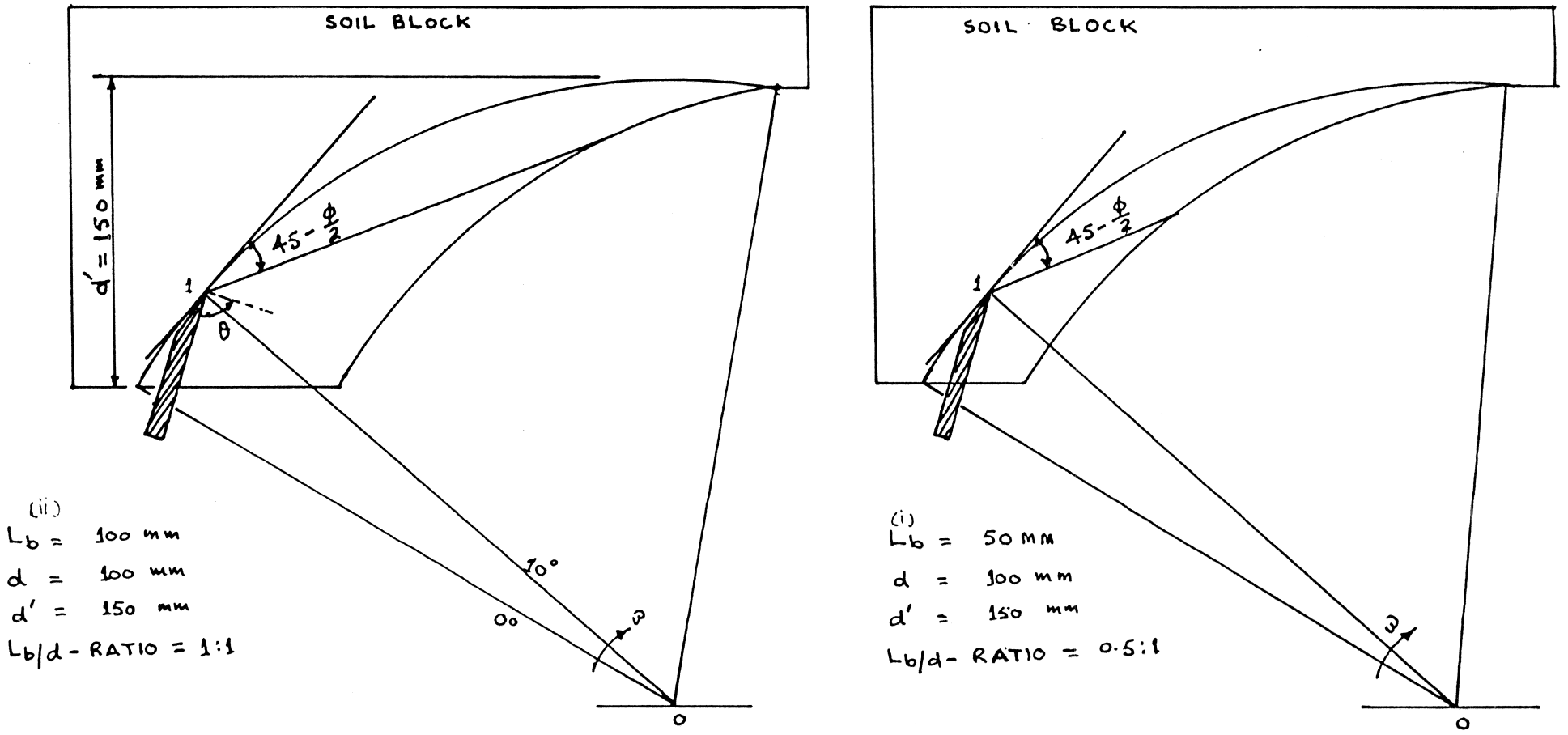

FIGURE 4·9b THEORETICAL SHEAR PLANES DEVELOPED BY A BLADE WITH VERTICAL AXIS OF ROTATION, FOR LESS THAN QUARTER OF A CIRCLE CUT

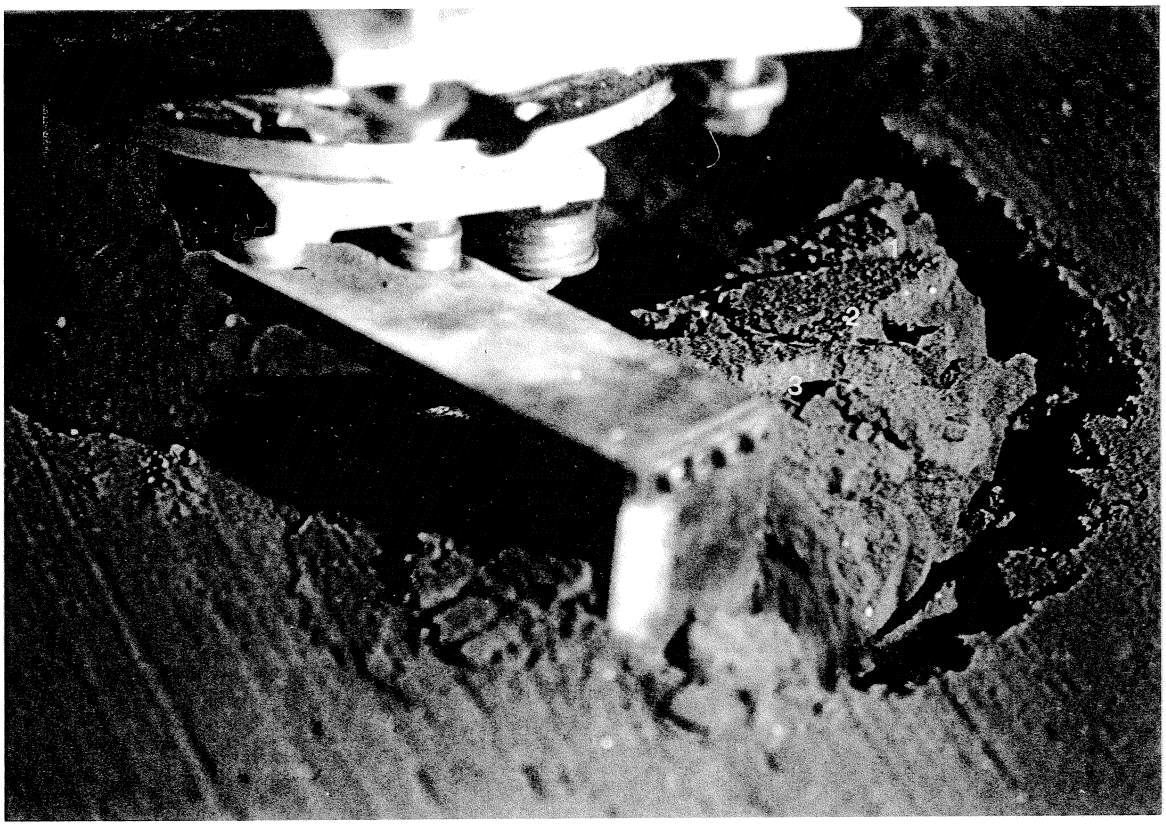

a. OBSERVED SHEAR PLANES

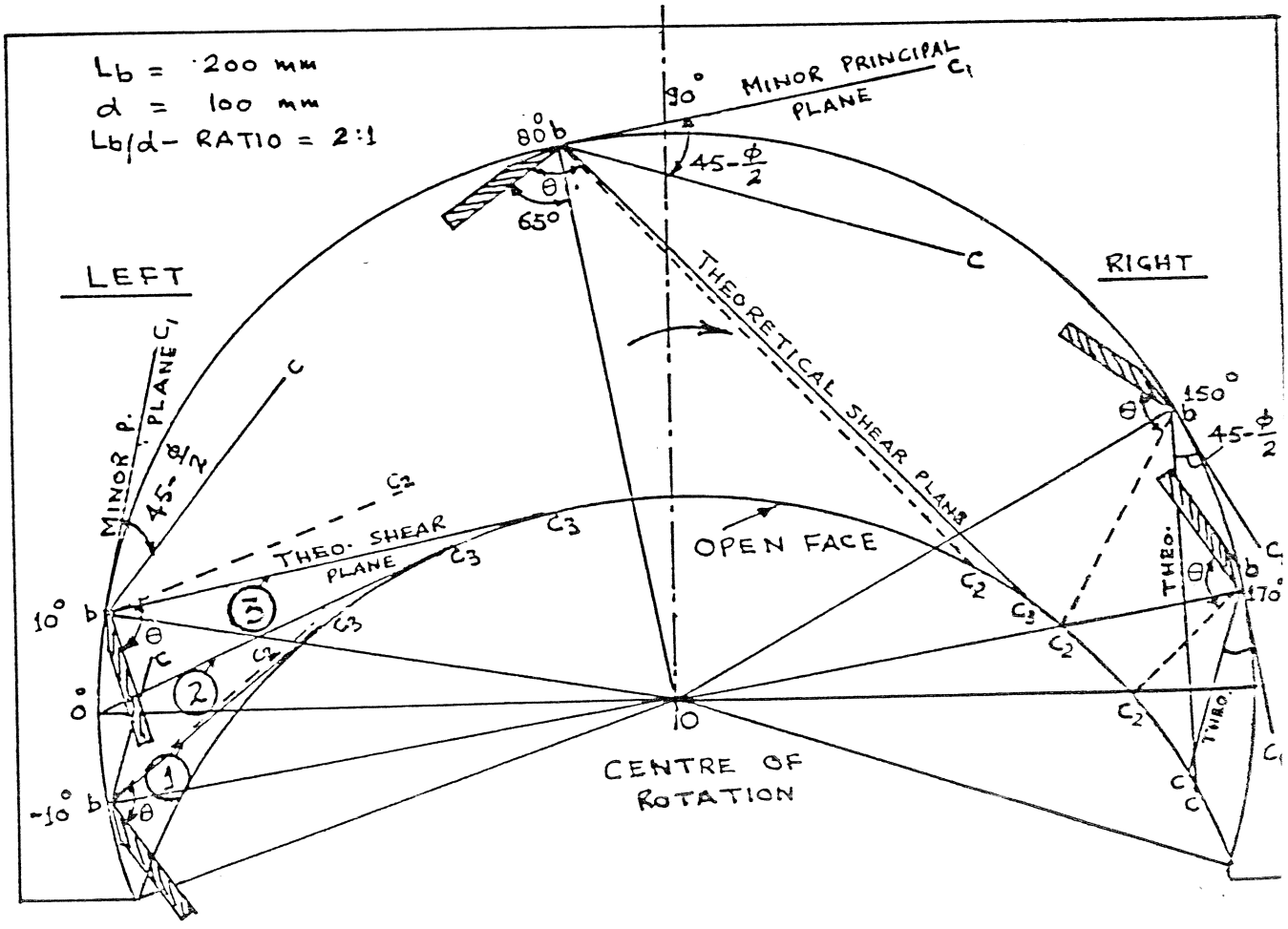

b. THEORETICAL SHEAR PLANES

FIGURE 4.15 OBSERVED AND THEORETICAL SHEAR PLANES DEVELOPED BY A BLADE, for HALE CIRCLE VERTICAL CUT

b. towards the base of the previous cut at an angle closest to $(45 - \frac{\phi}{2})$ degrees for the largest shear plane in cutting a full soil slice.

iii. The mechanics of a blade with vertical axis of rotation is not different than a blade with horizontal axis of rotation and the theoretical failure planes can be developed either;

a. according to (i) for very small bite length, or,

b. according to (ii.b) towards a break point on the curved free face at a shallowest angle closest to $(45 - \frac{\phi}{2})$ degrees.

5. DETERMINATION OF THE QUASI-STATIC FORCES ON A ROTATING BLADE AND A WIRE

5.1 Introduction

Many investigations have been carried out into the performance of soil engaging tools and the mathematical models have been established to predict the forces on the geometrically simple tools. Such models, however, assume two-dimensional flow of soil and disregard the soil flow around the cutting edge (tip) when operating at small rake angles. No cutting tool is perfectly sharp due to which a rear tip reaction on the cutting edge is produced. In the case of a sharp passive tool the 'tip-effect' may be insignificant in comparison to the higher magnitude of the passive soil reaction when operating at large depths. However, even for a sharp tool working at a shallow depth and a blunt tool working at a range of depths, the 'tip-effect' can not be neglected.

Very little work has been reported on the 'tip-effect' but the occurrence of this phenomenon has been observed and frequently used in the arguments of the experimental results by Seig (1982), and Harrison (1982) with the soil engaging tools and Boothroyd (1964) with the metal cutting tools. O'Dogherty (1964), however, predicted the tip force of a coal cutter using empirical equation. The tip force was found generally constant with the depth of cut and was thought to originate from the stresses acting at the edge of the cutter. In the case of a rotary tillage tool the geometrical and operational parameters are such that the tip of the blade becomes blunt only after a few hundred acres of work, V. Ya. Sal'nik (1960), which increase the cutting resistance many times.

The cutting edge of the blade which is practically, semi-circular in shape can be represented as a wire. Therefore, for the determination of 'tip-effect', the soil reactions on the wire is necessary. This chapter deals with the quasi-static forces acting on the cutting edge and the face of a rotating blade as it advances slowly in the soil. Two main sections on the wire and the blade are introduced with a brief review to explain the logic for that experiment and the relationship that it has with the complete mechanics of a rotating blade.

5.2 Experimental Variables

In addition to the variables described in Chapter 4, a limited number of experiments were conducted with a blade of 10^{o} tip angle in the frictional soil. The nature of reactions with 18^{o} tip angled blade and wire was also obtained for a purely cohesive artificial clay soil.

5.3 Experimental Technique

The method used for the measurement of the forces on a rotating blade and wire with horizontal axis of rotations was similar to the one described in Chapter 4 for the observations of the mechanism of soil failure. Before cutting a soil slice the rotor was cranked to bring the force measuring transducer upto its top most position which was considered as a zero reference point. The rotor was cranked at a slow speed of 5 r.p.m. and a permanent record of forces and resulting moment was obtained on a four-channels FM tape recorder which was replayed on a pre-calibrated X - Y plotter for further analysis. A wave like pattern of the forces was obtained due to successive failure and transitional periods while a new slice section was being stressed to failure. The number of shear planes in cutting a full soil slice were ascertained by conducting a joint analysis of the video film and X - Y plotter records. The position of shear planes and resulting magnitude of forces and moment were recorded using the method shown in Figure 5.1.

The method of analysis of force records for a blade with vertical axis of rotations was similar to the horizontal blade except a different experimental apparatus and signal conditioning equipment were used as described in Chapter 3.

The direction of the radial force towards the centre of rotation of the blade or the wire, taken with reference to the tangential component, was represented as a negative force and vice versa. The position of the resultant force was determined using the experimental values of the resultant force, moment and distance between the centroid of the transducer and tip of the blade (234 mm).

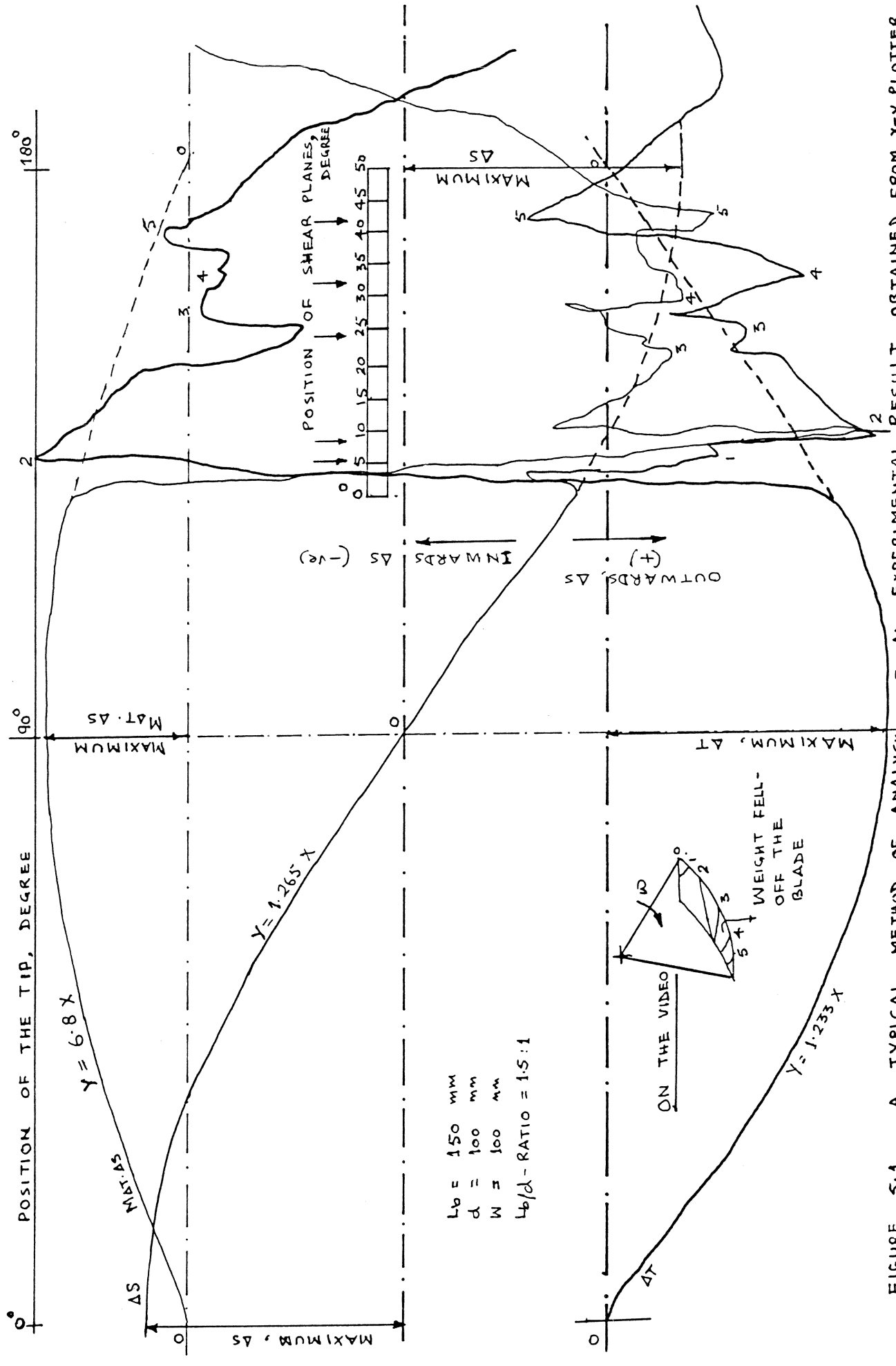

FIGURE 5.1 A TYPICAL METHOD OF ANALYSIS OF AN EXPERIMENTAL RESULT OBTAINED FROM X-Y PLOTTER

5.4 The Quasi-Static Soil Reactions Acting on a Wire

The failure of a soil slice by a rotary tiller blade is dependent upon the size and shape of the cutting edge. Zelenin (1950) compared the cutting resistance of a rope drawn scraper with the results obtained by Dalin (1943) for a rotary cultivator tine and found a close agreement between the results. Based on the magnitude of cutting resistance, he argued that the blade of a tiller works on the principle of frontal cutting. Dexter et.al.(1973 and 1978) reported the 'edge-effect' force on the geometrically simple tools by conducting analogous studies with probes of various types and sizes and concluded that the effect is mainly due to compression of the soil to the sides as it flows around the tool in agreement with Zelenin (1950) for a symmetrical knife operating near an open wall.

The 'tip-effect' of a blade can be determined by neglecting the face of a blade and defining the tip by a wire. Apparently, no theoretical investigations have been reported for the prediction of the tip forces based on the fundamental soil properties and soil behaviour equations. Only a few empirical relationships have been reported for the calculation of forces on a wire. Stefanelli (1968) studied the distribution of soil reaction by means of the funicular curve acquired by a wire during its uniform motion through the soil. From the form of the funicular curve he was able to determine the position of the resultant force using mathematical relationships. Stefanelli presented the cutting resistance as a function of water content and specific weight of soil, and the vertical pressure in relation to the sliding plane of wire. Godwin (1974), however, estimated the horizontal force of a vertical 20-gauge wire (tine edge) by pulling it horizontally and on the assumption that the force is proportional to the geostatic stress. A linear regression model was developed based on experimental results at two soil densities for a frictional soil. The steep increase in the horizontal force component for a 90^{o} rake angle tine near the origin of the force-width function was explained on the basis of the results obtained in soil cutting by a wire.

5.4.1 The Magnitude of the Resultant Force

The relationship between the magnitude of the resultant force and the angular position of the wire at different fetch-ratios for three depths of cut is shown in Figures 5.2 and 5.3. It can be deduced from the figures that the resultant force increases steeply to a peak value after approximately 15^{o} to 20^{o} of rotations of the wire into the soil for bite lengths less than 150 mm and thereafter the peak occurs after 25^{o} to 30^{o} of rotations. However, due to the deflection of the wire in the form of a funicular curve, Stefanelli (1968), the peak force may occur slightly earlier than the recorded peak. In general, at small bite lengths the peak resultant force does not show a single peak but the trend remains almost as a plateau upto approximately 90^{o} rotations of the wire from the horizontal axis of the rotor.
The reasons for this may be due to little variations in the size of the shear planes with the angular position of the wire in comparison to a large magnitude of the soil reaction due to the local shear failure which remains approximately constant during cutting a full soil slice. However, for large bite lengths of more than 150 mm the peak is clearly visible. Even for a small bite length of 25 mm, the resultant force is approximately 90 newtons for the depths of cut of 100 and 150 mm which may be due to considerably high magnitude of local soil reactions. At a smaller depth of cut (50 mm), the magnitude of the peak resultant force is approximately 50 % lower than the larger depths and may be because of lower confining stresses around the wire which remains always near the free horizontal soil surface.
The magnitude of the peak resultant force with fetch-ratios shown in Figure 5.4 reveals that the resultant force increases steeply at small fetch-ratios but the increase is at a decreasing rate as the ratio is increased. An eight fold increase in the bite length increased the resultant force by only approximately 2.5 times for the depths of cut of 100 and 150 mm and indicates a lower value of specific resistance with increasing fetch-ratios.

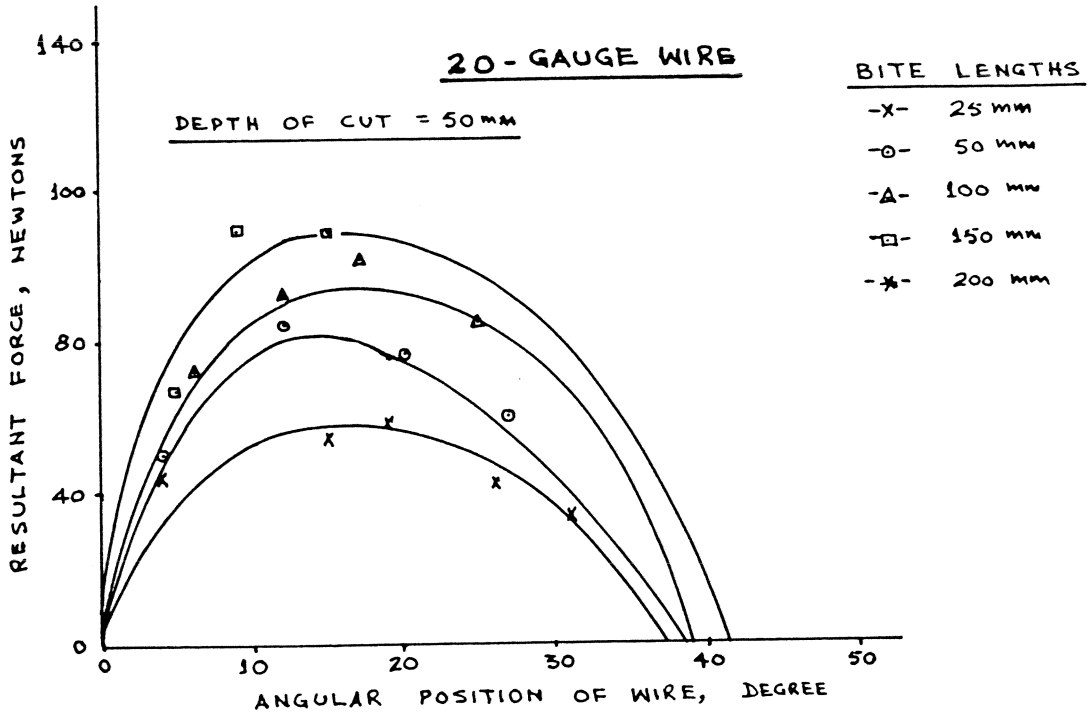

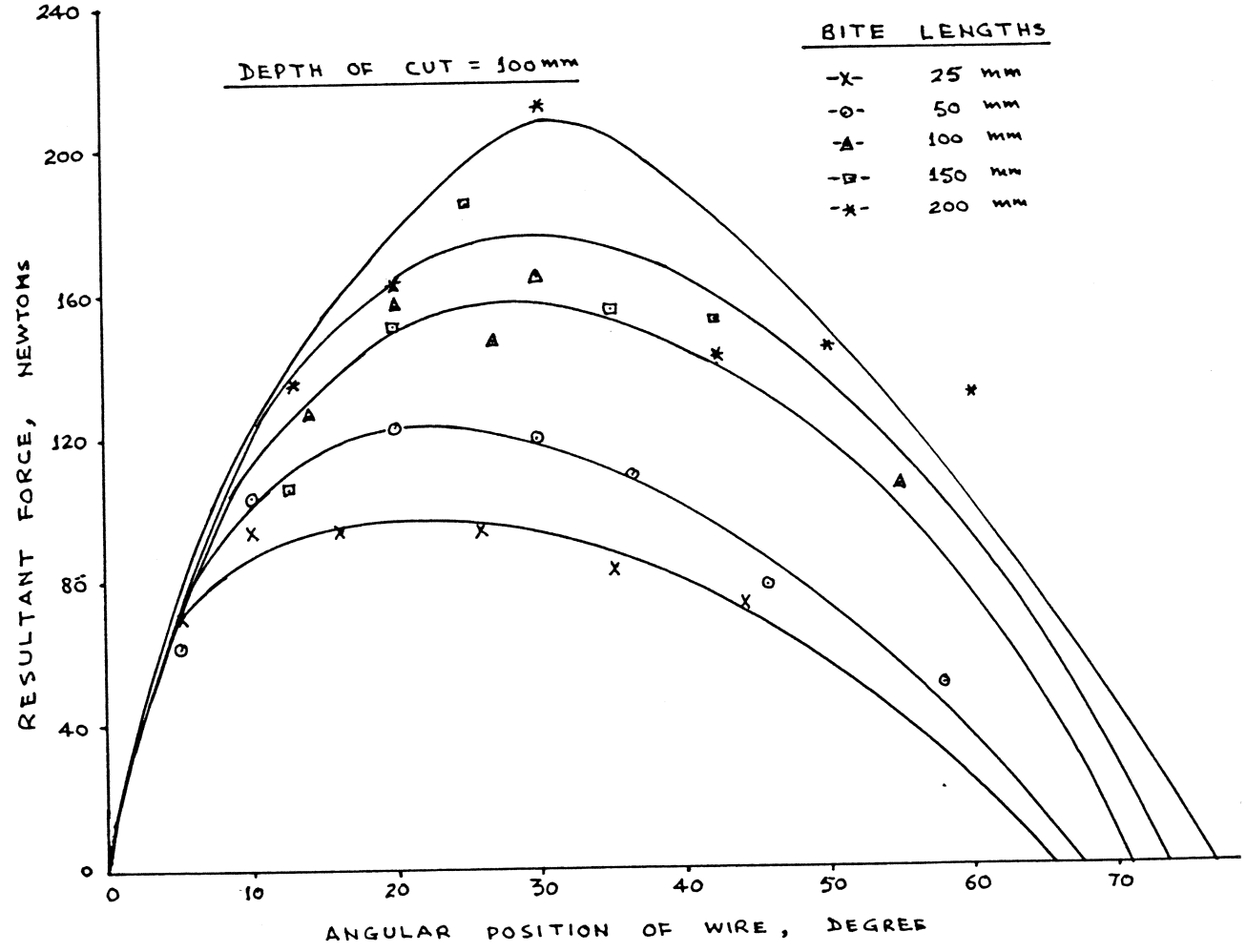

FIGURE 5.2 VARIATION OF RESULTANT FORCE WITH THE ANGULAR POSITION OF THE WIRE IN CUTTING A FULL SOIL SLICE AT DIFFERENT BITE LENGHS FOR 50 mm AND 100 mm DEPTHS OF CUT

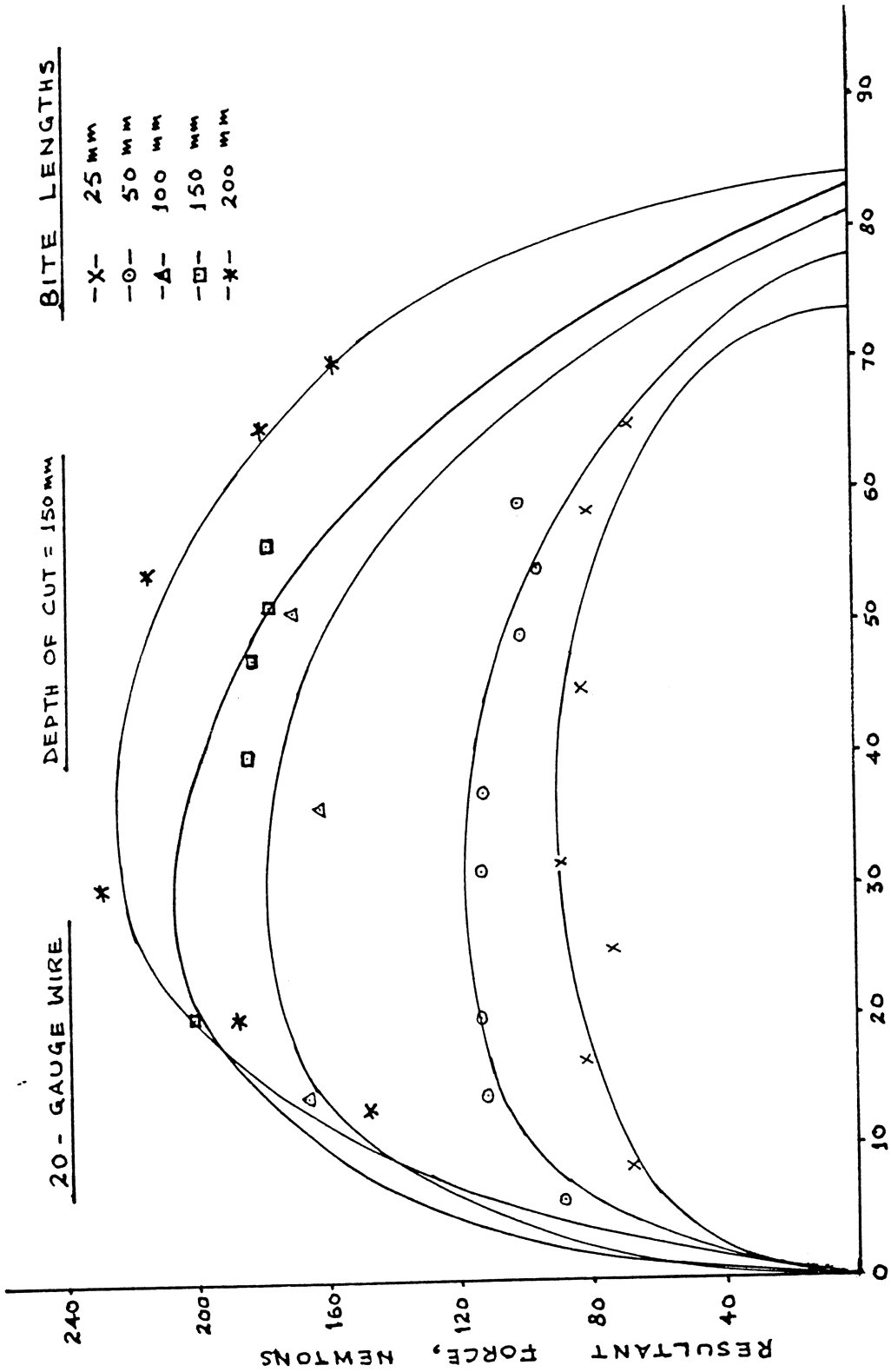

FIGURE 5·3 VARIATION OF RESULTANT FORCE WITH THE ANGULAR POSITION OF THE WIRE IN CUTTING A FULL SOIL SLICE AT DIFFERENT BITE LENGTHS FOR 150 MM DEPTH OF CUT

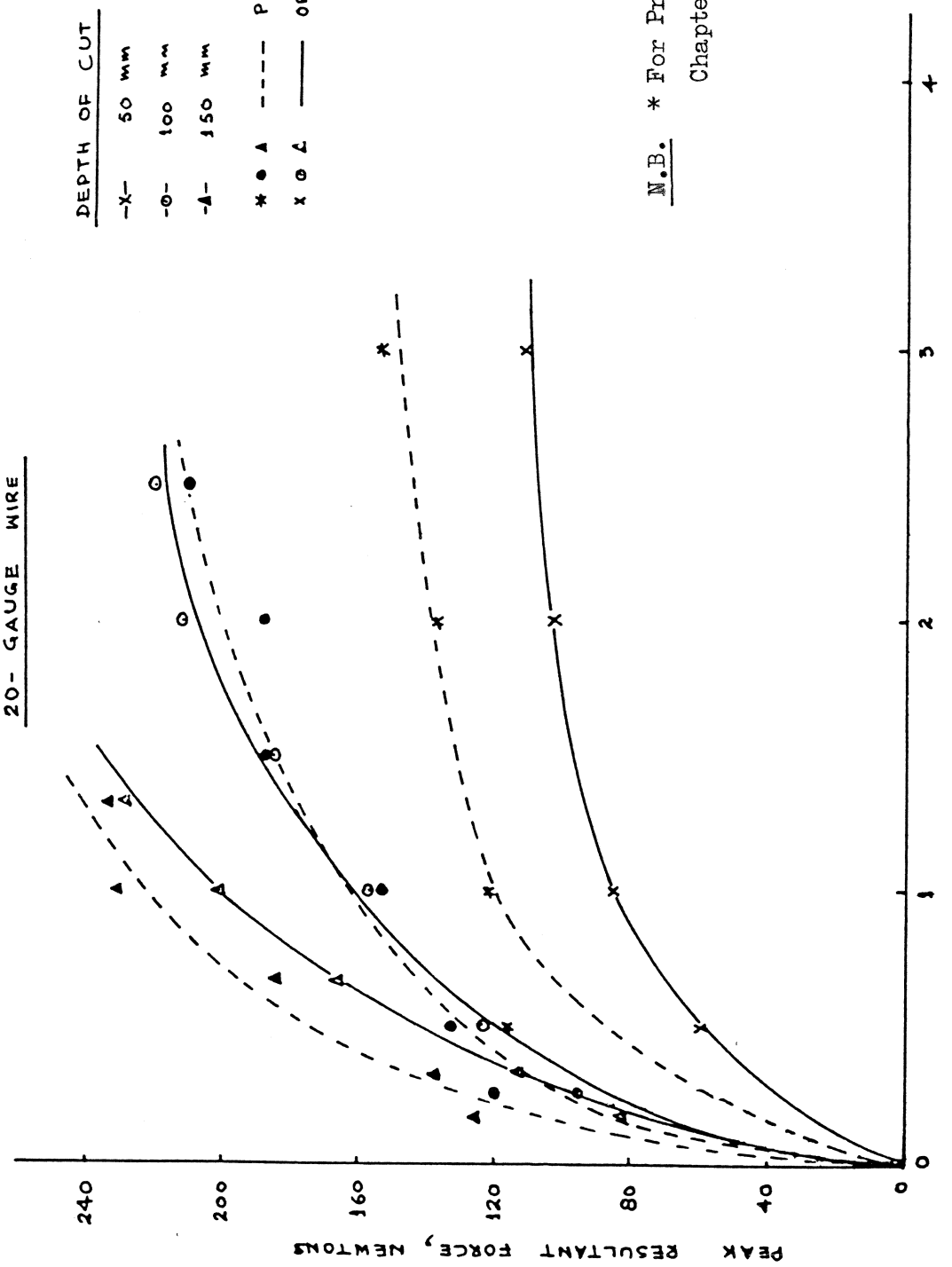

N.B. * For Predicted Results See Chapter - 8 and Table 8.1

FIGURE 5.4 OBSERVED AND PREDICTED VALUES OF PEAK RESULTANT FORCE IN CUTTING A FULL SOIL SLICE WITH 20-GAUGE WIRE AT DIFFERENT FETCH-RATIO

5.4.2 The Magnitude and Direction of the Radial Force

The variation of the radial force with the angular position of the wire in cutting a full soil slice is shown in Figure 5.5 for all the bite lengths at three depths of cut. The figure reveals that the magnitude of the radial force does not vary significantly with the angular position of the wire at different bite lengths. The magnitude of the radial force for the depths of cut of 100 mm and 150 mm is approximately in the same order and in correspondance with O'Dogherty (1964). However, for the small depth (50 mm), the radial force is approximately 30 - 40 % lower than the large depths. The reasons for this variation may be accounted for a comparatively lower value of local stresses when it operates close to a open free soil surface.

In a similar manner, it can be deduced from Figure 5.6 that at a particular depth of cut, the radial force at the peak resultant force remains almost constant with the change in bite lengths. A slight decrease in the radial force with increasing bite length may be due to comparatively large size of general shear plane and weight of the soil.

The net radial reaction always acts towards the centre of rotation of the rotor (-) irrespective of the depths of cut and bite lengths. It can be postulated that theoretically, there are two types of soil reactions acting on the wire simultaneously at a point of failure of a soil slice. The net radial reaction will be dependent upon the relative magnitudes of the resultant reactions due to general shear failure towards the free curved face of the slice and the local shear failure towards the undeformed soil. Therefore, for a particular depth of cut by increasing bite length, there may be a 'critical-fetch-ratio' after which the direction of net radial force may be positive. However, in the case of a wire the critical-fetch-ratio was not observed because of two possible reasons:

i. The mounting of the wire on the frame and its geometry of working in the soil is such that there is always a negative radial force due to the compressive soil reactions, even when there is no local

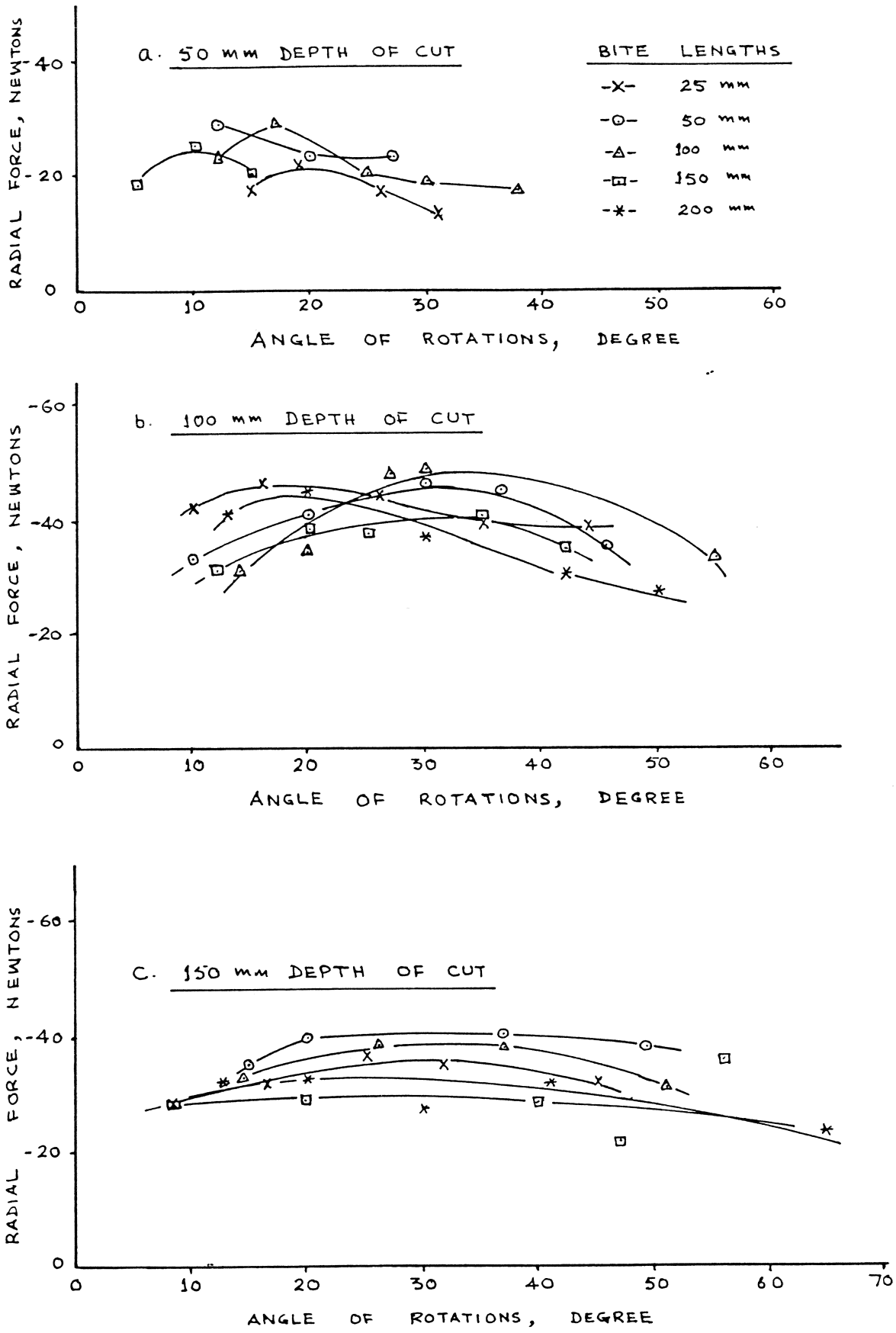

FIGURE 5.5 VARIATION OF RADIAL FORCE WITE THE ANGULAR POSITION OF THE WIRE IN CUTTING A FULL SOIL SLICE AT DIFFERENT BITE LENGTHS AND DEPTHS OF CUT

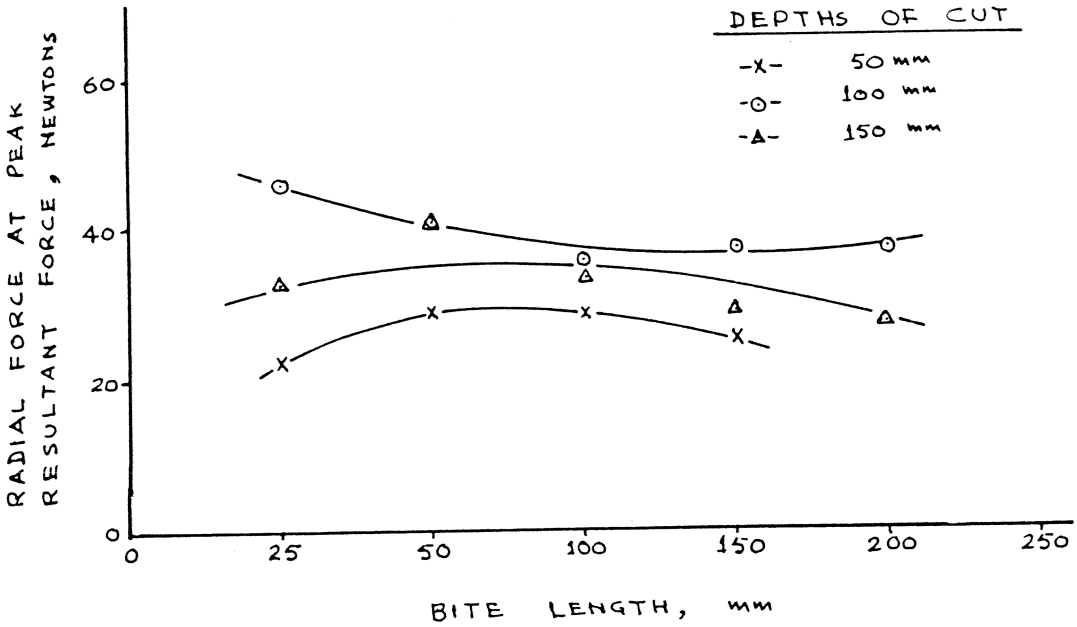

FIGURE 5·6 RELATIONSHIP BETWEEN THE RADIAL FORCE AT PEAK RESULTANT FORCE AND BITE LENGTH FOR THREE DEPTHS OF CUT (WIRE)

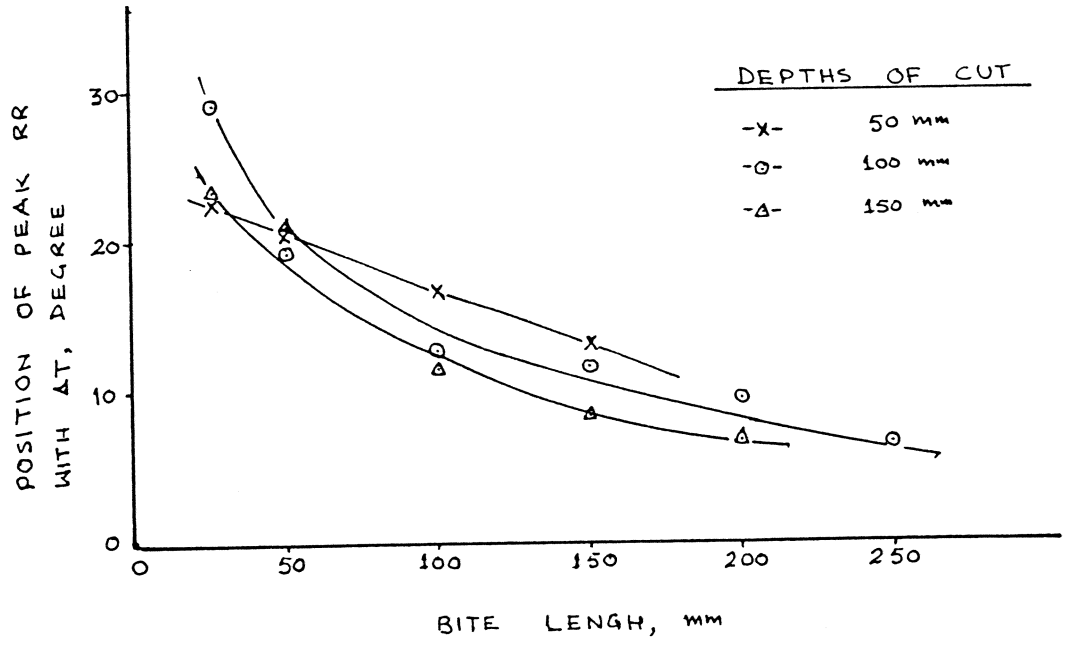

FIGURE 5·7 ANGULAR POSITION OF PEAK RESULTANT FORCE WITH TANGENTIAL FORCE AT DIFFERENT BITE LENGTHS AND DEPTHS OF CUT (WIRE)

shear failure of the soil. In practice, no wire is perfectly inextensible and inflexible due to which the wire will be always compressed towards the force measuring transducer which records a negative radial force.

ii. The total weight of the deformed soil can not rest on the wire. If at the place of the wire, an inextensible blade were used, the deformed soil may rest onto it which may produce a positive radial force.

There is a significant variation in the angular position of the peak resultant force with respect to the tangential force at increasing bite lengths as shown in Figure 5.7. It is evident from the figure that the inclination of the peak resultant force for a bite length of 25 mm is approximately 26^{o} whereas for the largest bite length of 250 mm the inclination is only approximately 6^{o}. This much variation in angular position of the resultant force is due to insignificant variation in radial force with fetch-ratios as seen in Figure 5.6. However, for any particular bite length, the variation in angular position of the resultant force was found to be insignificant among three depths of cut.

5.4.3 Cutting of the Artificial Clay Soil

A limited number of experiments were conducted at a constant depth of cut (100 mm) and bite lengths varying from 50 mm to 250 mm to test the validity of the force prediction model of a wire based on Meyerhof (1961) hypothesis. The clay soil blocks were prepared in a manner similar to the one used for sandy loam soil. However, when the block was inverted vertically in the soil bin, there was always a little bulging-out of the block which changed the width of cut from the standard width of 100 mm. This problem was alleviated by supporting the soil block until a cut was performed.

The results of the experiment shown in Figure 5.8a reveals that there is no significant variations in the magnitude of the resultant force either by increasing bite length or with the angular position

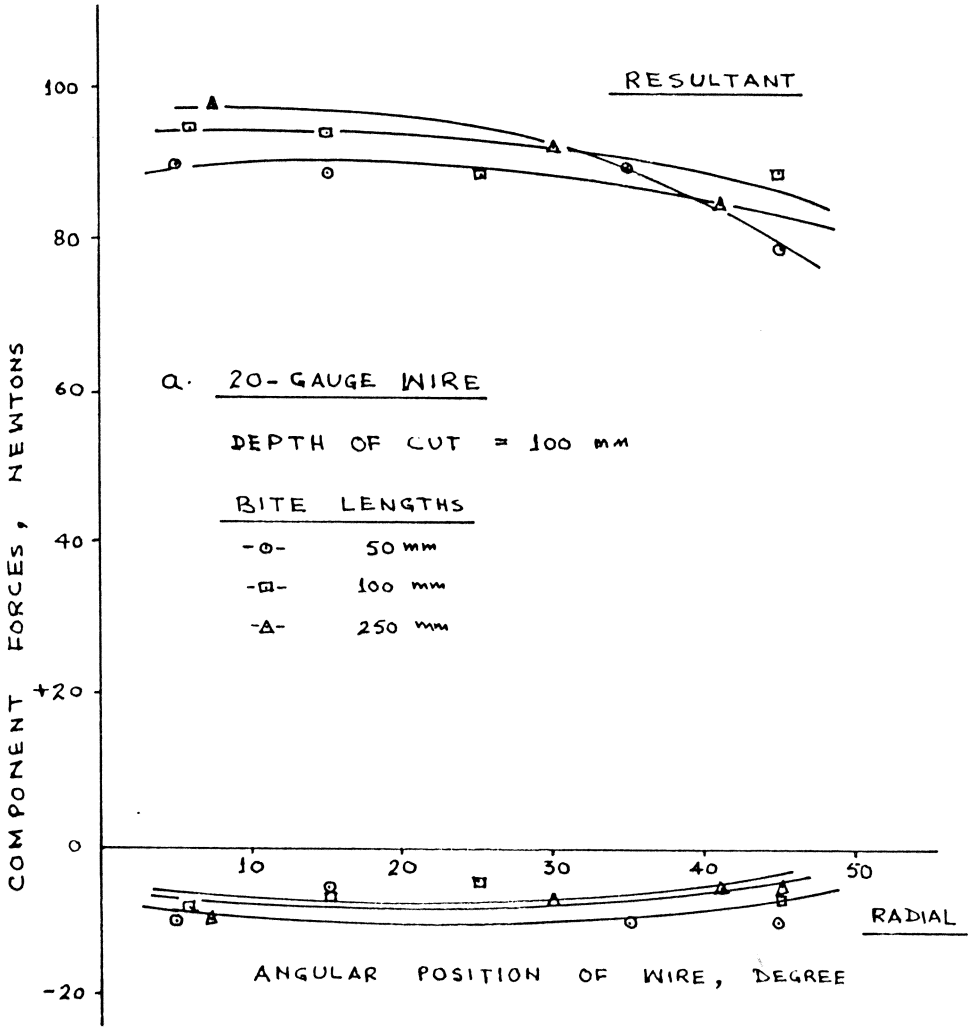

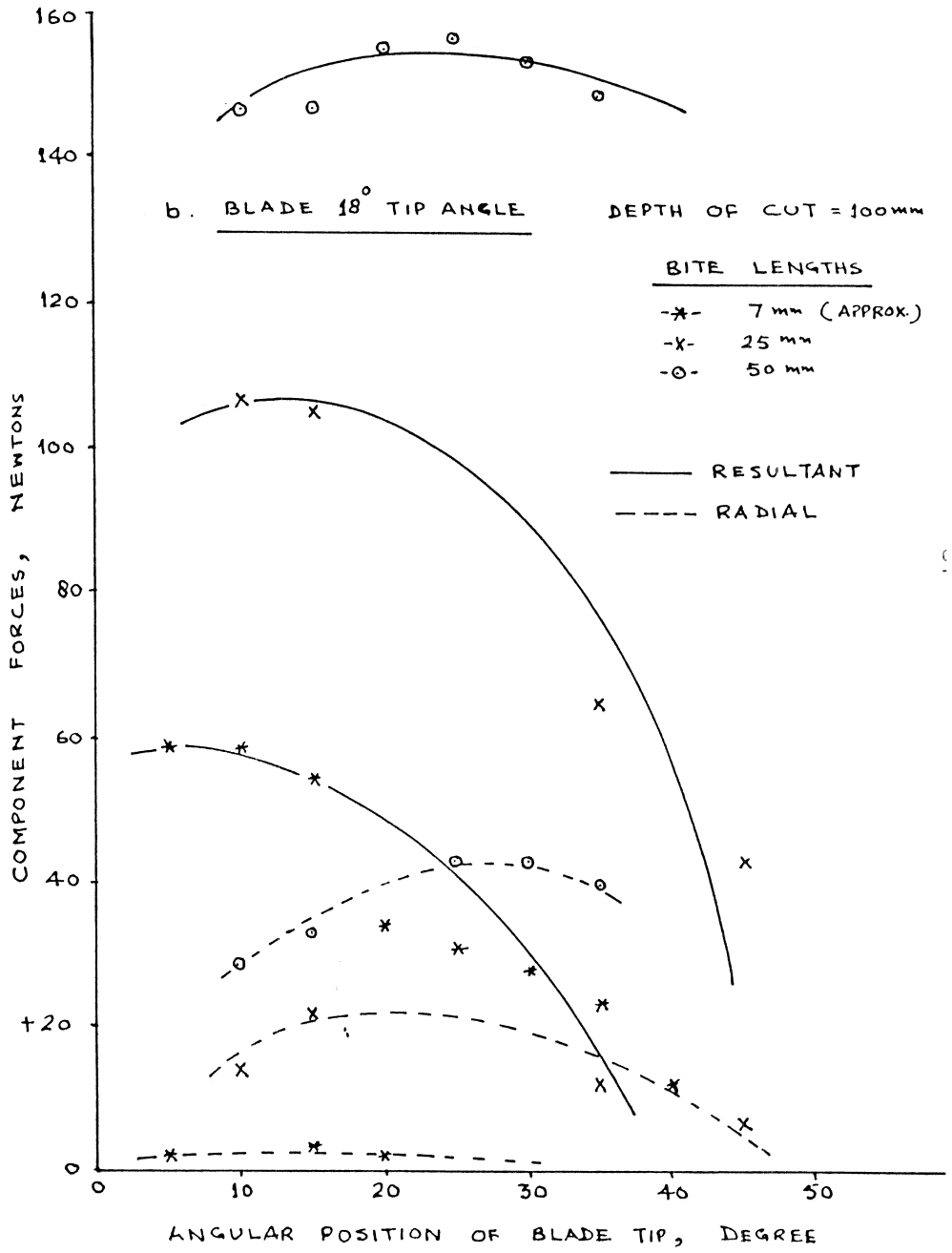

FIGURE 5·8 VARIATION OF COMPONENT FORCES WITH THE ANGULAR POSITION OF THE WIRE AND THE BLADE TIP IN CUTTING A FULL ARTIFICIAL CLAY SOIL SLICE

of the wire while cutting a full soil slice. Meyerhof (1951) reported only a slight increase in the base resistance of a footing with the depth in a purely cohesive media. Under these conditions, the skin friction was predominent compared to the base resistance. Since a wire may be considered as the base of a deep footing, a constant resistance with depth or bite length is inevitable according to Meyerhof observations.

It is also apparent from the Figure 5.8a that the magnitude of the net radial force remains invariably constant throughout the cutting of a slice for any fetch-ratio but remains always negative. Hypothetically, the mechanism of soil failure on both sides of the wire may be the same in contrast to a frictional soil where two types of failures takes place simultaneously at a particular position of the wire. The soil reactions on both sides of a wire in clay cutting should be in equilibrium and the net radial force should show a zero value. In this study, however, a net negative radial force of approximately 6 - 10 Newtons was recorded because of the compression of the wire due to the reasons outlined in Section 5.4.2 (i).

5.5 The Quasi-Static Soil Reactions Acting on a Blade

The process of soil cutting by a rotary tiller blade is cyclic. There is a sudden increase in the resultant force from the instant the blade enters in the soil. The position of the peak resultant force in a cutting cycle is dependent upon the design of the blade, working regime and soil physical conditions. According to Pavlov (1952) the resultant force increases to a maximum value by the time the rotor turned through an angle of 17^{o} to 21^{o} after the entry into the soil while Söhne (1959) reported a value around 10^{o} to 12^{o} but for a blade traversing in a circular trajectory. The findings of Bernacki (1962) were similar to Söhne for rigidly mounted blades working under real life situation, however, for the blades mounted on the rotor drum with intervening rubber insertions, the period of peak circumferential force was lengthened to 15^{o} - 20^{o} after the entry.

5.5.1 The Magnitude of the Soil Reactions

The relationship of the resultant force with the angular position of the tip after entry has been shown in Figure 5.9 for different bite lengths at three depths of cut. It is evident from the figure that while cutting a full soil slice, the resultant force increases rapidly upto a peak limiting value and drops down slowly to a zero value after approximately 40^{o} to 85^{o} of rotations of the tip depending upon the depths of cut and the bite lengths. The peak resultant force shows a clear peak which was absent in the case of soil cutting by a wire. It is also clear that the increase in the bite length at a constant depth of cut, changes the position of the peak forces in an increasing order. However, in general, the peak resultant force for bite lengths upto 150 mm was recorded after approximately 10^{o} of entry of the blade which increases to approximately 15^{o} for bite lengths greater than 150 mm.

The magnitude of the peak resultant force for the largest fetch-ratio is approximately twice the smallest ratio studied and is in correspondence with Pavlov (1952), Söhne (1959) and Surilov (1966). This, in fact, reveals that the specific resistance decreases with the increase in the fetch-ratio. The variations of the peak resultant force with fetch-ratios in Figure 5.10 shows that it does not increase in the same proportion but achieves a limiting value and thereafter becomes a plateau. This may be because of the reasons that the size of the largest shear plane in cutting a full soil slice increases at a decreasing rate with the increase in fetch-ratio.

The magnitude of the radial force at the point of peak resultant force varies significantly with the increase in fetch-ratio for all the depths of cut as shown in Figure 5.11. However, the negative radial force due to the 'tip-effect' remains almost constant with the bite lengths and depths of cut similar to the wire. The significant increase in radial force at large bite lengths may be attributed to the greater magnitude of the passive resistance force due to weight of the soil and general shear failure. In the similar manner, the angle of the peak resultant force to its tangential component shown in Figure 5.12, reveals that the inclination considered independently

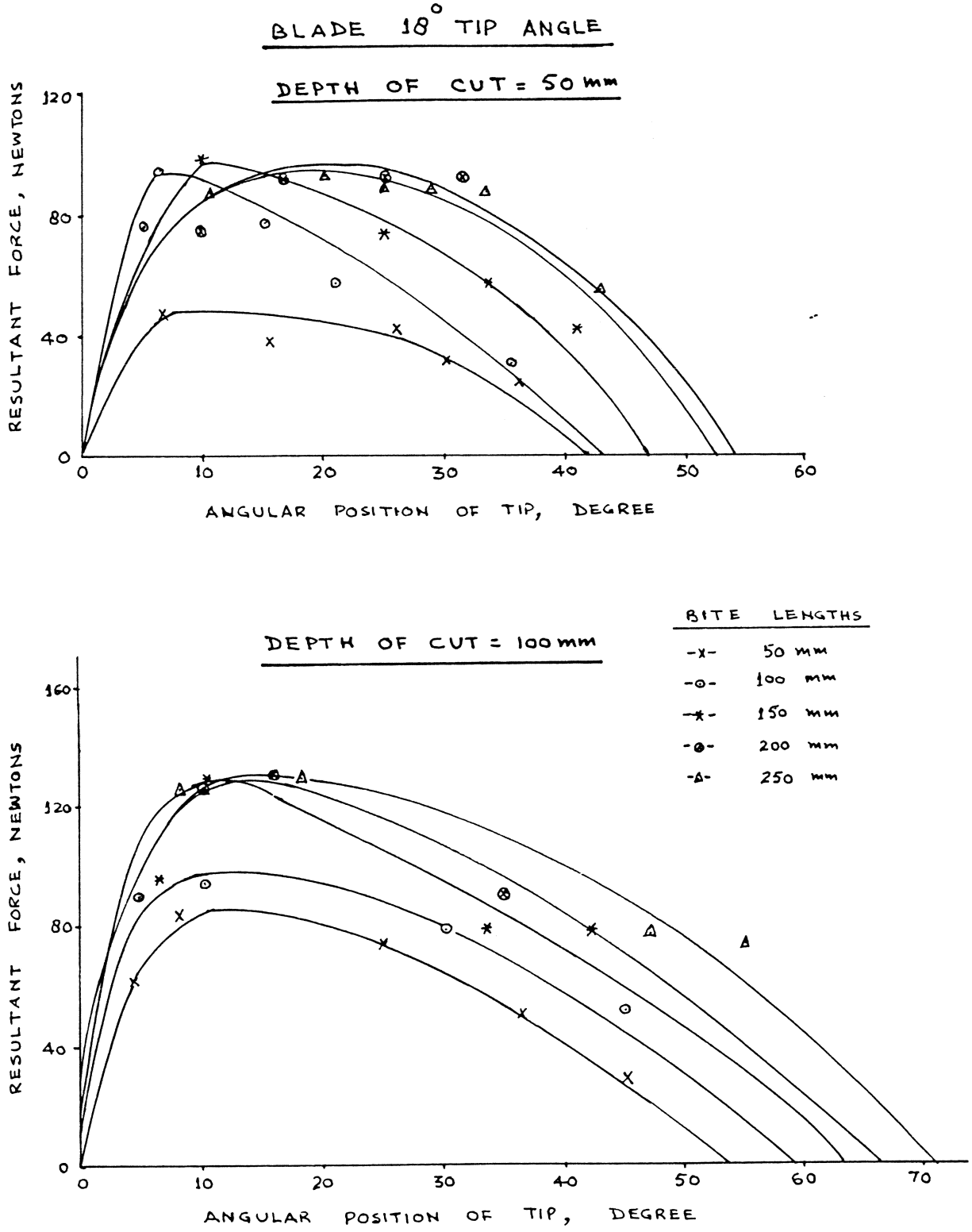

FIGURE 5.9a VARIATION OF RESULTANT FORCE WITH THE ANGULAR POSITION OF THE BLADE TIP IN CUTTING A FULL SOIL SLICE AT 50 mm AND 100 mm DEPTHS OF CUT

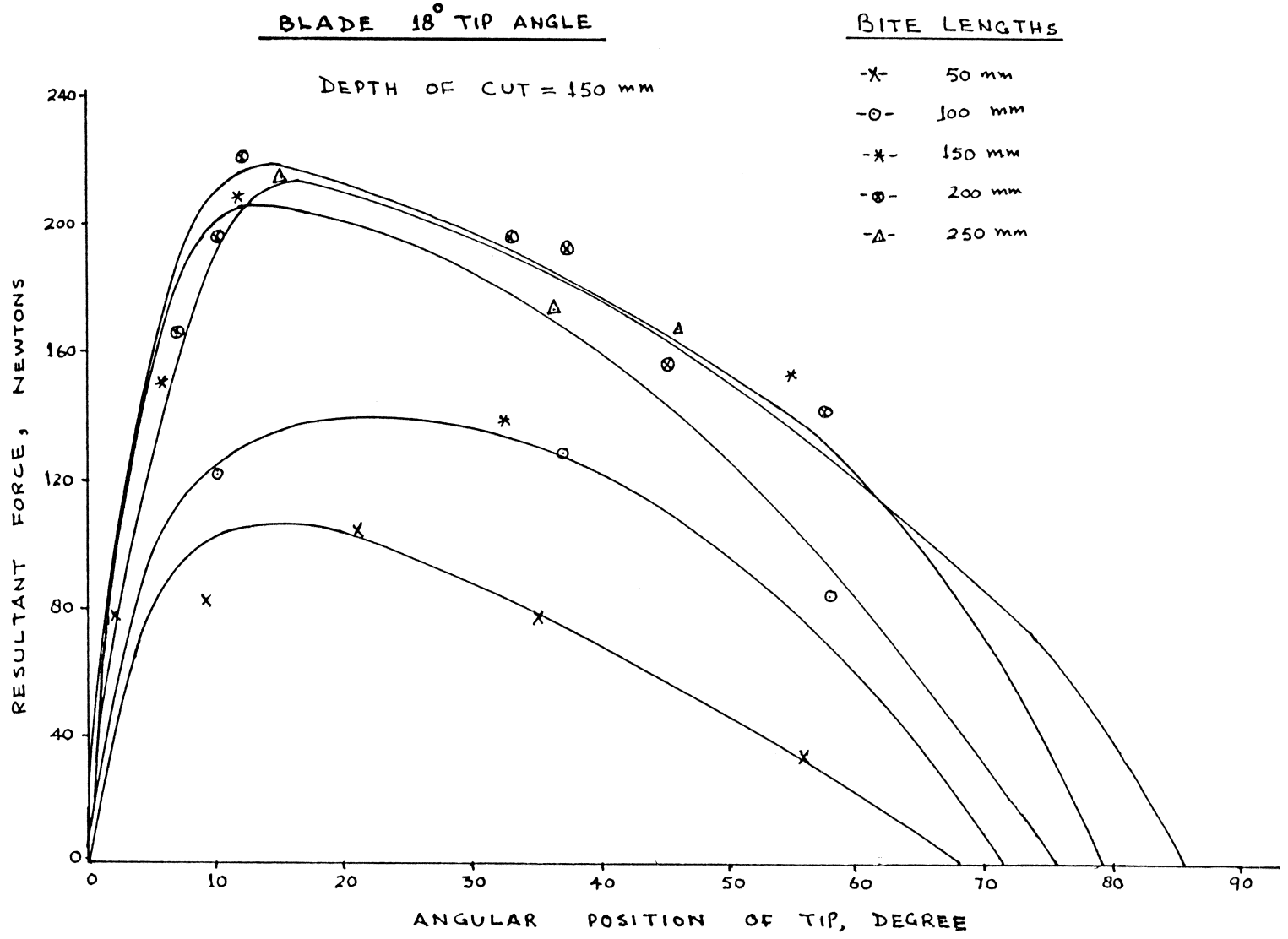

FIGURE 5.9b VARIATION OF RESULTANT FORCE WITH THE ANGULAR POSITION OF THE BLADE TIP IN CUTTING A FULL SOIL SLICE AT 150 mm DEPTH OF CUT

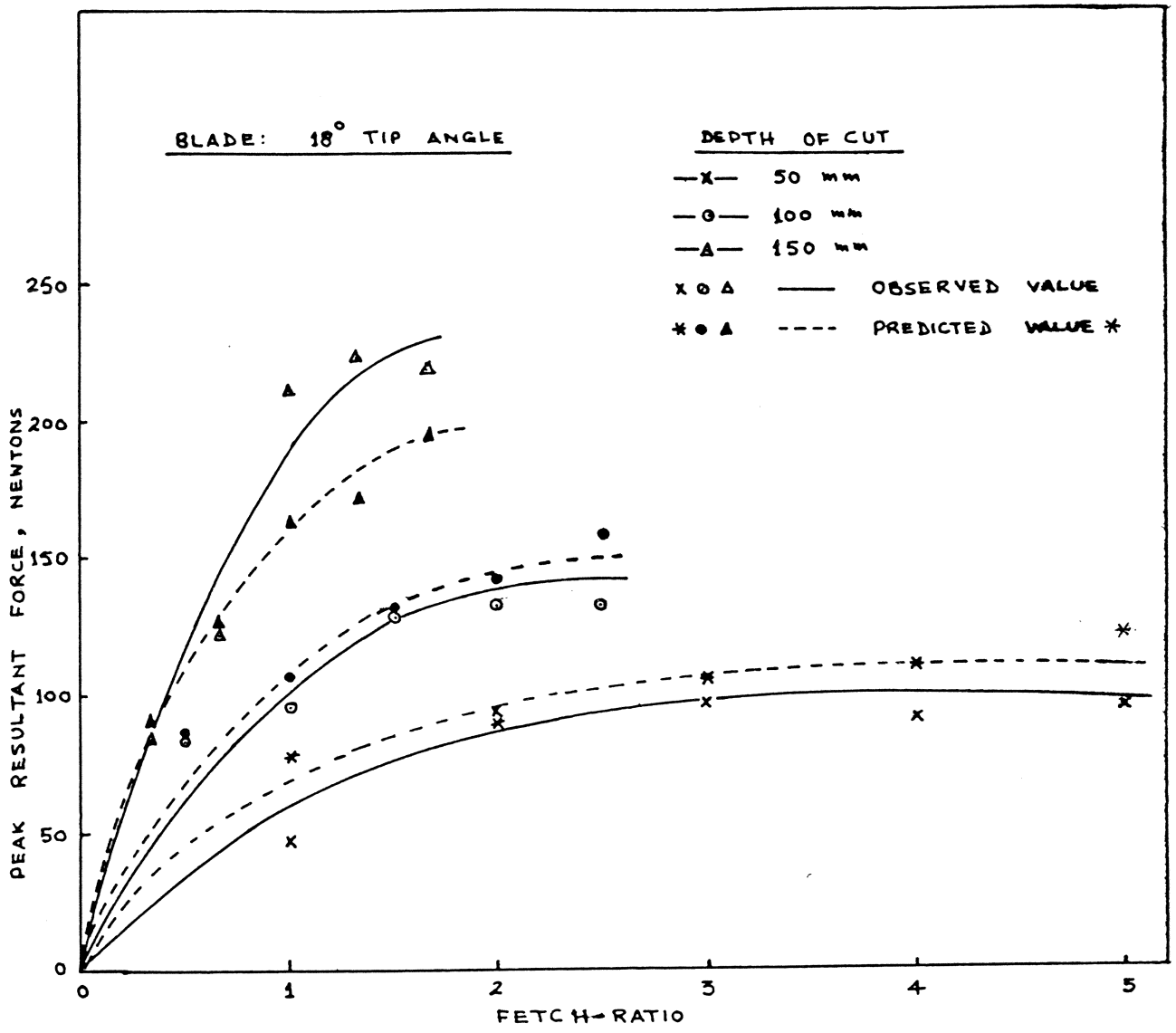

FIGURE 5·10 RELATIONSHIP BETWEEN OBSERVED AND PREDICTED VALUES OF PEAK RESULTANT FORCE IN CUTTING A FULL SOIL-SLICE AT DIFFERENT FETCH-RATIO (BLADE)

N.B. * For Predicted Values See Chapter-8 and Table 8.2

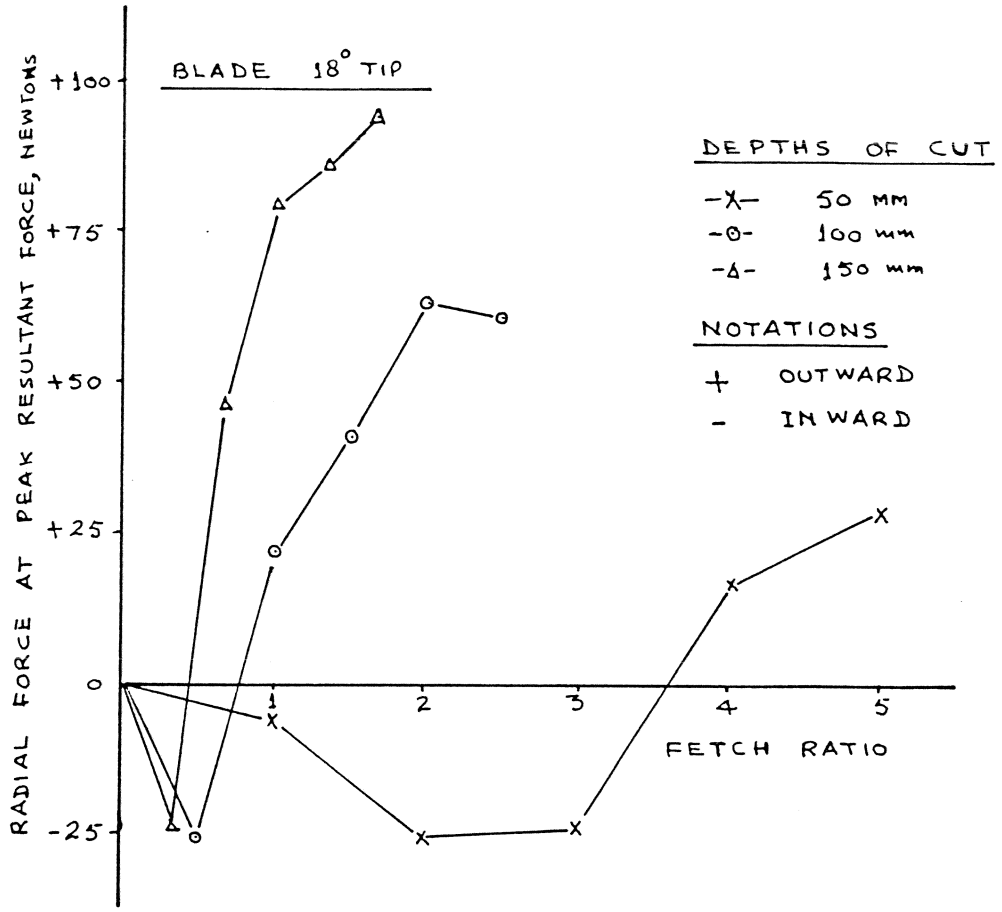

FIGURE 5·11 VARIATION OF RADIAL FORCE AT PEAK RESULTANT FORCE WITH FETCH-RATIO AT DIFFERENT DEPTHS OF CUT (BLADE)

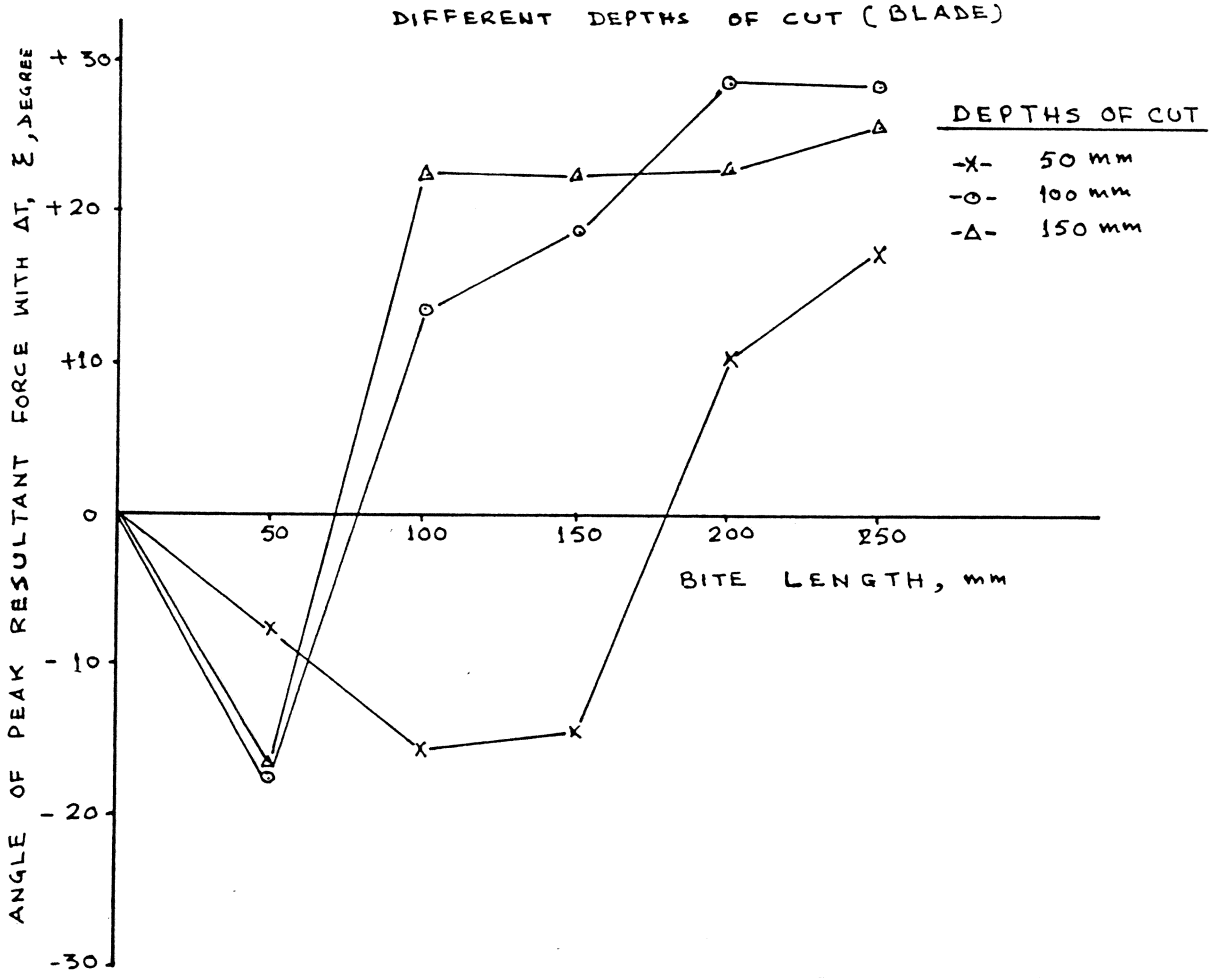

FIGURE 5·12 VARIATION IN ANGULAR POSITION OF PEAK RESULTANT FORCE WITH TANGENTIAL FORCE AT DIFFERENT BITE LENGTHS AND DEPTHS OF CUT (BLADE)

as the (+) and (-) sense does not change significantly with the bite lengths at different depths of cut. The reasons for the constant negative angle may be due to insignificant variations of the tangential force component in comparison to the large magnitude of the constant tip force. However, for the positive angle at large bite lengths the proportionate increase in the tangential force component is marginal in comparison to the radial force component.

5.5.2 The Direction and Position of the Resultant Force

The direction of the vertical force for the simple soil engaging tines and blades changes from upwards (-) to downwards (+) with the decrease in the angle of approach of the tool. The different values of approach angle have been quoted, at which this change in the direction occurs, depending upon the soil and tool variables by Payne and Tanner (1959), Dransfield et.al.(1964), Siemens et.al.(1965), and Godwin and Spoor (1977). An increase in the vertical reaction was reported by Krause (1973) with the increase in diameter of a rod weeder and with an increase in edge radius of a simple tine by Atkins and Harrison (1981). However, working with inclined tools at rake angles of 15^{o} to 45^{o} and varying edge radius, Harrison (1982) reported the net vertical reaction acting always downwards which was attributed to a comparatively large weight of the soil in contact with the blade.

Bernacki (1962) assumed the direction of the resultant force for the down-cut method of rotary tilling to be constant to permit the computation of the component forces from the torque records of the rotor. This, however, may not be true for the static component of the total force and in fact, varies with the fetch-ratios as shown in Figure 5.11. For any depth of cut, there is a 'critical-fetch-ratio' around which the radial force changes its direction from towards the centre of rotation (-) to outside the centre (+). In the present studies the 'critical-fetch-ratio' was observed at the 'fetch-ratios' 4:1, 1:1 and 0.66:1 for the depths of 50, 100, and 150 mm respectively. It is clear from the figure that at fetch-ratios less than critical, the radial force is negative and vice-versa and attributed to the reasons outlined in Section 5.4.2. It can also be noted from

Figure 5.13 and 5.14 that even at the 'critical-fetch-ratio' while cutting a full soil slice when the weight resting on the blade falls off around the end of cutting, the radial force again changes to negative. This indicates that the 'critical-fetch-ratio' is dependent upon the balance of the reactions acting at the front face and rear tip of the blade. It is evident that the rear tip force forms a small proportion of the cutting force at large bite lengths whereas at small bite lengths its contribution is significant.

The position of the resultant force in cutting a full soil slice at different bite lengths and depths of cut shown in Figure 5.13 and 5.14 reveals that it acts at the tip of the blade for fetch-ratios less than critical. However, for fetch-ratios greater than critical, the position of the resultant force is generally between the tip and half of the blade face and is in agreement with Harrison (1982) in the case of passive tools working at rake angles between 15^{o} and 45^{o}.

5.5.3 The Soil Reactions on a 10^{o} Tip Blade

A limited number of experiments were conducted with the 10^{o} tip angled blade to ascertain the 'tip-effect' phenomenon for a sharper blade with a clearance angle of 15^{o} instead of 7^{o} for the 18^{o} tip angled blade. The results of the experiments for two depths (100 and 150 mm) and three bite lengths (50, 100 and 200 mm) are presented in Figure 5.15 and 5.16. It can be deduced from the figures that the nature of variations of the resultant force is similar to the 18^{o} tip blade. The experiments with the 10^{o} tip blade were performed in a separate soil preparation, therefore, a direct comparison of the magnitude of the resultant forces with the 18^{o} tip blade may be unfair. The magnitude of the resultant force for a 10^{o} blade, however, is never greater than the 18^{o} tip blade.

The change in the direction of the radial force with increasing bite length is noticeable at both the depths of cut and is similar to the 18^{o} tip blade. The 'tip-effect' phenomenon with a 10^{o} tip blade, in fact, conforms with the effect noticed with sharpest metal machining tools of 0.005 - 0.03 mm edge radius. The reasons for high power

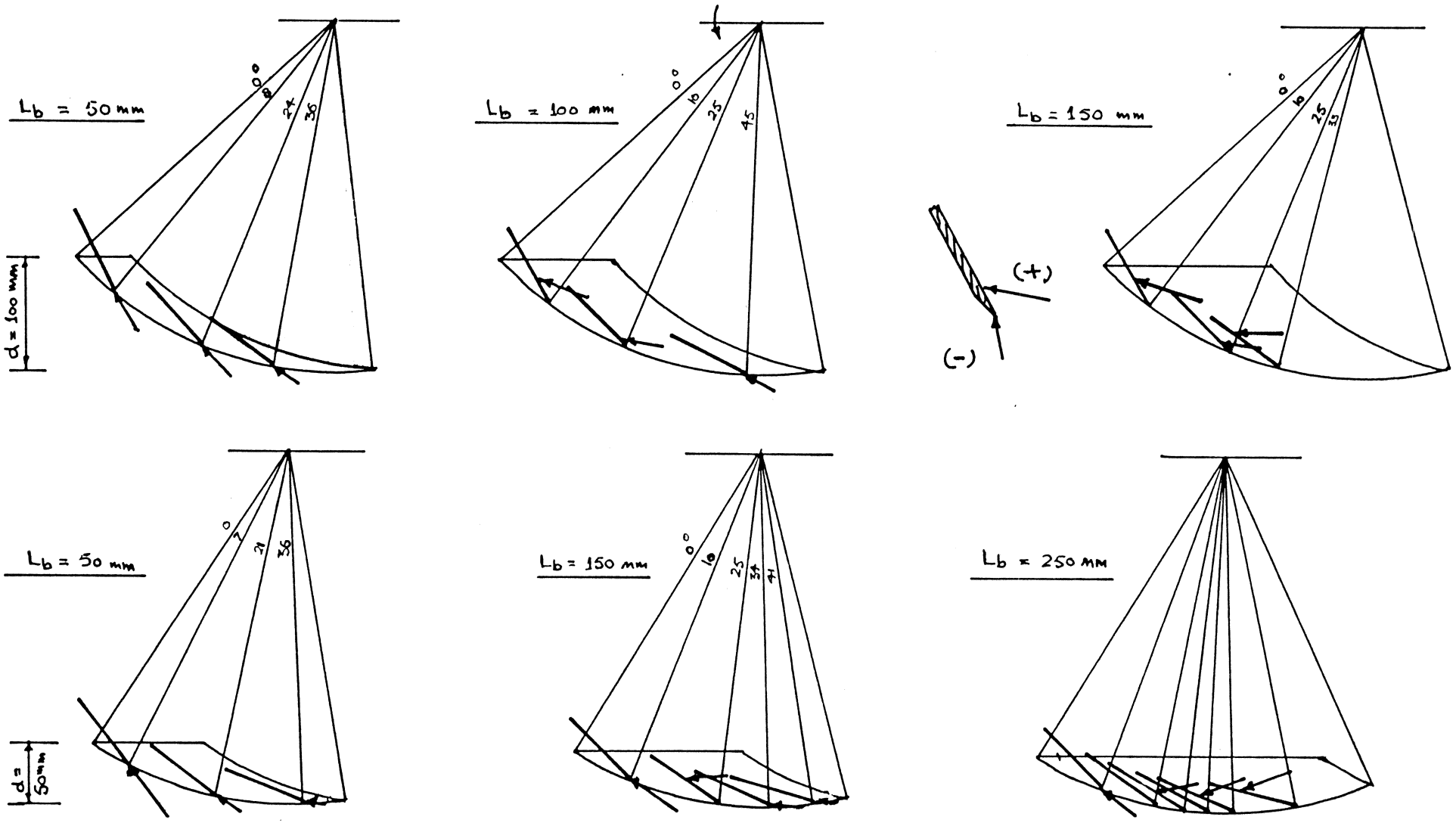

FIGURE 5·13 MAGNITUDE, DIRECTION AND POSITION OF RESULTANT FORCE ON THE BLADE (18° TIP) AT DIFFERENT BITE LENGTHS AND DEPTHS OF CUT

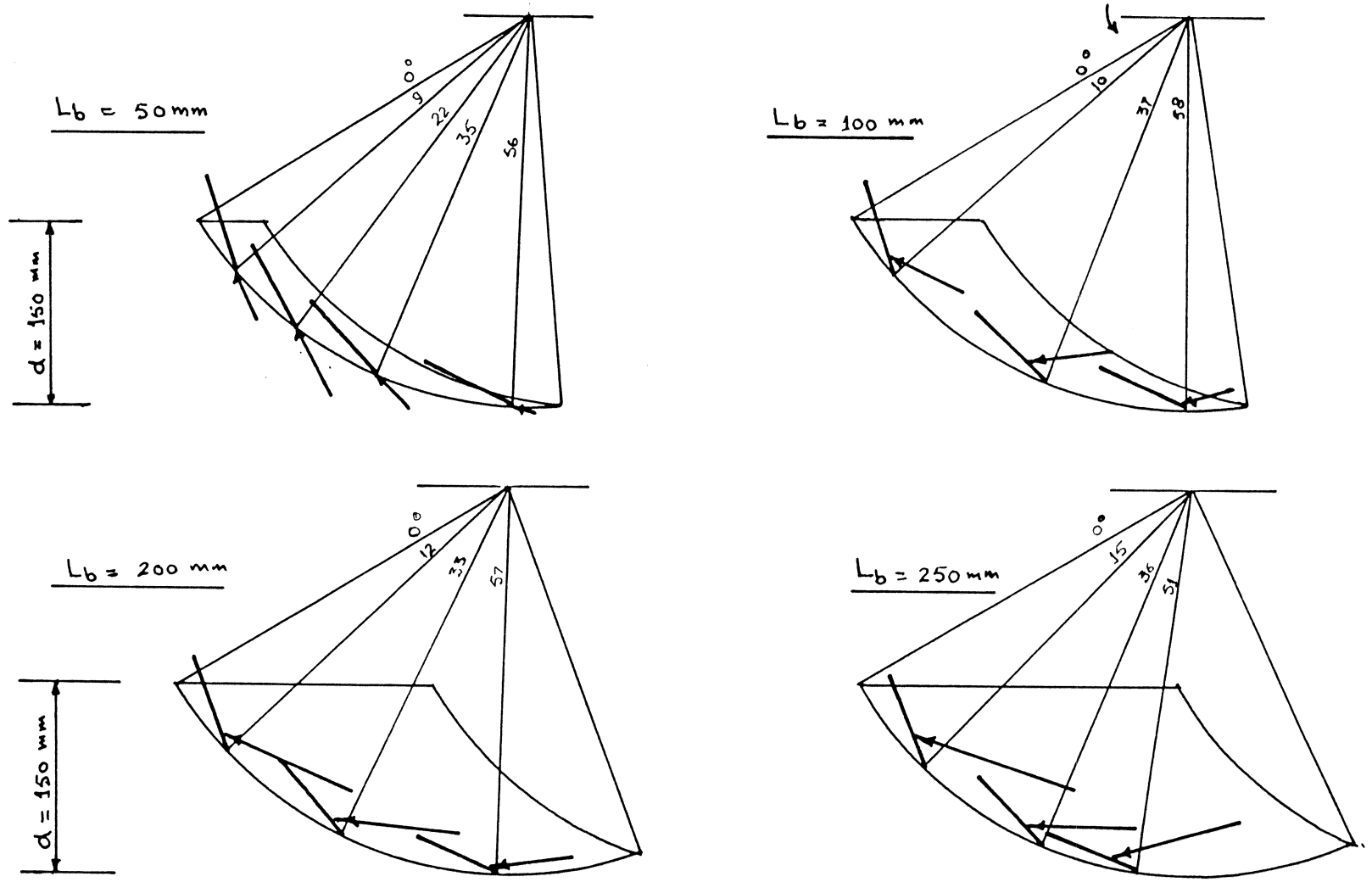

FIGURE 5.14 MAGNITUDE, DIRECTION AND POSITION OF RESULTANT FORCE OF THE BLADE (18° TIP) IN CUTTING A FULL SOIL SLICE AT DIFFERENT BITE LENGTHS AND

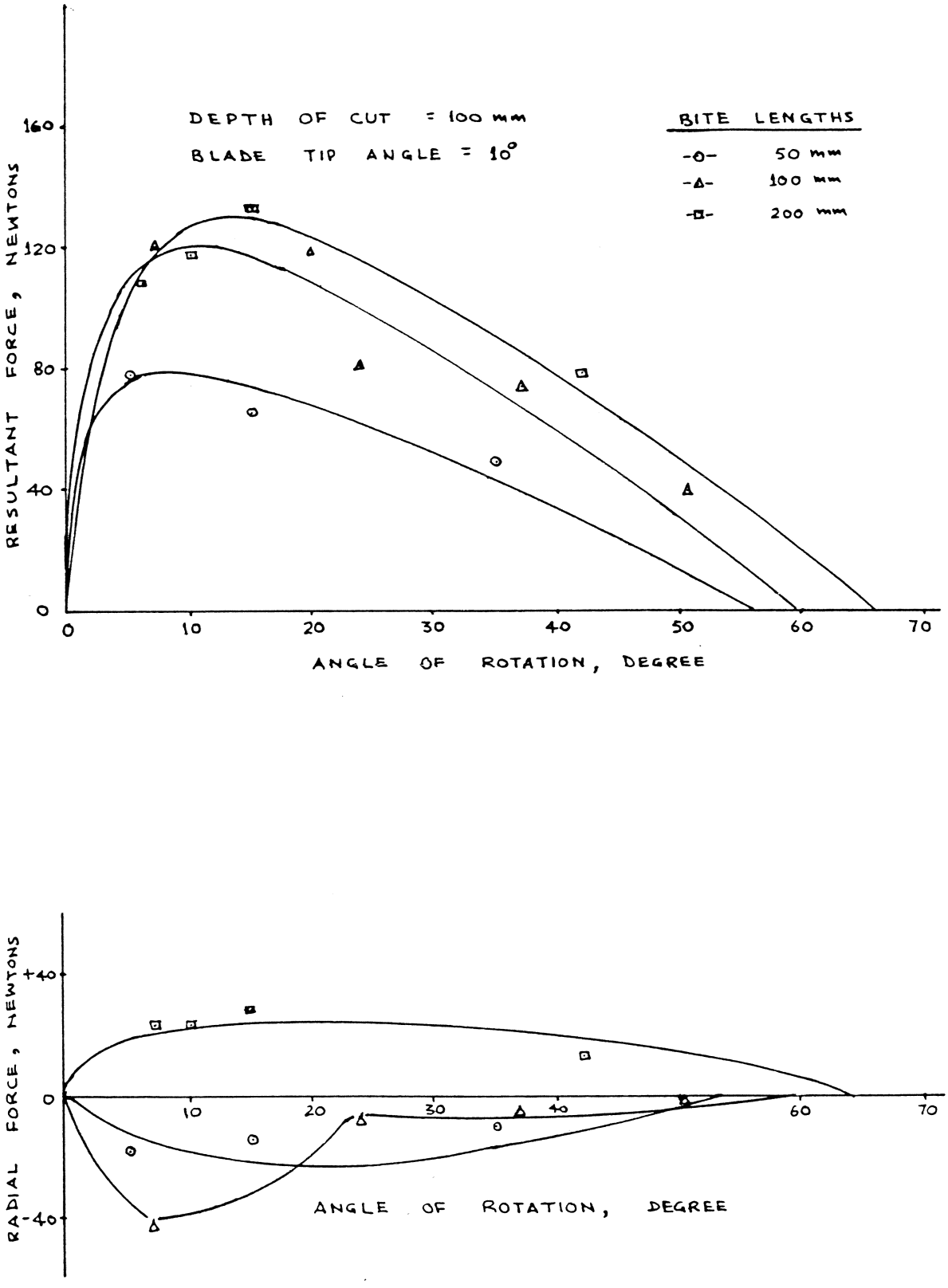

FIGURE 5.15 VARIATION OF RESULTANT FORCE AND RADIAL FORCE WITH THE ANGLE OF ROTATION OF THE BLADE TIP (10^{o}) FOR 100 mm DEPTH OF CUT

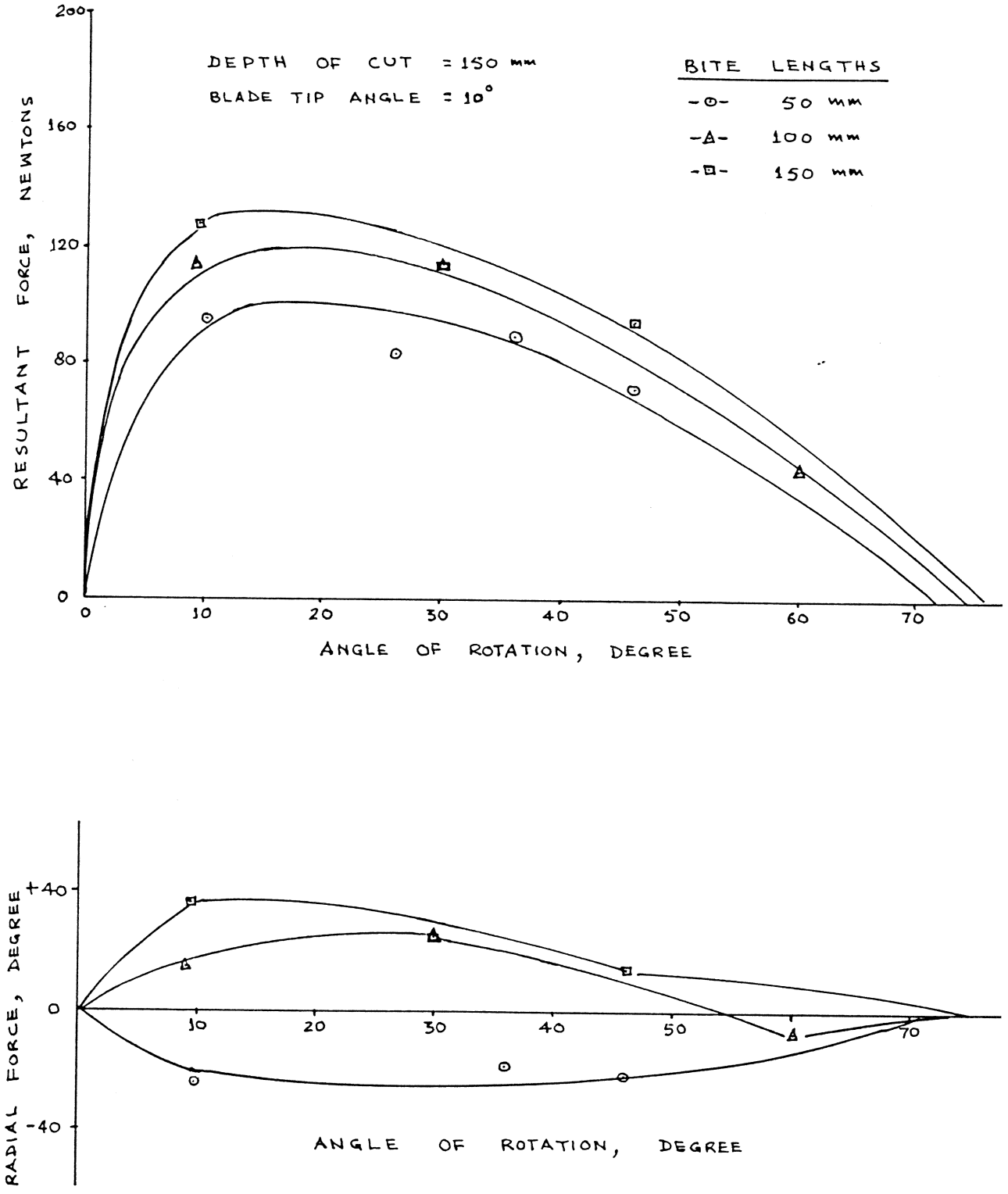

FIGURE 5·16 VARIATIONS OF RESULTANT FORCE AND RADIAL FORCE WITH THE ANGLE OF ROTATIONS OF THE BLADE TIP (10°) FOR 150 mm DEPTH OF CUT

consumption to remove a given volume of metal in processes such as grinding is believed to be due to the 'ploughing-force' at the bottom of the tools, Boothroyd (1964).

5.5.4 Soil Reactions in Cutting of Artificial Clay Soil

This set of experiments was conducted with an objective to record the variation of forces in comparison to a wire under similar conditions. The result of the experiment is shown in Figure 5.8b, for the 18^{o} tip blade cutting the soil at a constant depth (100 mm) and three bite lengths ranging from approximately 7 mm to 50 mm. The bite lengths greater than 50 mm were abandoned because of the difficulties in providing sufficient torque to turn the rotor.

It can be deduced from the Figure 5.8b that the component forces increase steeply with the increase in bite lengths in contrast to the wire which showed constant soil reactions with any combination of the bite lengths. The mechanism of soil failure under this extreme condition was less clearly visible. No distinct general shear plane failure was noticed, however, the soil adhered with the blade face while cutting the full soil slice. The increase in component forces may be attributed to the greater magnitude of the adhesive force as well as some tearing of the soil around the tip of the blade. It can be noticed that for a bite length of 50 mm, the peak resultant force occurs after 20^{o} to 25^{o} of blade entry when the full interface comes into contact with the soil. The radial force always remained positive even for a bite length of 7 mm and is due to the reasons outlined as above.

5.5.5 The Soil Reactions on a Blade with Vertical Axis of Rotation

5.5.5.1 Introduction

The soil reactions on a vertical blade were studied on a limited number of bite lengths and a single depth (100 mm) to obtain the preliminary information to test and extend the hypothesis developed for a blade with horizontal axis of rotation. Two sets of experiments

were planned according to the Figure 5.17. In both of the cases, the rotor traversed in a circular trajectory at a slow speed of 5 r.p.m. to minimize the acceleration forces. The geometry and mounting of the blade on the vertical rotor was exactly similar to the horizontal rotor except for the basic difference that the width of cut in the horizontal mode was equivalent to the depth of cut in the vertical mode.

In the first set of experiments, the rotor traversed within an arc less than a quarter of a circle such that a side cut (d') was equivalent to the actual depth of cut in horizontal rotor. The second set, however, consisted of a full half circle cut as in the actual working conditions. All the experiments were replicated three times to minimize any variations due to preparation of the soil block.

5.5.5.2 Experimental Results

The variations in the magnitude of the peak component forces with the bite length is shown in Figure 5.18 for the side cut (d') of 100 mm and 150 mm. The figures show an increase in force components with the increasing bite lengths which are similar to a blade with horizontal axis of rotation as shown in Figure 5.21. The experiments with both the axis of rotations were conducted on the same apparatus, however, the method of soil preparation was entirely different. The soil density achieved for the experiments with the vertical axis blade was approximately 2 % less. Therefore, a strict comparison between the two sets of data can not be made. A general comparison of Figure 5.18a and Figure 5.21 shows that at small bite lengths of 50 mm and 100 mm, there is a marginal difference between the component forces. However, for a bite length of 200 mm, the peak resultant force for a vertical axis blade is approximately 20 % greater than horizontal axis blade due to a significant variation in radial force component. This can be explained by the presence of the bottom failure plane and friction at the bottom end of the blade when operating in vertical axis. The angular position of the peak resultant force was similar in both the axis of rotation.

The results of the experiments in half a circle cutting are shown in Figures 5.19 and 5.20 for a vertical blade operating at a constant

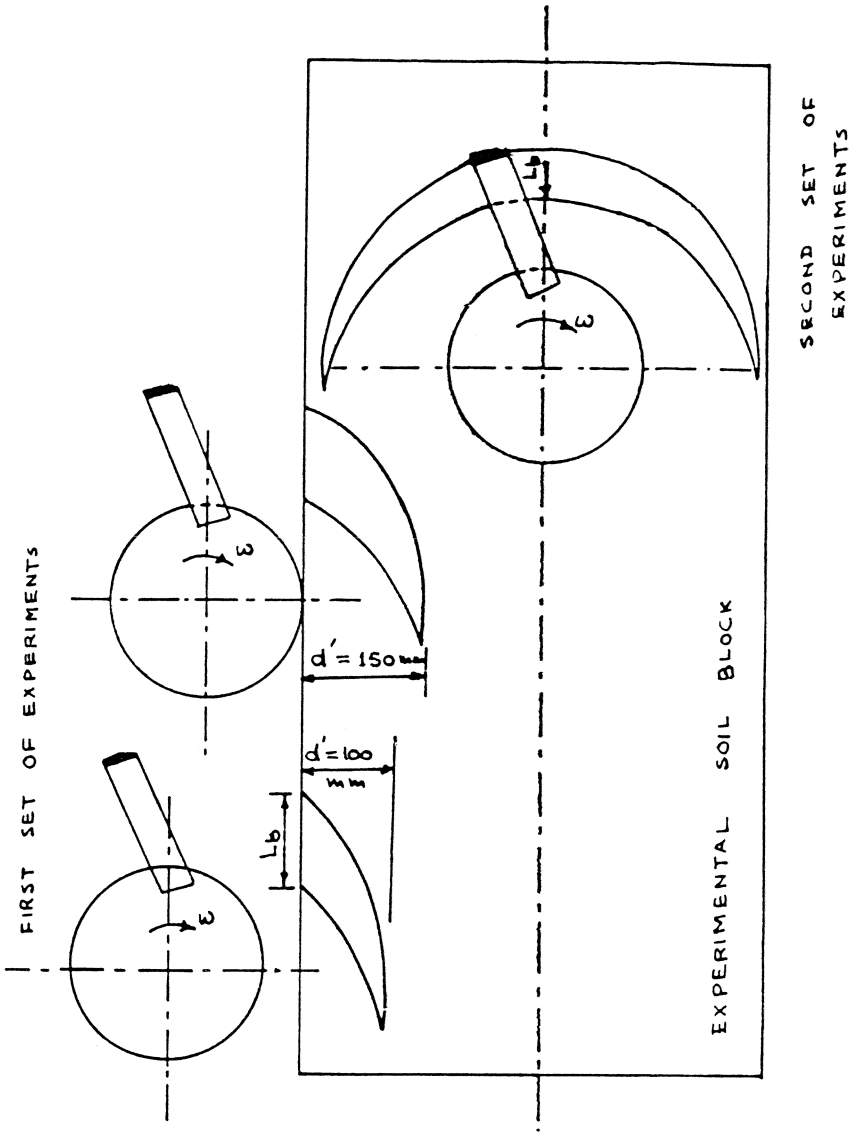

ROTOR SPEED = 5 rpm
DEPTH OF CUT = 100 mm

FORWARD SPEED = ZERO

TREATMENT NO.	SIDE CUT d', mm	BITE LENGTH Lb, mm	EXTENT OF CUTTING		REMARKS
			LESS THAN $\frac{1}{4}$TH OF CIRCLE	HALF CIRCLE	
T_{V_1}	100	50	YES	-	FIRST SET
T_{V_2}	100	100	YES	-	OF
T_{V_3}	100	200	YES	-	EXPERIMENTS
T_{V_4}	150	50	YES	-	
T_{V_5}	150	100	YES	-	
T_{V_6}	150	200	YES	-	
T_{V_7}	-	50	-	YES	SECOND
T_{V_8}	-	100	-	YES	SET
T_{V_9}	-	200	-	YES	OF EXPERIMENTS

FIGURE 5.17 EXPERIMENTAL PLAN FOR THE BLADE WITH VERTICAL AXIS OF ROTATION

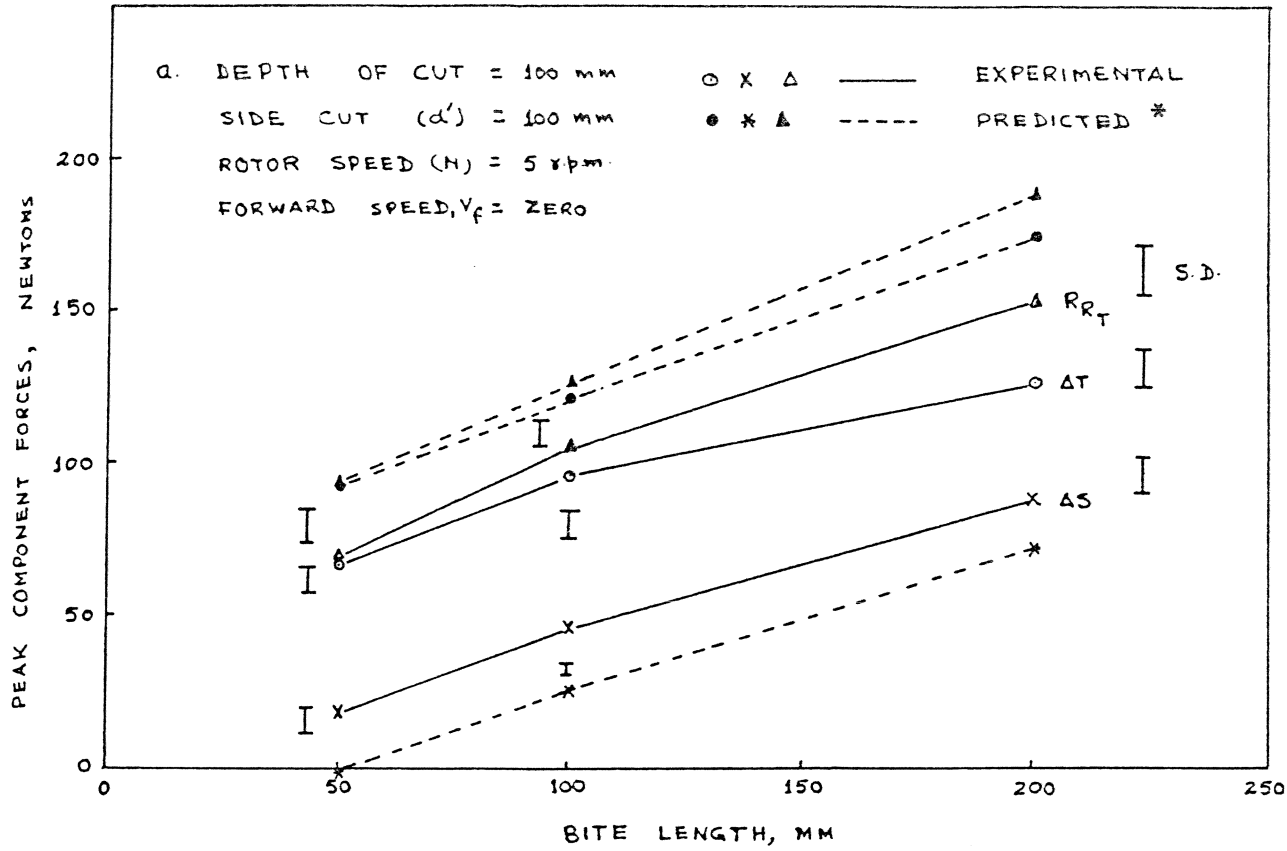

N.B. * For Predicted Results See Chapter-8 and Table 8.5b

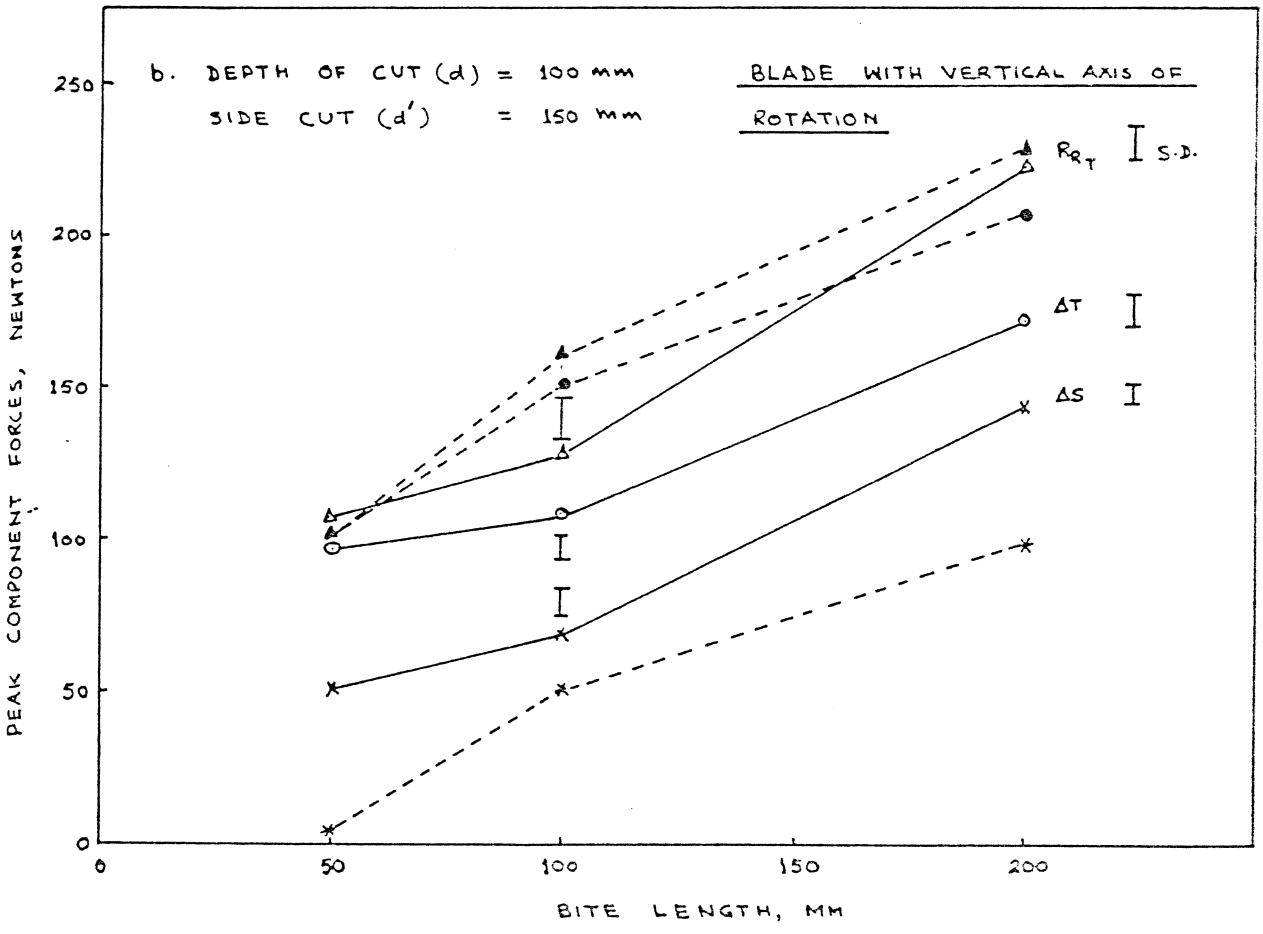

FIGURE 5.18 VARIATION OF COMPONENT FORCES AT DIFFERENT BITE LENGTHS AND DEPTHS OF CUT IN CUTTING A SOIL SLICE WITHIN AN ARC LESS THAN $\frac{1}{4}$TH OF A CIRCLE BY A BLADE WITH VERTICAL AXIS OF ROTATION

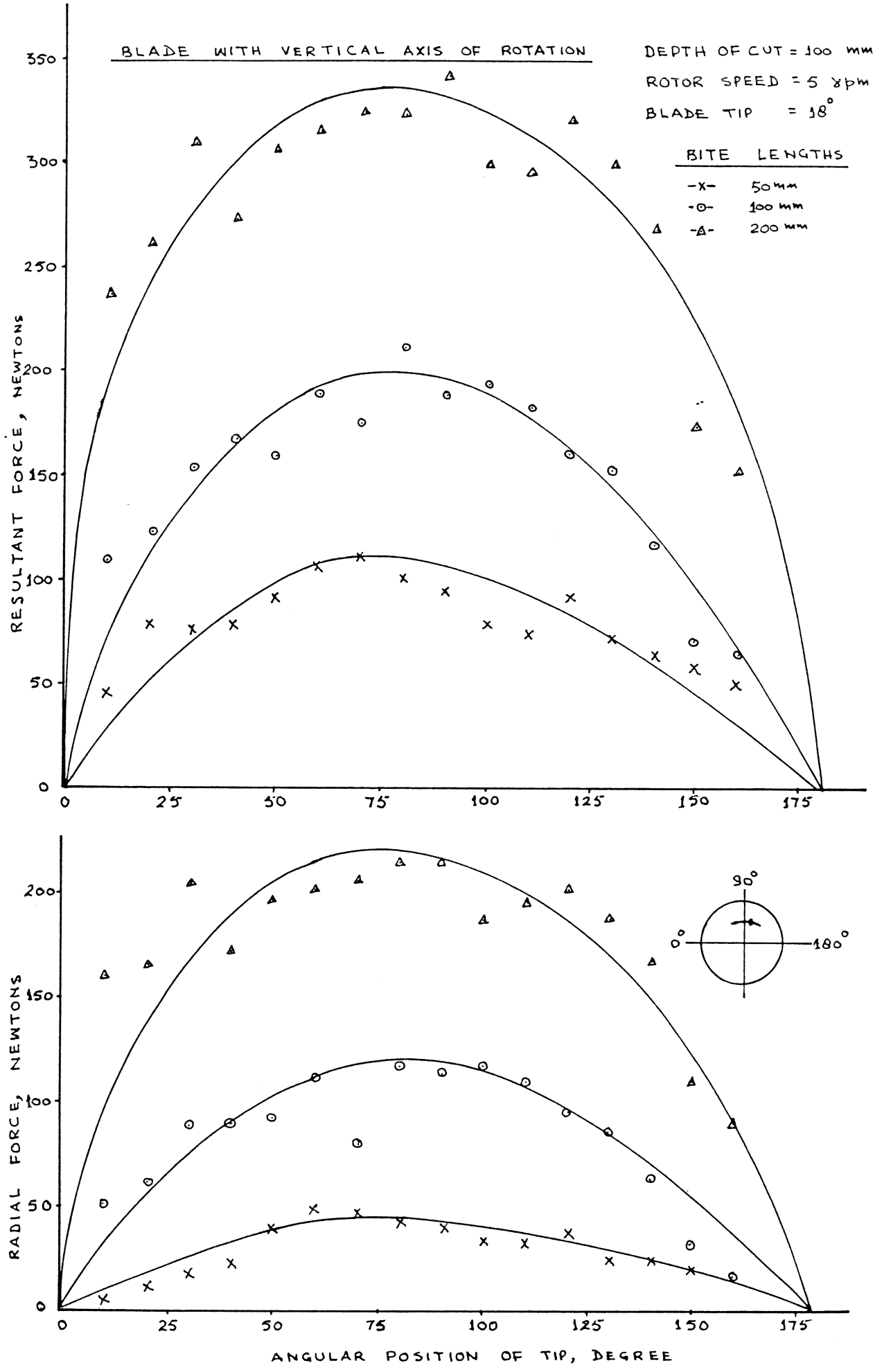

FIGURE 5·19 VARIATION OF RESULTANT AND RADIAL FORCES WITH THE ANGULAR POSITION OF THE BLADE TIP IN VERTICAL

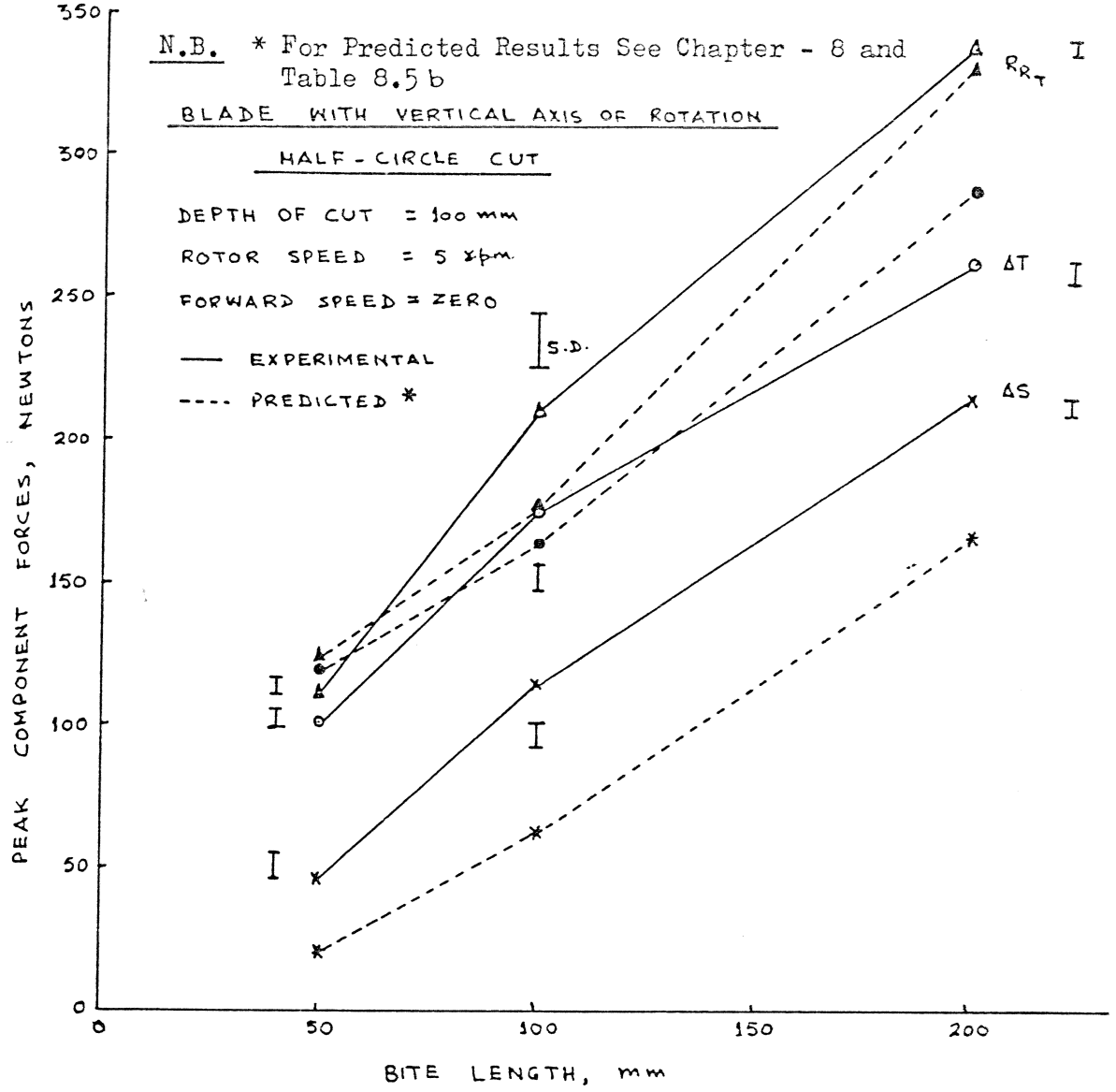

FIGURE 5.20 VARIATION OF PEAK COMPONENT FORCES AT DIFFERENT BITE LENGTHS IN CUTTING A SLICE IN A HALF CIRCLE BY A BLADEWITH VERTICAL AXIS OF ROTATION

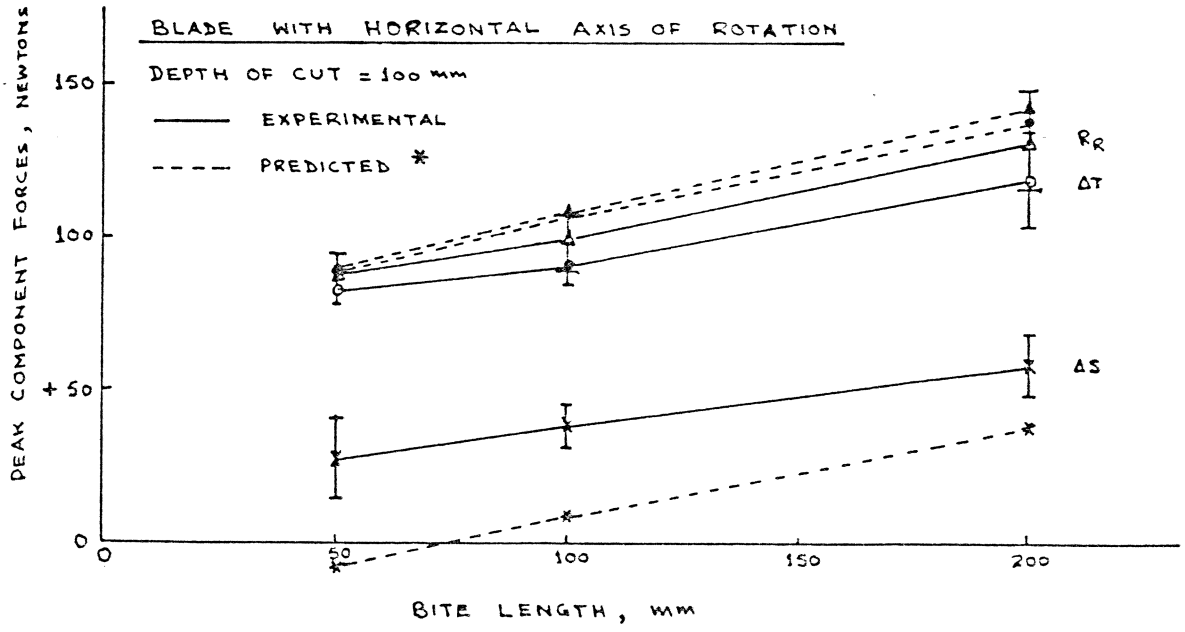

FIGURE 5.21 VARIATION OF COMPONENT FORCES WITH BITE LENGTH FOR A BLADE WITH HORIZONTAL AXIS OF ROTATION

depth (100 mm) and varying bite lengths of 50 - 200 mm. It can be deduced from the Figure 5.19 that the peak forces for different bite lengths occur before the central axis of a cut (90^{o}) at approximately $85^{o} \pm 5^{o}$ from the start of a cut. The slight asymmetry in the peak forces is due to the length of the shear planes being longer in the region prior to the central position. These shear planes develop at the shallowest angle with respect to the $(45 - \frac{\phi}{2})$ degree plane, which cut the free curved face. In general, the variation in magnitude of the forces with the angle of rotation of the blade at both sides from the peak is approximately constant. There is, however, an indication that the forces towards the end of the cut are lower than those at the start. The reasons for this may be due to deviation of shear planes from $(45 - \frac{\phi}{2})$ degrees with the major principal stress. The magnitude of the peak component forces in Figure 5.20 reveal increases in the radial and tangential forces with bite length. This is in contrast to the cutting by a blade with horizontal axis when after a limiting fetch-ratio, no increase in forces occur. This may be explained on the basis of increased size of the bottom shear plane with the bite lengths for a vertical axis blade which was absent in the case of a horizontal axis blade.

5.6 Conclusions

The following general conclusions can be drawn for the quasi-static forces acting on a rotating blade and a wire at different fetch-ratios:

i. The resultant force acting on a blade and a wire varied significantly with their angular position in cutting a full soil slice and the angular position of the peak force changed in an increasing order with fetch-ratios. The peak resultant force for a wire occurred approximately after 15^{o} of penetration for fetch-ratios less than at a bite length of 150 mm which increased to approximately 25^{o} for larger fetch-ratios. For a blade, the peak occurred earlier after 10^{o} and 15^{o} of the penetration in an order to that with a wire because of the effect of the blade interface.

ii. There was a critical-fetch-ratio around which the radial force changed its direction from towards the centre of rotation (-) to outwards (+) as the fetch-ratio was increased and is dependent upon the balance of reactions acting upon the blade interface and the tip.

iii. There was insignificant variation in the magnitude of the radial force with the angular position of a wire in cutting a full soil slice at all fetch-ratios. The radial force on a blade, however, varied significantly at fetch-ratios greater than critical because of the weight resting on the blade and size of the shear plane but remained insignificant at ratios less than critical due to a constant tip force.

iv. The peak resultant force acted at the tip of the blade for fetch-ratios less than critical. For larger fetch-ratios the position moved from the tip towards a position midway along the interface.

v. The component forces on a wire in artificial clay cutting remained almost constant with its angular position for all the fetch-ratios in contrast to the blade.

6. DETERMINATION OF THE DYNAMIC SOIL REACTION ON A ROTATING BLADE

6.1 Introduction

Chapter 5 described the static soil reaction forces on a blade and a wire as they rotated slowly into the soil in a circular trajectory. In the actual dynamic situations the blade traverses in a cycloidal trajectory and in addition to the quasi-static forces the dynamic forces are introduced due to the acceleration of the deformed soil slice. In the studies of the dynamic forces on a rotating blade, the effects of the λ-ratio i.e. $\frac{Vc}{Vf}$ - ratio, is an important variable parameter. Hence, for a given rotor radius λ-ratio can be varied either by changing peripheral speed (V_c) or forward speed (V_f). However, a disproportionate increase in either of the speeds in comparison to the other causes the back face of the blade to compress the undeformed soil and increases the resistance to manyfold.

This Chapter deals with (i) the static forces on the blade traversing in a cyloidal trajectory; (ii) the dynamic forces due to the acceleration of the deformed soil slice and (iii) the dynamic forces due to negative effective clearance angle, $(\delta_1 - \Delta\delta) \leq 0$, obtained by increasing forward speed at constant rotor speed.

6.2 Objectives

i. To study the effect of rotor speed on the dynamic force of resistance at a constant bite length and depth of cut with:

   (a) the zero forward speed of the rotor.

   (b) the varying forward and rotor speed as in the actual working conditions.

ii. To study the effect of λ-ratio by changing forward speed at constant rotor speed on the nature and magnitude of soil reaction forces for different depths of cut.

6.3 Experimental Technique

The experiments were conducted on the apparatus described in Section 3.7.2 with the following variables:

a. The Effect of Rotor Speed on Dynamic Forces

ii. The Rotor Traversing in a Circular Trajectory:
Blade tip angle = 18^{o}
Bite length, depth of cut and width of cut = 100 mm

Treatment No.	T_1	T_2	T_3	T_4	T_5	T_6
Rotor speed (N, r.p.m.)	5	10	20	40	80	120
Peripheral speed (V_c, m/sec)	0.161	0.322	0.645	1.290	2.58	3.87

ii. Varying Forward Speed and Rotor Speed for a Constant Bite Length:
Bite length, depth of cut and width of cut = 100 mm

Treatment No.	T_7	T_8	T_9	T_{10}	T_{11}	T_{12}
Forward speed (V_f, m/sec)	0.014	0.038	0.066	0.133	0.266	0.399
Rotor speed (N, r.p.m.)	4.38	11.54	20	40	80	120

The Effective Clearance Angle = $+2.3^{o}$ at the beginning of a cut (Table 6.2)

b. The Effect of Forward Speed at Constant Rotor Speed on the Dynamic Forces:

Depths of cut / Treatments (mm)			Forward speed (m/sec)	Rotor speed (r.p.m.)	λ-ratio	Bite length (mm)
50	100	150				
T_{13}	T_{17}	T_{21}	0.011	5	14.60	66.26
T_{14}	T_{18}	T_{22}	0.014	5	11.03	87.75
T_{15}	T_{19}	T_{23}	0.014	3	6.61	146.22
T_{16}	T_{20}	T_{24}	0.038	5	4.19	230.87

The sets of variables described at (a) were planned to study the effect of speed on the acceleration forces at the positive effective clearance angle, $(\delta_1 - \Delta\delta) > 0$, whereas the variables described at (b) were selected such that the acceleration forces are kept minimum with increasing forward speed to give conditions where the effect associated with the positive and negative effective clearance angle can be studied. The soil blocks were prepared according to the method described in Section 3.9.3. Each treatment was replicated three times and randomised in the blocks to minimize any variation due to the soil preparations.

6.4 The Effect of Rotor Speed at Constant Bite Length

6.4.1 Introduction

An important parameter affecting the magnitude of the reaction on the rotating blade is the cutting speed because of a definite portion of the soil slice is cut-off and accelerated at approximately peripheral speed of the blade. The increase in the resistance of a tiller blade has been found proportional to the square of the circumferential speed by Zhuk (1952), Bernacki (1962), Lisunov (1968) and Ahmad (1980). According to Bernacki, the dynamic force of resistance appears as a result of the impact of the blade on the soil at the initial instant of cutting. Dalin (1950) working at slow cutting speeds (2 - 4 m/sec) pointed out that resistance to cutting increases at a slower rate than the cutting speed and found an increase of 10 % in the resistance to cutting for a twofold increase in the cutting speed.

The cutting resistance of an analogous passive tillage tool such as a mouldboard plough is dependent upon the type of soil, amount of soil, trajectory of deformed soil and working speed. The effect of speed on the resistance to motion of a mouldboard plough has been widely studied and quantitatively established. Söhne (1956), and Gill and Vanden Berg (1968) reported an increase in draught force proportional to the square of the speed which is attributed primarily to the intertia forces of the mass of soil. Reaves and Schafer (1974), however, postulated the dependance of draught on speed between a linear and square relationship. The influence of speed on the interaction between narrow tines and soil is less clear. There are conflicting opinions reported both as to the magnitude of the effect of speed and on the relationship between draught of tine and speed. Dransfield et.al.(1964) detected no change in draught with speed for three out of four soils similar to Payne (1956) who observed a rise of only 20 - 30 % over a speed range of 0.2 to 2.7 m/s. In contrast, Siemans et.al.(1965), and Luth and Wismer (1969) observed a 100 % increase of draught in the range of 0.2 - 0.9 m/sec and 0.2 - 2.5 m/sec respectively.

6.4.2 Experimental Results

Observations were made on the two important aspects of soil cutting under dynamic situations as described below:

6.4.2.1 The Mechanism of the Soil Failure

The failure of a soil slice was observed on the video film monitor alongwith the positions of peak forces in cutting a full soil slice due to development of the shear planes obtained on the force records.
The observations have revealed that as the blade enters into contact with the soil, there is a sudden rise in the forces due to impact of the cutting edge. The blade penetrates to approximately 10^{o} of rotation during which period an elastic - plastic deformation occurs. Soon after, a crack in the form of a shear plane is developed and its magnitude is recorded as the first peak around 15^{o} of penetration on the force record as shown in Figures 6.1 and 6.2. After the first peak the forces

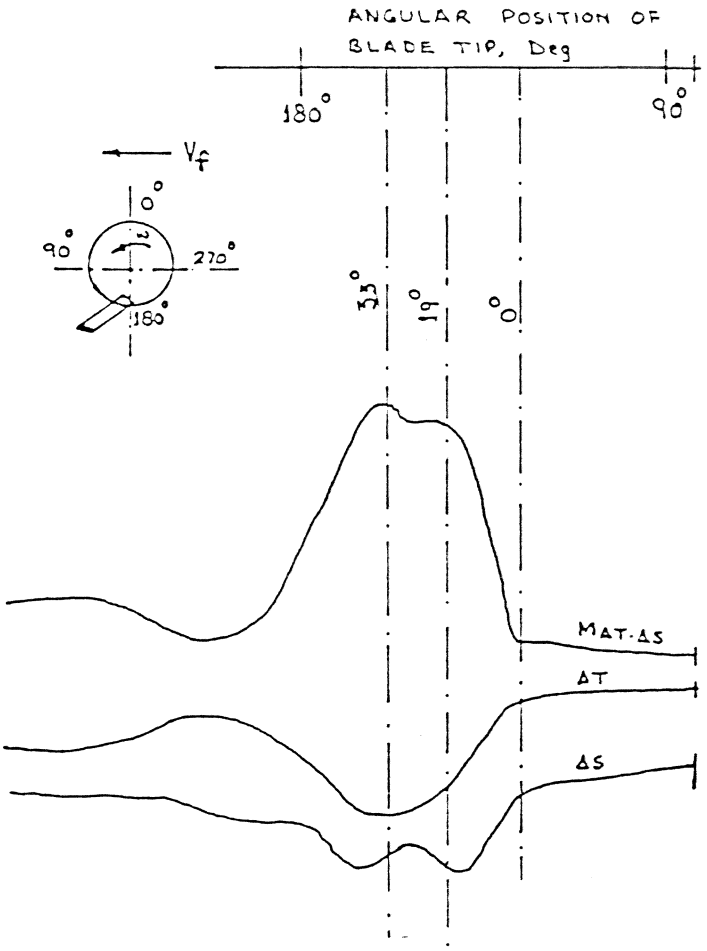

TREATMENT NO· T_5 :

ROTOR SPEED = 80 r.p.m.
FORWARD SPEED, V_f = ZERO
$L_b = d = w$ = 100 mm

COMPONENTS		FIRST PEAK 19 Deg	SECOND PEAK, 33°	CONSTANTS
ΔT	Cm	1·0	1·35	121·21 N/Cm
	N	121·21	163·63	
ΔS	Cm	+0·95	+0·90	77·66 N/Cm
	N	+73·77	+69·89	
$M_{\Delta T \cdot \Delta S}$	Cm	1·80	3·10	10·81 N-m/Cm
	N-m	19·45	33·51	
R_{RT}	N	141·89	177·93	

FIGURE 6·1 VARIATION OF COMPONENT FORCES WITH ANGULAR POSITION OF THE BLADE TIP AT 80 r.p.m. FOR CIRCULAR TRAJECTORY

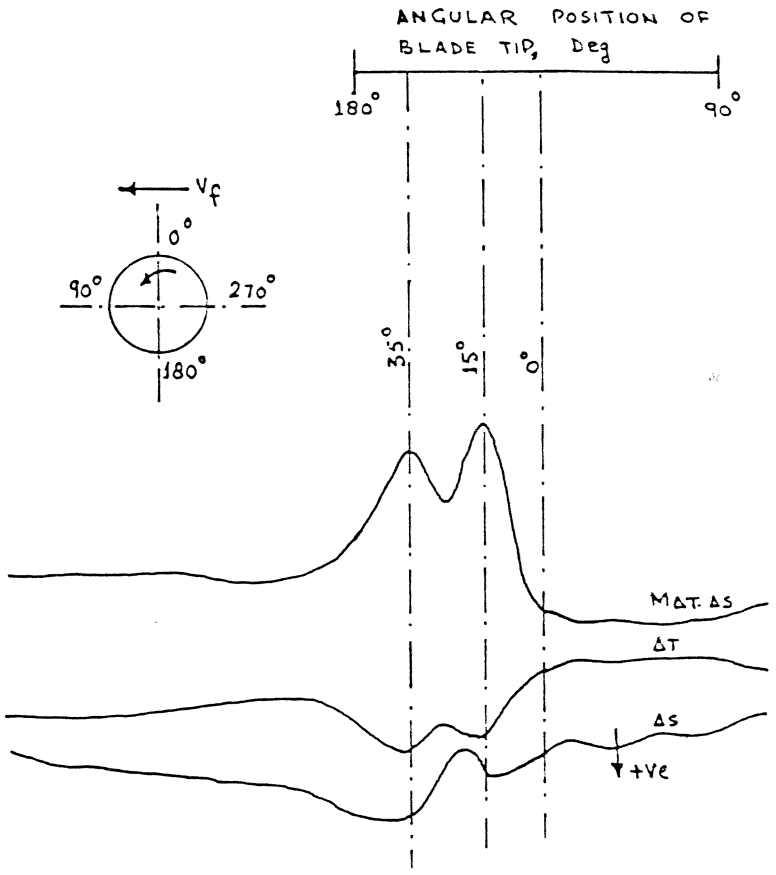

TREATMENT NO. T_{11}

ROTOR SPEED = 80 r.p.m.

FORWARD SPEED, Vf = 0.26 m/sec

Lb = d = w = 100 mm

COMPONENTS	FIRST PEAK AT 15°	SECOND PEAK AT 35°
ΔT, N	96.96	109.09
ΔS, N	+23.30	+46.60
$M_{\Delta T.\Delta S}$, N-m	27.56	21.62
R_{RT}, N	99.72	118.62

FIGURE 6.2 VARIATION OF COMPONENT FORCES WITH ANGULAR POSITION OF THE BLADE TIP AT 80 r.p.m. FOR CYCLOIDAL TRAJECTORY

drop only slightly because the force of inertia, force of gravity and resistance to rupture of the remaining undetached part of the slice are still acting on the blade. After the formation of the first shear plane, the kinetic energy of the rotating blade is transferred to the deformed slice, impelling it with an acceleration determined by the movement of the blade. Because of this inertia force, the forces again rise to the second peak observed approximately 35^{o} of the blade entry as shown in Figure 6.2. At this stage, the blade reaches almost to the end of cutting and the mass of the slice begins to leave the blade surface and the forces start declining. A further separation of the slice begins from the bottom, however, its magnitude is not detectable on the force record because of the size of the slice and resolution of the recording system.

The observations of the effect of speed on the shape of the failure planes have shown no noticeable changes even at the largest peripheral speed of 3.87 m/sec studied, and agree with the results of Vinogradov (1968) who observed no change in the nature of rupture at circumferential speeds between 1.5 to 7 m/sec. The shear planes still develop at $(45 - \frac{\phi}{2})$ degrees with the tangent drawn at the tip of the blade parallel to the direction of tangential force. It can be deduced that the orientation and size of the shear planes in a cycloidal trajectory is similar to a circular trajectory and the magnitude of the forces would, theoretically, be similar between the two cases provided the effective clearance angle remains positive.

6.4.2.2 The Magnitude of the Dynamic Forces

The observations of the cyclic variations of the forces in cutting a full soil slice reveal that at slow speeds, there are a number of distinct maxima corresponding to the development of the shear planes and the peak force occurs after approximately 10^{o} entry of the blade into the soil. As the cutting speed is increased, however, there are only two distinct maxima forces as shown in Figures 6.1 and 6.2. The variations of forces in cutting a full soil slice at different cutting speeds (Table 6.1) shows that at a rotor speed of 40 r.p.m., the first peak occurs between 10^{o} to 15^{o} and the second peak between

25^{o} to 30^{o} of the blade entry into the soil. The first peak, however, is approximately 20 percent greater than the second peak force. The position of the peak resultant force in cutting a full slice also changes with the increase in the rotor speed. It is evident from Figures 6.1 and 6.2 that the first and the second peak resultant force for 80 r.p.m. rotor speed occurs at approximately 15^{o} to 20^{o} and 30^{o} to 35^{o} after penetration respectively. For a further increase in rotor speed to 120 r.p.m., the position of the first peak does not change but the second peak moves further ahead to about 40^{o} to 45^{o} after penetration. It can be noted that the second peak force at the higher speeds of 80 and 120 r.p.m. is approximately 15 to 25 percent greater than the first peak force which shows a complete change in the phenomenon from slow speeds and may be attributed to the reasons described in Section 6.4.2.1.

The maxima forces at two positions of the blade in cutting a full slice has been recorded, Vinogradov (1968), with the first peak after about 20 to 30 mm of penetration while the second peak around two-third of the way along the full length of the cutting arc. Unfortunately, Vinogradov did not mention the working regime of the tiller. However, for an assumed depth of cut of 100 mm, the second peak corresponds to approximately 31^{o} of penetration which recorded the peak resultant force in cutting a full slice. Vinogradov results are in agreement with Harral (1977) who recorded the peak resultant force at least 30^{o} after entry but in complete contrast to Bernacki (1962) and Söhne (1957) who reported the peak force after 10^{o} to 12^{o} of the blade entry even under dynamic conditions.

The relationship between the component forces and the rotor speed for a single bite length and depth of cut at zero forward speed, and varying forward and rotor speeds for a single bite length similar to the one used for zero forward speed is shown in Figures 6.3 and 6.4 respectively. It can be noted from the figures that the nature of variation of the resultant force in both the conditions (circular and cycloidal trajectories) of the blade are identical. At a very slow speed of 0.161 m/sec (5 r.p.m.) the peak static force of approximately 90 Newtons was recorded with no significant variation in the magnitude for both the trajectories of the blade. This may be attributed to the

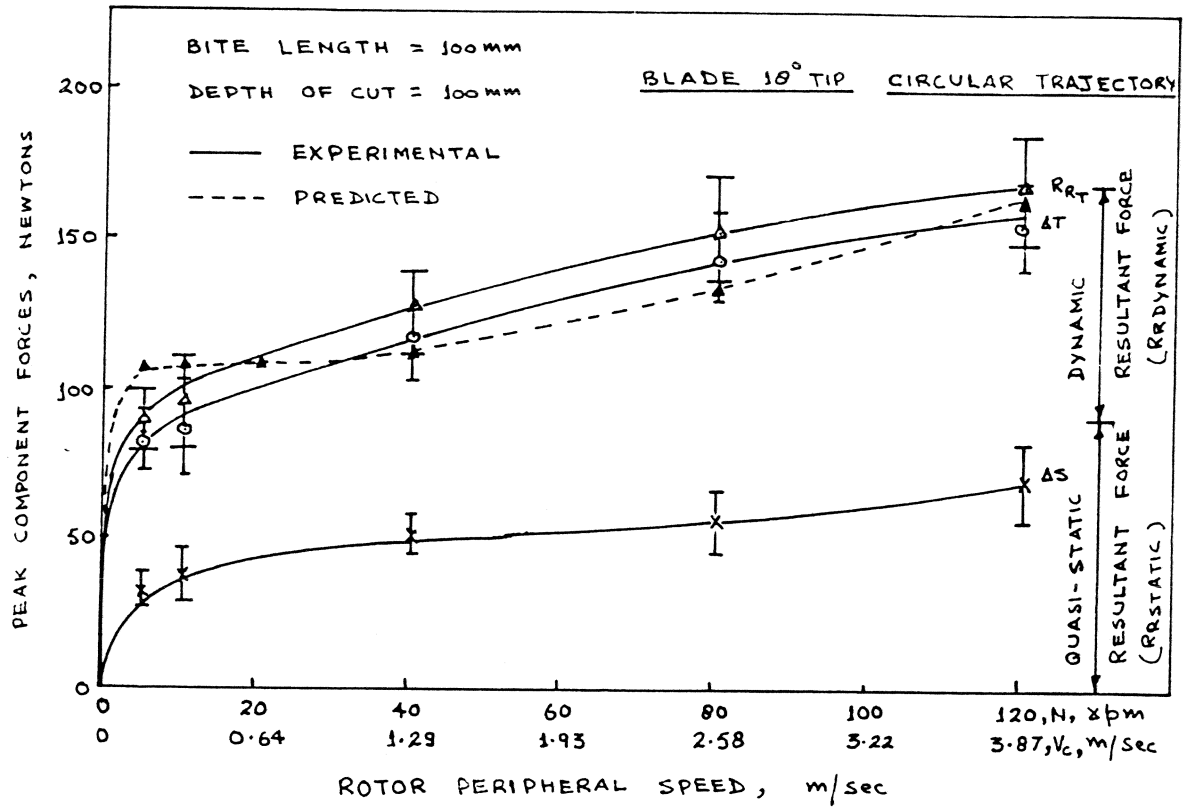

FIGURE 6·3 VARIATION OF COMPONENT FORCES (PEAK) WITH ROTOR PERIPHERAL SPEED FOR A BLADE TRAVERSING IN A CIRCULAR TRAJECTORY AT CONSTANT BITE LENGTH AND DEPTH OF CUT

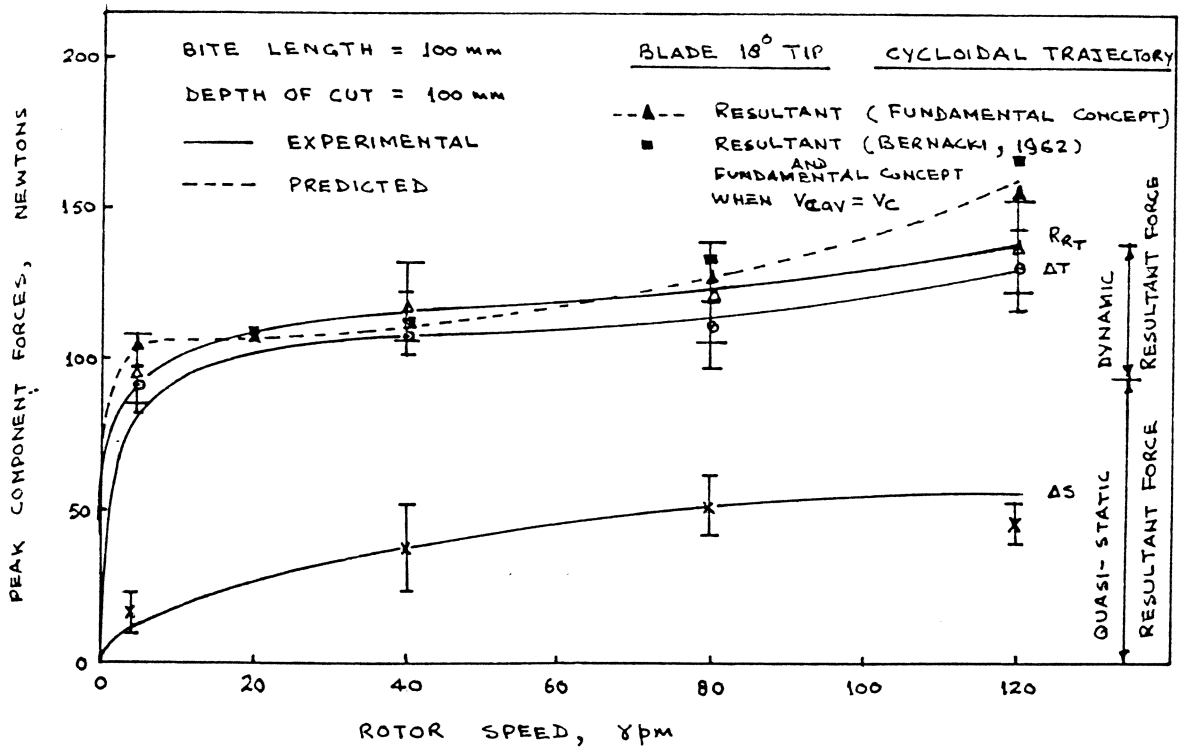

FIGURRE 6·4 VARIATION OF PEAK COMPONENT FORCES WITH VARYING ROTOR AND FORWARD SPEEDS FOR A BLADE TRAVERSING IN A CYCLOIDAL TRAJECTORY AT A CONSTANT BITE LENGTH AND DEPTH OF CUT

similar mechanism of soil failure described in Section 6.4.2.1. At a maximum peripheral speed of 3.87 m/sec, the total dynamic force increased approximately two fold to that of the minimum recorded speed which shows a slower rate of increase in the dynamic force than the speed of the blade in agreement with Dalin (1950).

6.5 The Effect of Forward Speed at Constant Rotor Speed

6.5.1 Introduction

The bite length in rotary tilling can be changed by changing the rotor diameter, number of blades and the λ-ratio. However, for a given tiller the first two parameters are seldom varied and a change in bite length is obtained by altering λ-ratio which changes the effective clearance angle such that either adequate clearance at the back face of the blade exists or the face presses into the undeformed soil. This unwanted phenomenon contributes to a significant increase in the dynamic forces and a tendency for the tiller blade to 'walk-out' of the soil. According to Beeny and Greig (1965), and Mursch (1957) an increasing λ-ratio obtained either by increasing rotor radius and speed or decreasing forward speed increases the specific power requirement. However, decreasing λ-ratio does not decrease the specific power requirement except within certain limits.

For a given rotor geometry, increasing λ-ratio by increasing peripheral speed results in the greater acceleration of the soil particles. Kisu et. al. (1966) presented the relationship between power requirement and bite length by varying λ-ratio by two different methods. It was postulated that increasing bite length by varying rotor speed at constant forward speed decreased the cutting path per unit slice volume; however, as the rotor speed reached some point, the power requirement began to rise again. Similarly, increasing bite length by increasing forward speed at constant rotor speed increased the volume of soil slices and the specific power requirement decreased upto a certain point. According to Dalin and Pavlov (1950) an increase of forward speed by a factor of five at constant rotor speed was accompanied by only a three fold increase of power requirement for tilling at a depth of 150 mm which was later substantiated by Furlong (1956).

Hendrick and Gill (1971) in their review on the effect of λ-ratio on the tiller design concluded that:

i. Decreasing λ-ratio by increasing forward speed results in an increase in the power requirement, but a reduction in specific power requirement provided the geometry of the soil - tool system is not varied too greatly.

ii. Decreasing λ-ratio by decreasing rotor speed decreases the power requirement and the specific power, again this occurs until the geometry of soil - tool system is extended beyond a favourable relationship.

iii. Increasing λ-ratio results in a greater value of the ratio between cutting area and volume per soil slice cut.

6.5.2 Experimental Results

A typical force record for a negative clearance angle i.e. $(\delta_1 - \Delta\varepsilon) < 0$, at a bite length of 231 mm and depth of cut of 100 mm is shown in Figure 6.5. The top of the figure shows the event marker record from no. 9 to no. 18 with the normal angular position of 4.09^{o} equivalent to 20 mm between two successive marks. The figure represents the treatment no. 20 with the effective clearance angles at the point of entry and 10^{o} after entry of the tip in the range of -4.76^{o} and -3.15^{o} respectively shown in Table 6.2. The following significant conclusions can be drawn from the force record:

i. All the component forces increase steeply after the entry of the blade and the maxima for the radial force is recorded after approximately 6 - 7^{o} of penetration. The reason for this maxima may be attributed to the fact that the full chamfer back of the blade comes into contact with the uncut soil approximately around this angle and records the maximum radial force which is dependent on the area of the face in contact with uncut soil and the magnitude of the negative clearance angle. After further entry of the blade the radial force increases only marginally upto about 12^{o} of

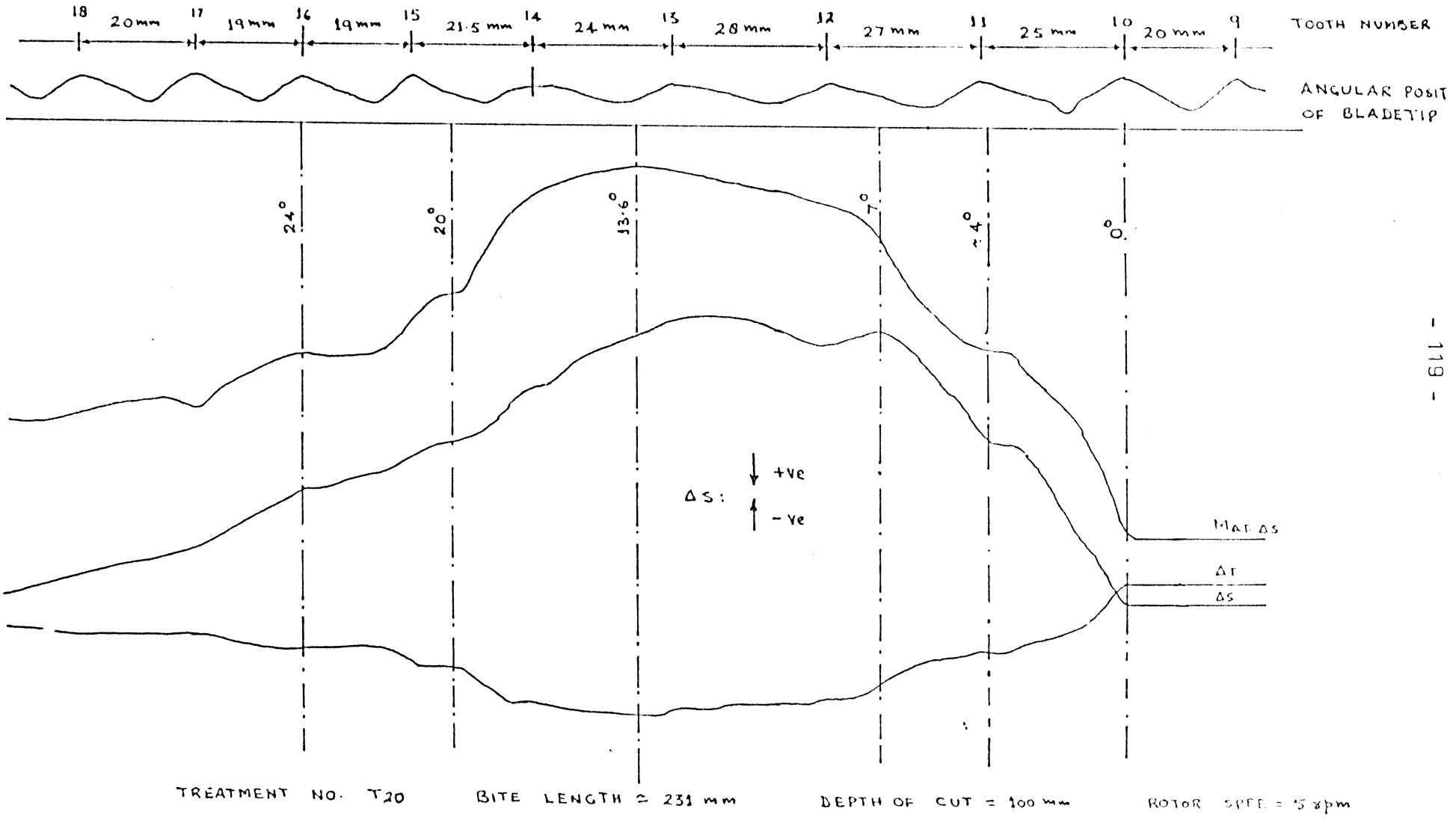

FIGURE 6.5 A TYPICAL FORCE RECORD FOR A NEGATIVE EFFECTIVE CLEARANCE ANGLE i.e. ($\delta_1 - \Delta\delta \leq 0$)

penetration and afterward drops down slowly. It can be noted that after about 14^{o} entry of the blade the first largest shear plane is developed as can be seen by peak tangential force; however, at this position of the blade the radial force is lower than its peak value and may be because of the weight of the deformed soil slice resting on the blade which reduces the net radial force.

ii. The observation of the distance between two events marks shows a varying distance from the normal 20 mm equivalent to 4.09^{o}. The maximum variations between event points are recorded after the entry of the blade till the blade back face comes into contact with uncut soil and is approximately 27 - 28 mm distance equivalent to 4.09^{o}. This phenomenon shows that the blade had been momentarily retarded due to the large magnitude of the negative radial force which restricted further penetration of the blade and in the ultimate could cause the blade to 'walk-out' of the soil.

The relationship between the magnitude of the component forces and the bite length at three depths of cut is shown in Figures 6.6, 6.7 and 6.8, and the respective effective cutting angle and clearance angle at the point of entry and 10^{o} after entry into the soil are presented in Table 6.2. The Figures show the component forces for the two different types of situation as no scrubbing, $(\delta_1 - \Delta\delta) > 0$, and scrubbing $(\delta_1 - \Delta\delta) \leq 0$, of the chamfered back face of the blade with the undeformed soil. It can be deduced from the Figures that for all the positive effective clearance angles, $(\delta_1 - \Delta\delta) > 0$, the magnitude of the component forces increase marginally but the forces at the negative clearance angles, $(\delta_1 - \Delta\delta) \leq 0$, increase very steeply because of the compression of the uncut soil by the blade. For about 3.5 fold increase in the forward speed the tangential and radial forces increase by approximately 3.5 and 18 times respectively for 50 and 100 mm depths of cut. However, for the 150 mm depth the increase is in the order of 1.8 and 13 times. It is evident that the increase in the peak resultant force at any depth of cut is mainly due to a substantial increase in the radial force component at negative clearance angle.

In the course of increasing the forward speed, the effective cutting angle for the depths of cut of 50, 100 and 150 mm decreases from 23^{o} to

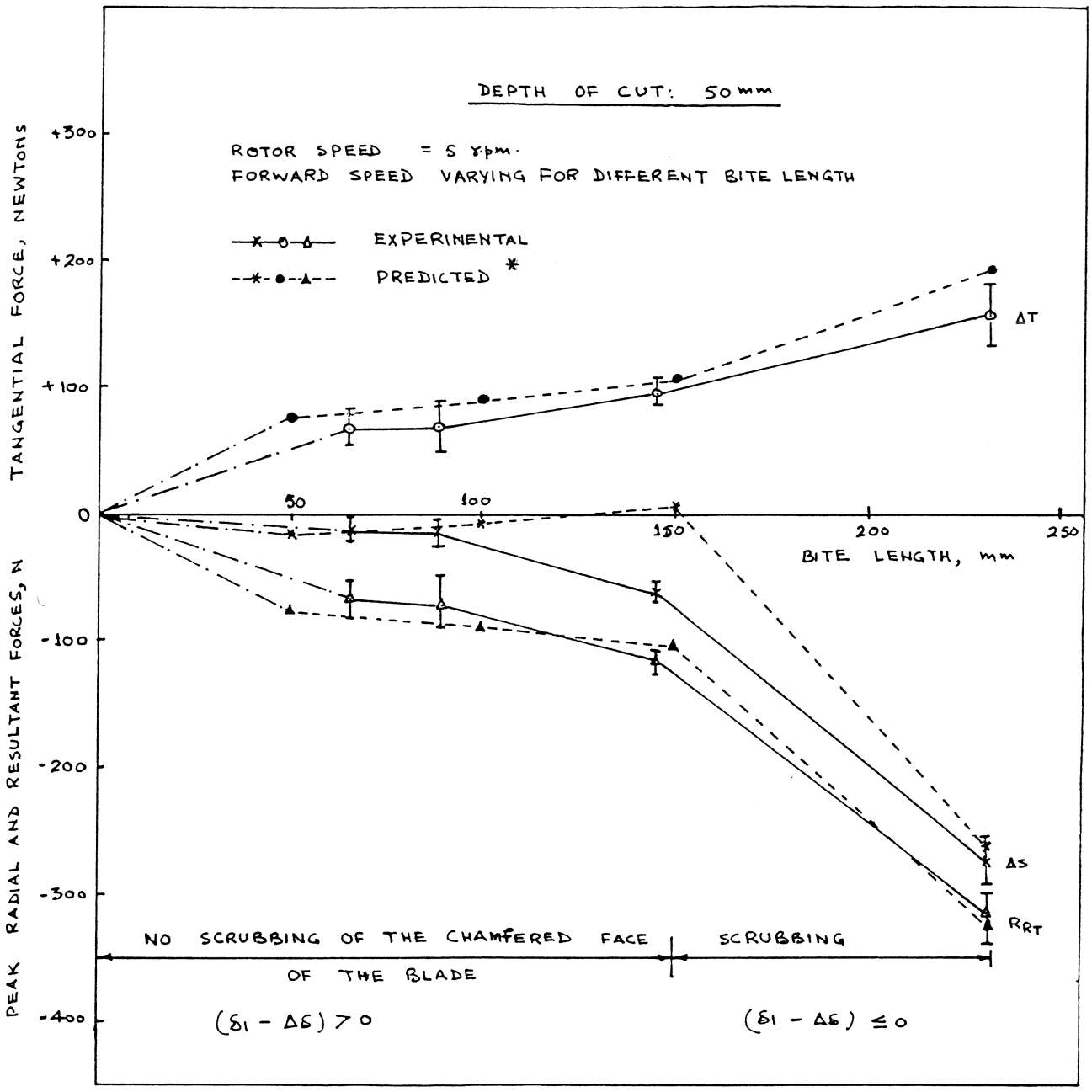

FIGURE 6.6 EFFECT OF FORWARD SPEED AT CONSTANT ROTOR SPEED ON THE PEAK DYNAMIC FORCES OF THE BLADE FOR 50 mm DEPTH OF CUT

N.B. * For Predicted Results See Chapter-8

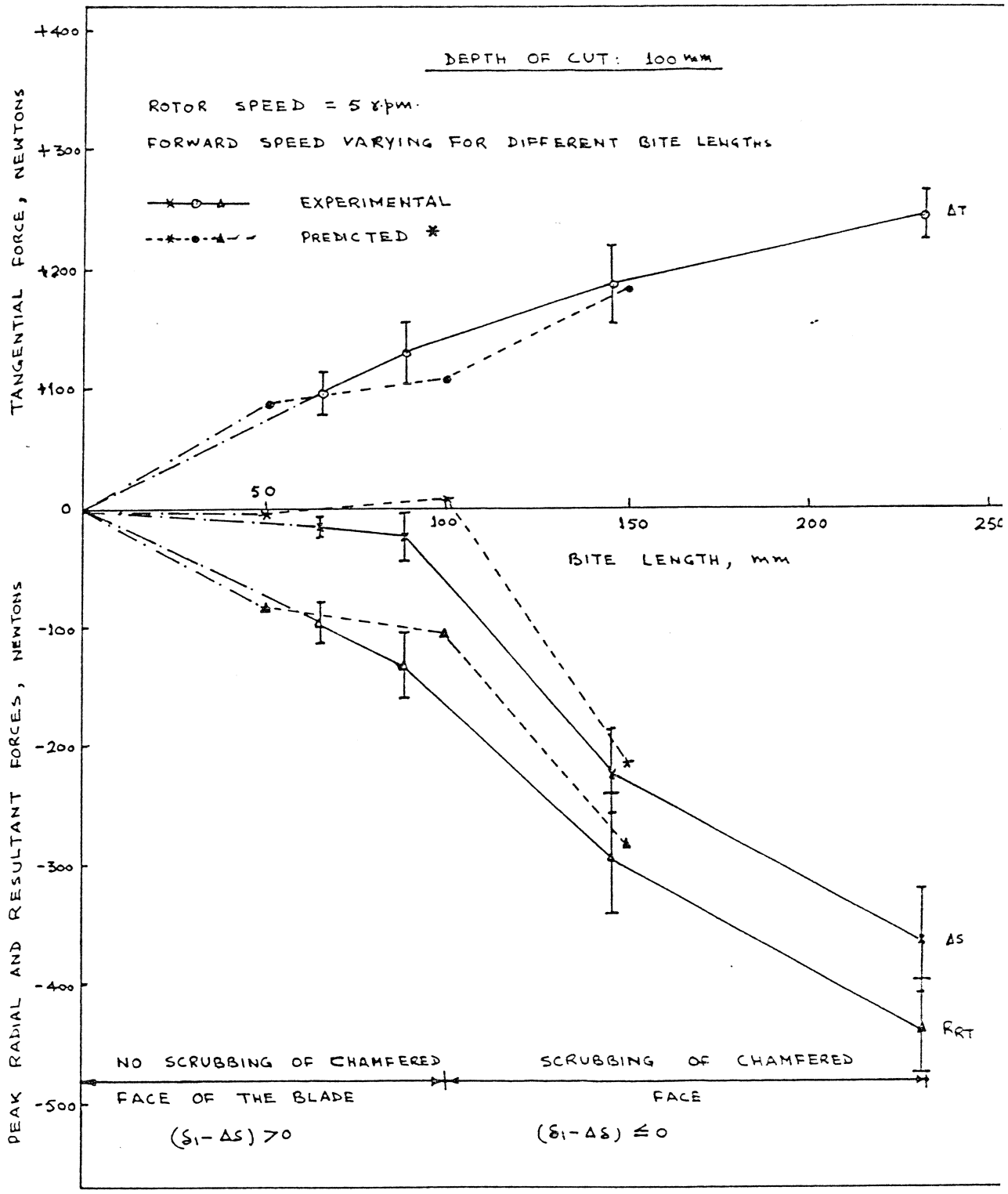

FIGURE 6·7 EFFECT OF FORWARD SPEED AT CONSTANT ROTOR SPEED ON THE PEAK DYNAMIC FORCES OF THE BLADE FOR 100 mm DEPTH OF CUT

N.B. * For Predicted Results See Chapter-8

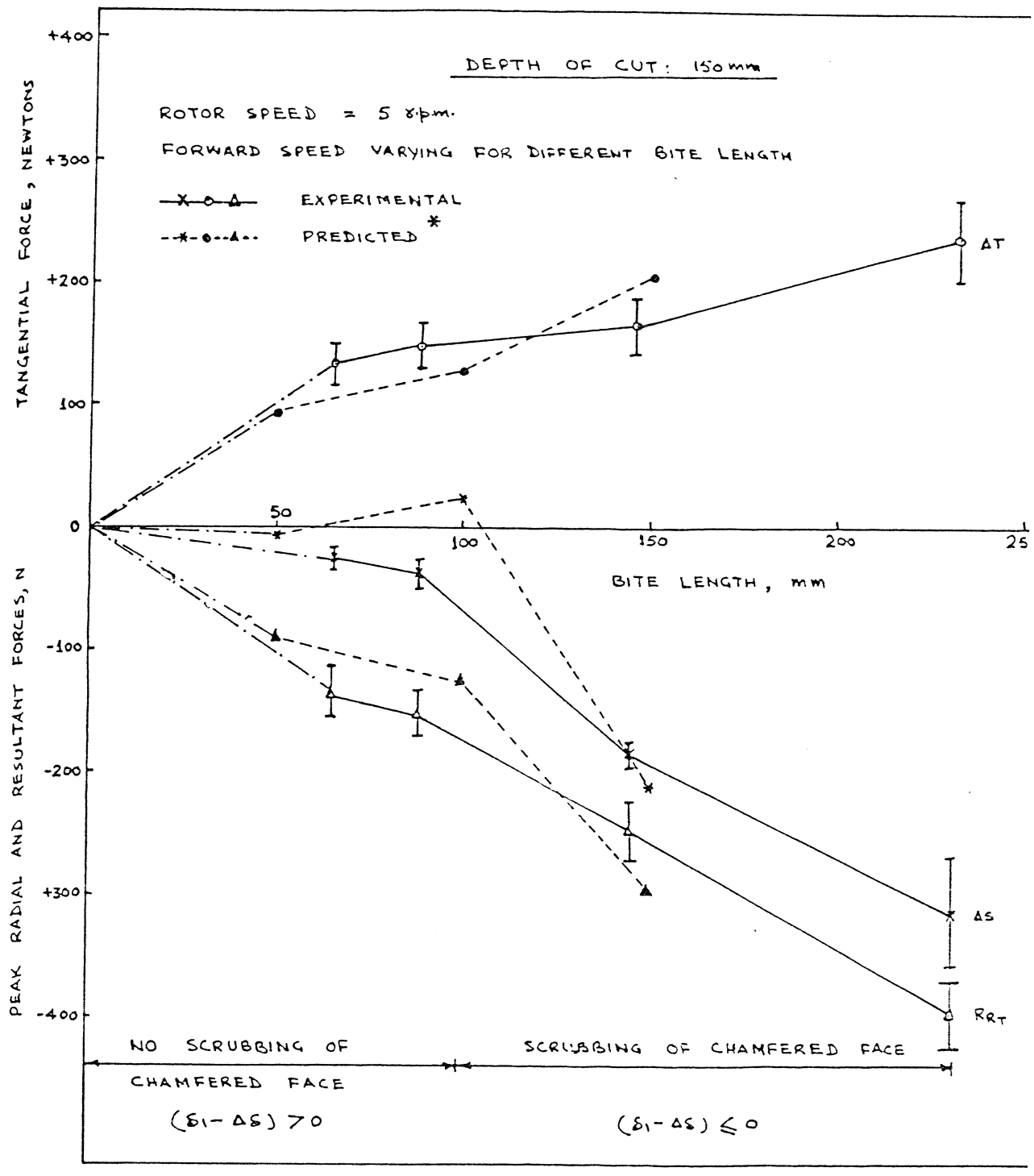

FIGURE 6.8 EFFECT OF FORWARD SPEED AT CONSTANT ROTOR SPEED ON THE PEAK DYNAMIC FORCES OF THE BLADE FOR 150 mm DEPTH OF CUT

N.B. * For Predicted Results See Chapter-8.

18^{o}, 22.5^{o} to 15^{o} and 22^{o} to 13^{o} respectively after 10^{o} entry of the blade in the soil as shown in Table 6.2. According to Söhne (1957) for a blade traversing in a circular trajectory a cutting angle of approximately 20^{o} recorded the least cutting resistance. In the present set of experiments the bite length and the effective cutting angle change at every point during cutting of a slice because of the cycloidal trajectory of the blade, therefore, it was difficult to determine the percentage contribution of forces to the resultant force exclusively due to the variation in the effective cutting angle. However, a blade with smaller cutting angle can record a comparatively lower value of resistance to cut-off a slice provided the effective clearance angle at the back face of the blade remains positive.

6.6 Conclusions

i. There was no appreciable change in the mechanism of soil failure whether the blade cuts-off the slice in a circular or a cycloidal trajectory. The size, shape and orientation of the shear planes in both the cases were identical and developed at an angle of $(45 - \frac{\phi}{2})$ degrees with the tangent drawn at the tip of the blade parallel to the direction of rotation (major principal stress).

ii. The mechanism of soil failure at a higher speed of 3.87 m/sec was similar to that at the lower speeds.

iii. There were two force component maxima in cutting-off a full soil slice with the first maxima after 15^{o} to 20^{o} and the second maxima after 30^{o} to 45^{o} of the blade entry into the soil for rotor speeds greater than 1.3 m/sec. The position of the second maxima changed with increasing speed of cutting and with an indication to appear after larger penetration of the blade. At higher cutting speeds, the second maxima of the cutting force appeared higher. However, the largest shear plane did not alter with the speed and occurred at around 10^{o} of the blade entry for the fetch-ratio (1:1) studied.

iv. All the component forces increased with the increasing peripheral speed of the blade but at a slower rate.

v. Increasing the bite lengths or reducing the λ-ratio by increasing the forward speed whilst maintaining constant rotor speed, significantly increased the component forces.

vi. The tangential force increased by about 2.4 times for about 3.5 fold increase in the forward speed whereas the radial force increased by almost 18 times (irrespective of the depths of cut). The large increase in the radial force was mainly due to the compression of the undeformed soil at negative effective clearance angles.

7. DEVELOPMENT OF THE FORCE PREDICTION MODEL

7.1 Introduction

This chapter deals with the force prediction model developed for a simple rotating powered blade cutting a two-dimensional soil slice, where the effect of the leg has been neglected. The predicted model is based upon the theories of Mohr-Coulomb soil mechanics and the bearing capacity of deep footings developed and extended by Meyerhof (1951 and 1961) from Terzaghi (1943) bearing capacity theory.

The mechanics of soil cutting by a powered blade has been explained on the basis of the 'blade-effect' causing a passive soil failure and the 'tip-effect' causing a local shear failure similar to a wire for determination of forces in a quasi-static condition. For dynamic conditions, the model incorporates an inertia term due to the acceleration of the deformed soil slice and a compressive force component for a special case. The applicability and limitations of the model developed for the blade with horizontal axis of rotations have been validated for a blade with vertical axis of rotation by incorporating certain modifications.

7.2 The Concept of the Prediction Model

From the work conducted on the mechanism of soil failure by a rotating blade and a wire traversing in a circular trajectory (quasi-static condition) in Chapter 4 and a blade alone traversing in a cycloidal trajectory (quasi-static and dynamic condition) in Chapter 6, it is evident that the mechanism of soil failure under both the conditions are similar. The theoretical orientation and size of the shear planes under both the trajectories should, therefore, be similar as shown in Figure A2.1 and the quasi-static forces should remain constant. It was, therefore, considered logical to predict, first, the quasi-static forces on the blade for a circular trajectory which is equally applicable to the cycloidal trajectory.

It is reasonable to assume that a model based on the forces shown in Figures 7.1 and 7.2 will be realistic for the soil reaction on the rotating blade. The quasi-static soil reaction at a very slow rotor speed consists of a passive soil resistance, P_p, acting on the front face of the blade and a rear tip reaction, Q_R, acting on the tip from the undeformed soil as shown in Figure 7.1. At higher speeds of cutting, there is a dynamic reaction due to the acceleration of the deformed soil slice and this should be added to the quasi-static soil reaction. Moreover, in dynamic condition (cycloidal trajectory) due to improper selection of the combination of the rotor speed and forward speed, the effective clearance angle can become negative and the back face of the blade starts compressing and scrubbing the undeformed soil, Hendrick and Gill (1974). The soil reaction, Q_{RT}, due to the compression of the undeformed soil is assumed to be acting on the chamfered face of the blade as shown in Figure 7.2. The resultant reaction under this condition will be the sum of the quasi-static reaction and the dynamic reaction due to acceleration of the deformed soil slice and the compression of the undeformed soil.

Therefore, the total soil reaction on the blade may be expressed as:

$$R_{RT} = R_{R\ static} + R_{R\ dynamic} \qquad \ldots\ldots\ldots (7.1)$$

The individual soil reaction on the blade can be obtained as below:

a. The Quasi-Static Soil Reaction

The tangential and radial components of the quasi-static force can be determined from Figure 7.1. The relationship of passive resistance, P_p, with tangential force component, ΔT, is shown in Appendix 3. Therefore,

$$\Delta T = P_p \cos (90 - \beta - \delta_1 - \delta) + Q_R \cos (45 - \delta) \quad \ldots\ldots (7.2)$$

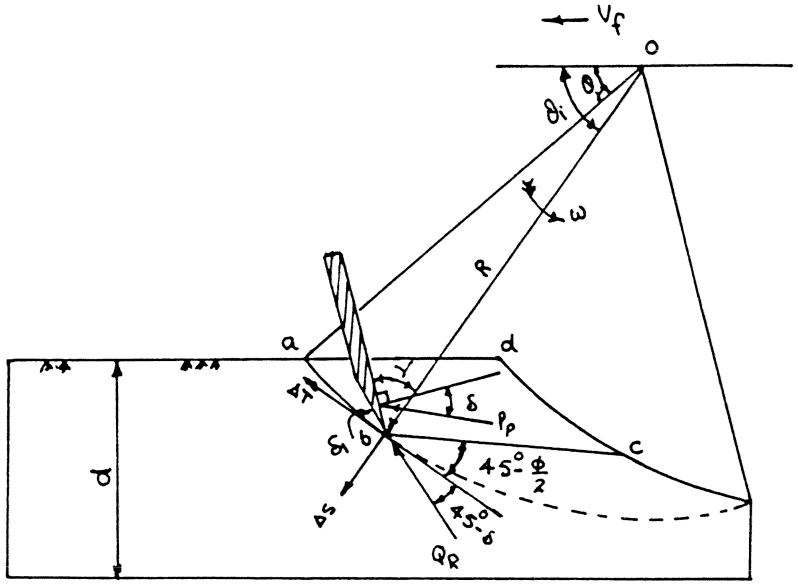

FIGURE 7·1 SOIL REACTION ON A POWERED ROTATING BLADE OPERATING AT POSITIVE EFFECTIVE CLEARANCE ANGLE i.e. $(\delta_1 - \Delta\delta) > 0$

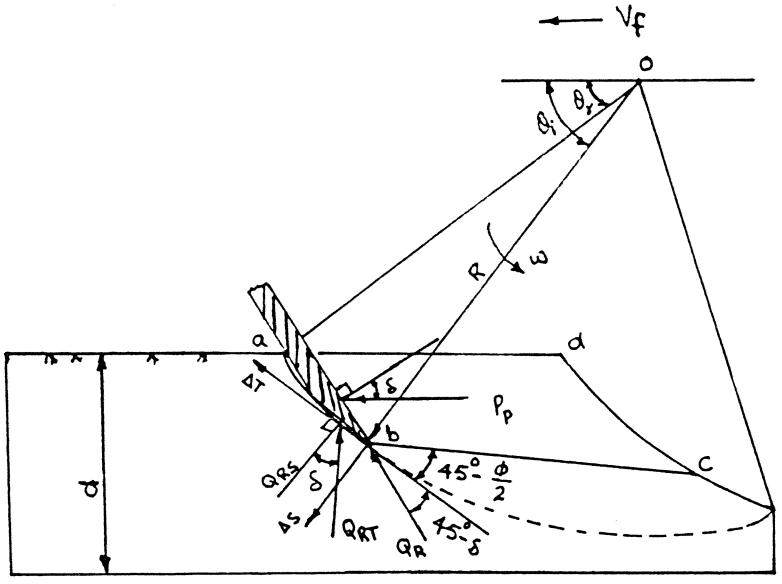

FIGURE 7·2 SOIL REACTION ON A POWERED ROTATING BLADE OPERATING AT NEGATIVE CLEARANCE ANGLE i.e. $(\delta_1 - \Delta\delta) \leq 0$

$$\Delta S = P_p \sin(90 - \beta - \delta_1 - \delta) - Q_R \sin(45 - \delta) \quad \ldots\ldots (7.3)$$

and $$R_{R\ static} = \sqrt{\Delta T^2 + \Delta S^2} \quad \ldots\ldots\ldots (7.4)$$

If ΔS is negative then the net force acts towards the centre of rotation of the blade.

b. The Dynamic Soil Reaction ($R_{R\ dynamic}$)

The total reaction under two dynamic conditions is given as the sum of acceleration force (I_F) and scrubbing force (Q_{RT}), hence when substituted into Equation 7.1 gives:

i. For positive effective clearance angle i.e. $(\delta_1 - \Delta\delta) > 0$

$$R_{RT} = R_{R\ static} + I_F \quad \ldots\ldots\ldots (7.5)$$

ii. For negative effective clearance angle i.e. $(\delta_1 - \Delta\delta) \leqslant 0$

$$R_{RT} = R_{R\ static} + I_F + Q_{RT} \quad \ldots\ldots\ldots (7.6)$$

The method for prediction of the individual soil reaction is described in detail in the following sections.

7.3 The Quasi-Static Force Prediction Model for a Blade with Horizontal Axis of Rotation

7.3.1 Determination of Passive Resistance of the Blade

7.3.1.1 Assumptions

i. The soil is homogeneous and isotropic.

ii. The shear failure towards the free curved face of the soil slice occurs as a result of sliding on a rupture surface within the soil mass. The Mohr-Coulomb soil failure condition is satisfied on the failure plane which develops at an angle of $(45 - \frac{\phi}{2})$ degrees

with the direction of major principal stress (tangent) in accordance with the observed mechanism of soil failure in Chapter 4.

iii. The soil reaction due to passive failure of the soil slice acts at an angle of friction (δ) with the normal to the interface in accordance with the observed mechanism of failure in Chapter 4 which showed that the failure plane develops from the tip of the blade and the full soil slice is pushed ahead by the interface.

iv. The mechanism of soil failure at slow and high peripheral speeds of the blade are similar. This assumption is in accordance with the observations in Chapter 6 for peripheral speeds of 0.16 m/sec (5 r.p.m.) to 3.87 m/sec (120 r.p.m.) which showed unaltered shape and orientation of the shear planes with speed and further substantiated by Vinogradov (1968) who reported an unaltered crack formation for peripheral speeds up to 7 m/sec.

7.3.1.2 The Model Development

A simple blade traversing in a circular trajectory is shown in Figure 7.3 at an angle of θ_i with the horizontal after 10^o of penetration in the soil. The line bc shows a potential shear plane towards the free curved face of the soil slice at an angle of $(45 - \frac{\phi}{2})$ degrees with the direction of major principal stress. At the time of incipient failure, there will be tangential (P) and normal (N) reaction forces acting on the failure plane. Therefore, equating the forces parallel to and normal to the failure plane bc and neglecting any surcharge force which is usually zero, the following equations are obtained (see Appendix 3 for relationship):

$$P = W \cos\left(\theta_i + 45 - \frac{\phi}{2}\right) + P_p \cos\left(45 + \frac{\phi}{2} - \delta - \beta - \delta_1\right) - C_a \cos\left(45 - \frac{\phi}{2} + \beta - \delta_1\right) \quad .. (7.7)$$

$$N = W \sin\left(\theta_i + 45 - \frac{\phi}{2}\right) - P_p \sin\left(45 + \frac{\phi}{2} - \delta - \beta - \delta_1\right) - C_a \sin\left(45 - \frac{\phi}{2} + \beta - \delta_1\right) \quad .. (7.8)$$

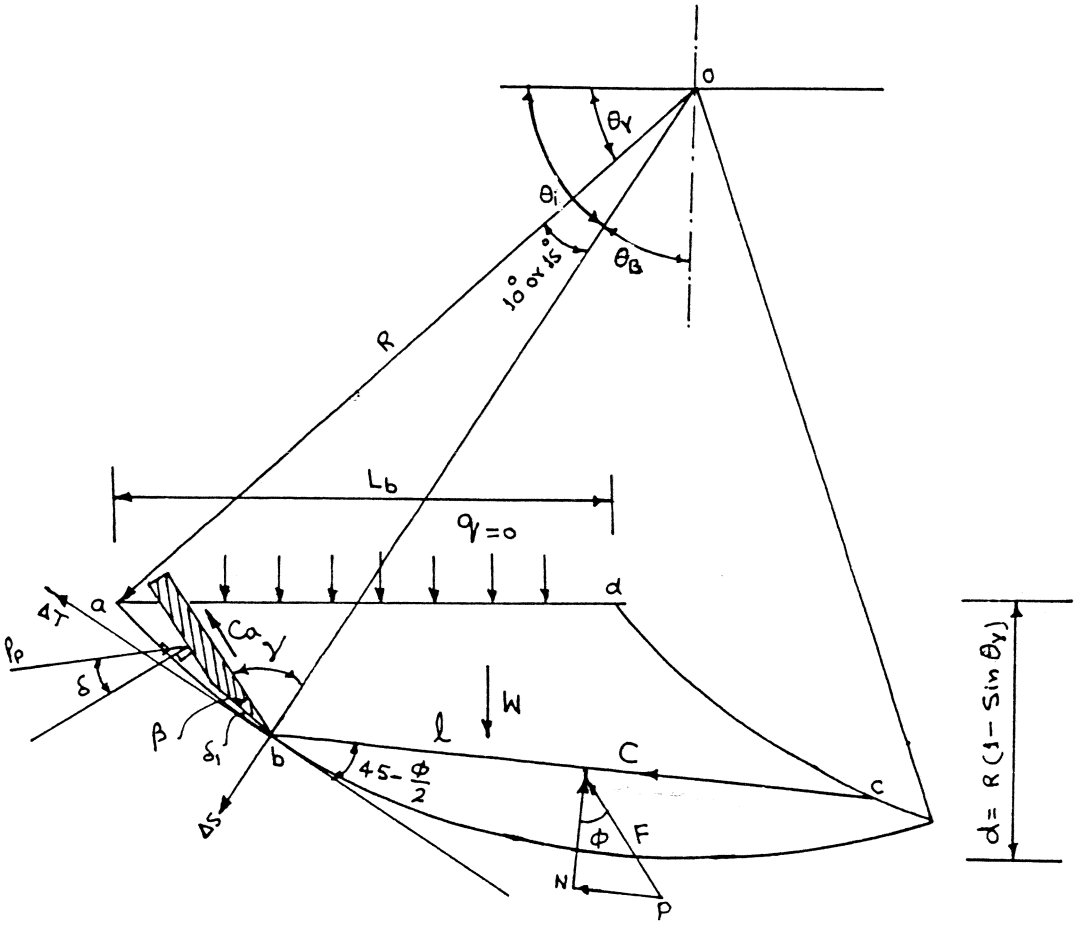

NOTATIONS:

R = RADIUS OF THE ROTOR
d = DEPTH OF CUT
L_b = BITE LENGTH
w = WIDTH OF CUT (NOT SHOWN)
ℓ = LENGTH OF THE SHEAR PLANE, bc
β = BLADE SHARPENING ANGLE
δ_1 = CLEARANCE ANGLE BETWEEN THE CHAMFERED BACK FACE OF THE BLADE AND A TANGENT TO THE CIRCLE INSCRIBED BY THE TIP
ψ = BLADE MOUNTING ANGLE
P_p = PASSIVE RESISTANCE FORCE
C = COHESION (FORCE) ALONG PLANE, bc
C_a = ADHESION ALONG THE INTERFACE
W = WEIGHT OF THE DEFORMED SOIL SLICE, abcd
δ = ANGLE OF SOIL-METAL FRICTION
ϕ = ANGLE OF SOIL SHEARING RESISTANCE
ΔT = TANGENTIAL SOIL REACTION
ΔS = RADIAL SOIL REACTION
q_Y = SURCHARGE
SUFFIX i FOR θ_i DENOTES ANY POSITION OF TIP FROM HORIZONTAL

FIGURE 7·3 PASSIVE SOIL REACTION IN ROTARY TILLING OF THE SOIL

The Mohr-Coulomb soil failure conditions must be satisfied on the failure plane bc so that,

$$P = C + N \tan \phi \qquad \ldots\ldots\ldots (7.9)$$

Now, substituting the values of P and N from Equations 7.7 and 7.8 in Equation 7.9 and solving for P_p, the following is obtained:

$$P_p \left[\text{Cos}\ (45 + \frac{\phi}{2} - \delta - \beta - \delta_1) + \text{Sin}\ (45 + \frac{\phi}{2} - \delta - \beta - \delta_1) \cdot \tan\phi\right]$$
$$= C + \left[\text{Sin}\ (\theta_i + 45 - \frac{\phi}{2}) \cdot \tan\phi - \text{Cos}\ (\theta_i + 45 - \frac{\phi}{2})\right] W$$
$$+ \left[\text{Cos}\ (45 - \frac{\phi}{2} + \beta - \delta_1) - \text{Sin}\ (45 - \frac{\phi}{2} + \beta + \delta_1) \cdot \tan\phi\right] C_a$$

Let,

$$(45 + \frac{\phi}{2} - \delta - \beta - \delta_1) = \alpha_1$$
$$(45 - \frac{\phi}{2} + \beta + \delta_1) = \alpha_2$$
$$(45 - \frac{\phi}{2} + \theta_i) = \alpha_3$$

$$P_p = \left[\frac{1}{\text{Cos}\,\alpha_1 + \text{Sin}\,\alpha_1 \cdot \tan\phi}\right] C + \left[\frac{\text{Sin}\,\alpha_3 \cdot \tan\phi - \text{Cos}\,\alpha_3}{\text{Cos}\,\alpha_1 + \text{Sin}\,\alpha_1 \cdot \tan\phi}\right] W$$
$$+ \left[\frac{\text{Cos}\,\alpha_2 - \text{Sin}\,\alpha_2 \cdot \tan\phi}{\text{Cos}\,\alpha_1 + \text{Sin}\,\alpha_1 \cdot \tan\phi}\right] C_a$$

Allowing T_C, T_γ and T_{C_a} to represent the terms enclosed in the brackets, the passive resistance is given by:

$$P_p = T_C \cdot C + T_\gamma \cdot W + T_{C_a} \cdot C_a \qquad \ldots\ldots\ldots (7.10)$$

where T-values are dependent upon the geometry of the blade and the properties of the soil.

7.3.2 Tip Effect (Wire) Force Prediction Model

7.3.2.1 Introduction

The theory of bearing capacity by Terzaghi (1943) has been used for predicting forces on a tine at depths greater than the critical depth defined by Payne (1956), Kostritsyn (1956), O'Callaghan and Farrelly (1964). Meyerhof (1948), however, noticed that the assumption made by Terzaghi regarding the mechanism of soil failure was not in accordance with the observed soil movement. For a deep foundation Terzaghi method suffers from the difficulty that when the failure surface no longer reaches ground level, the height over which the shearing strength of the soil is mobilized becomes very uncertain and must be assumed. Meyerhof (1951) overcame these limitations by extending Terzaghi analysis of the plastic equilibrium for a flat surface footing to shallow and deep foundations considering the soil to fail in a logarithmic spiral pattern until it interfaced either with the vertical face of the footing or intersected the soil surface. This type of failure is in accordance with Jacki (1948) for footing and Prandtl (1920) for punched indentation. The soil failure mechanism by a very narrow tine at depths greater than critical depth was observed by Godwin (1974) and Godwin and Spoor (1977) similar to Meyerhof (1951) assumptions for a footing at great depths and solution obtained for the forces on the face of a flat tine using appropriate N-factors.

7.3.2.2 The Concept of the Prediction Model

The conceptual mechanism of soil failure by a wire under two contrasting situations is shown in Figure 7.4. The failure mechanism by a wire drawn through a semi-infinite homogeneous soil mass can be considered similar on both sides from its centre and the soil reaction acting on both halves of the wire could balance each other as shown in Figure 7.4a. However, when the wire is working near an open wall, the failure mechanism becomes asymmetrical as in Figure 7.4b. There may be a general shear failure towards the free face of the wall and a local shear failure on the opposite side similar to the symmetrical failure mechanism. Soil reactions due to different types

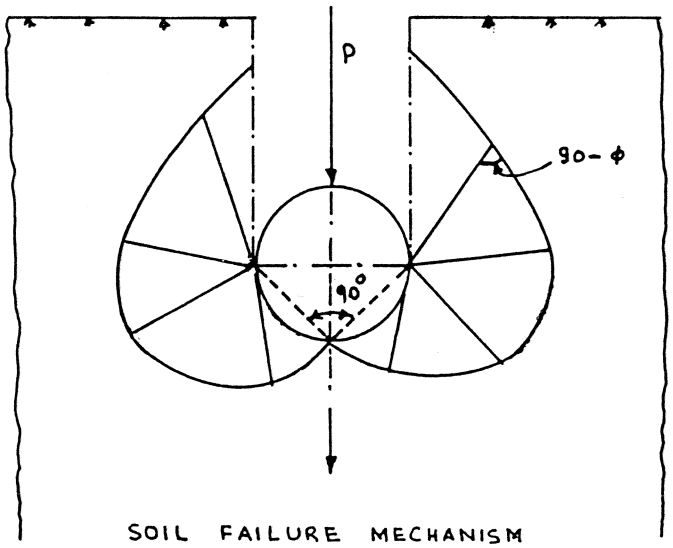

SOIL FAILURE MECHANISM

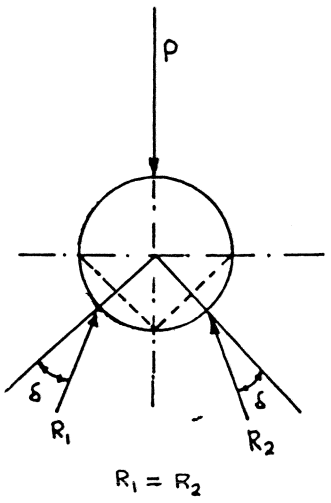

SOIL REACTION

a. SYMMETRICAL SOIL FAILURE MECHANISM IN A SEMI-INFINITE MASS BY A ROUGH WEDGE/WIRE

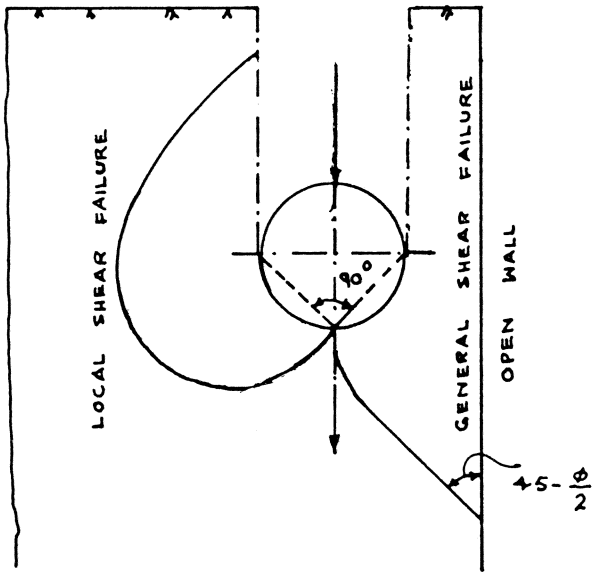

SOIL FAILURE MECHANISM

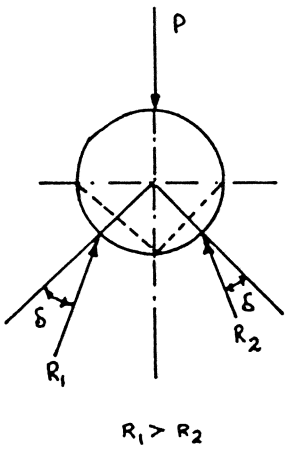

SOIL REACTION

b. ASYMMETRICAL SOIL FAILURE MECHANISM NEAR AN OPEN WALL

FIGURE 7.4 IDEALISED SYSTEMS OF FORCES ACTING ON A WIRE PUSHED THROUGH THE SOIL

of failure mechanism may be different on either side of the wire as shown in the figure.

The soil failure mechanism of a wire cutting a varying thickness of the soil slice as in rotary tilling can be considered asymmetrical as shown in Figures 7.5 and 7.6. The general shear failure planes develop towards the free curved face at an angle of $(45 - \frac{\phi}{2})$ degrees with the direction of major principal stress in cutting a full soil slice in accordance with the observations in Chapter 4. The passive resistance of the wire, P_{PW}, can be calculated by constructing a force polygon from the soil reaction acting on the soil slice shown in Figure 7.5a. The rear tip force, Q_R, is determined from Meyerhof (1961) theory for wedge shaped foundation and a second force polygon is constructed from P_{PW} and Q_R to determine the total force acting on the wire (Figure 7.5b). The component forces on the wire may be determined from the following equations:

$$\Delta T_W = P_{PW} \text{ Cos } (45 - \delta) + Q_R \text{ Cos } (45 - \delta) \quad \ldots\ldots\ldots (7.11)$$

$$\Delta S_W = P_{PW} \text{ Sin } (45 - \delta) - Q_R \text{ Sin } (45 - \delta) \quad \ldots\ldots\ldots (7.12)$$

and

$$R_{RW} = \sqrt{\Delta T_W^2 + \Delta S_W^2} \quad \ldots\ldots\ldots (7.13)$$

The method for calculating the individual reactions, P_{PW} and Q_R, are described below:

7.3.2.3 Assumptions

The assumptions for passive cutting and rear tip reaction are given as below:

i. The assumptions (i) and (ii) of Section 7.3.1.1 also apply for this model.

ii. The wire is considered like a wedge with included angle of 90^o in accordance with Zelenin (1950).

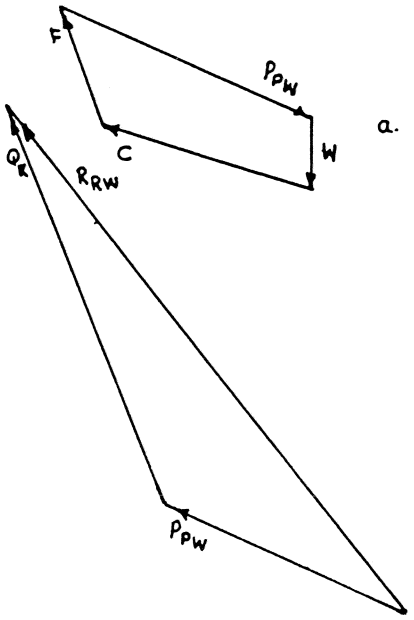

a. PASSIVE SOIL RESISTANCE OF A DEFORMED SOIL SLICE

b. TOTAL SOIL REACTION ON THE WIRE AT 'b'

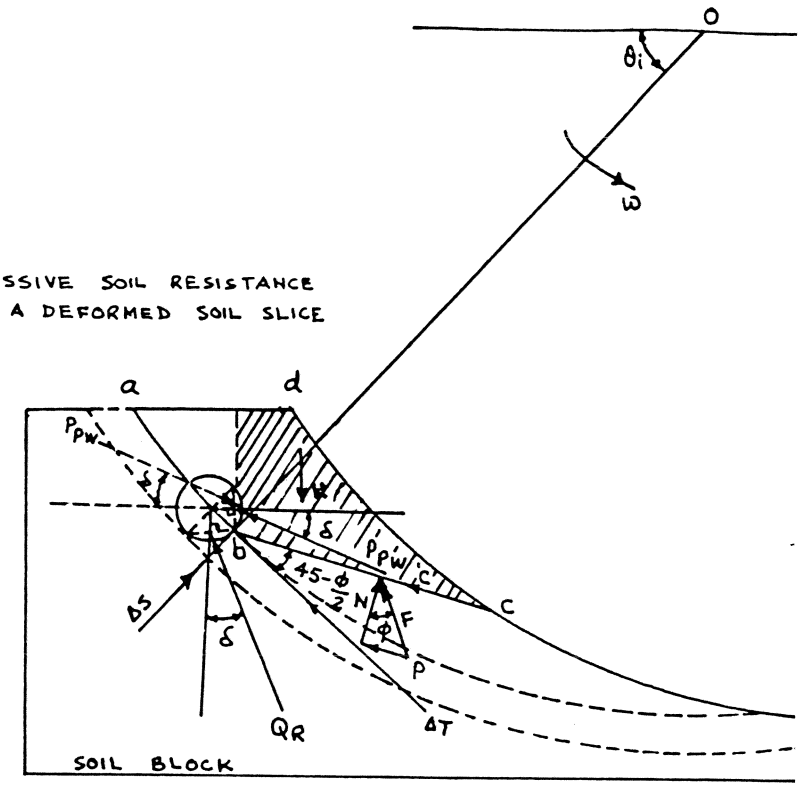

FIGURE 7·5 SOIL REACTION ON A ROTATING WIRE

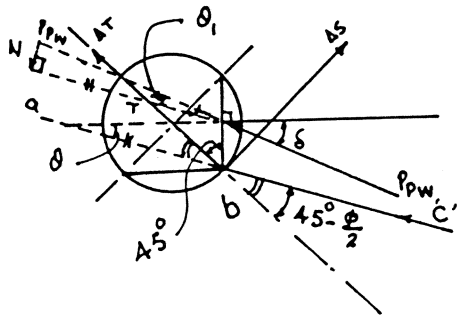

C. ENLARGED VIEW OF WIRE AT 'b'

$$\theta = 180^\circ - (90^\circ + 45 + 45 - \frac{\phi}{2}) = \frac{\phi}{2}$$

THE RELATIONSHIP BETWEEN THE DIRECTION OF P_{PW} AND 'C' IS GIVEN AS,

$$\theta_1 = \delta - \frac{\phi}{2}$$

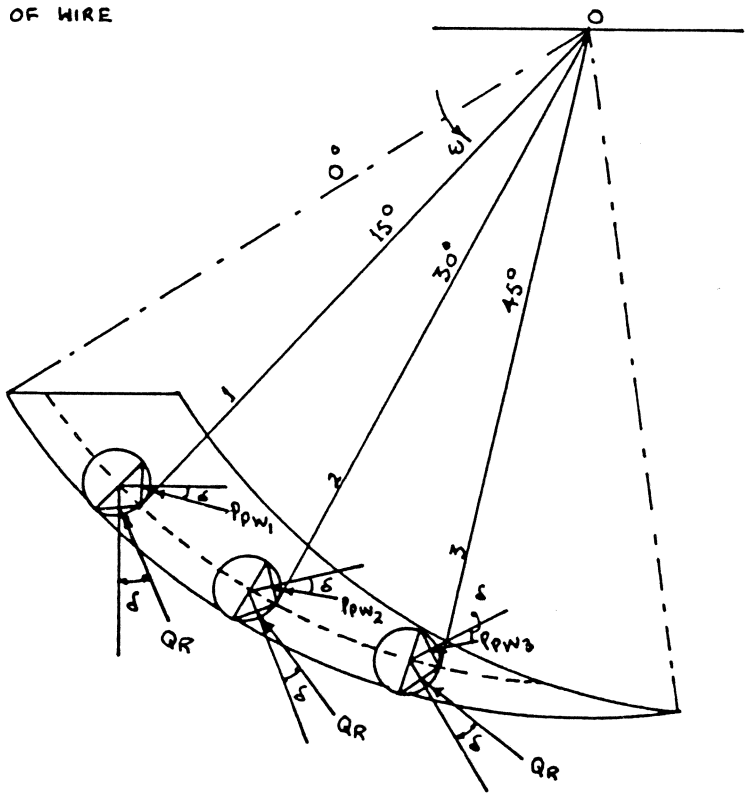

FIGURE 7·6 SOIL REACTION AT DIFFERENT POSITION OF A ROTATING WIRE IN CUTTING A FULL SOIL SLICE

iii. The wire can be divided in two halves with respect to the tangent at a point under consideration during the cutting process and

(a) The soil failure for half portion towards free curved face is in accordance with (i) and

(b) The failure for the other half towards undeformed soil mass is due to local shear failure similar to a wedge-shaped foundation at great depth (depth/width-ratio $\geqslant$ 4) suggested by Meyerhof (1961) and substantiated by Godwin (1974) with a very narrow tine working in sandy loam soil at a density around 1500 kg/m^3.

iv. The reactions P_{PW} and Q_R on both half portions of the wire are considered to be acting at an angle of friction, δ, with the normal to the face of the 90^o wedge.

7.3.2.4 The Model for the Passive Resistance of the Wire

A wire cutting the soil slice is shown in Figure 7.5 at an angle of θ_i with the horizontal after 15^o of the penetration in the soil. Equating the soil reaction parallel to and normal to the failure plane, bc, similar to Section 7.3.1.2 and neglecting any surcharge and adhesive force, the following Equations are obtained:

$$P = W \cos\left(\theta_i + 45 - \frac{\phi}{2}\right) + P_{PW} \cos\left(\delta - \frac{\phi}{2}\right) \quad \ldots\ldots\ldots \quad (7.14)$$

$$N = W \sin\left(\theta_i + 45 - \frac{\phi}{2}\right) + P_{PW} \sin\left(\delta - \frac{\phi}{2}\right) \quad \ldots\ldots\ldots \quad (7.15)$$

Also, the Mohr-Coulomb soil failure conditions must be satisfied on the failure plane, bc, therefore;

$$P = C + N \tan\phi \quad \ldots\ldots\ldots \quad (7.16)$$

Now, substituting the values of P and N from Equations 7.14 and 7.15 in Equation 7.16 and solving for P_{PW}, the following is obtained:

$$P_{PW}\left[\text{Cos}\left(\delta-\frac{\phi}{2}\right)-\text{Sin}\left(\delta-\frac{\phi}{2}\right).\tan\phi\right]=C+\left[\text{Sin}\left(\theta_i+45-\frac{\phi}{2}\right).\tan\phi-\text{Cos}\left(\theta_i+45-\frac{\phi}{2}\right)\right]W$$

$$\therefore\ P_{PW}=\left[\frac{1}{\text{Cos}\left(\delta-\frac{\phi}{2}\right)-\text{Sin}\left(\delta-\frac{\phi}{2}\right).\tan\phi}\right]C+\left[\frac{\text{Sin}\left(\theta_i+45-\frac{\phi}{2}\right).\tan\phi-\text{Cos}\left(\theta_i+45-\frac{\phi}{2}\right)}{\text{Cos}\left(\delta-\frac{\phi}{2}\right)-\text{Sin}\left(\delta-\frac{\phi}{2}\right).\tan\phi}\right]W$$

Allowing T_{CW} and $T\gamma_W$ to represent the terms given in the brackets, the passive resistance of a wire is given by:

$$P_{PW} = T_{CW}.C + T\gamma_W.W \qquad \text{..... (7.17)}$$

where T-values are dependent only on the soil properties and position of the wire during cutting.

7.3.2.5 The Model for the Rear Tip Force of a Wire and a Blade

The force acting on half thickness $(\frac{t}{2})$ of the wire or blade tip due to local shear failure towards undeformed soil can be determined using Meyerhof (1961) solution for a wedge-shaped foundation at great depth. The stress on the face of the wire for weightless soil is given as:

$$q = C\,N_c' + p_o\,N_q' \qquad \text{..... (7.18)}$$

where

q = stress upon the wire face

c = cohesion

N_c' = cohesive N-factor

N_q' = surcharge N-factor

The N-factors have been determined by Meyerhof for limiting conditions of perfectly smooth and perfectly rough wedges of varying semi-angles. For rough wedges, the factors are sensibly unaffected by the wedge angle (false base) except for semi-angles of about $< 30^o$ when the factors increase rapidly with smaller angles. The factors for smooth wedges are much smaller than those for rough wedges. The respective N-factors are plotted for a wedge semi-angle of 45^o applicable to the tip or a wire as shown in Figure 7.7. The bearing capacity factors for intermediate degrees of roughness can be found by linear interpolation between the two extreme limits with good approximation.

The geostatic stress, P_o, acting normal to the equivalent free surface defined by Meyerhof is given by Equation 7.19 below:

$$P_o = K_o \gamma z \qquad \ldots\ldots\ldots (7.19)$$

where K_o = the ratio of horizontal and vertical stress for soil at rest and given to about 0.5 for sand and 1.0 for clays, Meyerhof (1951 and 1961). However, the experimental values of this coefficient are modelled by $K_o = 1 - \sin \phi$, (Lambe and Whitman, 1968).

γ = soil bulk unit weight

z = depth of wire from horizontal soil surface

The total force on $\frac{t}{2}$ thickness of the wire is obtained from Equation 7.20 given below:

$$Q_R = \frac{t}{2} \cdot c \cdot N_c' \cdot w + K_o \cdot \gamma \cdot z \cdot w \cdot \frac{t}{2} \cdot N_q' \qquad \ldots\ldots (7.20)$$

where t = thickness of the tip or diameter of wire

w = width of cut

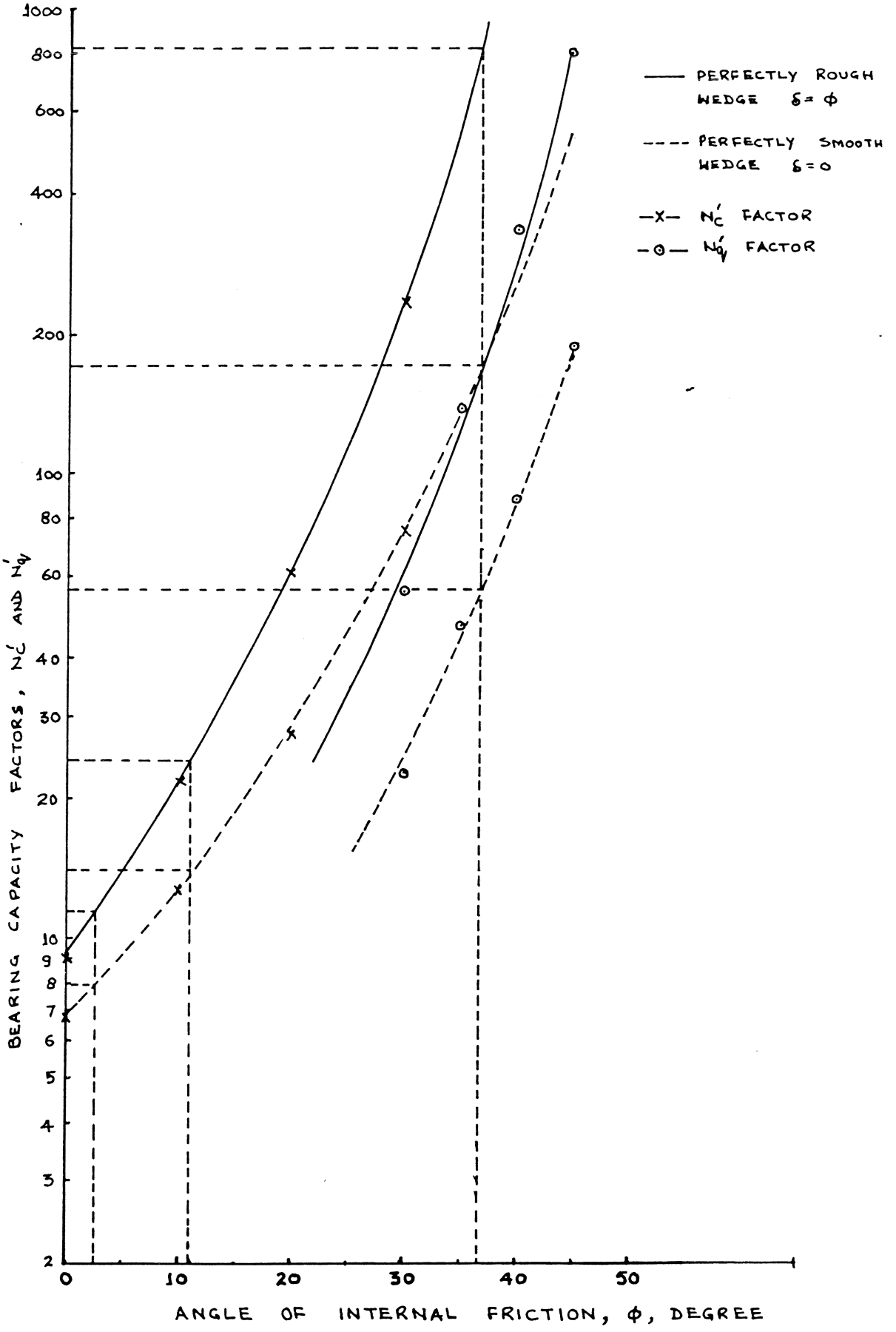

FIGURE 7.7 RELATIONSHIP BETWEEN BEARING CAPACITY FACTORS AND ANGLE OF INTERNAL FRICTION FOR A DEEP WEDGE SHAPED FOOTING WITH INCLUDED TIP ANGLE OF 90 DEGREE (MEYERHOF, 1961).

7.4 Dynamic Soil Reactions on the Blade

7.4.1 Dynamic Reaction in Throwing a Slice, I_F

Bernacki (1962) postulated that the forces acting on the blade of a tiller are mainly due to the static force in cutting the soil slice at infinitesimal circumferential and forward speeds and throwing the slice. He derived the conditions of the movement of particles of the soil slice along the surface of the blade. In a similar approach Poltavtsev (1954) suggested an approximate equation to determine the resistance to the ejection of the slice. However, their methods were purely theoretical in nature and so complex to use in practice that they resorted to empirical coefficients. For practical purposes, the following fundamental equation can be derived for the dynamic force.

7.4.1.1 The Fundamental Concept

In the rotary tilling process, the position of the blade in cutting a soil slice and the velocity of the deformed soil slice are known, therefore, the dynamic force can be considered as a function of position. Under this condition a model based on the 'Work - Energy - Principle' may be an appropriate solution.

7.4.1.2 Assumptions

In order to simplify the complex problem the following assumptions are made:

i. The soil slice is cut in a complete block and is intact with the interface during cutting the full slice. The initiation of the motion of the deformed slice alongwith the blade is considered after approximately 10^{o} of penetration of tip when the major portion of the slice is detached in accordance with observations in Chapter 5. The peak dynamic force in Chapter 6 was observed to occur around 30^{o} to 40^{o} penetration of the blade and is equivalent to approximately 80^{o} of blade rotation from the

horizontal axis of the rotor. Therefore, it may be reasonable to assume that the full separation of the soil slice from the blade occurs at its bottom most position i.e. after 90^{o} rotation of the tip from the horizontal axis.

ii. The trajectory of the motion of the slice is a continuous curve between the start of detachment and end of separation from the blade.

iii. The soil slice moves with the blade at an absolute velocity equal to the velocity of the blade plus speed of advance of the rotor. Since the velocity of the blade varies with its angular position, the slice is thrown from the blade at a velocity equal to the average velocity between that at the start of the shear plane and end of cut.

7.4.1.3 The Model Development

The resistance to throw the soil slice is the measure of kinetic energy restored in the soil mass and is given as:

$$K.E. = \tfrac{1}{2}\, m\, v_c^2 \qquad \ldots\ldots\ldots (7.21)$$

where m = mass of the soil slice

$$\left(\frac{Lb \times d \times w}{g}\right).\gamma$$

γ = bulk unit weight

g = acceleration due to gravity

v_c = peripheral speed of the blade

Hendrick and Gill (1971) reported the work conducted on rotary tillers by Frevert (1940), and Grinkchuk and Matyashin (1969) who postulated the expenditure of tilling energy proportional to the length of cutting path. Hence, the work done in throwing a slice can be taken as the product of dynamic force (I_F) acting on the slice and the distance (L) travelled by the blade from the detachment of the slice

and the end of cutting. This force is equivalent to the kinetic energy of the deformed slice given in Equation 7.21, from which;

$$I_F \times L = \frac{1}{2} \frac{Lb \times d \times w}{g} \gamma v_c^2$$

$$I_F = \frac{1}{2} \frac{Lb \times d \times w}{g \times L} \gamma v_c^2 \qquad \ldots\ldots\ldots (7.22)$$

The individual parameters are obtained as below:

a. The Blade Traversing in a Circular Trajectory

i. $$L = R\theta_B \qquad \ldots\ldots\ldots (7.23)$$

where θ_B = angle between detachment of slice and end of cutting

ii. $$v_c = \frac{\pi D N}{60} \text{ m/sec} \qquad \ldots\ldots\ldots (7.24)$$

where D = diameter of the rotor, m
N = speed of the rotor, r.p.m.

b. The Blade Traversing in a Cycloidal Trajectory

i. Length of cycloidal path (L)

$$L = R\theta_B - \frac{Lb \cdot z_1}{2\pi R} (2Rd - d^2)^{\frac{1}{2}} \qquad \ldots\ldots\ldots (7.25)$$

where z_1 = number of blades on one side of the rotor

ii. Velocity of the Blade (v_c):

The velocity of any point in cycloidal trajectory is a combination of the rotor forward speed, rotational speed and the distance from the rotational axis to the point of interest. Hendrick and Gill (1978) suggested an useful concept which permits the use of the simplifying 'Instant-Centre-Technique' for determining the velocity of a point in cycloidal trajectory. The velocity of a point is given as:

$$v_c = |\omega| \, l_1 \qquad \ldots\ldots\ldots (7.26)$$

where $|\omega|$ = angular velocity of the blade about its axis

l_1 = distance between Instant Centre and the point of interest

and $$l_1 = R\left[1 + (\lambda)^{-2} - 2(\lambda)^{-1} \cdot \sin\alpha\right]^{\frac{1}{2}} \qquad \ldots\ldots\ldots (7.27)$$

where λ = ratio between circumferential and forward speed of the rotor i.e. $\frac{Vc}{Vf}$

α = angular rotation, measured from the x - axis in the direction of rotation

The average velocity of the blade is given as:

$$v_{cav} = \frac{\omega R}{2}\left[(1 + (\lambda)^{-2} - 2(\lambda)^{-1} \cdot \sin\theta_i)^{\frac{1}{2}} + (1 + (\lambda)^{-2} - 2(\lambda)^{-1} \cdot \sin 90)^{\frac{1}{2}}\right] \qquad \ldots\ldots (7.28)$$

7.4.1.4 Bernacki Concept on Dynamic Force

For practical purposes Bernacki (1962) suggested an empirical Equation for the calculation of dynamic force of resistance which is presented overleaf for comparison with the results obtained from the fundamental concept.

$$P_d = 0.01\ w \cdot d \cdot \alpha_u \cdot V_f \cdot V_c \qquad \ldots\ldots\ldots (7.29)$$

where P_d = average dynamic force, kg

w = width of cut, dm

d = depth of cut, dm

V_f = forward speed, m/sec

V_c = circumferential speed, m/sec

α_u = coefficient of dynamic resistance,

$$\frac{kg - sec^2}{m^4}$$

$$= 400 - 500\ kg \cdot sec^2/m^4$$

For a medium textured soil with density around 1600 kg/m^3, Bernacki used a value of α_u = 400 kg . sec^2/m^4 for verification of his experimental results.

7.4.2 Dynamic Force due to Compression/Scrubbing of the Undeformed Soil (Q_{RT})

7.4.2.1 The Concept of the Model

The clearance angle (δ_i) changes at various positions of the blade in a cutting cycle when traversing in a cycloidal trajectory. The correction angle ($\Delta\delta$) can be determined for any position of the blade from the equation given below:

$$\tan \Delta\delta = \frac{V_f \cos \theta_i}{V_c - V_f \sin \theta_i}$$

where θ_i = angular position of the tip of the blade from x - axis in the direction of travel

$$\therefore \tan \Delta\delta = \frac{\cos \theta_i}{\lambda - \sin \theta_i} \qquad \ldots\ldots\ldots (7.30)$$

The effective cutting angle (the angle between the front face of the blade and a tangent to the cycloid at the point of interest) then becomes equal to $(\beta + \delta_1 - \Delta\delta)$ degree and the effective clearance angle becomes $(\delta_1 - \Delta\delta)$ degree. By increasing the forward speed of the rotor at constant rotational speed, the effective clearance angle becomes negative at a certain combination due to which the back chamfered face 'compresses' the undeformed soil. This undesirable phenomenon termed as trowelling, Hendrick and Gill (1974), restricts the penetration and produces a tendency for the blade to 'walk-out' of the soil. Although it is never recommended that rotary tillers should be operated at such a combination of speeds, it is desirable to know the nature and magnitude of the force penalty caused by this effect.

As a first hand approximation the load - sinkage results of a flat plate seemed to be a feasible solution to determine the reaction due to compression of the soil. Various approaches have been reported to understand off - the - road vehicle mechanics by using the plate sinkage test Bekker (1960), Reece (1965), Youssef and Ali (1982) but all the methods are essentially empirical in nature and the constants have to be determined empirically from experimental data. Godwin et.al. (1978) reported the load - sinkage relationship of a 125 x 100 mm size flat plate for sandy loam soil similar to the one used in the current experiments at two soil densities as shown in Figure 7.8a. These results were obtained by loading the plate and measuring the sinkage under stationary condition (Figure 7.8b). Since a blade of the rotor penetrates and compresses the soil simultaneously, a load - sinkage result with a moving plate would have been more appropriate for the present condition. However, in lack of any such information, the results of Godwin et.al. (1978) were used for determination of the soil reaction due to compression and scrubbing of the blade.

7.4.2.2 Assumptions

i. The blade is penetrating downwards, and compressing and scrubbing the undeformed soil simultaneously. The compression force (Q_{RT}) may be assumed to be acting at an angle of friction (δ) with the normal to the chamfered back face as shown in Figure 7.2.

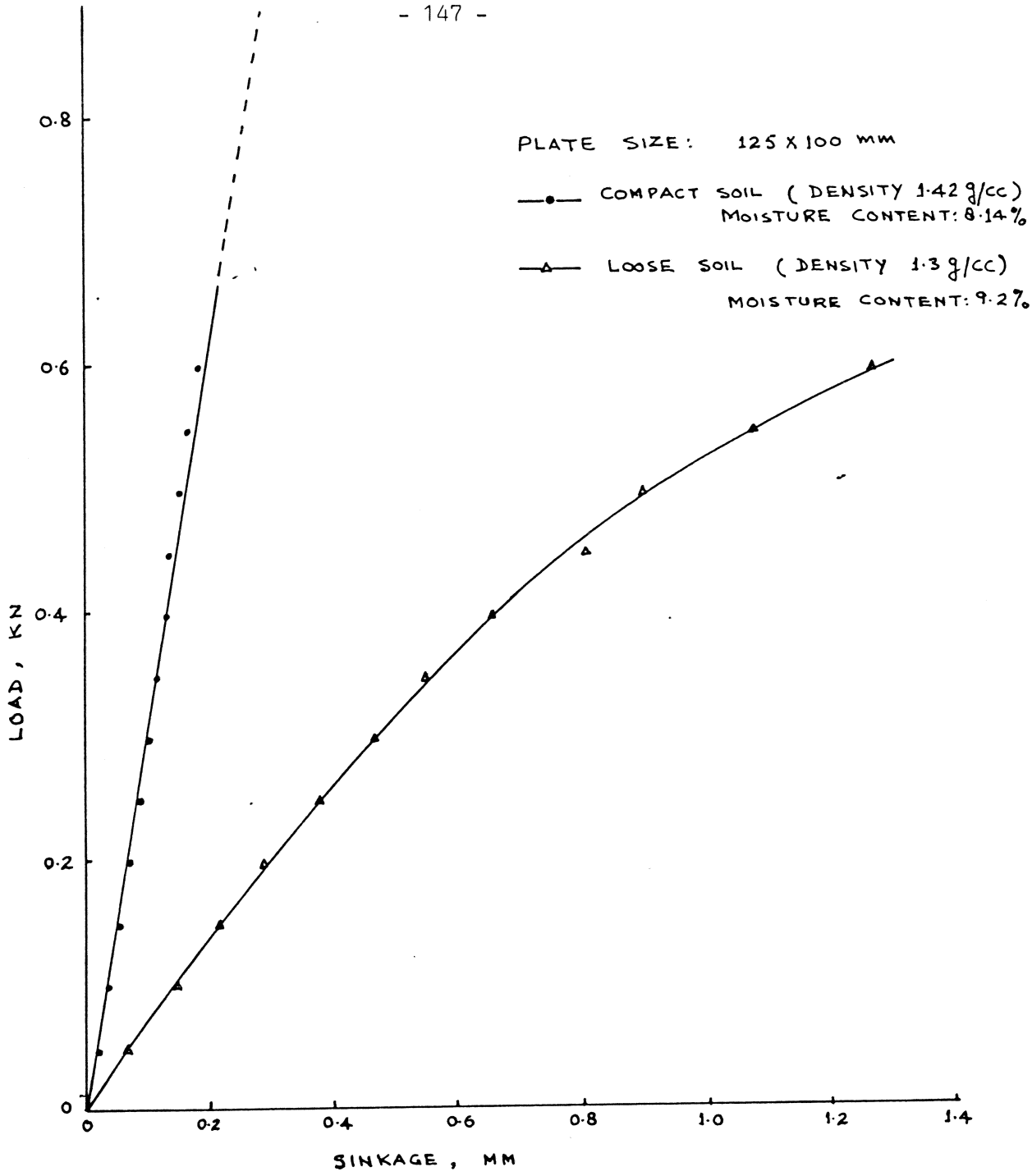

FIGURE 7·8a LOAD-SINKAGE RELATIONSHIP OF A PLATE (GODWIN et. al. 1978)

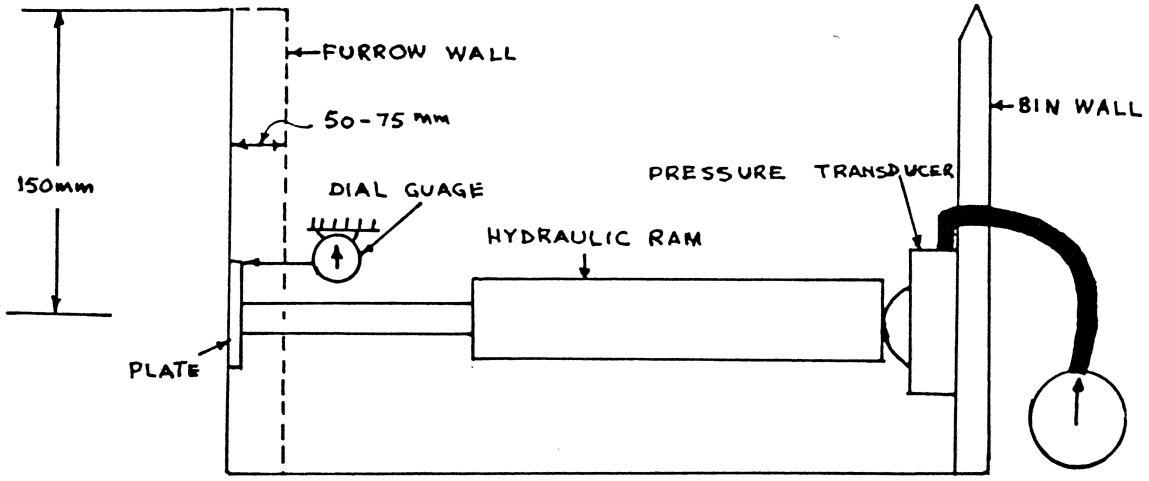

FIGURE 7·8b SOIL-PLATE SINKAGE EQUIPMENT

ii. The compression force is considered due to the sinkage of the blade and a load - sinkage relationship of a flat plate in static condition is equally applicable to the dynamic situation.

iii. The area of the back face of the blade in contact with the soil and the degree of sinkage is varying from the beginning of penetration. At the point of entry of the blade the negative clearance angle is larger which reduces as the blade penetrates downwards (Table 6.2) whereas the area of the back face is smaller at the entry and increases with penetration. The maximum soil reaction due to compression of the blade is obtained after full penetration of the chamfered back face. For the present geometry of the blade, the back face comes into contact with soil after 5^{o} of penetration and the forces increase very steeply after this position of the tip as described in Chapter 6. Therefore, the average sinkage of the blade at 5^{o} of penetration is considered for determination of the peak compression force.

7.4.2.3 The Model Development

From Figure 7.2 the force (Q_{RT}) due to compression of the chamfered back face is obtained as below:

$$Q_{RT} = Q_{RS} \text{ Sec } \delta \qquad \ldots\ldots\ldots (7.31)$$

where Q_{RS} = the force due to sinkage of the chamfered back face obtained from simple analogous plate - sinkage tests.

The tangential ($\Delta T'$) and radial ($\Delta S'$) components of the compression force are determined as below:

$$\Delta T' = Q_{RS} \cdot \text{Sec } \delta \cdot \text{Sin } (\delta - \delta_1) \qquad \ldots\ldots\ldots (7.32)$$

$$\Delta S' = Q_{RS} \cdot \text{Sec } \delta \cdot \text{Cos } (\delta - \delta_1) \qquad \ldots\ldots\ldots (7.33)$$

7.5 The Quasi-Static Force Prediction Model for a Blade with Vertical Axis of Rotation

7.5.1 The Model for Less than a Quarter of a Circle Cut

7.5.1.1 The Concept of the Model

The reactions acting on a blade with vertical axis of rotation and on the deformed soil slice is shown in Figure 7.9. The mechanism of the soil failure under this condition is similar to a blade with horizontal axis of rotation (Chapter 4). The main difference, however, under this condition is that there is a bottom shear plane a'b'c'd' with the weight of the deformed soil slice acting upon the plane. The reaction due to different failure regime can be determined in a manner similar to the one described for a blade with horizontal axis of rotation in Section 7.3.

7.5.1.2 Assumptions

i. The major shear plane, bc, develops at an angle of $(45 - \frac{\phi}{2})$ degree with the direction of major principal stress (tangent) according to observations in Chapter 4 and the resistance force is only due to cohesion on the failure plane. The resistance force is considered to be acting at an angle of soil-metal friction (δ) with the interface.

ii. The total weight of the soil block, abcd, acts on the bottom shear plane, a'b'c'd' and the passive resistance acts at an angle of friction with the interface.

iii. The frictional force due to sliding of the bottom end of the blade is neglected.

iv. The tip reaction on its half thickness acts similar to the wire or a blade with horizontal axis of rotations but in the vertical plane.

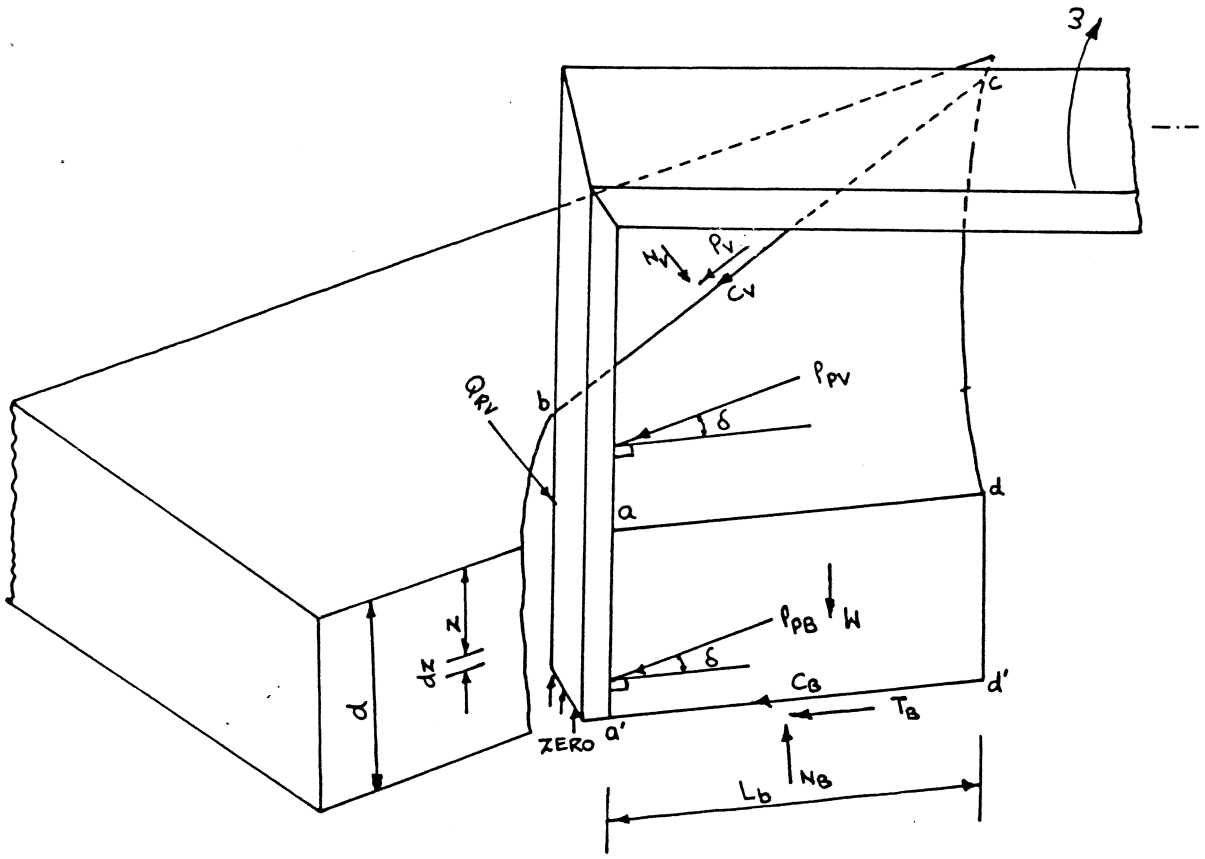

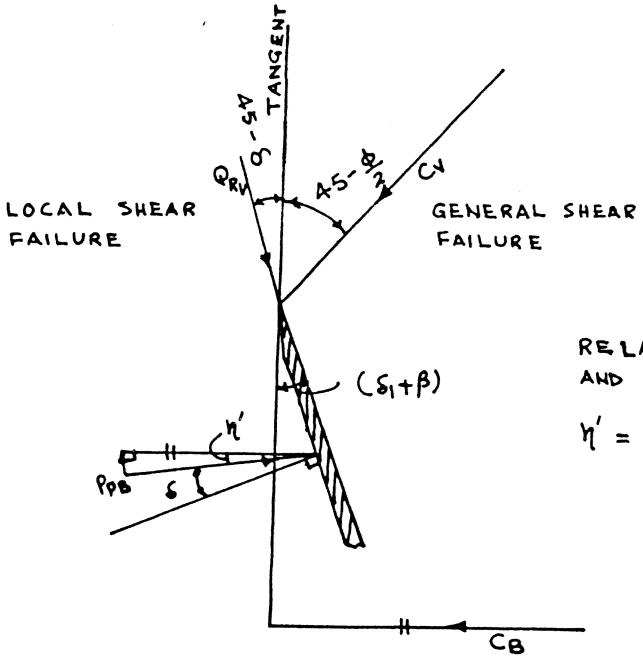

RELATIONSHIP BETWEEN P_{PB} AND C_B IS GIVEN AS:

$$\eta' = (\delta_1 + \beta - \delta) \text{ deg}$$

FIGURE 7·9 FORCES ACTING ON THE BLADE WITH VERTICAL AXIS OF ROTATION FOR LESS THAN $\frac{1}{4}$TH OF A CIRCLE CUT

7.5.1.3 Development of the Passive Resistance Model

The shear force (T_B) and normal force (N_B) on the bottom shear plane, a'b'c'd', is given from the relationship in Figure 7.9 as below:

$$T_B = P_{PB} \text{ Cos } (\beta + \delta_1 - \delta) \quad \ldots\ldots\ldots (7.34)$$

$$N_B = -P_{PB} \text{ Sin } (\beta + \delta_1 - \delta) + W \quad \ldots\ldots\ldots (7.35)$$

According to Mohr-Coulomb criteria of soil failure;

$$T_B = C_B + N_B \tan \phi \quad \ldots\ldots\ldots (7.36)$$

Now, substituting the value of T_B and N_B in Equation 7.36 from Equation 7.34 and 7.35;

$$P_{PB} = \left[\frac{1}{\text{Cos } (\beta + \delta_1 - \delta) + \text{Sin } (\beta + \delta_1 - \delta) \cdot \tan\phi}\right] C + \left[\frac{\tan \phi}{\text{Cos } (\beta + \delta_1 - \delta) + \text{Sin } (\beta + \delta_1 - \delta) \cdot \tan\phi}\right] W$$

Allowing T_{CV} and $T_{\gamma V}$ to represent the terms given in the brackets, the passive resistance due to bottom failure plane is given by:

$$P_{PB} = T_{CV} \cdot C + T_{\gamma V} \cdot W \quad \ldots\ldots\ldots (7.37)$$

The resistance due to the general shear failure along the plane, bc, can be determined using the relationship between the shear plane and the passive resistance, P_P, and has been derived for the blade in horizontal axis of rotation, therefore,

$$P_{PV} = T_C \cdot c \cdot l \cdot d \quad \ldots\ldots\ldots (7.38)$$

The total passive force on the blade is given as:

$$P_{P\ Total} = P_{PB} + P_{PV} \qquad \ldots\ldots\ldots (7.39)$$

The tangential (ΔT_V) and radial (ΔS_V) components of the resistance on the vertical blade due to total passive resistance ($P_{P\ Total}$) and rear tip force (Q_{RV}) can be determined using Equations 7.2 and 7.3.

7.5.1.4 Determination of Rear Tip Force

From Equations 7.19 and 7.20, the stress acting upon an element, dz, at a depth z (Figure 7.9) is given as:

$$q_V = C\ N_c' + K_o \gamma z\ Nq'$$

The total force acting upon half portion ($\frac{t}{2}$ thickness) of the tip of the blade is therefore:

$$Q_{RV} = \frac{t}{2} \cdot C \cdot N_c' \int_0^d dz + K_o \gamma\ Nq' \frac{t}{2} \int_0^d z\ dz$$

$$\therefore Q_{RV} = \frac{t}{2} \cdot C \cdot N_c' \cdot d + \tfrac{1}{4} K_o \gamma\ Nq' \cdot t \cdot d^2 \qquad \ldots\ldots (7.40)$$

7.5.2 The Model for Half-Circle Cut

7.5.2.1 The Concept of the Model

The soil reactions acting on the blade with vertical axis of rotation traversing in a half circle are similar to the quarter of a circle cut shown in Figure 7.9. However, there are variations in the boundary condition in that the general shear plane, bc, does not develop at an angle of $(45 - \frac{\phi}{2})$ degrees with the direction of major principal stress but takes the path of least resistance towards the

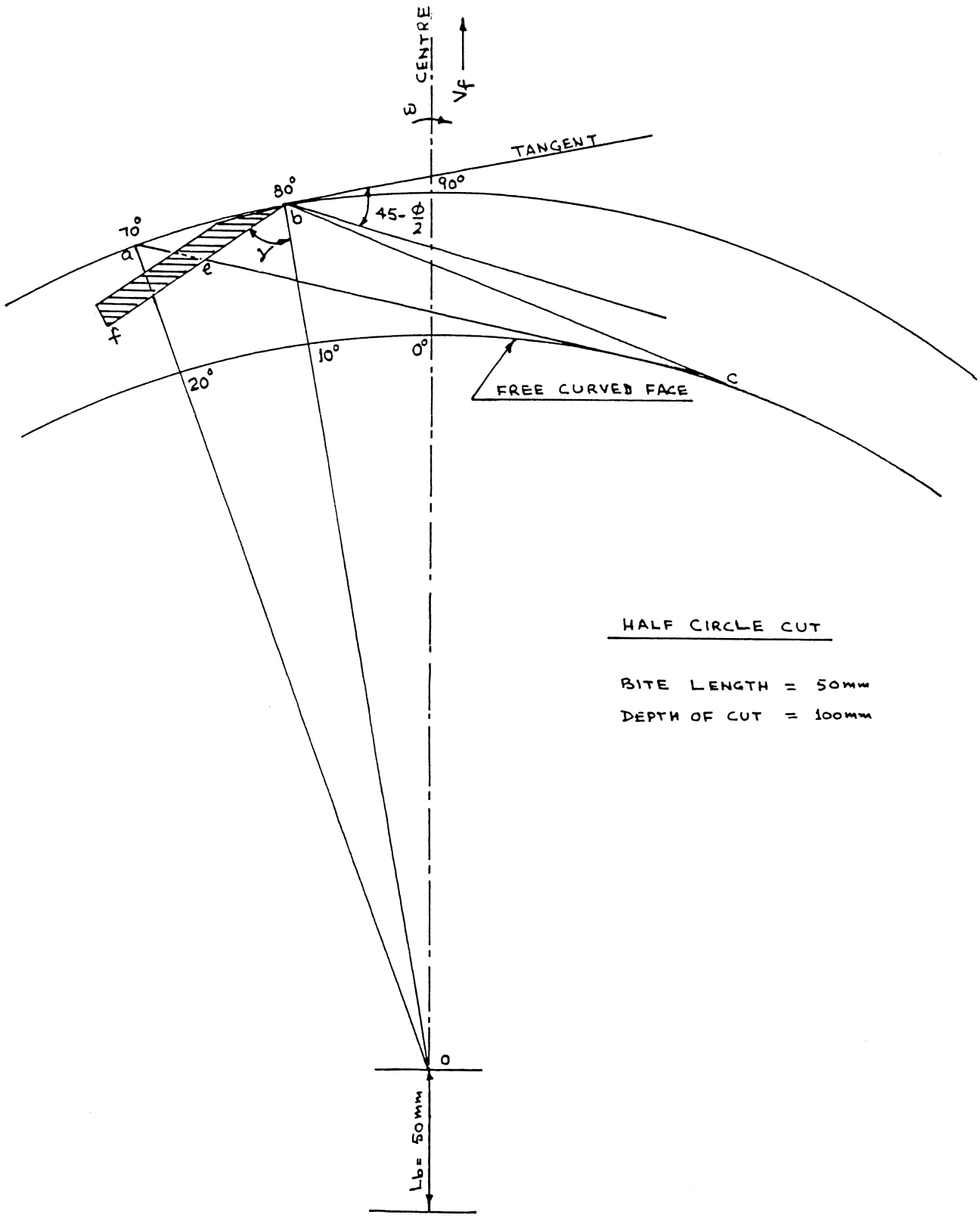

FIGURE 7.10 CONCEPTUAL MECHANISM OF SOIL FAILURE FOR A BLADE WITH VERTICAL AXIS OF ROTATION OPERATING IN A HALF CIRCLE

free curved face at a shallowest angle of $(45 - \frac{\phi}{2} + \psi)$ in accordance with observations in Chapter 4. The value of angle, ψ, increases with the bite length. The peak resultant force for cutting a full half circle was observed at an angle of $80^{o} \pm 5^{o}$ from the start of the cut as described in Chapter 5. Therefore, the peak forces can be determined using the following assumptions.

7.5.2.2 Assumptions

i. The assumptions i to iv of Section 7.5.1.2 also apply in this case with an extension in (i) that the general shear plane bc develops at $(45 - \frac{\phi}{2} + \psi)$ degrees with the major principal stress at a shallowest angle towards the curved face.

ii. The peak forces occur at 10^{o} before the central axis of rotation i.e. 90^{o} considered on the line of the direction of travel for all the bite lengths and the shear planes develop after every 10^{o} of rotation. Therefore, the reactions of the failed soil at the front face of the blade, ef, (Figure 7.10) is neglected.

iii. The soil failure occurs in a complete block abc.

The total passive resistance ($P_{p\ Total}$) and component forces are determined in the manner similar to Section 7.5.1.3.

A sample calculation for determination of forces on a blade / wire with horizontal axis of rotation in a frictional and pure cohesive soil and a blade with vertical axis of rotation is given in Appendix 4.

8. DISCUSSION OF EXPERIMENTAL AND PREDICTED RESULTS

8.1 Introduction

This chapter describes the results obtained using the prediction model developed in Chapter 7 in association with the experimental results reported in Chapters 5 and 6. The sample calculations for the prediction of the forces on the blade and the wire under different working regimes are reported in Appendix 4 and the magnitude of the predicted force components together with the experimental results are presented in Tables 8.1 to 8.5. The discussion of the experimental results has already been reported with details in the relevant chapters. This chapter, therefore, concentrates on the correlation between the observed and predicted results with a brief scientific reasoning wherever appropriate.

8.2 Predicted Quasi-Static Forces on the Wire

8.2.1 For Frictional Soil

The sample calculation described in Section A4.1 was used to determine the predicted force components presented in Table 8.1. The peak forces have been determined after 15^{o} entry of wire into the soil for bite lengths upto 150 mm and after 25^{o} entry for greater bite lengths for all the depths of cut based upon the observations in Chapter 5. The relationship between the observed and predicted sets of data at different 'fetch-ratios' is shown in Figure 5.4. The figure shows a very close association between the two sets of results for depths of cut of 100 mm and 150 mm with an exception for the very small 'fetch-ratio' when the model over predicts the resultant force. A similar trend can be noticed at the lower depth of 50 mm for all the 'fetch-ratios'. The overall association between experimental and predicted results shown in Figure 8.1 shows a high correlation coefficient (γ = 0.9359) which can be further improved if the results at very small 'fetch-ratio' and depth of cut are not considered alongwith the general model. The deviation between the two data sets where there is greater

deviation in the association can be explained as follows: The over-estimation of the lower magnitude expected forces occurs at smallest 'fetch-ratio' and depth of cut. It was observed that under these conditions, there is multiplicity of general shear failure planes which manifest a possibility that the full local shear failure towards the undeformed soil may not be fully mobilised. The determination of the rear tip force, Q_R, is based upon the assumption that the failure mechanism is similar irrespective of the 'fetch-ratios' for all the depths of cut. A constant magnitude of Q_R would, therefore, over-estimate the magnitude of lower expected forces when operating in the vicinity of a free surface.

8.2.2 For Pure Cohesive Media (Artificial Clay)

The predicted force on the wire in a purely cohesive media is presented in Section A4.1.2. Under this condition, an average experimental force of approximately 90 Newtons was recorded with insignificant variation with the angular position of the wire during cutting a full soil slice. The predicted values of 77.76 N and 48.03 N are determined assuming the wire as perfectly rough and perfectly smooth respectively. It can be noticed that the force on the wire is under predicted by approximately 15 % when wire is assumed as perfectly rough. However, because of the interaction between c and ϕ, when an upper 95 % confidence limit of ϕ (11.34^{o}) is chosen with the lower 95 % confidence limit of c (40.61 kN/m^2), the resultant force is predicted as 89.08 N and 51.96 N for the perfectly rough and perfectly smooth interface respectively. It is evident from this analysis that the association between the experimental and predicted results is very close when the interface is assumed as rough in agreement with Meyerhof (1961) who postulated that the cone resistance and the point resistance of brass piles in clays agree close to theoretical estimates based on perfectly rough tips.

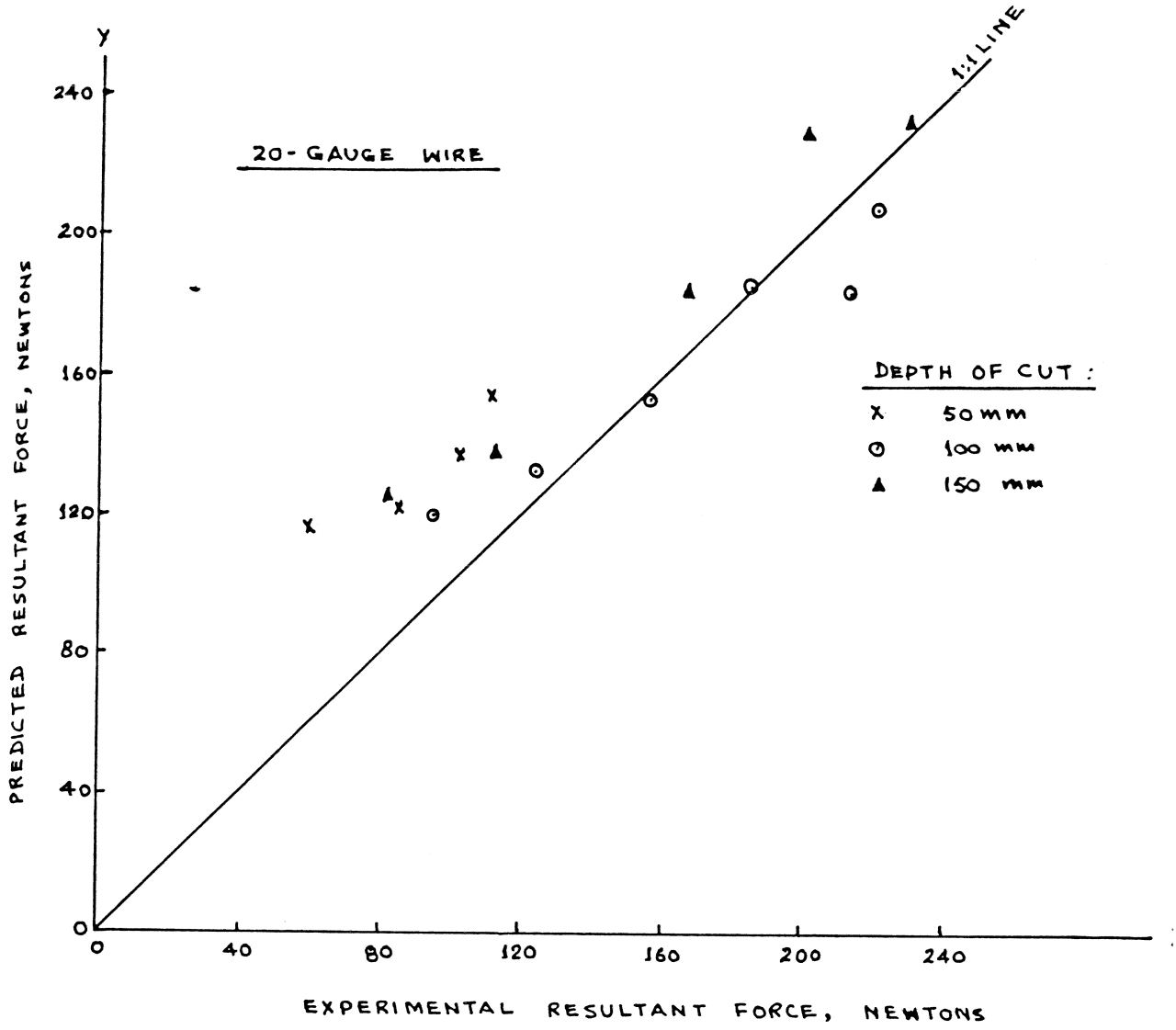

STATISTICS:

CORRELATION COEFFICIENT, r = 0.9359

REGRESSION COEFFICIENT, b = 0.6658

95% UPPER CONFIDENCE LIMIT, b = 0.8159

95% LOWER CONFIDENCE LIMIT, b = 0.5157

INTERCEPT, a = 67.0137

95% UPPER CONFIDENCE LIMIT, a = 89.943

95% LOWER CONFIDENCE LIMIT, a = 44.084

FIGURE 8.1 RELATIONSHIP BETWEEN EXPERIMENTAL AND PREDICTED PEAK RESULTANT FORCE IN CUTTING A FULL SOIL SLICE WITH A WIRE

8.3 Predicted Forces for the Blade with Horizontal Axis of Rotation

8.3.1 Predicted Quasi-Static Forces

The procedure outlined in Section A4.2.1 was used to derive various force components of a rotating blade at different bite lengths and depths of cut as shown in Table 8.2. The peak resultant force in cutting a full soil slice has been calculated at 10^{o} entry of the tip for bite lengths upto 150 mm and at 15^{o} for bite lengths greater than 150 mm for all the depths of cut. The relationship between the observed and predicted results of the peak resultant force at different 'fetch-ratio' are presented in Figure 5.10. In general the predicted results adequately reflect the experimental values.

Figure 8.2 shows the overall relationship between the experimental and predicted peak resultant force. The statistics given, accompanying the figure, enable an estimation of the performance of the model to be made. If there was a one to one correspondance between the predicted set of data and the experimental set of data the regression equation linking the two data sets is given as:

$$y = a + bx \qquad \ldots\ldots\ldots (8.1)$$

where y = predicted data

x = experimental data

The Equation 8.1 would have the parameter values as the intercept, $a = 0.0$ and the regression coefficient, $b = 1.0$.

The closeness of the association between the two sets of data is given by r, the correlation coefficient, the closer the magnitude of r to unity then closer the association between two data sets.
The value of the regression coefficient was less than unity with an intercept greater than zero, indicating that the model slightly under predicts the magnitude of the higher expected forces and over predicts some of the lower expected forces. However, the overall association between the two data sets is good with acceptable correlation coefficient.

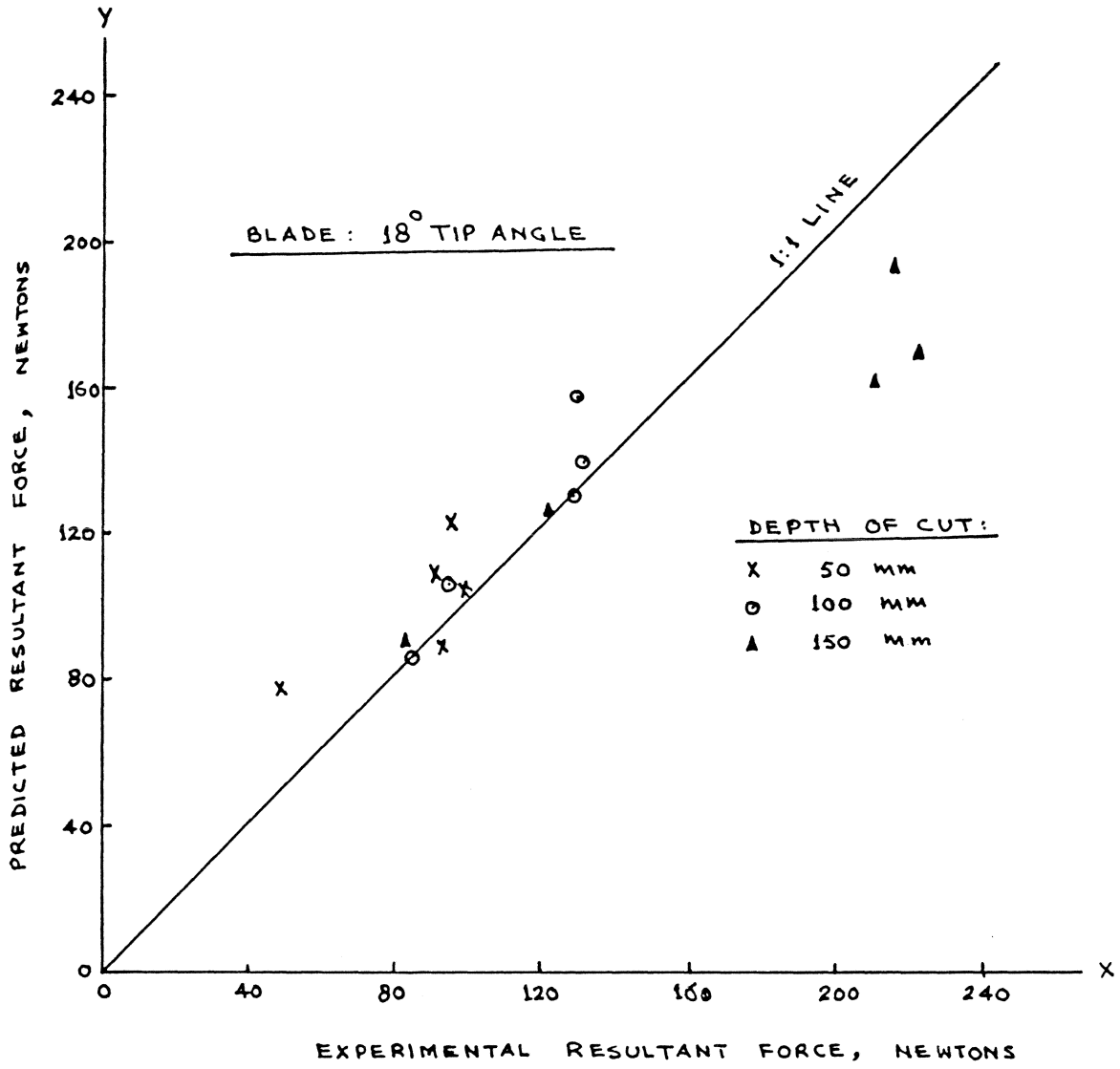

STATISTICS:

CORRELATION COEFFICIENT, r	= 0.9194
REGRESSION COEFFICIENT, b	= 0.5995
95% UPPER CONFIDENCE LIMIT, b	= 0.7530
95% LOWER CONFIDENCE LIMIT, b	= 0.4459
INTERCEPT, a	= 51.742
95% UPPER CONFIDENCE LIMIT, a	= 72.278
95% LOWER CONFIDENCE LIMIT, a	= 31.206

FIGURE 8.2 RELATIONSHIP BETWEEN EXPERIMENTAL AND PREDICT PEAK RESULTANT FORCE IN CUTTING A FULL SOIL SLI WITH A BLADE

8.3.2 Predicted Dynamic Forces

8.3.2.1 Dynamic Force due to the Acceleration of the Deformed Soil Slice

A sample calculation of the acceleration force is given in Section A4.2.2.1 of Appendix 4 for the blade traversing in the circular and cycloidal trajectories. The resultant force for the circular trajectory has been determined using the fundamental concept only (Table 8.3) because the Bernacki concept (1962) on dynamic force can not be used for a blade with zero forward speed. Nevertheless, both the concepts have been used for the blade with cycloidal trajectory for the comparison of the results as shown in Table 8.4.

The quasi-static force remains constant with the peripheral speed of the blade and added to the dynamic force due to acceleration of the deformed soil slice to obtain the total predicted dynamic force as shown in Figure 6.3. In general, the predicted results reflect the experimental results well. The predicted dynamic forces with increases in peripheral speed, however, are slightly less than the experimental but remain always within the limit of standard deviation of three replicates of the experiments. The general trend of both the sets of data is similar in that the forces increase with the speed of cutting. It is also evident from the figure that at the largest peripheral speed of 3.87 m/sec (120 r.p.m.), the experimental and predicted results are approximately equal. The reason for this may be accounted for by the aerodynamic and ventilation losses of deformed soil mass which increase with the speed of cutting whereas the prediction model does not incorporate any such kind of losses.

A similar trend can be noticed with the observed and predicted dynamic forces for the cycloidal trajectory as shown in Figure 6.4. The predicted force at all the speeds except the largest speed of 3.87 m/sec is very close to the experimental force. A slight over-prediction of approximately 12 % at the largest speed can be due to the soil mass losses mentioned earlier. Even so the predicted dynamic force is always within the standard deviation of the experimental set of data. Both the dynamic force according to Bernacki (1962) concept

and the fundamental concept assuming throwing velocity of the slice equal to the peripheral speed of the blade (V_c) as in circular trajectory, have been determined. With this assumption the predicted results by both the concepts are approximately equal as shown in Table 8.4. The Bernacki concept over predicts the dynamic force by approximately 20 % from the average experimental force at the largest speed but remains close to the extreme variation of the observed dynamic force. It is quite probable that a blade with a large effective clearance angle instead of 2.31^{o} at the entry of the blade in the soil, used in the current experiments, may restore the two sets of data closer by neglecting any scrubbing force at the chamfered face of the blade due to slight variation in the cutting and forward speeds. Since there is no difference in the predicted results by Bernacki concept and fundamental concept when the speed of throwing is assumed equal to V_c instead of V_{cav}, the fundamental concept can reasonably be accepted for all practical purposes considering the complexity of determining the magnitude of V_{cav}.

8.2.2.2 Dynamic Force due to Scrubbing of the Chamfered Back Face of the Blade

The sample calculation for prediction of forces under this condition is given in Section A4.2.2.2 and the relationship between the experimental and predicted results is presented in Figures 6.6 to 6.8 for three depths of cut. The figures show the association between two data sets when the effective clearance angle is positive i.e. $(\delta_1 - \Delta\delta) > 0$ and that when the angle is zero or negative i.e. $(\delta_1 - \Delta\delta) \leq 0$. The predicted quasi-static forces for the circular trajectory (Table 8.2) are shown in the figures alongwith experimental forces for the cycloidal trajectory when $(\delta_1 - \Delta\delta) > 0$. The association between the two data sets is very close for all the depths of cut. For $(\delta_1 - \Delta\delta) \leq 0$, the dynamic component forces have been added to the respective quasi-static components which again show a close agreement between the data sets. However, for the depths of cut of 100 mm and 150 mm, at largest bite length, it was not possible to predict the forces because of the limit of the range of the plate-sinkage tests shown in Figure 7.8a.

8.4 Predicted Forces for the Blade with Vertical Axis of Rotation

A sample calculation for the prediction of the component forces under the vertical working regime of the blade given in Section A4.3 was used to determine the component forces shown in Table 8.5a and b. The association between the two data sets is shown in Figure 5.18 for side cuts (d') of 100 mm and 150 mm at different bite lengths. In general, the model over predicts the resultant force by approximately 20 % but the general trend of the results is similar in both the sets. For a side cut of 150 mm, the predicted resultant force is nearly equal to the experimental value with a slight over prediction.

The association of the results with half-circle cuts (Figure 5.20) is much better than the less than a quarter of a circle cut (Figure 5.18). However, the resultant force is under predicted with very less variation. The reasons for over predicted results in less than a quarter of a circle cuts and under prediction in half circle cuts may be because of the assumption made for the prediction model which assumes that the soil slice fails by developing a general shear plane and the bottom shear plane in a complete block. This may not be true with half circle cuts in which case the soil will crumble and develop slightly more experimental failure force than the predicted values.

9. CONCLUSIONS

The following conclusions relate to studies conducted with a powered rotating blade operating at a constant cutting angle (25^{o}) and a range of 'Fetch-Ratios' (0.33 : 1 to 5 : 1) with three depths of cut (50, 100 and 150 mm) using a sandy loam soil of friable consistency and a specified density state of 1450 kg/m^3:

i. Investigations showed that there are two modes of soil failure, a general shear failure towards the free curved face of a previous cut and a local shear failure due to 'tip-effect' towards the undeformed soil, occurred simultaneously. The boundary of the general shear failure plane for most practical cases was recorded at an angle of $(45 - \frac{\phi}{2})$ degrees with the direction of major principal stress. The direction of which, is a tangent to the cutting path at the point of the tip for both circular and cycloidal trajectories. The orientation of the principal planes, therefore, changed with the angular position of the tip in cutting a full soil slice. The orientation of rupture plane at large 'fetch-ratios', however, had two main exceptions:

   a. that the first few shear planes before the largest plane developed towards the horizontal free surface, the mechanics of which was similar to a passive inclined blade and;

   b. that the first largest shear plane (fetch-ratio > 1 : 1 for depth of cut, 150 mm) deviated from the general concept towards the base of a previous cut at an angle shallowest to $(45 - \frac{\phi}{2})$ degrees plane.

ii. The presence of a blade face had no significant effect on the shape and orientation of the shear planes which generated as a straight line for all the 'fetch-ratios' as the fundamental failure patterns were common for both a simple cutting tip (wire) and a full blade.

iii. The mechanics of a tip (wire) causing local shear failure was assumed to be similar to the ultimate bearing capacity of a

wedge shaped footing with 90^{o} included angle, operating at great depths. Predictions using this theory gave good agreement with experimental results.

iv. The magnitude of the peak resultant force in cutting a full soil slice occurred after approximately 10^{o} - 15^{o} penetration of the blade tip with an indication to occur after greater penetration with increases in 'fetch-ratio'. The force prediction models developed on the basis of the Mohr-Coulomb soil mechanics both for the tip (wire) and the blade have reflected the experimental results with reasonable degree of accuracy.

v. There was no significant change in the mechanism of soil failure upto the blade tip peripheral speed of 3.87 m/sec (120 r.p.m.) studied in the present investigation. However, there were only two maxima forces in cutting a full soil slice at rotor speed of 80 r.p.m. and more. The peak force (second maxima) occurred after 30^{o} to 45^{o} of blade tip penetration with a larger magnitude with increases in cutting speed.

The dynamic force prediction model incorporated two major components, a quasi-static force component at infinitesimal slow speed due to passive soil failure and a 'tip-effect'; and a dynamic force component due to acceleration of the deformed soil slice. The quasi-static and dynamic force prediction models based upon the Mohr-Coulomb soil mechanics and 'work energy' principle respectively have reflected the experimental results well in close agreement with Bernacki dynamic force concept based upon empirical coefficient.

iv. A disproportionate increase in forward speed in relation to the rotor speed resulted in a several times increase in the radial force component and was noticed due to compression / sinkage of the back chamfered face of the blade. An empirical model based upon analogous flat plate - sinkage results has predicted the experimental values with acceptable association.

vii. From a limited number of experiments on the blade with vertical axis of rotation, the mechanism of soil failure has been found

similar to a blade with horizontal axis of rotation and the failure planes developed either;

a. at $(45 - \frac{\phi}{2})$ degrees with the major principal plane (tangent) for very small 'fetch-ratios', or

b. at an angle shallowest to the tangent upto a break point on the curved free surface similar to a condition described in i(b).

The adaption of the force prediction model developed for the horizontal axis of rotation to the vertical axis mode has produced predicted values which agree closely to the experimental results.

viii. The results of this study have been of value in the understanding of fundamental mechanics of many powered rotary machines such as rotary tillers, spading machines, rotary ditch/canal diggers and end blades of post hole diggers. This mechanics should eventually enable design improvements to be made by reducing the amount of costly empirical (cut and try) development in the future generation of these machines.

LIST OF REFERENCES

Ahmad, B.D. 1980 - 81. An investigation into the mechanics of rotary tillage. M.Sc. Thesis, N.C.A.E., Silsoe.

Baker, H.W. 1969. Modern workshop technology, Part II, Machine tools and manufacturing processes. Cleaver Hume Press Ltd. London. pp. 116 - 123.

Baver, L.D. 1932. The physical properties of soil of interest to Agricultural Engineers. Agril. Engng. December.

Beeny, J.M.; Greig, D.J. 1965. The efficiency of a rotary cultivator. J. Agric. Engng. Res., 10 (1).

Beeny, J.M.; Khoo, D.C.P. 1970. Preliminary investigations into the performance of different shaped blades for the rotary cultivation of wet rice soil. J. Agric. Engng. Res., 15 (1).

Beeny, J.M. 1973. Rotary cultivation of wet rice land - comparison of blade shape. J. Agric. Engng. Res., 18 pp. 249.

Bekker, M.G. 1960. Off - the - road locomotion - Research and development in terramechanics. Univ. of Michigan Press, Ann Arbor, Michigan, U.S.A.

Bernacki, H. 1962. Dynamic forces acting during rotary tiller operation. Inst. Mech. Elec. Agril., Warsaw. Bulletin No. 2. (Translated from Polish).

Boothroyd, G.; Wallace, P.W. 1964. Tool forces and tool-chip friction in orthogonal machining. J. Mech. Engng. Sc., 6 (1) pp. 74 - 87.

Chamen, W.C.T. 1971 - 73. Studies to investigate the design of a rotary digging machine. Dept. Note DN/TC/377/1260, Natn. Inst. Agric. Engng., Silsoe.

Chamen, W.C.T.; Cope, R.E.; Patterson, D.E. 1979. Development and performance of a high output rotary digger. J. Agric. Engng. Res., 24 pp. 301.

Christopherson, D.G.; Oxley, P.L.B.; Palmer, W.B. 1958. Orthogonal cutting of work-hardening material. Engineering, (186) pp. 113.

Clyd, A.W. 1937. Load studies on tillage tools. Agric. Engng., 18 (3).

Cook, N.H.; Rabinowicz, E. 1963. Physical measurement and analysis. Addison - Wesley Pub. Co. New York.

Dalin, A.D.; Pavlov, P.V. 1950. Rotatsionnye gruntoobrabaty - vayushchie i zemleroinye machiny (Rotary soil-working and earth moving machines). Mashgiz, Moscow.

Dalin, A.D. 1951. Issledovanie po rezaniyu gruntov plyzhnymi i frezermymi nozhami (Study of soil cutting with plow and rotary knives). Sb. Rezanie Gruntov, Izd - Vo AN SSSR. Moscow.

Dexter, A.R.; Stafford, J.V.; Tanner, D.W. 1978. Edge effects on soil engaging tools. J. Agric. Engng. Res., 23 (1) pp. 59 - 66.

Dransfield, P.; Willatt, S.T.; Willis, A.H. 1964. Soil - to - implement reaction experienced with simple tines at various angles of attack. J. Agric. Engng. Res., 9 (3).

Eaczmarek, J. 1976. Principles of machining by cutting, abraison and erosion. Peter Peregrinus Ltd., Stevenage Wydawnictwa Naukowo - Techniczne, Warsaw, pp. 262 - 290.

Eggenmüller, A. 1959. Querlpfluge unter besonderer berucksichtigung des aratore civello. Grundlagen der Landtechnik, No. 11.

Elgin, P. 1979. Prediction models for torque requirements of rotary tillage machines. B.Sc. Thesis, N.C.A.E., Silsoe.

Evans, I.; Murrell, S.A.F. 1957. The mechanics of wedge penetration into coal. National Coal Board. M.R.E. Report No. 2059.

Evans, I. 1959. A theory of the basic mechanics of coal ploughing. National Coal Board. M.E.R. Report No. 2151.

Furlong, D.B. 1956. Rotary tiller performance tests on existing tines. Technical Report No. 1049. F.M.C. Corp., San Jose, Calif., September.

Gill, W.R.; Vanden Berg, G.E. 1968. Soil dynamics in tillage and traction. U.S.D.A. Agril. Handbook No. 316. pp. 263.

Ghosh, B.N. 1967. The power requirement of a rotary cultivator. J. Agric. Engng. Res., 12 (1).

Godwin, R.J. 1974. An investigation into the mechanics of narrow tines in frictional soils. Ph.D. Thesis. University of Reading.

Godwin, R.J. 1975. An extended octagonal ring transducer for use in tillage studies. J. Agric. Engng. Res., 20 (4).

Godwin, R.J.; Spoor, G. 1977. Soil failure with narrow tines. J. Agric. Engng. Res., 22 (3).

Godwin, R.J.; Spoor, G.; Pullen, D.W.M.; Johnson, G.C.; Watts, C. 1978. The effects on plough forces of minor changes in the orientation of the plough body. Report compiled by N.C.A.E., Silsoe.

Godwin, R.J.; Spoor, G.; Kilgour, J. 1980. The design and operation of a simple low cost soil bin. J. Agric. Engng. Res., 20 pp. 99.

Goryachkin, V.P. 1937. Sobranie sochinenii. T. IV (Collected Works, Vol. IV). Sel'khozgiz, Moscow.

Harral, B.B. 1977. The effect of some rotary digger parameters on the power requirement. Dept. Note DN/CU/757/1270, Natn. Inst. Agric. Engng., Silsoe.

Harrison, H.P. 1978. Design of vertical rotary tiller blades for reforestation. Trans. Am. Soc. Agric. Engrs., 12 (6).

Harrison, H.P.; Atkins, R.P. 1981. Soil reacting forces for rod weeder from field measurements. Trans. Am. Soc. Agric. Engrs., 24 (3).

Harrison, H.P. 1982. Soil reactions from laboratory studies with an inclined blade. Trans. Am. Soc. Agric. Engrs., 25 (1).

Hendrick, J.G.; Gill, W.R. 1971a. Rotary tiller design parameters, I : Direction of rotation. Trans. Am. Soc. Agric. Engrs., 14 (4).

Hendrick, J.G.; Gill, W.R. 1971b. Rotary tiller design parameters, II : Depth of operation. Trans. Am. Soc. Agric. Engrs., 14 (4).

Hendrick, J.G.; Gill, W.R. 1971c. Rotary tiller design parameters. III : Ratio of peripheral and forward velocities. Trans. Am. Soc. Agric. Engrs., 14 (4).

Hendrick, J.G.; Gill, W.R. 1973. Soil reaction to high speed cutting. Trans. Am. Soc. Agric. Engrs., 16 (3).

Hendrick, J.G.; Gill, W.R. 1974. Rotary tiller design parameters, IV : Blade clearance angle. Trans. Am. Soc. Agric. Engrs., 17 (1).

Hendrick, J.G.; Gill, W.R. 1978. Rotary tiller design parameters, V : Kinematics. Trans. Am. Soc. Agric. Engrs., 12 (4).

Hettiaratchi, D.R.P. 1965. The present state of the theory of soil cutting. Journal of Terramechanics, 2 (1).

Hettiaratchi, D.R.P.; Witney, B.D.; Reece, A.R. 1966. The calculation of passive pressure in two dimensional soil failure. J. Agric. Engng. Res., 11 (2).

Hettiaratchi, D.R.P.; Reece, A.R. 1967. Symmetrical three dimensional soil failure. Journal of Terramechanics, 4 (3).

Hettiaratchi, D.R.P. 1967. The mechanics of soil cultivation. Paper No. 3/245/C/28, Ag. Engng. Sym. Ins. Agric. Engrs. Silsoe.

Hettiaratchi, D.R.P.; Reece, A.R. 1974. The calculation of passive soil resistance. Geotechnique, 24 (3).

Jacky, J. 1948. On the bearing capacity of piles. Proc. Second Int. Conf. Soil Mech., 1 pp. 100.

Joshida, T. 1965. On the shape of the flatknife tines 'Natabo' for garden type rotary tillers. Tokyo.

Kempster, M.H.A. 1968. Principles of jig and tool design. The English Universities Press Ltd., London.

Kisu, M.; Kohda, Y.; Yagi, S.; Seyama, K. 1966. Studies on trafficability, tractive and rotary tilling performance of tractor. Technical Report Inst. of Agric. Machinery, Omiya, Japan. pp. 108.

Kostritsyn, A.K. 1956. Cutting of a cohesive medium with knives and cones. N.I.A.E. Trans. No. 58.

Krause, R. 1973. Der verdraengungsvorgang um untergrundwerkzeuge in trockenem sand. Unpublished Doctoral Dissertation, Technical University of Braunschweig, West Germany.

Lambe, T.W.; Whitman, R.V. 1969. Soil mechanics. John Wiley and Sons, New York.

Lawrance, S. 1978. Failure, displacement and compaction of cohesive, plastic soil about tines of different geometries. M.Sc. Thesis, N.C.A.E., Silsoe.

Lee, E.H.; Shaffer, B.W. 1951. The theory of plasticity applied to a problem of machining. J. Appl. Mech., (18) pp. 405.

Lisunov, F.A. 1968. Expenditures of energy for rotary tilling soil. Mech. i. Electrif. Sots. Sel'khoz., 10 pp. 36 - 37.

Luth, H.J.; Wismer, R.D. 1969. Performance of plane soil cutting blades in sand. A.S.A.E., Paper No. 69 - 115.

Matsuo, M. 1965. Studies on the up-cut method of rotary cultivation - Load characteristics of rotary up-cut method. J. Soc. Agril. Mach., Japan, 25 (4) No. 83.

Merchant, M.E. 1945. Mechanics of metal cutting process. J. Appl. Phys., (16) pp. 267.

Meyerhof, G.G. 1948. An investigation of the bearing capacity of shallow footings on dry sand. Proc. Second Int. Conf. Soil Mech. 1 pp. 237.

Meyerhof, G.G. 1951. The ultimate bearing capacity of foundations, Geotechnique, No. 2.

Meyerhof, G.G. 1961. The ultimate bearing capacity of wedge shaped foundations. Proceedings, 5th Int. Conf. on Soil Mechanics and Foundations Engineering, Paris.

Mursch, B. 1957. Investigations on a rotary cultivator. Landtech. Forsch, 7 (4).

Nichols, M.L. 1930. Dynamic properties of soil affecting implement design. Agric. Engng., 11 (6).

Nichols, M.L. 1931. The dynamic properties of soil, II, soil and metal friction. Agril. Engng., 12 (8).

O'Callaghan, J.R.; Farrelly, K.M. 1964. Cleavage of soil by tined implements. J. Agric. Engng. Res., 9 (3).

O'Dogherty, M.J. 1964. A laboratory examination of the effect of rake angle and back clearance angle on cutter pick performance in Cwmtillery (Graw) Coal. National Coal Board. M.R.E. Report No. 2258.

O'Dogherty, M.J. 1975. A dynamometer to measure the forces on a sugarbeet topping knife. J. Agric. Engng. Res., 20 (4).

Omer, A.B. 1977. Narrow tines failure of cohesive soils. M.Sc. Thesis, N.C.A.E., Silsoe.

Osman, M.S. 1963. The mechanics of soil cutting blades. J. Agric. Engng. Res., 9 (4).

Panov, I.M.; Melikhov, V.V. 1963. Rotatsionnye Pochvoobrabatyvayushchie mashiny i orudiya (Rotary soil - working machines and implements). Is INTIAM, Moscow.

Papov, G.F. 1963. K raschetu rabochikh organov pochvoobratatyushchikh frez (The design of the cutting tools of rotary tillers). Traktory i Sel'khozmashiny. No. 2.

Pascal, J.A. 1967. Rotary soil working machines. Farm Mechanization, 19 (211).

Pavlov, P.V. 1952. Issledovanie sil v pochvennykh frezakh (Study of forces in rotary tillers). Trudy VIM, 15. Moscow.

Payne, P.C.J. 1956. The relationship between the mechanical properties of soil and the performance of simple cultivation implement. J. Agric. Engng. Res., 1 (1).

Payne, P.C.J. 1959. The mechanical properties of soil in relation to the design of cultivation implements. J. and Proc. Inst. of British Agril. Engrs., 15 (2).

Payne, P.C.J.; Tanner, D.W. 1959. The relationship between rake angle and the performance of simple cultivation implements. J. Agric. Engng. Res., 4 (4).

Perdok, U.D.; Burema, H.J. 1977. Power requirements of rotary tiller blades in clay and sandy soils. Inst. of Agric. Engng., Wageningen, Netherlands, Research Report 77 - 1.

Poltavtsev, I.S. 1954. Frezernye kanavokopateli (Rotary canal diggers). Mashgiz, Moscow, Kiev.

Prandtl, L. 1920 Uber die harte plastischer karper (The hardness of plastic bodies). Nachr. Kgl. Ges. Wiss Gottingen Math. Phys. Klasse. 506.

Radford, J.D.; Richardson, D.B. 1980. Production Engineering Technology. The Macmillan Press Ltd. London. pp. 165 - 177.

Reece, A.R. 1965. Principles of soil - vehicle mechanics. Proc. of Ins. of Mech. Engrs. (Auto. Div.) 180. Part 2A.

Reeves, C.A.; Schafer, R.L. 1974. Force versus width of cut of mouldboard bottoms. A.S.A.E. Paper No. 74 - 1588.

Romig, B.E. 1971. Performance tests of rotary tiller blades. Trans. Am. Soc. Agric. Engrs., 14 (6).

Sakai, J. 1979. Engineering characteristics of rotary tillage resistance of Japanese rotary tillers with tractors. The 8th Conf. ISTRO, Bundesrepublik Deutschland.

Sakai, J.; Hai, L.V. 1982. The reduced tillage energy of Japanese rotary blade - study on the single-edged blade. Proc. ISTRO. pp. 639.

Sal'nik, V.Y. 1980. Iznashivanie nozhei pochvoobrabatyvayushchikhfrez (Wear of the knives of rotary tillers). Sb. Povyshenie Dolgovachnosti Rabochikh Detalei Poschvoobrabatyvayushchikh Mashin. Mashgiz. Moscow.

Seig, D.A.T. 1981 - 82. An investigation into the forces acting on plough share points. M.Sc. Thesis, N.C.A.E., Silsoe.

Siemens, J.C.; Weber, J.A.; Thornburn, T.H. 1965. Mechanics of soil as influenced by model tillage tools. Trans. Am. Soc. Agric. Engrs., 8 (1).

Söhne, W. 1957. Influence of shape and arrangement of tools on driving - moments of rotary hoes. Grundlagen der Landtechnik - Dusseldorf, 9 pp. 69 - 87. (N.I.A.E. Translation).

Söhne, W.; Eggenmüller, A. 1959. Fast-running rotary cultivators and slow-running rotary diggers - Investigations on individual tools. Grundlagen der Landtechnic, (II). (N.I.A.E. Translation No. III).

Söhne, W.; Moller, R. 1962. The design of mouldboards with particular reference to high speed ploughing. Grundl. Landtech., 15 (15) (N.I.A.E. Translation No. 146).

Sokolovski, V.V. 1956. Statics of soil media. Butterworth, London.

Spoor, G. 1969. Design of soil engaging implements. Farm Machine Design Engineering, December.

Spoor, G. 1982. Lecture notes on 'Theory and Practices of Cultivation'. N.C.A.E., Silsoe.

Stafford, J.V. 1979. The performance of a rigid tine in relation to soil properties and speed. J. Agric. Engng. Res., 24 (1).

Steel, R.G.P.; Torrie, J.H. 1960. Principles and procedures of statistics. McGraw - Hill Book Co. Inc., New York.

Steffanelli, G. 1968. Soil resistance to cutting with a wire. Transactions of 5th Int. Congress of Soil Science, 1 Paper 75.

Surilov, V.S. 1966. Opredelenie optimal'nykh parametrov frezernogo kultivatornogo agregata (Determination of the optimum parameters of the rotary cultivator). Trudy SibVIM, (3) Novosibirsk.

Terzaghi, K. 1943. Theoretical soil mechanics. John Wiley and Sons, New York.

Tinker, D.B. 1981. Studies on the power requirements of rotary cultivators and shallow leading tines. M.Sc. Thesis. N.C.A.E., Silsoe.

Umeda. 1958. Characteristics of soil resistance to rotary tillage tires. Bulletin, University of Osaka Prefecture, Series B, Vol. 8.

Vinogradov, V.I.; Leont'ev, Yu. S. 1968. The interaction of rotary working tools with soil. Traktory i sel'skhozmashiny (9). N.I.A.E. Translation.

Webb, D.R. 1981. Vertical crack formation with narrow drainage tines. M.Sc. Thesis, N.C.A.E., Silsoe.

Yatsuk, E.P.; Panov, I.M.; Efimov, D.N.; Marchenko, O.S.; Chernenkov, A.D. 1981. Rotary soil working machines - Construction, calculation and design. Mashinostroenie publishers, Moscow, 1971. Translated from Russian. Published for U.S.D.A. Washington, D.C., by Amerind Pub. Co. Pvt. Ltd. New Delhi.

Youssef, A.F.A.; Ali, G.A. 1982. Determination of soil parameters using plate test. J. Terramechanics, 19 (2).

Zelenin, A.N. 1950. Fizicheski Osmovie Terorii Rezaniya Gruntor. (Basic physics pf the theory of soil cutting). Akademia Nawk USSR, Moscow - Leningrad. (N.I.A.E. Translation).

Zhuk, Ya. M. 1952. Issledovanie frezerovaniya pochvy (Study of the rotary tilling of soil). Nauchnye Trudy VIM, 15. Moscow.

TABLES

Table 6.1 Variation of Forces at Different Rotor Speed for a Blade Traversing in a Circular Trajectory, for a Bite Length and Depth of Cut of 100 mm

(* Peak Resultant Force in Cutting a Full Soil Slice)

Rotor Speed, N r.p.m.	Average Component Forces/Moment		Angle of Rotations of the Blade Tip, , Degrees									
			5	10	15	20	25	30	35	40	45	50
5	ΔT,	N	74.74	82.82	64.64	72.72	60.60	50.50				
	ΔS,	N	+38.83	32.36	9.06	27.18	19.41	-2.59				
	$M_{\Delta T.\Delta S}$,	N-m	12.97	16.03	13.33	15.13	14.05	9.73				
	R_{RT},	N	82.44	89.22*	65.35	78.03	64.60	52.15				
10	ΔT,	N	78.78	86.86	54.54	75.75	84.84	72.72	48.48	60.60	-	-
	ΔS,	N	+46.60	37.54	15.53	19.41	27.18	21.35	7.76	15.53	-	-
	$M_{\Delta T.\Delta S}$,	N-m	16.21	17.11	12.43	15.67	17.29	16.28	12.97	11.35	-	-
	R_{RT},	N	91.53	94.62*	56.70	78.19	89.08	75.79	49.09	62.56	-	-
40	ΔT,	N	-	109.09	115.15	80.63	94.94	48.48	-	63.63	-	39.39
	ΔS,	N	-	46.60	53.39	7.76	50.48	23.30	-	29.12	-	-15.53
	$M_{\Delta T.\Delta S}$,	N-m	-	23.24	24.86	14.45	23.06	14.59	-	14.05	-	9.45
	R_{RT},	N	-	118.62	126.93*	81.00	107.52	53.78	-	69.97	-	42.34
80	ΔT,	N			109.09			142.01				
	ΔS,	N			+73.73			+55.65				
	$M_{\Delta T.\Delta S}$,	N-m			22.70			27.74				
	R_{RT},	N			131.69			152.63*				
120	ΔT,	N			113.13					153.53		
	ΔS,	N			+69.89					67.56		
	$M_{\Delta T.\Delta S}$,	N-m			26.84					3.07		

Table 6.2 Variation of Effective Cutting Angle and Clearance Angle under Dynamic Situation

Items	Treatment Number	Forward Speed, V_f m/s	Rotor Speed, N r.p.m.	Peripheral Speed, V_c m/s	λ-Ratio V_c/V_f	Bite Length L_b mm	Correction Angle $\Delta\delta$, Degrees Start	Correction Angle $\Delta\delta$, Degrees 10^o After	Effective Cutting Angle (25 - $\Delta\delta$) Degrees Start	Effective Cutting Angle (25 - $\Delta\delta$) Degrees 10^o After	Effective Clearance Angle (7 - $\Delta\delta$) Degrees Start	Effective Clearance Angle (7 - $\Delta\delta$) Degrees 10^o After
d = 100 mm	T_7 to	0.014 to	4.38 to	0.141 to	9.67	100	4.68	3.92	20.31	21.07	2.31	3.07
	T_{12}	0.399	120	3.87								
d = 50 mm cutting starts at $\theta_y = 56.89^o$ from horizontal	T_{13}	0.011	5	0.161	14.60	66.26	2.27	1.64	22.72	23.35	4.72	5.35
	T_{14}	0.014	5	0.161	11.03	87.75	3.06	2.22	21.93	22.77	3.93	4.77
	T_{15}	0.014	3	0.096	6.61	146.21	5.39	3.94	19.60	21.06	1.60	3.05
	T_{16}	0.038	5	0.161	4.19	230.86	9.24	6.83	15.75	18.16	-3.75*	0.16
d = 100 mm $\theta_y = 42.48^o$	T_{17}	0.011	5	0.161	14.60	66.26	3.01	2.52	21.98	22.47	3.98	4.47
	T_{18}	0.014	5	0.161	11.03	87.75	4.04	3.40	20.95	21.59	2.95	3.59
	T_{19}	0.014	3	0.096	6.61	146.21	7.02	5.96	17.97	19.03	-0.028*	1.03
	T_{20}	0.038	5	0.161	4.19	230.86	11.76	10.15	13.23	14.84	-4.76*	-3.15*
d = 150 mm $\theta_y = 20.86^o$	T_{21}	0.011	5	0.161	14.60	66.26	3.48	3.10	21.51	21.89	3.51	3.89
	T_{22}	0.014	5	0.161	11.03	27.75	4.66	4.16	20.34	20.83	2.34	2.83
	T_{23}	0.014	3	0.096	6.61	146.21	8.02	7.23	16.97	17.76	-1.027*	-0.237*
	T_{24}	0.038	5	0.161	4.19	230.86	13.14	12.07	11.86	12.92	-6.14*	-5.07*

* Negative sign shows scrubbing of the back face of the blade and compression of the undeformed soil slice

Table 8.1 Observed and Predicted Quasi-Static Force Components for a 20-Gauge Wire

Depth of cut,	Bite Length	Length of Shear Plane	Weight of Slice	T-Values		Passive Resistance	Tip Force	Tangential Force		Radial force		Resultant Force	
								Observed	Predicted	Observed	Predicted	Observed	Predicted
d, mm	L_b, mm	l, mm	W, N	T_{CW} -	$T_{\gamma W}$ -	P_{PW}, N	Q_R, N	ΔT_W, N	N	ΔS_W, N	N	R_{RW}, N	N
50	25	22	0.18	1.083	0.9652	9.71	109.88	55.15	111.64	-22.70	-35.89	59.42	117.27
	50	36	0.56	1.083	0.9652	16.14	109.88	79.51	117.65	-29.65	-33.59	84.85	122.35
θ_γ= 56.89°	100	76	2.23	1.083	0.9652	35.08	109.88	98.14	135.33	-29.73	-26.80	102.54	137.96
	150	116	4.12	1.083	0.9652	54.23	109.88	108.67	153.21	-25.29	-19.94	111.57	154.50
100	25	30	0.42	1.083	0.6980	13.29	109.88	82.97	114.99	-46.33	-34.61	95.03	120.08
	50	62	2.063	1.083	0.6980	28.29	109.88	116.38	129.00	-40.94	-29.23	123.37	132.27
θ_γ= 42.48°	100	116	5.98	1.083	0.6980	54.42	109.88	153.01	153.39	-34.48	-19.87	156.84	154.67
	150	186	11.66	1.083	0.6980	88.71	109.88	181.03	185.40	-37.71	-7.58	184.91	185.56
	200	174	13.95	1.083	0.8893	87.78	109.88	209.05	184.53	-36.63	-7.92	212.23	184.70
	250	224	18.76	1.083	0.8893	113.72	109.88	218.75	208.75	-24.78	+1.38	220.15	208.75
150	25	44	0.89	1.083	0.4495	19.46	109.88	75.43	120.75	-32.32	-32.40	82.06	125.02
	50	80	3.04	1.083	0.4495	36.02	109.88	106.68	136.21	-34.48	-26.47	112.11	138.76
θ_γ= 30.86°	100	190	11.15	1.083	0.4495	87.32	109.88	162.71	184.10	-33.40	-8.08	166.10	184.28
	150	298	20.02	1.083	0.4495	138.09	109.88	198.27	231.50	-28.01	+10.11	200.23	231.72
	200	280	27.45	1.083	0.6648	139.54	109.88	228.45	232.85	-26.94	+10.63	229.98	233.10

Table 8.2 Observed and Predicted Quasi-Static Force Components for the Blade (18^{o} Tip)

Depth of cut,	Bite Length	Length of Shear Plane	Weight of Slice	T-Values		Passive Resistance	Rear Tip Force	Tangential Force		Radial Force		Resultant Force	
				T_C	T_γ			Observed	Predicted	Observed	Predicted	Observed	Predicted
d, mm	L_b, mm	l, mm	W, N	-	-	P_P, N	Q_R, N	ΔT, N	N	ΔS, N	N	R_R, N	N
50	50	37	1.28	0.8644	0.7013	13.69	71.79	47.85	77.35	-6.32	-16.74	48.26	79.14
	100	86	2.27	0.8644	0.7013	31.33	71.79	90.83	90.66	-25.06	-5.17	94.22	90.81
$\theta_\gamma = 56.89^{o}$	150	135	5.55	0.8644	0.7013	50.57	71.79	95.70	105.19	-24.50	+7.45	98.78	105.45
	200	148	9.67	0.8644	0.7705	58.62	71.79	90.38	111.26	+16.60	+12.73	91.89	111.99
	250	186	11.66	0.8644	0.7705	73.29	71.79	90.83	122.34	+28.45	+22.36	95.18	124.36
100	50	70	3.15	0.8644	0.4741	25.69	71.79	80.30	86.41	-25.30	-8.87	84.19	86.87
	100	142	8.0	0.8644	0.4741	52.89	71.79	92.40	106.94	+22.13	+8.97	95.01	107.31
$\theta_\gamma = 42.48^{o}$	150	220	11.75	0.8644	0.4741	81.64	71.79	120.03	128.63	+41.10	+27.83	128.35	131.61
	200	240	18.15	0.8644	0.5571	93.09	71.79	115.16	137.27	+63.20	+35.34	131.36	141.75
	250	290	23.12	0.8644	0.5571	113.15	71.79	115.10	152.41	+61.60	+48.50	130.54	159.95
150	50	91	4.18	0.8644	0.2684	32.58	71.79	79.48	91.61	-23.71	-4.35	82.94	91.71
	100	214	11.78	0.8644	0.2684	77.15	71.79	113.58	125.25	+46.95	+24.89	122.90	127.70
$\theta_\gamma = 30.86^{o}$	150	326	15.75	0.8644	0.2684	116.95	71.79	195.06	155.28	+79.81	+50.99	210.75	163.44
	200	320	20.31	0.9003	0.4649	124.68	71.79	204.93	161.12	+86.85	+56.07	222.57	170.60
	250	346	33.07	0.9469	0.5813	150.27	71.79	195.06	180.43	+93.89	+72.86	216.48	194.59

Table 8.3 Experimental and Predicted Peak Dynamic Forces for the Blade (Circular Trajectory)

Treatment Number	Rotor Speed N, r.p.m.	Tip Peripheral Speed, V_c, m/sec	Acceleration Force, I_F*, N	Total Dynamic Force, R_{RT}, N Experimental	Predicted*
T_1	5	0.161	0.093	29.22	107.68
T_2	10	0.322	0.374	94.62	107.68
T_3	20	0.645	1.495	-	108.80
T_4	40	1.29	5.981	126.93	113.29
T_5	80	2.58	23.925	152.63	131.23
T_6	120	3.87	53.833	167.88	161.143

* Column 4 (I_F) is added to 107.31 N (the Quasi-Static Component) to obtain R_{RT} (Predicted) in Column 6

Table 8.4 Experimental and Predicted Peak Dynamic Forces for the Blade (Cycloidal Trajectory)

Treatment Number	1 Rotor Speed N, r.p.m.	2 Tip Peripheral Speed V_c, m/sec Circular	3 Average Tip Speed V_{cav} m/sec Cycloidal	4 Acceleration Force, I_F, N For V_c	5 Acceleration Force, I_F, N For V_{cav}
T_7	4.38	0.142	0.128	0.081	0.067
T_8	11.54	0.372	0.338	0.563	0.466
T_9	20	0.645	0.586	1.692	1.399
T_{10}	40	1.29	1.173	6.766	5.597
T_{11}	80	2.58	2.346	27.066	22.387
T_{12}	120	3.87	3.519	60.899	50.370

Treatment Number	6 Experimental	7 Total Dynamic Force, R_{RT}, Newtons Predicted (Fundamental) For V_c, m/sec*	8 Total Dynamic Force, R_{RT}, Newtons Predicted (Fundamental) For V_{cav}, m/sec	9 Predicted (Bernacki, 1962) Pd	10 Predicted (Bernacki, 1962) Total R_{RT}*
T_7	95.42	107.39	107.37	0.081	107.39
T_8	-	107.87	107.77	0.560	107.87
T_9	-	109.00	108.71	1.685	108.99
T_{10}	119.24	114.07	112.90	6.747	114.06
T_{11}	123.48	134.37	129.69	26.910	134.30
T_{12}	139.36	168.21	157.68	60.728	168.04

* Predicted forces are approximately equal by both the concepts

.e 8.5 Observed and Predicted Quasi-Static Forces for the Blade with Vertical Axis of Rotation

a. Less than a Quarter of a Circle Vertical Cut — Rear Tip Force, Q_{RV} = 71.05 N, d = 100 mm

de	Bite Length	Length of Vertical Shear Plane	Area of Bottom Shear Plane	Weight of Soil	T-Values		Passive Resistance			Tangential Force		Radial Force		Resultant Force	
					T_{CV}	$T_{\gamma V}$	P_{PV}	P_{PB}	P_p Total	Observed	Predicted	Observed	Predicted	Observed	Predicted
mm	L_b, mm	l, mm	A_B, cm	W, N	-	-	N	N	N	ΔT_V, Newton		ΔS_V, Newton		R_{RV}, Newton	
]	50	70	22.14	3.15	0.9871	0.7438	25.85	11.08	36.93	66.67	94.20	+19.41	-1.23	69.68	94.21
	100	142	56.25	8.00	0.9871	0.7438	49.09	28.16	77.25	95.45	124.63	+47.57	+25.21	106.76	127.15
	200	240	127.60	18.15	0.9871	0.7438	82.98	63.88	146.86	127.27	177.16	+88.02	+70.88	154.76	190.82
]	50	91	29.39	4.18	0.9871	0.7438	31.46	14.71	46.17	96.97	101.18	+50.48	+4.83	109.32	101.29
	100	214	82.85	11.78	0.9871	0.7438	73.99	41.47	115.46	109.09	153.47	+69.89	+50.29	129.94	161.50
	200	320	142.80	20.31	0.9871	0.7438	115.24	71.48	186.72	172.73	207.25	+143.68	+97.04	224.69	228.85

b. Half a Circle Vertical Cut — Rear Tip Force, Q_{RV} = 71.05 N, d = 100 mm

	50	164	25.00	3.55	0.9871	0.7438	58.79	12.51	71.30	101.51	120.14	46.60	+21.31	111.69	122.02
	100	260	47.60	6.77	0.9871	0.7438	106.87	23.83	130.70	175.65	164.97	115.20	+60.28	210.07	175.64
	200	386	89.32	12.70	0.9871	0.7438	246.57	44.72	291.29	262.62	286.17	214.88	+165.64	339.32	330.65

APPENDICES

APPENDIX 1

EXTENDED OCTAGONAL RING TRANSDUCER DESIGN

The material selected for the transducer was an alloy steel, EN 24A, subsequently heat treated to an Ultimate Tensile Stress of 1132 MN/m^2 (73.5 $tons/in^2$) and yield stress of 1052 MN/m^2 (6.83 $tons/in^2$) giving high strength for compactness. The Modulus of Elasticity was known as 206.7 GN/m^2 (30 x 10 $lbsf/in^2$).

Design Requirements

Assumed moment 250 N-m (1000 N at 250 mm), Söhne (1959).
Factor of safety of 4, to ensure linearity within the working range.
Designed applied moment, M = 1 KN-m.

Design Details

Working stress = 558.63 MN/m^2

The size of EN 24A stock readily available and requiring least machining resulted in a K value of 2.5.

For K = 2.5, from Cook and Rabinowicz (1963), the following was achieved:

$$\text{The strain dimensionless group } \frac{\varepsilon E b t^2}{M} = 0.3 \quad \ldots\ldots \text{A1.1}$$

$$\text{The deflection dimensionless group } \frac{\phi E b t^3}{M \cdot r} = 0.18 \quad \ldots \text{A1.2}$$

However, the sensitivity determined experimentally by Godwin (1975) for the moment bridge was 1.35 times larger than that expected from the prediction Equation A1.1 for the extended ring transducers. Therefore, a value of 1.35 times to those given in Equation A1.1 was taken for strain dimensionless group as:

$$\frac{\varepsilon E b t^2}{M} = 0.405 \qquad \text{..... A1.3}$$

where:

$K = \frac{L}{r}$

$2L$	=	distance between ring centres	(75 mm)
r	=	radius of ring	(15 mm)
E	=	modulus of elasticity	(206.7 GN/m^2)
b	=	width of transducer	(50 mm)
M	=	applied moment	(1 KN-m)
σ	=	working stress	
ε	=	strain	
t	=	ring thickness	
ϕ	=	angular deflection in radians	

For a perfectly elastic material $E = \frac{\sigma}{\varepsilon}$, hence, Equation A1.3 becomes:

$$\frac{\sigma b t^2}{M} = 0.405 \qquad \text{..... A1.4}$$

which solving for t using the design working stress gives a ring thickness of 3.8 mm. From Equation A1.2 the transducer deflection is 4.76×10^{-3} radians (0.27^{o}).

The working drawing and heat treatments are given in Figure A1.1.

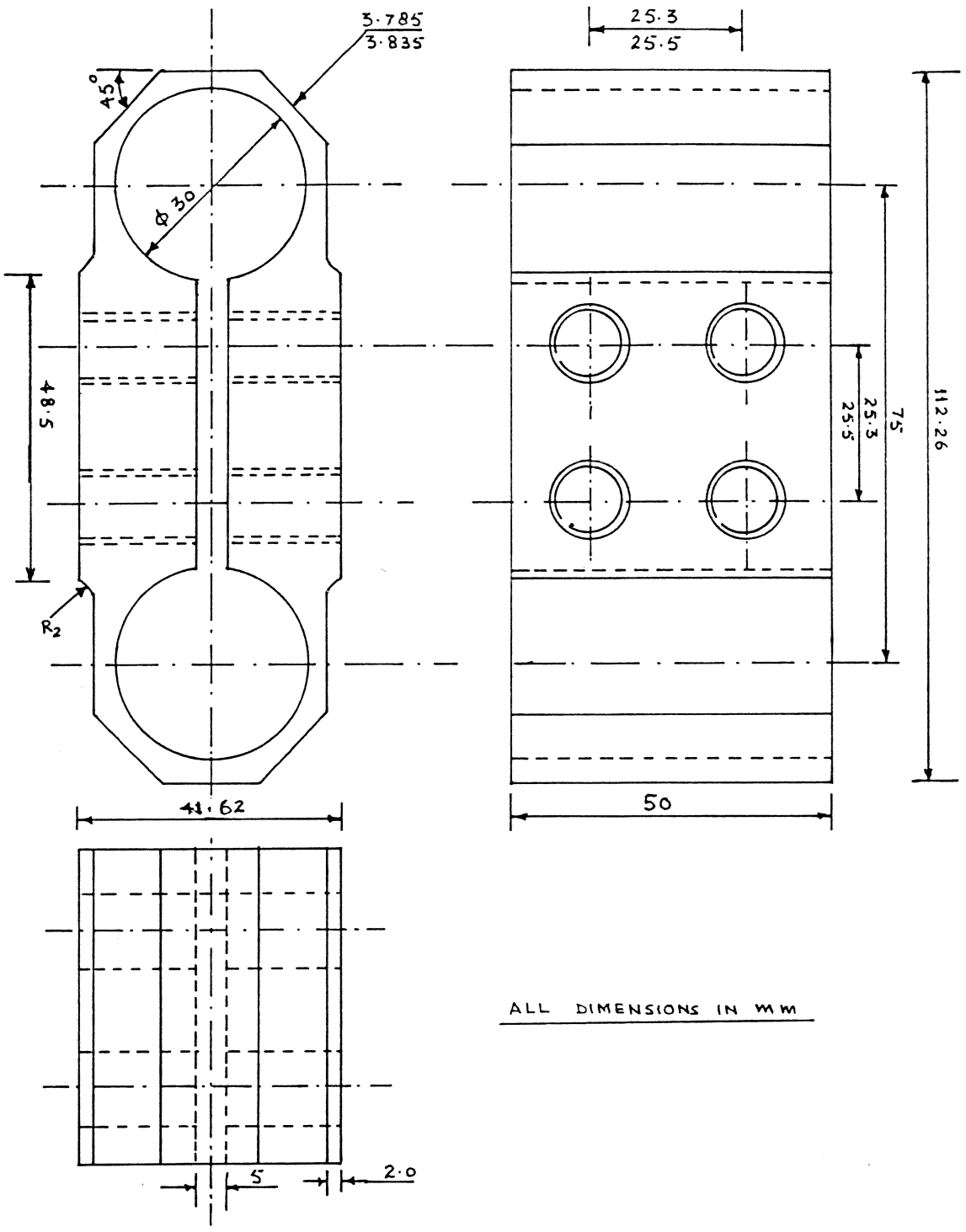

NATIONAL COLLEGE OF AGRICULTURAL ENGINEERING		
MATL. EN 24 A STEEL HEAT TREATMENT. OIL QUENCH 850°C, TEMPER 560°C		
HARDNESS TEST. PREFRRED 416, MINIMUM 363 BRINELL SCALE		
TOLERANCE. 0·25 UNLESS STATED OTHERWISE		
SURFACE FINICE. 0·4 – 0·6 μM FOR STRAIN GAUGES ≃ 0·8 μM BY GRINDING		
SCALE. FULL SIZE	DATE. 11. 6. 82	DRG. NUMBER TT85/1
NAME. EXTENDED OCTAGONAL RING TRANSDUCER		
DRAWN. T. C. THAKUR	CHECKED. R. J. GODWIN	

FIGURE A1.1 WORKING DRAWING AND HEAT TREATMENTS OF THE EXTENDED OCTAGONAL RING TRANSDUCER

APPENDIX 2

METHOD TO CONSTRUCT A CYCLOIDAL TRAJECTORY DESCRIBED BY A ROTATING TOOL

The blade of a rotary tiller executes a complex motion consisting of relative - rotary motion around the axis of the cutter drum with a velocity, V_c, and translatory forward motion with a velocity, V_f. Different ratios of the rotary and translatory velocities of motion, $\lambda = \frac{V_c}{V_f}$ give different trajectories of motion of the blade. The coordinates of a point in the path are given by the parametric equations of the cycloid:

$$X = V_f \cdot t + R \cos \omega t \quad \ldots\ldots\ldots \text{A2.1}$$

$$Y = R \sin \omega t \quad \ldots\ldots\ldots \text{A2.2}$$

where:

R = radius of the circle described by the blade edge during rotation

ω = angular speed of the blade

ωt = angle of rotations in the time, t

The X and Y coordinates have been calculated as an example given overleaf:

Table A2.1 Coordinates of Cycloidal Trajectory

Treatment No. T_7 - T_{12}

R = 308 mm; N = 120 r.p.m.; V_f = 0.399 m/sec; L_b = d = w = 100 mm

θ_i deg	$\omega t = \frac{\pi \theta_i}{180}$ arc	t sec	$s = V_f t$ cm	Cos ωt	R Cos ωt cm	X	Sin ωt	Y
0	0	0	0	1	30.80	30.80	0	0
10	0.174	0.013	0.554	0.984	30.33	30.88	0.173	5.34
20	0.349	0.027	1.108	0.939	28.94	30.05	0.342	10.53
30	0.523	0.041	1.662	0.866	26.67	28.33	0.50	15.40
40	0.698	0.055	2.216	0.766	23.59	25.80	0.643	19.79
50	0.872	0.069	2.770	0.642	19.79	22.56	0.766	23.59
90	1.570	0.124	4.987	0.00	0.00	4.98	1.00	30.80
180	3.141	0.249	9.975	-1.00	-30.80	-20.82	0.00	0.00
270	4.712	0.373	14.962	0.00	0.00	14.96	-1.00	-30.80
360	6.283	0.498	19.95	1.00	30.80	50.75	0.00	0.00

The cycloidal trajectory for 0 to 90^o rotations of the blade is shown in Figure A2.1 drawn from the Table A2.1. However, this can also be constructed by the graphic method shown in Figure A2.1. In the graphic method, a circle is drawn equal to the radius, R and divided into 10^o sections. The distance, S, travelled by the blade when rotating through 10^o is found from the following relationships:

$$V_c = \frac{\pi RN}{30} \text{ cm/sec} \qquad \text{..... A2.3}$$

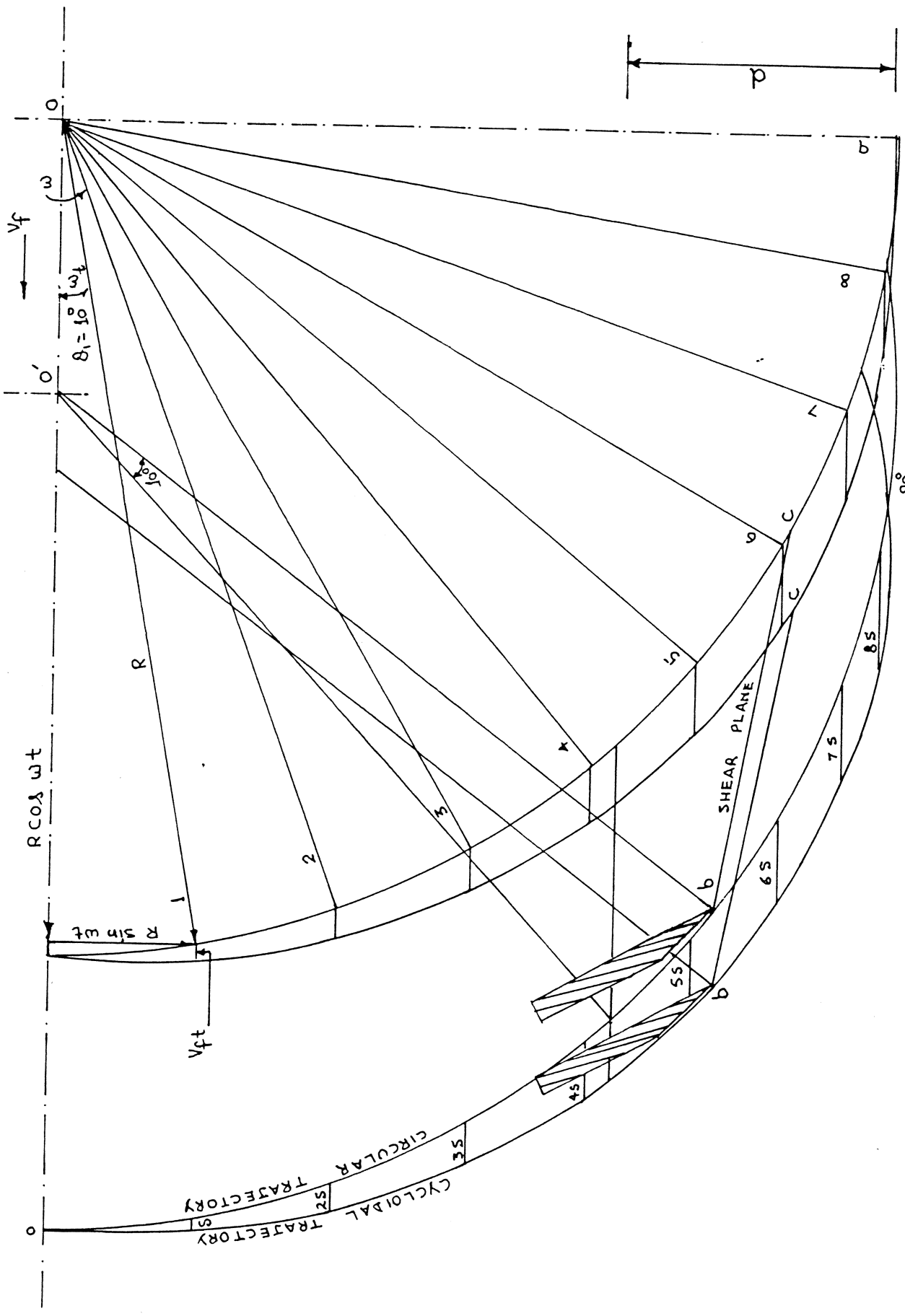

FIGURE A2.1 METHOD FOR DETERMINING THE CYCLOIDAL TRAJECTORY TRACED BY A TIP

and $$t = \frac{R\pi\theta_i}{180.V_c} \text{ sec}$$

or $$t = \frac{\theta_i}{6N} \text{ sec} \qquad \ldots\ldots\ldots \text{A2.4}$$

$$S = \frac{V_f \cdot \theta_i}{6N} \text{ cm} \qquad \ldots\ldots\ldots \text{A2.5}$$

where, N = speed of the rotor, r.p.m.

For 10^o rotations S = 0.554 cm

Starting from line '0' in the figure, the linear distance (S) is added geometrically at the end of line 1 (10^o) and the distance 2S is similarly added at the end of line 2 (20^o) and so on. Thus, the cycloidal path being covered is determined.

APPENDIX 3

RELATIONSHIP OF PASSIVE RESISTANCE (P_p) WITH SHEAR PLANE AND THE TANGENTIAL FORCE (ΔT)

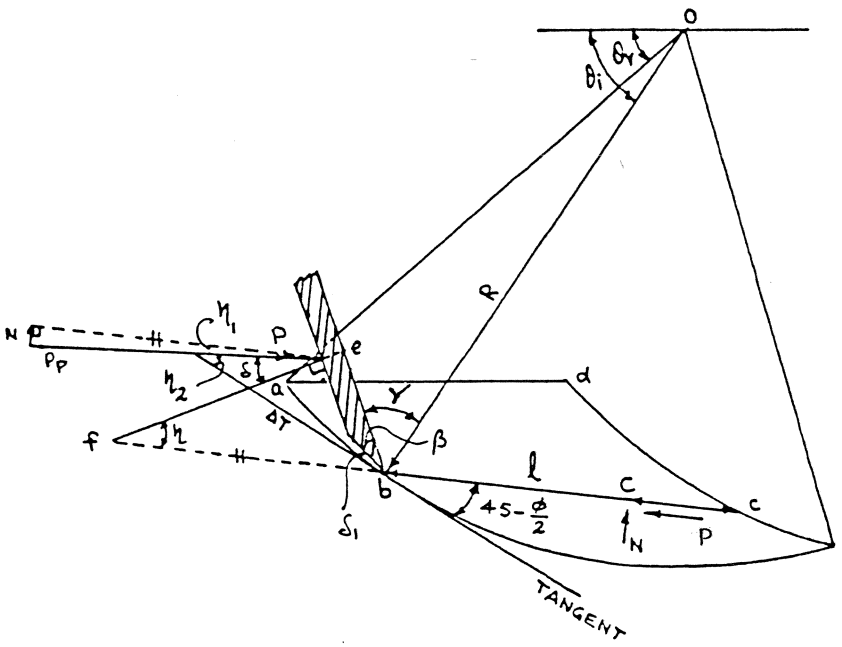

FROM TRIANGLE efb

$$90^\circ + \eta + 45^\circ - \frac{\phi}{2} + \delta_1 + \beta = 180^\circ$$

$$\therefore \eta = (45 + \frac{\phi}{2} - \delta_1 - \beta) \text{ deg}$$

THEREFORE, THE ANGLE (η_1) BETWEEN P_p AND A PLANE ALONG THE SHEAR PLANE, bc, IS GIVEN AS BELOW:

$$\eta_1 = (45 + \frac{\phi}{2} - \delta_1 - \beta - \delta) \text{ deg.}$$

AND THE RELATIONSHIP OF P_p WITH ΔT IS GIVEN AS:

$$\eta_2 = 180^\circ - 90^\circ - \delta - \delta_1 - \beta$$

$$\therefore \eta_2 = (90^\circ - \delta - \delta_1 - \beta) \text{ deg.}$$

APPENDIX 4

A SAMPLE CALCULATION FOR DETERMINATION OF FORCES ON A WIRE AND THE BLADE

A4.1 Determination of Forces on a Wire

A4.1.1 For Frictional Soil (Sandy-Loam)

Working Regime:

Bite length, L_b = 50 mm
Depth of cut, d = 100 mm
Width of cut, w = 100 mm

Soil Properties:

γ = 1450 kg/m^3 = 14224.5 N/m^3
C = 4000 N/m^2; ϕ = 37^o
δ = 24^o Ca = 0.0 kN/m^2

Diameter (thickness) of the wire, t = 0.914 mm (20-gauge)

a. Rear Tip Reaction, Q_R:

The N-factors are calculated from Figure 7.7 as; pp. 140

$$N_c' = (N_c' - N_c')\frac{\delta}{\phi} + N_c'$$
$$\delta=\delta \quad \delta=\phi \quad \delta=0 \quad \delta=0$$

$$\therefore N_c' = (820 - 170)\frac{24}{37} + 170 = 591.62$$

Similarly,

$$N_q' = (N_q' - N_c')\frac{\delta}{\phi} + N_q'$$
$$\delta=\phi \quad \delta=0 \quad \delta=0$$

$$\therefore N_q' = (170 - 56)\frac{24}{37} + 56 = 129.94$$

From Equation 7.20, the reaction, Q_R, is calculated as: pp. 139

$$Q_R = \frac{0.914}{2} \times \frac{1}{1000}(m) \times 4000 \left(\frac{N}{m^2}\right) \times 591.62 \times \frac{100}{1000}(m) + (1 - \text{Sin } 37^o)$$

$$\times 14224.5 \left(\frac{N}{m^2}\right) \times \frac{51.70}{1000}(m) \times \frac{100}{1000}(m) \times \frac{0.914}{2} \times \frac{1}{1000}(m) \times 129.94$$

$$Q_R = 108.15 + 1.73 \qquad \therefore Q_R = 109.88 \text{ Newtons}$$

b. Determination of Passive Resistance, P_{PW}:

The length of shear plane after 15^o entry in the soil, l = 62 mm

Angular position of the wire, $\theta_i = 42.48 + 15 = 57.48^o$

Cohesive force along the shear plane, $C = c \cdot l \cdot w$

$$= 4000 \times \frac{62}{1000} \times \frac{100}{1000}$$

$$= 24.80 \text{ N}$$

The T-values from Equation 7.17 are determined as: pp. 138

$$T_{CW} = \frac{1}{\text{Cos}\left(24 - \frac{37}{2}\right) - \text{Sin}\left(24 - \frac{37}{2}\right) \text{Tan } 37} \qquad \therefore T_{CW} = 1.083$$

$$T_{\gamma W} = T_{CW} \text{ Sin } (57.48 + 45 - \frac{37}{2}) \text{ . Tan } 37 - \text{Cos } (57.48 + 45 - \frac{37}{2})$$

$$\therefore T_{\gamma W} = 0.698$$

$$\text{Soil weight on the shear plane } (W) = 145.2 \times \frac{1}{10} (m)^{3} \times 14224.5 \ (\frac{N}{m})$$

$$W = 2.06 \text{ N}$$

$$P_{PW} = 1.083 \times 24.80 + 0.698 \times 2.06$$

$$= 28.29 \text{ N}$$

c. Determination of Component Forces:

From Equations 7.11 and 7.12 pp. 135

$$\Delta T_{W} = 28.29 \text{ Cos } (45 - 24) + 109.88 \text{ Cos } (45 - 24)$$

$$= 128.99 \text{ N}$$

$$\Delta S_{W} = 28.29 \text{ Sin } (45 - 24) - 109.88 \text{ Sin } (45 - 24)$$

$$= -29.24 \text{ N}$$

Resultant force, $R_{RW} = 132.26$ N

Position of R_{RW} with ΔT_{W}, $\epsilon = 12.77^{o}$

A4.1.2 Pure Cohesive Soil (Artificial Clay)

Soil Properties:

$$\gamma = 1757 \text{ kg/m}^3$$

$$C = 50.05 \begin{matrix} 59.92 \\ 40.61 \end{matrix} \text{ kN/m}^2$$

$$\phi = 7.16^{\circ} \begin{matrix} 11.34^{\circ} \\ 3.01^{\circ} \end{matrix}$$

$$C_a = 0.85 \text{ kN/m}^2 \qquad C_a = 0.0 \text{ (for wire)}$$

$$\delta = 28.30^{\circ}$$

In the case of a wire in artificial clay soil, there was no general shear failure and the soil failed by flowing around the wire assumed to be due to local shear failure. Therefore, the full thickness of the wire should be considered for calculating forces using Equation 7.20 and neglecting the surcharge term (N_q') which is insignificant for clay. The equation 7.20 can be rewritten as:

$$R_{RW} = t \cdot c \cdot N_c' \cdot w$$

From Figure 7.7

$$\left.\begin{matrix} N_c' = 17 \\ N_c' = 10.5 \end{matrix}\right\} \phi = 7.16^{\circ}$$

17 (perfectly rough interface)

10.5 (perfectly smooth interface)

The resultant force for perfectly rough and perfectly smooth interface is determined as below:

i. $$R_{RW} = 0.914 \times \frac{1}{1000} \text{ (m)} \times 50050 \left(\frac{N}{m^2}\right) \times 17 \times \frac{100}{1000} \text{ (m)}$$

$$= 77.76 \text{ N} \quad \text{(Perfectly rough)}$$

similarly,

ii. $$R_{RW} = 48.03 \text{ N} \quad \text{(Perfectly smooth)}$$

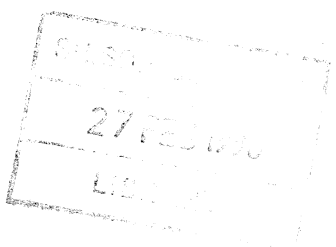

Average experimental force = 90 N (Approximately)

A4.2 Determination of Forces on a Blade with Horizontal Axis of Rotation

A4.2.1 Quasi-Static Forces on the Blade

i. Blade Geometry: Tip angle, β = 18^{o}
Clearance angle, δ_1 = 7^{o}
Thickness of tip, t = 0.6 mm

ii. Working Regime: L_b = d = w = 100 mm
Angular position of tip, θ_i = (42.48 + 10) degrees

iii. Soil Properties: Similar to Section A4.1.1 for wire

a. Determination of P_p from Equation 7.10 pp. 132

Length of shear plane, l = 142 mm

Cohesive force on the shear plane, C = c . l . w

$$= 4000 \left(\frac{N}{m^2}\right) \times \frac{142}{1000} (m) \times \frac{100}{1000} (m)$$

$$= 56.8 \text{ N}$$

$$\text{Weight of soil, } W = \frac{56.25}{10000} (m^2) \times \frac{100}{1000} (m) \times 14224.5 \left(\frac{N}{m^3}\right)$$

$$= 8.00 \text{ N}$$

T-values are given as:

$$\alpha_1 = 45 + \frac{\phi}{2} - \delta - \beta - \delta_1 = 14.5^{o}$$

$$\alpha_2 = 45 - \frac{\phi}{2} + \beta + \delta_1 = 51.5^{o}$$

$$\alpha_3 = 45 - \frac{\phi}{2} + \Theta_i = 78.98^{o}$$

$$\therefore T_C = \frac{1}{\text{Cos } 14.5 + \text{Sin } 14.5 \times \text{Tan } 37} = 0.8644$$

$$T_\gamma = T_C \text{ (Sin } 78.98 \times \text{Tan } 37 - \text{Cos } 78.98) = 0.4741$$

$$P_p = 0.8644\ C + 0.4741\ W = 52.89\ N$$

b. Determination of Rear Tip Force, Q_R

From Equation 7.20 pp. 139

$$Q_R = \frac{0.6}{2} \times \frac{1}{1000} (m) \times 4000 \left(\frac{N}{m^2}\right) \times 591.62 \times \frac{100}{1000} (m) + (1 - \text{Sin } 37^{o})$$

$$\times 14224.5 \left(\frac{N}{m^2}\right) \times \frac{36.30}{1000} (m) \times \frac{100}{1000} (m) \quad \frac{0.6}{2 \times 1000} (m) \times 129.94$$

$$= 70.994 + 0.801 = 71.79\ N$$

c. Determination of Components of the Resultant Force

From Equations 7.2 and 7.3 pp. 127

$\Delta T = 52.89 \text{ Cos } (90 - 18 - 7 - 24) + 71.79 \text{ Cos } (45 - 24) = 106.94 \text{ N}$

$\Delta S = 52.89 \text{ Sin } (90 - 18 - 7 - 24) - 71.79 \text{ Sin } (45 - 24) = +8.97 \text{ N}$

Determination of the Magnitude of the Resultant Force

$$R_{R \text{ Static}} = \sqrt{(106.94)^2 + (8.97)^2} = 107.31 \text{ N}$$

Determination of the Direction of the Resultant Force

$$\psi = \text{Tan}^{-1} \frac{\Delta S}{\Delta T} = +4.79^{\circ}$$

A4.2.2 Dynamic Forces on the Blade

A4.2.2.1 Force due to Acceleration of the Soil Slice

The blade geometry, working regime and soil properties are the same as in Section A4.1.1

Rotor radius, R = 308 mm; Number of blades, n = 2

Rotor speed, N = 120 r.p.m.

a. Circular Trajectory

Treatment number, T_6, $V_f = 0$

Angle of rotation of the blade after detachment of the soil slice and the end of cutting is:

$$\theta_B = (90 - \theta_i)^o = (90 - 52.48)^o = 37.52^o$$

$$\text{Length of cutting path, } L = R \cdot \theta_B = 308 \times \frac{\pi \times 37.52}{180}$$

$$= 201.7 \text{ mm}$$

$$\text{Cutting speed of the blade, } V_c = \frac{\pi D N}{60} = \frac{\pi \times 2 \times 0.308 \times 120}{60}$$

$$= 3.87 \text{ m/sec}$$

From Equation 7.22 pp. 143

$$I_{F\ Circular} = \frac{0.1 \times 0.1 \times 0.1 \times 1450 \times 9.81}{2 \times 9.81 \times 0.2017} (3.87)^2$$

$$= 53.83 \text{ N}$$

b. Cycloidal Trajectory

Treatment Number = T_{12} V_f = 0.399 m/sec

i. Fundamental Concept

$$\omega = \frac{N}{30} \text{ rad/sec} = \frac{\pi \times 120}{30} = 4 \text{ rad/sec}$$

$$\lambda = \frac{V_c}{V_f} = 9.67$$

$\alpha_s = \theta_i = 52.48^0$ (at the start of detachment)

$\alpha_e = 90^0$ (at the end of cut)

Average speed of cutting from Equation 7.28

$$V_{cav} = 4\pi \times 0.308 \left[\frac{\sqrt{1 + (9.67)^{-2} - 2(9.67)^{-1} \text{ Sin } 52.48)^{\frac{1}{2}}}}{} \right.$$

$$\left. \frac{+ (1 + (9.67)^{2} - 2(9.67)^{-1} \text{ Sin } 90)^{\frac{1}{2}}}{2} \right]$$

$= 3.52$ m/sec

Length of cutting path from Equation 7.25 pp. 143

$$L = 20.17 - \frac{10 \times 2}{2\pi \times 30.8} (2 \times 30.8 \times 10 - 10^2)^{\frac{1}{2}}$$

$= 17.83$ cm

From Equation 7.22 pp. 143

$$I_{F \text{ cycloidal}} = \frac{0.1 \times 0.1 \times 0.1 \times 1450 \times 9.81}{2 \times 9.81 \times 0.1783} (3.52)^2$$

$= 50.38$ N

When the speed of cutting is assumed equal to the peripheral speed of the blade according to Bernacki (1962) i.e. $V_{cav} = V_c = 3.87$ m/sec

$I_{F \text{ cycloidal}} = 60.89$ Newtons

ii. Bernacki Dynamic Force Model

From Equation 7.29 pp. 145

$$Pd = 0.01 \times 0.1 \times 10\ (dm) \times 0.1 \times 10\ (dm) \times 400 \times 9.81\ \left(\frac{N - sec^2}{m^4}\right)$$

$$\times 0.399\ (m/sec) \times 3.87\ (m/sec)$$

$$= 60.59 \text{ Newtons}$$

A4.2.2.2 Determination of Force due to Compression of Undeformed Soil, Q_{RT}

The blade geometry and soil properties are the same as in A4.1.1.

Working Regime: Treatment Number T_{16}

Bite length = 230.87 mm
Depth of cut = 50 mm
Width of cut = 100 mm

T_C = 0.8644 and T_γ = 0.7705

a. Determination of Quasi-Static Force

Using the procedure outlined in Section 4A.2.1

Length of shear plane at 15^o after penetration, L = 176 mm

$$\text{Shear force on the failure plane, } C = \frac{176}{1000} \times 4000 \times \frac{100}{100}$$

$$= 70.4 \text{ N}$$

Weight of soil mass = 10.50 N

Passive resistance force, P_p = 0.8644 x 70.4 + 0.7705 x 10.50

= 68.94 N

The component forces are obtained as:

ΔT = 119.05 N (from Equation 7.2)

ΔS = +19.50 N (from Equation 7.3)

$R_{R\ Static}$ = 120.63 N

b. Determination of Dynamic Forces

i. $I_{F\ cycloidal} \simeq$ zero (at rotor speed of 5 r.p.m.)

ii. Determination of Force due to Compression / Sinkage

Effective clearance angle at the start of cut = -3.75^{o}
(From Table 6.2)

Effective clearance angle after 5^{o} of penetration = -1.106^{o}

Average sinkage of the chamfered face of the blade = $\frac{0 - 1.106}{2}$

= -0.553^{o}

Sinkage = width of the back face x Sin $(-0.553)^{o}$

= 32.5 mm x 9.56 x 10 = 0.31 mm

Sinkage load = 0.9 kN (from Figure 7.8)

Area of the plate = (0.125 x 0.1) m^2

$\therefore$ stress on the plate = 72 kN/m^2

Area of the chamfered face of the blade $= \frac{32.5}{1000} \times \frac{100}{1000}$

$= 3.25 \times 10 \quad m^2$

Sinkage force, $Q_{RS} = 72 \times 3.25 \times 10^{-3} = 0.234$ kN

Compression force, $Q_{RT} = 0.256$ kN (from Equation 7.31) pp. 148

The component force due to compression is obtained as:

$\Delta T' = 74.84$ N (from Equation 7.32) pp. 148

$\Delta S' = 244.81$ N (from Equation 7.33) pp. 148

Therefore, total force on the blade for negative clearance angle is determined as below:

Total tangential force, $\Delta T_T = \Delta T + \Delta T'$

$= 119.05 + 74.84 = 193.89$ N

Total radial force, $\Delta S_T = \Delta S + \Delta S'$

$= 19.50 + 244.81 = 264.31$ N

Total resultant force, $R_{RT} = 327.80$ N

A4.3 Determination of Forces on the Blade with Vertical Axis of Rotation (<Quarter of a Circle Cut)

The blade geometry, working regime and soil properties are identical to the blade in horizontal axis of rotation. However, with the vertical blade,

Width of cut (w) in horizontal axis = Depth of cut (d) in vertical axis

Depth of cut (d) in horizontal axis = side cut (d') in vertical axis

Determination of Total Passive Resistance ($P_{P\ Total}$)

i. Passive resistance (P_{PV}) due to general shear failure plane bc (Figure 7.9) pp. 150

Cohesive force on the plane, C = c . l . d

$$= 4000 \left(\frac{N}{m^2}\right) \times \frac{142}{1000} (m) \times \frac{100}{1000} (m)$$

$$= 56.8\ N$$

The T_C-value is the same as with the horizontal axis blade = 0.8644

$P_{PV} = T_C \cdot C = 0.8644 \times 56.8\ N$

$= 49.09\ N$

ii. Passive resistance force (P_{PB}) due to bottom shear plane

Using Equation 7.37; pp. 151

$$T_{CV} = \frac{1}{\text{Cos } (18 + 7 - 24) + \text{Sin} \cdot (18 + 7 - 24) \text{ Tan } 37} = 0.9871$$

and $T_{\gamma V} = T_{CV} \cdot \text{Tan } \phi = 0.7438$

Area of bottom shear plane a'b'c'd' = $56.25 \times 10^{-4}\ m^2$

Weight of soil mass = $56.25 \times 10^{-4}\ (m^2) \times 14224.5 \left(\frac{N}{m^3}\right) \times \frac{100}{1000} (m)$

$= 8.00\ N$

Cohesive force on the plane a'b'c'd' = area x cohesion

$= 56.25 \times 10^{-4}\ m^2 \times 4000\ N/m^2$

$= 22.50\ N$

$P_{PB} = 0.9871 \times 22.50 + 0.7438 \times 8$

$= 28.16\ N$

$\therefore P_{P\ Total} = 49.09 + 28.16 = 77.25\ N$

Determination of Rear Tip Force, Q_{RV}

From Equation 7.40; pp. 152

$$Q_{RV} = \frac{0.6}{2} \times \frac{1}{1000}(m) \times 4000\ (\frac{N}{m^2}) \times 591.62 \times \frac{100}{1000}(m) + \frac{1}{4}(1 - \text{Sin } 37^{o})$$

$$\times 14224.5\ (\frac{N}{m^3}) \times 129.94 \times \frac{0.6}{2} \times 10^{-4}\ (m) \times \frac{100^2}{1000^2}(m)^2$$

$\therefore Q_{RV} = 70.994 + 0.055\ N = 71.05\ N$

The tangential (T_V) and radial (S_V) components are determined using Equations 7.2 and 7.3 as below: pp. 127

$T_V = 77.25\ \text{Cos}\ (90 - 18 - 7 - 24) + 71.05\ \text{Cos}\ (45 - 24)$

$= 124.63\ N$

$S_V = 77.25\ \text{Sin}\ (90 - 18 - 7 - 24) - 71.05\ \text{Sin}\ (45 - 24)$

$= +25.21\ N$

$R_{RV} = 127.156\ N$